GEOCHEMISTRY AND MINERALOGY OF THE PHONOLITE LAVA LAKE, MOUNT EREBUS VOLCANO, ANTARCTICA: 1972 to 2004 AND COMPARISON WITH OLDER LAVAS

by
Peter J. Kelly

Submitted in Partial Fulfillment
of the Requirements for the Degree of
Master of Science in Geochemistry
May, 2006

Department of Earth and Environmental Science
New Mexico Institute of Mining and Technology
Socorro, New Mexico, USA

ABSTRACT

A detailed 31-year record of the magmatic composition of the lava lake at Mount Erebus volcano, Ross Island, Antarctica, is compared to 0 ± 4 ka to 17 ± 8 ka-age lavas from the summit plateau. $^{40}Ar/^{39}Ar$ age determinations are used to refine the younger (< 180 ka) geologic history of Mt. Erebus.

The geochemistry of the lava lake is examined by analyzing major and trace element and oxygen isotope compositions of matrix glass and minerals in lava bombs erupted from the lake and associated vents between December 1972 and January 2004. Olivine, clinopyroxene, titanomagnetite, fluor-apatite, and matrix glass compositions are invariant and show that the magmatic temperature (~1000°C) and oxygen fugacity (ΔlogFMQ = -0.9) have been constant. Anorthoclase phenocrysts up to 10 cm in length show complex textural and compositional zoning that reflects growth during convection in a P_{H2O} gradient under isothermal conditions. Bomb textures and anorthoclase compositions suggest that crystallization occurs at low degrees of effective undercooling and is controlled by shallow degassing of water in the conduit.

Eleven lavas were analyzed and show a restricted compositional range that is controlled by anorthoclase content. They are indistinguishable from modern bulk tephra compositions and demonstrate that Mt. Erebus has been erupting lava and tephra from the summit region with the same bulk composition for ~17 ka.

Oxygen isotopes measured on 4 anorthoclase samples separated from bombs, 1 anorthoclase separate from a 6 ± 4 ka-age lava, and 2 matrix glass separates from bombs have a small range of primitive mantle-like values. Anorthoclase $\delta^{18}O$ range from 5.71‰ to 5.92‰ and matrix glass have $\delta^{18}O$ values of 5.29‰ and 5.57‰ (typical 1σ analytical uncertainty = ± 0.17‰). The phonolite is a highly differentiated residual melt (F = 0.24) derived from basanite by fractional crystallization, and large amounts of fractionation should lead to small predictable increases in $\delta^{18}O$. The low $\delta^{18}O$ values may be a consequence of CO_2 with a mantle-like $\delta^{18}O$ signature degassing from deep in the system. CO_2 saturates and exsolves at ~ 8 to 13 km and passes through a chamber of phonolite magma which resides higher in the crust. The upper level phonolite magma chamber is connected by an open conduit to the lava lake, where deep CO_2 and volatiles that saturate at lower pressures (i.e. H_2O) degas and deplete ^{18}O in the melt. The model is in accord with measured CO_2 fluxes, which are too large to be accounted for by observed magma fluxes, and helps explain how observed volatile fluxes are sustained at Mt. Erebus.

Six new $^{40}Ar/^{39}Ar$ age determinations provide a more complete record of the eruptive history of Mount Erebus volcano and development of the summit region. The new dates support the presence of a second, younger, superimposed caldera near the southwestern margin of the summit plateau. A pre-caldera lava sample from the southeastern caldera margin has an age of 172 ± 10 ka which is significantly older than any previously dated sample from the summit region and extends the age of lavas exposed in the caldera walls by ~70 ka. Trachyte lava from "Ice Station" on the eastern flank is 159 ± 2 ka, similar to two other trachyte lavas found on Mount Erebus. Trachyte

lavas were erupted from the eastern periphery of Mt. Erebus at ~160 ka, in close temporal and spatial proximity to Si-undersaturated lavas erupted from the modern-day summit region.

ACKNOWLEDGMENTS

There are many people I wish to thank for contributing to my professional and personal growth during the process of completing this project. I owe a debt of gratitude to my principle advisor, Philip Kyle, *il miglior fabbro*, for being my best critic and most constant source of encouragement. Nelia Dunbar was actively involved in nearly all aspects of this work and her enthusiasm, dedication, generosity, and friendship are gratefully acknowledged. Nelia deserves additional thanks along with Lynn Heizler for allowing me so much time on the electron probe and for patiently helping me operate the instrument. I am indebted to Rich Esser and Lisa Peters, who individually and collectively taught and helped me with many things, usually with a cheerful grin or a wry smile. Matt Heizler and Bill McIntosh provided invaluble expertise for the argon geochronolgy portion of this work. Additional thanks are in order to Bill McIntosh for his mischevious spirit and unfailingly sound guidance. Andy Campbell is thanked for many helpful conversations and for allowing me free reign in his isotope lab.

Warm thanks are extended to Ken Sims at the Woods Hole Oceanographic Institution, where oddly enough my career at NMT began. Under Ken's guidance I learned many of my research skills, and he has been extremely generous with his time and friendship. While at WHOI, Sylvain Pichat and Jerzy Blusztajn taught me much and made working there a pleasure.

My understanding of Mt. Erebus has benefitted from conversations and adventures in Antarctica with Harry Keys, Clive Oppenheimer, and Kurt Panter, all of whom are graciously thanked. Thank you to the denizens of the Lower Erebus Hut; you all made a wonderfully alien place feel like home. I am mightly indebted to the numerous workers who collected the samples I examined for this project over the last 30-plus years. Without their efforts this investigation would have been impossible.

Thank you to Ryan Jakubowski, Garrett Kramer, Shauna Mikelich, and Robert L. Wyckoff for your friendship and love these past years.

Finally, I must thank my family. They have supported me in all my endeavors all my life. Extra thanks are afforded to my Parents, who pushed me to go forward with this wild Antarctic stuff when I was ready to choose a more practical, if not boring, path. Thank you.

TABLE OF CONTENTS

LIST OF TABLES

LIST OF FIGURES

This thesis is accepted on behalf of the
Faculty of the Institute by the following committee:

Philip R Kyle
Advisor

Kenneth Rundle

Nina W. Dunbar

17 May 06
Date

I release this document to the New Mexico Institute of Mining and Technology.

Student's Signature

17 May 06
Date

PREFACE

Mount Erebus volcano, Ross Island, Antarctica, is a rare volcano. It is noteworthy not because it is the southernmost active volcano in the world, but because of its persistent activity and lake of convecting magma. The number of persistently active volcanoes worldwide is small, and only a handful feature active lava lakes comparable to Mt. Erebus. Examples include Kilauea (e.g Tilling, 1987; Garcia et al., 2003), Erta 'Ale, Ethiopia (e.g. Le Guern et al., 1979; Oppenheimer et al., 2004), Nyiragongo, Democratic Republic of Congo (e.g. Tazieff, 1984), Masaya, Nicaragua (e.g. Stoiber et al., 1986) and Villarrica, Chile (Witter et al., 2004). Among these volcanoes Mt. Erebus is the only one with phonolite magma which contains huge anorthoclase feldspar phenocrysts.

Yet for all its exotic flair, Mt. Erebus offers an exceptional opportunity to examine some fundamental igneous processes common to active and fossil systems worldwide. For example, the study of magma chambers and their dynamics is typically an inherently indirect endeavor, because they are located several kilometers underground. At Mt. Erebus, the lava lake gives us a direct view into the top of an active magma chamber. Here we can directly constrain parameters like temperature, and observe processes like convection instead of inferring its occurrence (e.g. Tait et al., 1989).

The primary focus of this study is to relate the composition of the lava lake over the last 31 years to observed behavior. This is accomplished by analyzing the major and trace element and oxygen isotope compositions of matrix glass and minerals from lava

bombs erupted between December 1972 and January 2004. From these data, it is possible to infer the controls on crystallization and eruption, and some of the fundamental characteristics and dynamics of the lava lake/upper-level magmatic system. To put recent activity in context, the compositions of modern bombs are compared to 0 ± 4 ka to 17 ± 8 ka-age phonolite lavas.

A second focus is to refine the younger (< 180 ka) geologic history of Mt. Erebus. The eruptive history of Mt. Erebus has been examined by Esser et al. (2004) and Harpel et al. (2004) using high-precision $^{40}Ar/^{39}Ar$ age determinations. Here we report new $^{40}Ar/^{39}Ar$ age determinations from key areas where age control was lacking that compliment and extend these previous efforts.

The two main research goals of this work are sufficiently different that they have been divided into two mutually exclusive papers. Part A encompasses the geochemical investigation of bombs and lavas. Part B discusses the $^{40}Ar/^{39}Ar$ age determinations and volcanic geology of Mt. Erebus. Both papers have been prepared and formatted for submission to the Journal of Volcanology and Geothermal Research. A comprehensive combined reference list encompassing all works cited by both papers is given with the appendices.

REFERENCES

Esser R.P., Kyle P.R., McIntosh W.C., 2004. $^{40}Ar/^{39}Ar$ dating of the eruptive history of Mount Erebus, Antarctica: Volcano evolution. Bull. Volcanol. 66, 671–686.

Garcia, M.O., Pietruszka, A.J., Rhodes, J. M., 2003. A petrologic perspective of Kilauea Volcano's summit magma reservoir. Journal of Petrology. 44, 2313-2339.

Harpel, C.J., Kyle P.R., Caldwell, D.A., McIntosh W.C., Esser R.P., 2004. $^{40}Ar/^{39}Ar$ dating of the eruptive history of Mount Erebus, Antarctica: summit flows and caldera collapse. Bull. Volcanol. 66, 687–702.

Le Guern, F., Carbonelle, J., Tazieff, H., 1979. Erte 'Ale lava lake: Heat and gas transfer to the atmosphere, J. Volcanol. Geotherm. Res. 6, 27– 48.

Oppenheimer, C., McGonigle, A.J.S., Allard, P., Wooster, M.J., Tsanev, V., 2004. Sulfur, heat, and magma budget of Erta 'Ale lava lake, Ethiopia. Geology. 32, 509-512.

Stoiber, R., Williams, S., Huebert, B., 1986. Sulfur and halogen gases at Masaya caldera complex, Nicaragua: Total flux and variations with time. J. Geophys. Res. 91, 2215–2231.

Tait, S.R., Wörner, G., Bogaard Pvd., Schmincke H-U., 1989. Cumulate nodules as evidence for convective fractionation in a phonolite magma chamber. J. Volcanol. Geotherm. Res. 37, 21-37.

Tazieff, H., 1984. Nyiragongo: Renewed activity of the lava lake. J. Volcanol. Geotherm. Res., 20, 267– 280.

Tilling, R.I., 1987. Fluctuations in surface height of active lava lakes during 1972-1974 Mauna Ulu eruption, Kilauea Volcano, Hawaii. J. Geophys. Res. 92, 13721-13730.

Witter, J.B., Kress, V.C., Delmelle, P., Stix, J., 2004. Volatile degassing, petrology, and magma dynamics of the Villarrica Lava Lake, Southern Chile. J. Volcanol. Geotherm. Res. 134, 303-337.

Geochemistry and mineralogy of the phonolite lava lake, Mount Erebus volcano, Antarctica: 1972 to 2004 and comparison with older lavas

Abstract

Mount Erebus, Ross Island, Antarctica, is a large (3794 m) alkaline open-conduit stratovolcano that hosts a persistently convecting and degassing lake of anorthoclase-phyric phonolite magma. The composition of the lava (magma) lake over the last 31 years was investigated by examining glass and mineral compositions in lava bombs erupted between December 1972 and January 2004. Olivine, clinopyroxene, titanomagnetite, fluor-apatite, and matrix glass compositions are invariant and show that the magmatic temperature (~1000°C) and oxygen fugacity (ΔlogFMQ = -0.9) have been constant. Anorthoclase phenocrysts up to 10 cm in length show complex textural and compositional zoning that reflects growth during convection in a P_{H2O} gradient under isothermal conditions. Bomb textures and anorthoclase compositions suggest that crystallization occurs at low degrees of effective undercooling and is controlled by shallow degassing of water in the conduit. Minor variations in eruptive activity in the last 31 years are decoupled from magma compositions. The variations probably relate to changes in conduit geometry within the volcano and/or variable input of CO_2-rich volatiles into the upper-level magma chamber from deeper in the system.

Eleven bulk samples of phonolite lava from the summit plateau that range in age from 0 ± 4 ka to 17 ± 8 ka were analyzed for major and trace elements. Small compositional variations are controlled by anorthoclase content. The lavas are indistinguishable from modern bulk tephra compositions and demonstrate that Mt. Erebus

has been erupting lava and tephra from the summit region with the same bulk composition for ~17 ka.

Oxygen isotopes were measured on 4 anorthoclase samples separated from bombs, 1 anorthoclase separate from a 6 ± 4 ka-age lava, and 2 matrix glass separates from bombs. The samples have a small range of primitive mantle-like values with anorthoclase $\delta^{18}O$ from 5.71‰ to 5.92‰ and matrix glass $\delta^{18}O$ values of 5.29‰ and 5.57‰ (typical 1σ analytical uncertainty = ± 0.17‰). The phonolite is a highly differentiated residual melt (F = 0.24) derived from basanite by fractional crystallization, and large amounts of fractionation should lead to small predictable increases in $\delta^{18}O$. The low $\delta^{18}O$ values may be a consequence of degassing of CO_2 with a mantle-like $\delta^{18}O$ signature from deep in the system. CO_2 saturates and exsolves at ~ 8 to 13 km and passes through a chamber of phonolite magma which resides higher in the crust. The upper level phonolite magma chamber is connected by an open conduit to the lava lake, where deep CO_2 and volatiles that saturate at lower pressures (i.e. H_2O) degas and deplete ^{18}O in the melt. The model is in accord with measured CO_2 fluxes, which are too large to be accounted for by observed magma fluxes, and helps explain how observed volatile fluxes are sustained at Mt. Erebus.

1. Introduction

Persistently active volcanoes and those with prolonged eruption cycles offer outstanding opportunities to directly study the time scales of magmatic processes because data can be collected in robust time series (e.g. Francalanci et al., 1999; Devine et al., 2003). Geochemical time series have been used to constrain important parameters like differentiation and mixing rates (Reagan et al., 1987), magma residence times (Albarède, 1993; Francalanci et al., 1999) and can potentially aid in forecasting major eruptions (Chen et al., 1993). The rates of magmatic processes can also provide insight into fundamental characteristics of magmatic systems, such as the factors controlling crystallization and differentiation (Hawkesworth et al., 2000; Hawkesworth et al., 2004). In the case of recently active volcanoes, the geochemical record can often be integrated with observations of eruption style and magnitude, gas emissions, ground deformation, and seismicity to give a complete picture of the volcanic activity. Data from modern integrated monitoring efforts (e.g. Soufrière Hills volcano, Monserrat) have helped uncover links between subvolcanic processes and volcanic behavior, and are pushing toward better physical models and improved eruption forecasting (Sparks, 2003a).

Mount Erebus volcano, Ross Island, Antarctica, (Fig. 1) presents an excellent opportunity to study a large (3794 m elev., 2170 km^3), stable, slowly evolving, highly differentiated, persistently active magmatic system (Esser et al., 2004; Kyle, 1977; Kyle et al., 1992; Caldwell and Kyle, 1994). Mt. Erebus is an alkaline open-conduit stratovolcano that hosts a persistently convecting and degassing lake of anorthoclase-phyric phonolite magma (herein referred to as the "lava lake," as per convention). There

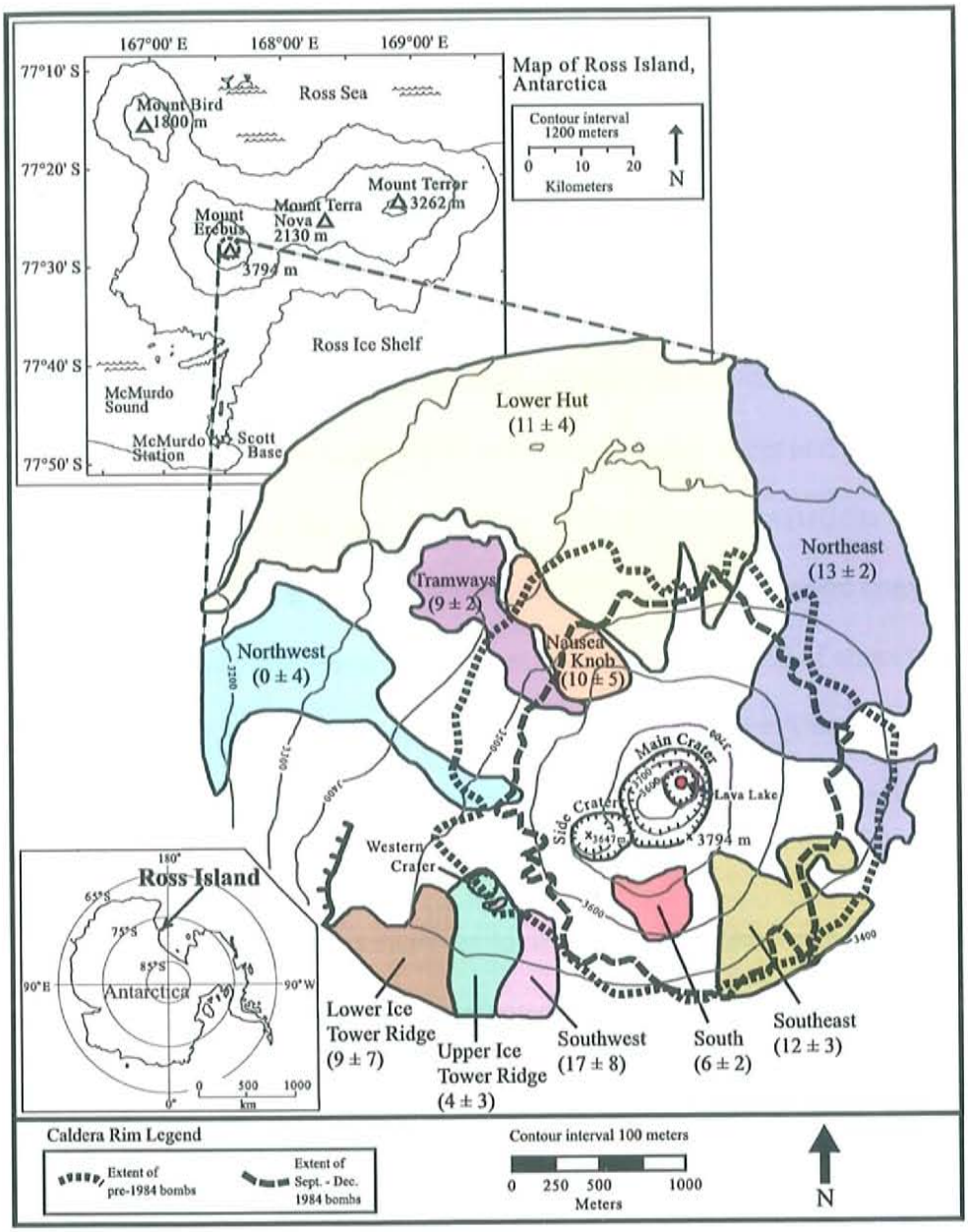

Figure 1. Geologic map of the summit of Mt. Erebus volcano showing topography and lava flow units with their ages (in ka). The distribution of bombs erupted in late 1984 and at some unspecified time prior to that are shown. Insets show Ross Island and location in Antarctica. $^{40}Ar/^{39}Ar$ ages and 2σ errors from Harpel et al. (2004) and Kelly (Section B).

is evidence of a lava lake on an aerial photograph in 1963, and it was first directly observed by a scientific party in December, 1972 (Giggenbach et al., 1973; Kyle et al., 1982). Since 1972 the lava lake has always been present but has changed in size (5 – 60 m diameter), shape, and location (Kyle et al., 1982; Aster et al., 2003). Typical eruptive activity at Mt. Erebus includes up to six strombolian eruptions per day from the lava lake, continuous degassing and small bubble bursts at the lake and less frequent gas and ash eruptions from adjacent vents. Minor variations in the style and magnitude of activity between 1972 and the present (early 2006) include a period of larger and more frequent strombolian eruptions (September to December 1984) that briefly buried the lava lake under fresh ejecta (Kyle et al., 1986; Caldwell and Kyle, 1994), a phreatic eruption (1993), rare intra-crater lava flows on the Inner Crater floor, a period of almost no eruptions (2002 – 2004), the brief appearance of a second lava lake (December 2004), and a recent return to typical strombolian activity with up to 6 eruptions per day in mid-2005.

The main purposes of this study are to determine if the geochemical and mineralogic compositions of lava bombs erupted from 1972 – 2004 relate in any way to observed variations in eruptive activity, and if any evolutionary changes have occurred during this time. To put the composition of recently erupted tephra in context, a comparison is made between the modern phonolite lava bombs and older lavas. In an earlier study Caldwell and Kyle (1994) documented the nearly constant chemical composition and mineralogy of bombs erupted from 1972 – 1986. They raised the possibility that a batch of volatile-rich magma may have been injected into the system to

trigger the 1984 eruptions, and that the temperature of the magmatic system may be fluctuating.

We present major element, trace element, mineralogical, and oxygen isotope measurements made on volcanic bombs erupted between 1972 and 2004 as well as bulk major and trace element analyses of phonolite lavas erupted in the last ~17 ka. The data show that the Mt. Erebus magmatic system is extremely stable and that no change in bulk composition has occurred in ~17 ka. Important inferences about the structure and degassing of the Mt. Erebus magmatic system are revealed by oxygen isotope measurements, the first reported for rocks from Erebus volcano.

2. Mount Erebus Volcano

2.1 Volcanic geology

Mount Erebus volcano is the southernmost active volcano in the world. Intracontinental rifting and extension have resulted in voluminous alkaline volcanism in the western Ross Sea which is termed the McMurdo Volcanic Group (MVG) (Kyle and Cole, 1974; Kyle, 1990a). On Ross Island, Mt. Erebus and its subsidiary volcanic centers, Mt. Terror, Mt. Bird, and Hut Point Peninsula (Fig. 1) form part of the Erebus volcanic province (Kyle, 1990b). Ross Island overlies very thin (17 - 25 km) rifted continental crust at the southern terminus of the Terror Rift, a major graben located at the western margin of the West Antarctic rift system (Bannister et al., 2000; Cooper et al., 1987; Behrendt et al., 1991). About 4,520 km^3 of volcanic material has been erupted on Ross Island over the last ~4 Ma (Esser et al., 2004).

Temporal constraints on the volcanic evolution of Mt. Erebus have been obtained by comprehensive high-precision $^{40}Ar/^{39}Ar$ age-dating (Esser et al, 2004; Harpel et al, 2004; Kelly, Part B). Development of the Mt. Erebus edifice can be divided into three phases:

(I) proto-Erebus shield building phase (1.3 – 1.0 Ma)

(II) proto-Erebus cone building phase (1.0 Ma – 250 ka)

(III) the modern-Erebus cone building phase (250 ka – present)

The first phase represents a transition from subaqueous to subaerial activity at 1.3 Ma, and is represented by eruption of basanite. During the second phase more evolved phonotephrite lavas formed steep summit slopes that were subsequently destroyed by a caldera collapse event at ~750 ka and followed by a period of flank eruptions. The bulk of the present-day Erebus edifice was formed during the third phase, when activity increased and large volumes of anorthoclase-phyric tephriphonolite and phonolite lavas were extruded.

The present-day summit topography (Fig. 1) was formed by a major caldera collapse between 80 and 24 ka that created the summit plateau, and a second smaller nested caldera collapse that occurred between 25 and 11 ka (Harpel et al., 2004; Kelly, Part B). Post-collapse lava flows and pyroclastic deposits fill the calderas and form the summit cone, which consists of two craters, the Side Crater and Main Crater. All historic eruptive activity has originated from the lava lake and associated vents in the ~ 160 m diameter, ~ 100-m-deep Inner Crater which is nested in the Main Crater (500 by 600 m diameter, 120 m deep). Lava bombs ejected from the lava lake are on average ~1m in diameter and occasionally land on the main crater rim or travel 100's of meters beyond it.

During the increased activity in late 1984, bombs up to 10 m in diameter were thrown up to 1 km above the Main Crater rim and over 1 km from the lava lake (Caldwell and Kyle, 1994). Older bombs (pre-1972) are found up to 1.5 km from the Main Crater, indicating that 1984-like activity has occurred previously. A lag gravel formed by physical weathering of bombs that litter the summit area indicates that activity observed over the last 34 years is not abnormal and has been sustained for several centuries or millennia (Kyle et al., 1982; Harpel et al., 2004).

2.2 Petrology

The trace element concentrations of primitive Mt. Erebus basanites are similar to those at alkalic oceanic islands (OIB), and feature primitive Sr, Nd, and Hf ratios (e.g. $^{87/86}Sr \sim 0.70300$) and HIMU-like $^{206/204}Pb$ ratios (~19.95) (Sun and Hanson, 1975; Sun and Hanson, 1976; Kyle et al., 1992; Sims et al., in prep.). Alkaline, OIB-like basalts with low $^{87/86}Sr$ and HIMU enrichments are characteristic of Cenozoic West Antarctic rift volcanoes, although there is little agreement on their origin or significance here or in general (Finn et al., 2005; Panter et al., in press).

The basanite to phonolite lava suite found at Mt. Erebus, termed the "Erebus Lineage" (EL), is alkaline and strongly Si-undersaturated (Kyle, 1976; Kyle et al., 1992). EL lavas form continuous trends on major and trace element variation diagrams and have primitive, nearly invariant radiogenic isotope ratios (Sr, Nd, Hf, Pb) (Kyle et al., 1992; Sims et al., in prep.). They have been interpreted as a co-genetic sequence related by fractional crystallization (FC) (Kyle et al., 1992). FC models suggest bulk phonolite is a

23.5% residual melt of parental basanite (Kyle et al., 1992). Phonolite lavas have only been erupted recently in the history of Mt. Erebus. A shift from tephriphonolite to phonolite occurred at ~36 ka, after 1.3 Ma of eruption of less-differentiated material (Harpel et al., 2004; Esser et al., 2004). The oldest phonolite lavas are found on the flanks of Erebus volcano (Esser et al., 2004). Phonolite lavas from the summit region examined in this study range in age from 17 ± 8 to 0 ± 4 ka (Harpel et al., 2004; Kelly, Part B).

3. Sample descriptions, analytical methods, and results

3.1 Lavas

Phonolite lavas from the summit region have an extreme phaneritic texture. Abundant (~30 – 40 vol. %) anorthoclase feldspar crystals up to ~6 cm in length along with small amounts of olivine, opaque oxides, clinopyroxene, and apatite are found in a glassy groundmass that is black when fresh and weathers to lighter shades of gray. In hand specimen the individual summit lava flows are indistinguishable from each other (Harpel, 2004).

Preparing a representative bulk sample of Mt. Erebus lava and tephra is difficult because of the abundance and large size of the anorthoclase phenocrysts. To best approximate true bulk chemical composition Moore (1986) and Caldwell and Kyle (1994) jaw crushed one to five kilograms of sample and then split a fraction to prepare a fine (~5-10 μm) powder using a tungsten carbide swing mill. Eschenbacher (1998) followed a similar procedure to obtain a bulk chemical analysis of a bomb erupted in

1997. Tantalum contamination from the WC was monitored and corrected using quartz "blanks."

Eleven whole rock samples from ten lava flows from the summit plateau erupted in the last ~17 ka were analyzed for major elements by XRF and trace elements by ICP-MS. Results, analytical details, and $^{40}Ar/^{39}Ar$ ages from Harpel et al. (2004) and Kelly (Part B) are summarized in Table 1. Two samples (E87020 & E87034) collected from different locations 1.3 km apart on the Lower Hut flow were analyzed to assess intra-flow compositional variability.

In addition to data collected as part of this study, several other datasets were also considered. These include 97 previously unreported minor and trace element analyses of bulk lava samples from the summit plateau (Appendix C.3), as well as one previously unpublished whole-rock analysis of a bomb erupted in 1997 (Eschenbacher, 1998). Whole rock analyses of bombs erupted between 1972 and 1986 reported by Caldwell and Kyle, 1994 and bulk analyses of Erebus Lineage lavas (Kyle et al., 1992) are also included.

3.2 Tephra

The 32 lava bombs analyzed in this study were erupted from the lava lake or associated vents between December 1972 and January 2004 and collected from the Main Crater floor or around the crater rim. The exact time and date of eruption are known for some bomb samples and others were collected based on their fresh appearance. Recently erupted bombs have a distinctive metallic to iridescent vitreous luster that is quickly lost (~1 – 2 weeks) upon exposure to acid gases continuously emitted from the lava lake and

Table 1. Whole-rock analyses of phonolite lavas and a bomb erupted from Mt. Erebus volcano as determined by XRF and ICP-MS.

Sample	E87066	E87030	E87085	E87020	E87034	E87035	E87004	E87054	E87083	E87051	E87040	97018*
Age (ka)	17±8	13±2	12±3	11±4	11±4	10±5	9±2	9±7	6±2	4±3	0±4	erupted 21-Dec-1997
Location	Southwest flow	Northeast flow	Southeast flow	Lower Hut flow	Lower Hut flow	Nausea knob	Tramways flow	Lower Ice Tower Ridge	South flow	Upper Ice Tower Ridge	Northwest flow	collected from crater rim
SiO_2 (wt%)	56.02	56.49	56.59	56.05	55.80	56.72	57.64	56.22	56.15	55.97	56.77	56.23
TiO_2	0.98	1.08	1.13	1.11	1.10	1.00	0.89	1.09	1.00	1.11	0.96	0.99
Al_2O_3	19.88	19.73	19.88	19.71	19.62	19.94	20.27	19.60	19.38	19.61	20.11	19.82
$Fe_2O_3^T$	5.22	5.81	6.19	5.92	5.87	5.27	4.68	5.76	5.62	5.98	4.97	5.35
MnO	0.21	0.24	0.26	0.24	0.24	0.23	0.19	0.23	0.24	0.24	0.20	0.23
MgO	0.91	1.03	1.03	0.99	0.98	0.94	0.83	0.89	0.97	1.03	0.85	0.88
CaO	2.86	2.90	2.74	2.79	2.78	2.93	3.00	2.86	2.75	2.82	2.91	2.68
K_2O	4.40	4.46	4.71	4.59	4.58	4.38	4.21	4.47	4.45	4.43	4.33	4.51
Na_2O	8.13	8.05	8.18	8.32	8.35	8.10	8.02	8.16	8.10	8.11	8.10	8.38
P_2O_5	0.42	0.47	0.48	0.47	0.48	0.43	0.39	0.46	0.44	0.48	0.41	0.41
L.O.I.	-0.15	-0.18	-0.08	0.10	0.33	-0.11	-0.12	-0.21	-0.14	-0.14	-0.09	-0.16
Total	98.88	100.08	101.10	100.29	100.13	99.83	100.00	99.53	98.96	99.65	99.52	99.61
TiO_2 (wt%)	1.00	1.22	1.06	1.12	1.31	1.11	0.90	1.15	1.02	1.12	0.99	
Li (ppm)	17.8	23.2	26.3	27.6	30.6	26.4	19.9	24.2	20.2	22.7	21.1	
Be	8.66	9.64	9.35	9.50	10.82	9.24	7.07	8.70	8.29	8.82	7.78	
Sc	3.07	3.29	3.40	3.24	4.00	3.12	2.50	3.63	3.49	3.12	3.12	
V	4.97	7.79	6.08	5.88	7.31	6.19	5.05	7.72	5.66	6.88	5.20	8.5
Co	10.4	10.1	9.06	10.2	13.9	12.6	18.2	9.24	8.91	10.7	11.0	
Ni	1.9	0.61	0.64	0.80	0.98	0.88	0.61	0.58	0.76	0.54	0.51	4.5
Cu	6.8	5.6	5.1	5.4	6.2	5.6	4.3	5.3	5.1	5.1	5.0	4.5
Zn	115	138	128	129	151	136	98	128	128	128	107	127
Ga	22	26	23	22	27	24	23	23	23	22	22	27.2
Rb	95.8	107	104	107	119	100	80.8	99.2	96.3	100	90.0	107
Sr	1028	939	726	780	917	1145	1234	941	886	854	1120	914
Y	52.9	62.4	62.2	60.5	67.3	57.2	44.9	58.2	58.7	59.3	50.4	55.9
Zr	969	1092	1083	1084	1216	1018	799	1007	983	1024	907	1016
Nb	252	286	281	284	320	266	208	264	257	267	236	261
Cs	1.29	1.47	1.44	1.48	1.62	1.35	1.08	1.35	1.31	1.39	1.23	
Ba	1124	1075	881	889	1037	1271	1346	1103	1141	989	1224	1129
La	118	136	133	130	147	127	103	127	128	129	114	
Ce	226	259	255	249	279	241	193	242	246	247	215	
Pr	23.8	28.3	28.0	26.6	29.8	25.5	19.7	26.4	26.5	26.6	22.6	
Nd	82.5	96.3	93.5	90.9	102	88.1	70.2	89.9	90.4	90.8	79.3	
Sm	13.7	16.1	15.8	15.3	17.1	14.7	11.7	15.1	15.2	15.3	13.1	
Eu	4.12	4.44	3.97	3.91	4.45	4.55	4.26	4.31	4.34	4.11	4.24	
Gd	10.8	12.7	12.5	12.0	13.4	11.6	9.1	12.1	12.0	12.0	10.4	
Tb	1.67	1.94	1.92	1.86	2.07	1.79	1.41	1.85	1.85	1.84	1.60	
Dy	9.52	11.0	10.8	10.7	11.9	10.2	8.09	10.5	10.4	10.6	9.07	
Ho	1.88	2.16	2.14	2.12	2.34	2.03	1.58	2.06	2.06	2.08	1.80	
Er	5.23	5.95	5.90	5.80	6.47	5.55	4.39	5.63	5.59	5.67	4.91	
Yb	4.86	5.52	5.45	5.39	5.96	5.23	4.07	5.15	5.09	5.25	4.56	
Lu	0.757	0.854	0.859	0.851	0.937	0.809	0.640	0.805	0.805	0.820	0.716	
Hf	19.2	21.5	21.4	21.4	24.0	20.4	15.8	20.2	19.4	20.3	17.9	
Ta	14.7	16.3	16.1	16.3	18.5	15.4	12.2	15.5	14.7	15.5	13.7	
Pb	4.91	5.29	5.20	5.28	5.95	5.36	4.20	5.08	4.86	4.99	4.75	5.8
Th	24.0	26.2	26.6	26.5	29.6	25.1	19.5	24.7	23.3	25.1	22.0	26.4
U	6.85	7.55	7.42	7.52	8.45	7.39	5.50	7.11	6.66	7.11	6.32	6.7

Age = $^{40}Ar/^{39}Ar$ ages and 2σ errors from Harpel et al. (2004), except E87040 from Kelly (Section B). L.O.I. = Loss on ignition. Major elements analyzed by Philips PW2400 X-ray fluorescence (XRF) spectrometer at New Mexico Tech (NMT) (Hallett and Kyle, 1993). Typical major element XRF analytical precision is < 1%. Trace elements and TiO_2 analyzed by VG PQ ExCell quadrupole ICP-MS at Boston University following the procedures of Kelley et al. (2003) (except 97018*). Analytical precision for trace elements is < 3%. *Previously unpublished whole rock analysis of lava bomb from Eschenbacher (1998) for comparison; major and trace elements by XRF at NMT (typical trace element precision < 2%).

surrounding fumaroles. Based on their fresh condition, samples for which an exact date of eruption is unknown must have been erupted less than one month prior to collection.

Matrix glass major element compositions were determined by electron microprobe (EMP) and trace element compositions by ICP-MS; results and analytical details are summarized in Table 2. Minerals were analyzed by EMP; representative analyses and analytical details are given in Table 3, except anorthoclase feldspar (Table 4). Mineral modes for 7 bombs (Table 5) were calculated by least squares mass balance using major element whole rock analyses (Caldwell and Kyle, 1994; Eschenbacher, 1998) and mineral compositions from Tables 2, 3, and 4.

3.3 Oxygen Isotopes

A conventional extraction line was used to measure oxygen isotopes on 2 glass and 4 anorthoclase mineral separates from tephra and an anorthoclase separate from a 6 ± 4 ka-age anorthoclase phonolite lava (Kelly, Section B) following procedures outlined by Hallett (1994, and references therein). Results and analytical details are summarized in Table 6. Aliquots of glass were taken from samples prepared for trace element analysis. Anorthoclase feldspar were crushed, sieved, and etched in a 15% HF acid solution to remove melt inclusions following a procedure similar to Esser et al. (1997) and described in Kelly (Section B).

4. Whole rock geochemistry

4.1 Major and trace element concentrations of lavas

All the lavas are Si-undersaturated phonolites that show strong enrichments in alkali and incompatible elements (Figs 2 & 3a). The concentrations of some elements,

Table 2. Major and trace element analyses of matrix glass separated from tephra erupted from Erebus volcano between December 1972 and January 2004 as determined by EMP and ICP-MS.

Eruption date	26 Dec 1972	Dec 1974	Dec 1974	Dec 1975		Nov 1977	Nov 1977	26 Dec 1979	Nov 1980		Nov 1981		Dec 1982
Sample	25724G	2E2G	25721G	25723G	77015G	77016G	78325G	79302G	80300G	81003G	81401G	81410G	82416G
n	*20*	*17*		*18*	*13*		*16*	*16*	*6*	*15*	*17*	*10*	*9*
SiO_2 (wt.%)	55.62	55.75		55.70	55.78		55.78	55.73	55.01	55.74	55.08	55.69	55.02
TiO_2	1.05	1.02		1.03	1.01		1.02	1.02	0.99	1.02	1.01	1.01	1.01
Al_2O_3	19.58	19.67		19.60	19.65		19.61	19.63	19.98	19.64	20.05	19.71	20.07
FeO^T	5.59	5.38		5.52	5.42		5.41	5.41	5.34	5.49	5.31	5.43	5.37
MnO	0.28	0.28		0.29	0.27		0.28	0.26	0.26	0.27	0.27	0.28	0.28
MgO	0.86	0.83		0.85	0.83		0.80	0.83	0.82	0.84	0.80	0.82	0.84
CaO	1.85	1.88		1.92	1.84		1.89	1.83	1.89	1.86	1.86	1.84	1.89
Na_2O	8.82	8.85		8.73	8.86		8.80	8.85	9.09	8.82	9.09	8.80	9.04
K_2O	5.61	5.64		5.58	5.63		5.70	5.67	5.71	5.61	5.65	5.64	5.57
P_2O_5	0.28	0.28		0.29	0.26		0.26	0.27	0.23	0.28	0.26	0.28	0.28
SO_2	0.08	0.07		0.08	0.07		0.08	0.08	0.08	0.08	0.08	0.08	0.07
F	0.23	0.19		0.25	0.22		0.20	0.26	0.23	0.21	0.18	0.28	0.20
Cl	0.16	0.15		0.16	0.16		0.16	0.15	0.16	0.15	0.16	0.15	0.15
TiO_2 (wt %)	1.00		1.00	1.02		0.95	1.17	1.02	1.04	1.05	1.03		1.00
Li (ppm)	32.8		30.2	32.5		31.8	30.0	33.3	31.0	28.4	28.3		31.8
Be	12.7		12.3	13.4		12.5	12.4	12.9	11.8	10.1	10.1		12.8
Sc	4.34		5.05	4.89		4.92	4.70	4.46	4.95	5.04	4.74		5.12
V	2.20		2.49	2.59		2.10	4.28	2.62	2.06	1.86	1.86		2.68
Co	2.34		2.81	2.62		2.31	2.82	2.74	2.27	2.02	2.08		2.78
Cu	8.4		4.3	4.0		3.9	5.3	9.8	6.8	5.3	11.8		16.1
Zn	158		160	159		147	159	161	160	160	163		161
Ga	31		31	31		29	30	31	31	31	31		30
Rb	146		143	147		142	142	149	143	138	139		143
Sr	237		267	249		255	257	252	263	261	245		251
Y	85.8		86.2	85.8		80.7	84.0	85.6	83.0	76.3	79.8		85.7
Zr	1605		1569	1632		1541	1550	1615	1606	1592	1549		1572
Nb	411		399	418		394	399	415	415	414	407		402
Cs	2.00		1.95	2.02		1.94	1.95	2.02	1.91	1.79	1.78		1.95
Ba	435		460	451		461	456	454	465	460	436		445
La	165		168	166		156	165	166	164	153	161		166
Ce	319		326	321		299	315	319	315	294	311		318
Pr	33.9		34.8	33.8		31.8	33.4	34.0	33.9	31.6	33.4		33.8
Nd	113		116	113		106	112	113	112	103	110		114
Sm	19.1		19.9	19.3		18.0	19.0	19.2	19.2	17.7	18.9		19.4
Eu	3.65		3.80	3.70		3.52	3.71	3.69	3.73	3.56	3.63		3.70
Gd	17.0		17.5	17.1		16.0	16.9	16.9	15.7	13.6	14.4		17.1
Tb	2.66		2.73	2.67		2.52	2.63	2.65	2.48	2.24	2.34		2.67
Dy	14.4		14.7	14.6		13.9	14.3	14.4	14.0	12.7	13.3		14.6
Ho	2.83		2.86	2.86		2.72	2.80	2.85	2.78	2.56	2.66		2.85
Er	7.83		7.82	8.00		7.56	7.71	7.85	7.81	7.39	7.60		7.88
Tm									1.17	1.13	1.16		
Yb	7.50		7.49	7.64		7.30	7.33	7.54	7.50	7.16	7.28		7.52
Lu	1.16		1.16	1.19		1.15	1.15	1.18	1.17	1.12	1.14		1.17
Hf	31.4		30.7	32.7		30.5	30.8	31.8	31.9	31.3	30.6		31.4
Ta	23.6		22.8	24.4		23.0	23.4	23.9	23.7	23.1	22.4		23.6
Pb	7.83		5.82	6.13		6.07	6.26	9.70	7.78	6.06	6.67		7.53
Th	31.6		30.3	33.6		32.8	31.2	31.8	31.8	29.8	29.6		32.3
U	9.30		8.92	9.81		9.51	9.19	9.42	9.38	8.78	8.88		9.53

Table 2. *(continued)*

Eruption date			Dec 1983	Oct 1984	Dec 1984	Dec 1984	Dec 1985		22 Dec 1986	Dec 1988	Dec 1989	Jan 1991	Dec 1992	Dec 1992
Sample	82418G	83207G	83220G	84500G	84501G	84505G	85009G	85010G	86022G	88104G	89001G	91101G	92101G	Er92G
n	*12*	*14*	*6*	*16*		*12*	*13*		*12*	*17*	*20*	*19*	*20*	
SiO_2 (wt.%)	55.82	55.75	54.93	55.61		55.90	55.63		55.41	54.97	55.12	55.09	54.85	
TiO_2	1.00	0.99	1.03	0.98		0.98	0.97		1.01	1.03	0.99	1.01	1.02	
Al_2O_3	19.75	19.74	20.01	19.71		19.69	19.70		19.74	19.90	19.91	19.83	19.90	
FeO^T	5.50	5.52	5.41	5.57		5.40	5.45		5.48	5.45	5.46	5.43	5.50	
MnO	0.28	0.29	0.27	0.29		0.28	0.28		0.28	0.28	0.28	0.27	0.28	
MgO	0.85	0.84	0.82	0.93		0.83	0.92		0.83	0.84	0.83	0.84	0.84	
CaO	1.74	1.75	1.89	1.80		1.75	1.81		1.79	1.86	1.88	1.88	1.88	
Na_2O	8.96	8.99	9.14	8.96		8.99	8.93		9.04	9.13	9.02	9.06	9.15	
K_2O	5.35	5.41	5.67	5.42		5.43	5.50		5.62	5.65	5.59	5.65	5.65	
P_2O_5	0.27	0.27	0.26	0.27		0.28	0.28		0.26	0.29	0.30	0.28	0.29	
SO_2	0.06	0.07	0.07	0.07		0.07	0.08		0.09	0.07	0.08	0.08	0.07	
F	0.27	0.26	0.15	0.26		0.26	0.31		0.29	0.17	0.19	0.21	0.20	
Cl	0.15	0.14	0.15	0.15		0.14	0.15		0.16	0.15	0.16	0.16	0.15	
TiO_2 (wt. %)			1.04		1.02	1.06	1.00	1.12	1.07		0.98	1.03	1.06	1.07
Li (ppm)			28.6		28.4	29.0	28.1	30.0	29.0		30.0	28.8	28.6	28.8
Be			10.0		10.0	10.3	10.0	10.6	10.3		12.1	10.3	10.0	10.1
Sc			4.84		4.80	5.09	5.09	5.11	4.86		4.08	5.39	4.75	5.33
V			1.93		1.91	2.43	2.34	2.20	1.97		2.16	2.51	1.97	2.89
Co			2.18		2.23	2.44	2.15	2.47	2.31		2.39	2.23	2.20	2.22
Cu			8.6		8.0	11.4	6.6	9.2	7.3		6.1	16.2	8.8	11.6
Zn			161		161	177	171	173	167		157	178	164	180
Ga			30		30	36	38	33	33		31	39	32	39
Rb			137		137	140	139	144	140		143	140	140	141
Sr			273		258	273	273	221	250		272	252	239	264
Y			82.5		78.2	84.9	81.0	85.6	79.4		83.6	86.7	81.4	82.7
Zr			1549		1533	1576	1571	1626	1573		1554	1563	1569	1610
Nb			405		402	408	402	421	410		400	403	411	413
Cs			1.77		1.80	1.89	1.97	1.85	1.79		1.95	2.01	1.79	2.01
Ba			463		455	465	475	404	438		463	449	422	463
La			170		158	175	167	174	161		164	182	166	172
Ce			324		304	335	319	330	308		313	349	319	326
Pr			35.2		32.7	36.3	33.6	36.2	33.4		33.4	37.4	34.6	34.7
Nd			117		108	120	111	119	108		112	124	114	115
Sm			20.2		18.7	20.7	19.0	20.6	18.6		19.0	21.3	19.6	19.7
Eu			3.90		3.66	3.93	3.74	3.83	3.62		3.72	3.98	3.68	3.82
Gd			15.2		14.3	15.6	14.5	15.7	14.4		16.7	16.0	14.8	14.9
Tb			2.46		2.31	2.49	2.31	2.55	2.33		2.62	2.51	2.40	2.38
Dy			13.9		13.3	14.0	13.2	14.4	13.3		14.1	14.4	13.7	13.7
Ho			2.76		2.65	2.80	2.70	2.82	2.66		2.77	2.88	2.71	2.78
Er			7.82		7.55	7.98	7.67	8.08	7.57		7.59	8.18	7.79	7.86
Tm			1.20		1.17	1.22	1.20	1.22	1.15			1.26	1.17	1.23
Yb			7.37		7.27	7.51	7.34	7.61	7.20		7.19	7.59	7.32	7.45
Lu			1.16		1.14	1.16	1.13	1.21	1.12		1.12	1.16	1.14	1.15
Hf			30.6		30.8	30.4	29.7	32.3	30.6		30.3	29.9	30.6	30.7
Ta			22.4		22.6	22.4	22.5	23.6	22.7		22.7	22.6	22.7	23.3
Pb			6.74		7.15	7.45	6.37	7.05	6.39		5.83	7.46	6.58	11.26
Th			29.3		29.9	29.2	29.4	30.6	29.2		29.4	29.5	29.8	30.5
U			8.69		8.94	8.85	9.03	9.19	8.63		8.68	9.11	8.93	9.13

Table 2. *(continued)*

Eruption date	Dec 1993	Dec 1996	Dec 1996	21 Dec 1997	Dec 1997	Dec 1999	Dec 1999	Dec 2000	Dec 2000	Dec 2001	Jan 2004	mean	RSD	EAP
Sample	93102G	E96-01G	ER96G	97018G	Er97G	1999G	Er99G	DEC2000G	Er2000G	E2001G	JAN2004G		(%)	(%)
n	*17*	*20*		*18*		*16*		*11*		*20*	*15*	*435*		*20*
SiO_2 (wt.%)	55.17	55.12		55.11		55.00		54.73		54.94	54.95	55.35	0.68	1.0
TiO_2	1.01	1.02		1.03		1.02		1.02		1.02	1.04	1.01	1.8	3.0
Al_2O_3	19.79	19.91		19.85		19.83		19.93		19.92	19.87	19.80	0.72	1.1
FeO[7]	5.42	5.32		5.34		5.38		5.43		5.39	5.45	5.43	1.3	1.3
MnO	0.27	0.27		0.27		0.28		0.28		0.28	0.27	0.28	2.4	7.2
MgO	0.82	0.83		0.83		0.83		0.84		0.83	0.82	0.84	3.2	1.2
CaO	1.88	1.87		1.88		1.86		1.89		1.87	1.90	1.85	2.6	1.6
Na_2O	9.06	9.09		9.07		9.13		9.21		9.13	9.10	9.00	1.5	4.7
K_2O	5.64	5.64		5.65		5.68		5.73		5.67	5.65	5.61	1.7	1.6
P_2O_5	0.28	0.27		0.30		0.31		0.28		0.29	0.27	0.28	5.7	7.2
SO_2	0.08	0.08		0.08		0.08		0.08		0.08	0.09	0.08	7.6	26
F	0.23	0.21		0.25		0.24		0.20		0.22	0.23	0.23	16	26
Cl	0.15	0.15		0.16		0.16		0.16		0.16	0.16	0.15	4.1	13
TiO_2 (wt. %)	1.00		1.00		0.97		0.99		1.01	1.02	1.02	1.03	4.5	4.0
Li (ppm)	27.8		28.3		27.4		28.6		28.6	28.9	29.3	29.6	5.5	5.3
Be	9.9		10.0		9.6		10.2		10.2	10.1	10.5	10.9	11	9.0
Sc	4.81		5.19		4.90		4.84		5.00	4.93	5.26	4.91	5.8	2.3
V	2.37		2.51		2.16		2.36		2.46	2.30	2.43	2.36	20	8.0
Co	2.01		2.23		2.15		2.17		2.26	2.03	2.21	2.32	10	12
Cu	9.3		13.0						18.6	14.7	10.7	9.4	37	17
Zn	172		175		174		186		181	174	179	167	5.7	2.2
Ga	38		38		37		38		38	39	39	34	11	6.8
Rb	137		138		134		139		140	140	142	141	2.4	3.5
Sr	256		245		245		231		216	269	248	253	6.0	2.9
Y	81.8		82.5		77.9		79.5		83.9	80.6	81.8	82.5	3.4	5.8
Zr	1550		1603		1584		1576		1619	1579	1601	1580	1.7	1.9
Nb	398		405		397		403		412	405	411	407	1.7	1.1
Cs	1.97		1.95		1.91		2.01		2.01	1.99	2.06	1.93	4.7	7.8
Ba	454		436		442		429		405	475	454	449	4.1	2.2
La	171		171		161		163		175	166	169	166	3.8	4.7
Ce	327		328		305		311		333	316	321	319	3.6	5.7
Pr	35.0		34.8		32.3		33.1		35.3	33.2	34.4	34.1	3.9	8.1
Nd	115		115		106		109		118	109	113	113	4.1	8.2
Sm	19.7		19.7		18.1		18.6		20.1	18.7	19.5	19.3	4.3	8.6
Eu	3.78		3.73		3.52		3.59		3.73	3.68	3.75	3.72	3.0	5.7
Gd	14.9		15.0		13.8		14.2		15.2	14.2	14.8	15.4	7.5	11
Tb	2.37		2.36		2.21		2.29		2.43	2.27	2.37	2.45	6.2	9.9
Dy	13.5		13.6		12.7		13.2		13.9	13.1	13.7	13.8	4.2	6.9
Ho	2.74		2.74		2.59		2.68		2.81	2.66	2.76	2.75	3.1	5.2
Er	7.79		7.74		7.34		7.71		7.95	7.64	7.86	7.76	2.5	4.3
Tm	1.21		1.20		1.15		1.20		1.24	1.19	1.24	1.19	2.9	1.3
Yb	7.36		7.37		7.04		7.39		7.55	7.30	7.59	7.40	2.1	3.5
Lu	1.12		1.13		1.09		1.13		1.15	1.12	1.17	1.15	2.4	3.0
Hf	29.6		30.2		30.1		30.3		30.9	29.8	30.9	30.8	2.5	2.6
Ta	22.4		22.9		22.6		23.0		23.2	22.5	23.4	23.0	2.3	4.4
Pb	6.67		7.03						7.94	6.86	7.31	7.12	17	6.0
Th	29.5		29.7		29.2		30.0		30.3	29.1	30.5	30.4	4.0	6.8
U	9.03		8.86		8.68		9.16		9.22	9.00	9.39	9.08	3.3	6.8

All EMP analyses normalized to total 100 wt%. *n* = number of EMP analyses averaged; mean = average of dataset; RSD = relative standard deviation (1σ) of entire dataset; EAP = estimated analytical precision*. Major elements, SO_2, F, and Cl in matrix glass were analyzed with the Cameca SX-100 3-spectrometer electron microprobe (EMP) at New Mexico Tech. A 25μm beam at 15 kV and 10 nA was used to prevent volatilization of Na, S, F, and Cl. Count times = 20 sec, except S = 30 sec, F = 60 sec, Cl = 40 sec. Total Fe reported as FeO. Matrix glass for trace element analysis was lightly crushed in cloth sample bags, mafic minerals were removed using a hand magnet, and remaining crystals were removed by hand-picking under a low-power microscope. Trace elements and TiO_2 were analyzed by VG PQ ExCell quadrupole ICP-MS at Boston University following the procedures of Kelley et al. (2003).

*For EMP measurements EAP is a statistical estimate of analytical precision determined by calculating one standard deviation of 20 analyses of rhyolite glass reference material VG-568. For trace element measurements by ICP-MS, EAP was determined by performing replicate analyses on 3 samples and averaging the relative differences between the original and duplicate measurements. In this case EAP is a combination of analytical precision and matrix glass separate inhomogeneity. The precision estimates are larger than those expected by replicate analyses of standards at BU (typically < 3%), but give a more accurate appraisal of what constitutes significant variation in the data.

Table 3. Representative analyses of olivine, clinopyroxene, titanomagnetite, fluor-apatite, and pyrrhotite in tephra erupted from Erebus volcano between December 1972 and January 2004 as determined by EMP.

	Olivine		Clinopyroxene		Titano-magnetite		Fluor-apatite		Pyrrhotite	
	mean	2σ	mean	2σ	mean	2σ	mean	2σ	mean	2σ
n	*67*		*19*		*634*		*63*		*7*	
SiO_2 (wt %)	34.80	(0.43)	50.89	(0.30)			0.35	(0.10)		
TiO_2			1.35	(0.25)	24.52	(0.51)				
Al_2O_3	0.01	(0.01)	2.81	(0.12)	2.27	(0.17)				
Fe_2O_3					20.07	(0.73)				
FeO	38.33	(0.60)	9.54	(0.16)	47.80	(0.63)	0.51	(0.45)		
MnO	2.45	(0.15)	0.65	(0.03)	1.76	(0.11)	0.11	(0.05)		
MgO	23.53	(0.33)	12.23	(0.20)	2.89	(0.08)				
CaO	0.50	(0.09)	21.13	(0.33)			53.67	(0.98)		
Na_2O			0.93	(0.08)			0.12	(0.05)		
K_2O										
P_2O_5							41.07	(0.88)		
SrO										
BaO										
F							3.06	(0.43)		
Cl							0.13	(0.02)		
Mn									0.19	(0.01)
Fe									60.58	(0.26)
Cu									0.38	(0.01)
S									37.29	(0.30)
Sum							99.01			
O=F,Cl							1.32			
Total	99.67		99.53		99.30		97.70		98.44	
Fo (%)	50.7									
Fa	46.3									
Te	3.0									
Wo			46.1							
En			36.6							
Fs			17.3							
Ulvöspinel					71.5					

Mineral analyses by electron microprobe (EMP) showed no variation outside expected analytical precision (except anorthoclase*). Therefore, mean values are taken to be representative. Analytical precision estimates are based on repeat analyses except pyrrhotite which is based on counting statistics. A focused 1μm beam at 15 kV and 20nA was used, except for fluor-apatite where a 5μm beam was used. Count times = 20 sec. n = number of analyses averaged. Olivine endmembers: fayalite (Fa; Fe_2SiO_4), forsterite (Fo; Mg_2SiO_4), and tephroite (Te; Mn_2SiO_4). Clinopyroxene endmembers: wollastonite (Wo; $Ca_2Si_2O_6$), ferrosilite (Fs; Fe_2SiO_6), enstatite (En; $Mg_2Si_2O_6$). Ulvöspinel content of titanomagnetite calculated following the method of Stormer (1983).
*Discussed in section 5.6. Analytical information with Table 4.

Table 4. Representative analyses of anorthoclase feldspar in tephra erupted from Erebus volcano as determined by EMP.

	1	2	3	4	mean (n = 755)
SiO_2 (wt.%)	61.66	62.16	62.99	64.26	62.87
Al_2O_3	23.73	23.12	22.68	21.83	22.81
CaO	4.50	3.77	3.44	2.30	3.36
FeO^T	0.18	0.19	0.20	0.19	0.19
SrO	0.31	0.31	0.27	0.24	0.28
BaO	0.25	0.28	0.29	0.35	0.31
Na_2O	7.30	7.76	7.69	7.39	7.57
K_2O	2.40	2.70	2.97	4.28	3.12
Total	100.32	100.27	100.53	100.75	
Ab (%)	64.2	66.8	66.6	65.5	65.8
An	21.9	17.9	16.4	11.3	16.2
Or	13.9	15.3	17.0	24.9	17.9

The mean of all analyses (n = 755) is taken as representative of the anorthoclase solid composition and is used in models. Anorthoclase feldspar endmembers: anorthite (An; $CaAl_2Si_2O_8$), albite (Ab; $NaAlSi_3O_8$), orthoclase (Or; $KAlSi_3O_8$). A 10μm beam at 15 kV and 20nA was used. Count times = 90 sec. Based on counting statistics estimated analytical precision (2-sigma) for determinations are: SiO_2 ± 1%; Al_2O_3 ± 1%; CaO ± 2%; FeO^T ± 7%; SrO ± 7%; BaO ± 8%; Na_2O ± 2%; K_2O ± 2%.

Table 5. Modal mineralogy of bulk tephra calculated by mass-balance.

Mineral proportions (wt.%)	25724WR	2E2WR	77016WR	78325WR	25721WR	77015WR	97018WR
matrix glass	65.7	68.7	66.6	66.5	66.8	75.9	65.5
anorthoclase feldspar	31.2	28.7	30.9	30.1	30.6	21.6	30.6
titanomagnetite	1.2	1.0	0.9	0.9	0.9	0.9	1.7
olivine	0.8	0.6	0.6	1.3	0.4	0.6	1.3
clinopyroxene	0.5	0.5	0.5	0.7	0.8	0.6	0.4
fluor-apatite	0.5	0.5	0.5	0.5	0.5	0.5	0.6
Σr^2	0.05	0.09	0.09	0.02	0.14	0.12	0.08

Mineral modes calculated by major element least squares mass balance using whole rock (WR) tephra analyses from Caldwell and Kyle (1994) and Eschenbacher (sample 97018WR; 1998) and mineral compositions from Tables 2, 3, & 4. Σr^2 = sum of squares of residuals.

Table 6. Oxygen isotope ratios measured on glass and anorthoclase separated from lava and bombs erupted from Erebus volcano.

Sample ID	E86???	82416	84505	85010	Jan 2004
type	lava	bomb	bomb	bomb	bomb
eruption date	6 ± 4 ka*	Dec 1982	Dec 1984	Nov - Dec 1985	Jan 2004
$\delta^{18}O$ anorthoclase (‰)	5.92	5.73	5.77	5.86	5.71
$\delta^{18}O$ matrix glass			5.29	5.57	

Oxygen was liberated from samples by reacting them with ClF_3 at temperatures in excess of 450°C for 8 hours within a stainless steel, high vacuum extraction system. Product O_2 was converted to CO_2 by reaction with hot graphite and analyzed on a Thermo Finnigan Delta Plus XP isotope ratio mass spectrometer at New Mexico Tech. $\delta^{18}O$ values are reported in per mil (‰) notation relative to Standard Mean Ocean Water (SMOW; Craig, 1961). Based on analyses of 9 aliquots each of quartz standard NBS-28 and an in-house quartz standard (Capitan Quartz; A. Campbell, pers. comm. 2005) over 2 days the estimated analytical precision is ± 0.17‰ (1σ). All unknowns were corrected by + 0.25 ‰ based on the NBS-28 standard analyses (mean measured NBS-28 $\delta^{18}O$ = 9.39‰; reported NBS-28 $\delta^{18}O$ = 9.64‰; NIST). Replicate measurements were made of all unknowns and $\delta^{18}O$ values reported here are the mean of 2 analyses of each sample. $*^{40}Ar/^{39}Ar$ age from Kelly (Appendix F).

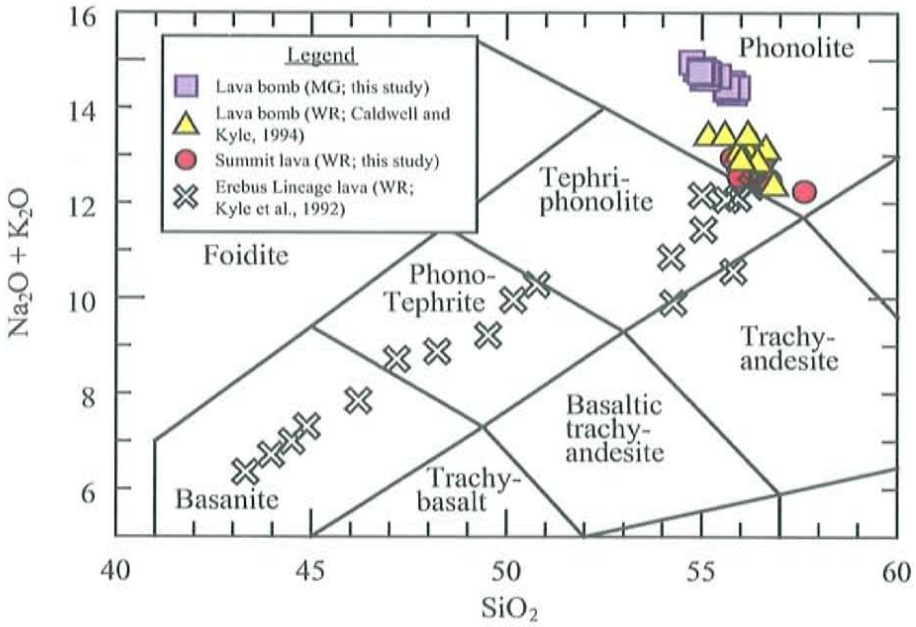

Figure 2. TAS classification (LeBas et al., 1986) of Mt. Erebus lavas and tephra. MG = matrix glass. WR = whole rock.

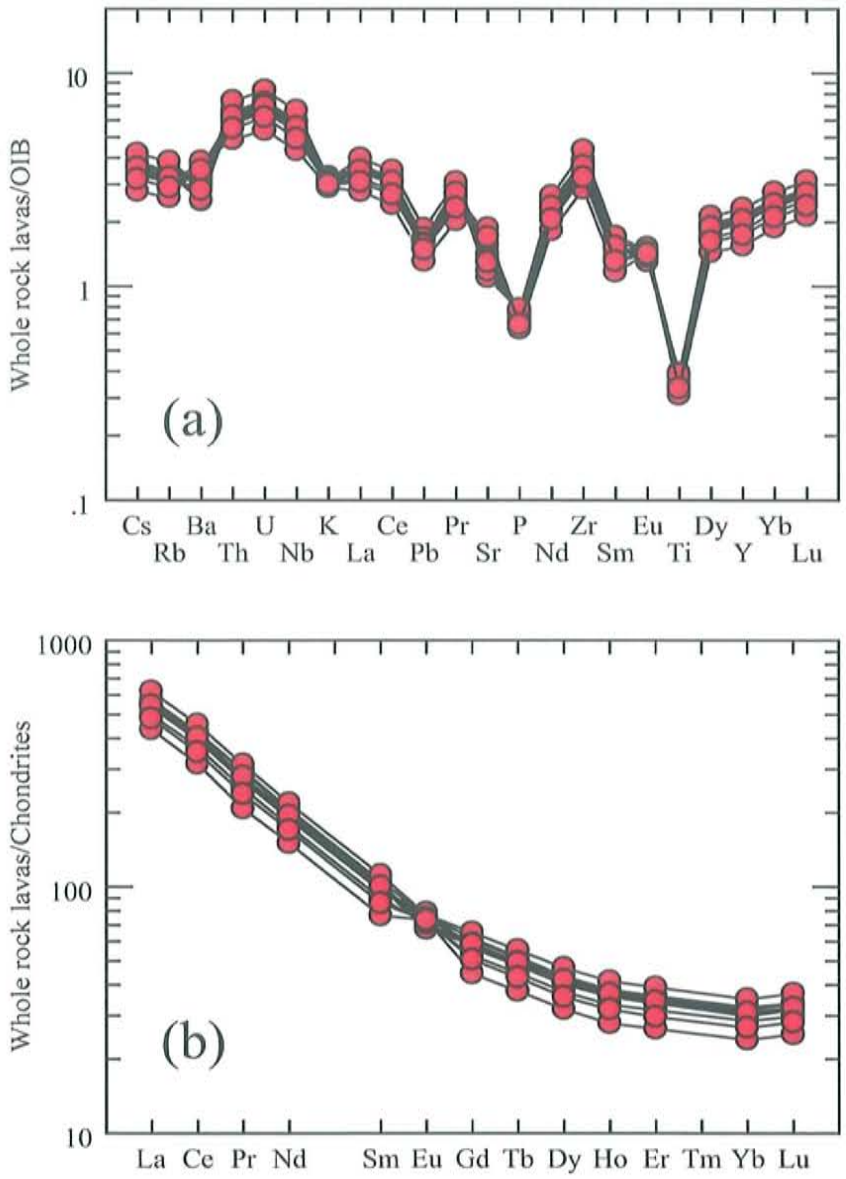

Figures 3. (a) Trace element concentrations from whole rock lava samples normalized to oceanic island basalt (OIB) (Sun and Hanson, 1989). (b) Rare earth elements (REE) from whole rock lavas normalized to chrondrites (Sun and Hanson, 1989).

such as Mn, Mg, Ca, Ti, Cr, P, and V are comparatively low due to extensive fractionation of clinopyroxene (52%), olivine (16%), Fe-Ti oxides (14%) and apatite (3%) during evolution from basanite to phonolite (Kyle et al., 1992) (Table 2 & Fig. 3a). The rare earth elements (REE) are enriched, and light REE are strongly enriched with respect to the heavy REE (La_N/Yb_N = 24.1–25.3). The REE concentrations and patterns reflect the highly differentiated nature of the samples and the importance of clinopyroxene and apatite fractionation during petrogenesis (Fig. 3b).

Some major and all trace element concentrations in the lavas show variations outside of analytical error. SiO_2, Al_2O_3, and Na_2O vary little about their mean concentrations (< 3%; 2σ, n = 11) whereas CaO and K_2O show somewhat larger variations (~ 6%; 2σ). Most trace element concentrations vary by 20-25% (2σ) about their mean values (n = 11). The largest absolute trace element variations are seen in elements that are either highly compatible or incompatible in anorthoclase feldspar. For example Sr varies from 726-1234 ppm and Zr varies from 799-1216 ppm. Samples from the same lava flow (E87020 & E87034) show compositional variations that are comparable to inter-flow variations (e.g. Zr = 1084 & 1216).

Strong correlations are observed between sets of elements that are either compatible or incompatible in anorthoclase feldspar (e.g. CaO vs. Sr, r^2 = 0.81; Sr vs. Ba, r^2 = 0.99; Zr vs. Th, r^2 = 0.99). On the other hand, plots comparing anorthoclase-compatible and incompatible elements are anti-correlated (e.g. Ba vs. Zr, r^2 = 0.51; Fig. 4). The correlations do not follow fractional crystallization differentiation trends but define mixing lines that relate to the relative accumulation or depletion (fractionation) of feldspar in each sample (Fig. 4). Accumulation of feldspar will enrich a sample in

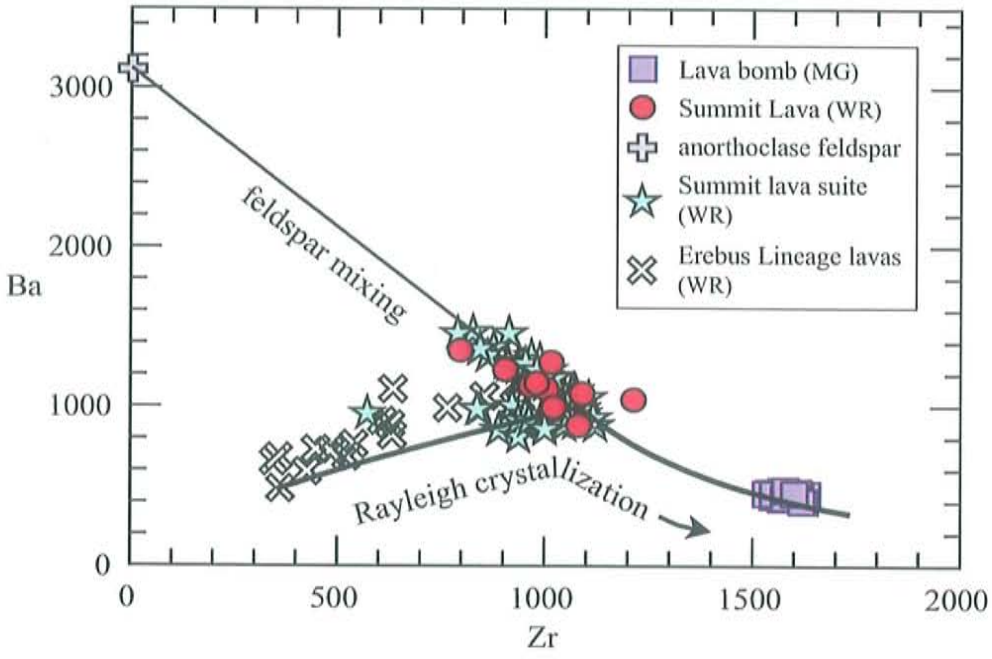

Figure 4. Rayleigh crystallization versus feldspar mixing trend. Analytical errors are approximately the same size as symbols. Note that accumulation or depletion of feldspar can explain the observed compositional variation in summit lavas from this study (red circles). Rayleigh crystallization trend calculated for two stages: (I) EL basanite 83435 to bulk phonolite using EL data (Kyle et al., 1992) and bulk lava data from this study: D_{Zr} = 0.15, D_{Ba} = 0.44; (II) bulk phonolite to matrix glass using bulk lava and matrix glass data from this study: D_{Zr} = 0.15, D_{Ba} = 3.00. Feldspar Ba composition from Table 4 and Zr from Dunbar et al. (1994). "Summit lava suite" is 97 previously unpublished analyses (P. Kyle) of lavas from Mt. Erebus summit region. Other symbols are the same as in Fig. 2.

feldspar-compatible elements (e.g. SiO_2, Al_2O_3, CaO, Sr, Ba, Eu) while diluting incompatible elements, and vice versa. This is further illustrated by chrondrite-normalized REE plots where small Eu anomalies vary inversely with other REE concentrations (Fig. 3b). There are no systematic temporal trends in lava composition.

Thus, it appears that compositional variations result from accumulation or fractionation of anorthoclase. Anorthoclase is less dense than residual melt ($\rho_{anorthoclase}$ = 2.58 g/cm^3; $\rho_{modern\ matrix\ glass}$ = 2.7 g/cm^3; Dunbar et al., 1994) which together with their large size may help facilitate physical re-distribution pre-, syn-, or post-eruption. Similar controls on lava bulk compositions have been noted at other volcanoes, for instance compositional variations in porphyritic lavas erupted between A.D. 1631 and 1944 from Vesuvius result from relative accumulation or fractionation of clinopyroxene in samples (Belkin et al., 1993). Also, some variability of lavas erupted from Kilauea relate to relative olivine content, but in that case compositional changes due to crystal accumulation and fractionation are superimposed upon source variations (Powers, 1955; Wright and Fiske, 1971; Garcia et al., 2003).

In light of these considerations, what constitutes true bulk composition of the phonolite lavas is in a strict sense unknown. However, compositions of some lava samples (e.g. E87054 & E87030) agree closely with those predicted by Rayleigh crystallization trends (Fig. 4) and are probably the best estimates of true bulk phonolite composition.

4.2 Incompatible element ratios

Most incompatible element ratios (IERs) in the lavas are very constant. For example, Zr/Rb, Zr/Th, U/Th, and Nb/Ta show less variation than expected by analytical uncertainty (< 4.2%; compound error). Some IERs are unaffected by anorthoclase content and can be used as a measure of differentiation. For example, Lu and Hf are strongly fractionated by apatite (D_{Lu} = 13.8-21.5, D_{Hf} = 0.730-0.878; Fujimaki, 1986) and Lu/Hf shows a progressive decreasing trend during magmatic evolution because the melt is saturated with respect to apatite, and apatite is fractionated at every stage of differentiation (Fig. 5). Within the 11 lava samples analyzed here Lu/Hf varies by only 3.2% about the mean (2σ), indicating they have all reached the same degree of bulk differentiation. This reinforces the point that the observed compositional variations are controlled by the physical distribution of crystals within lava flows, and not differences in parental melt composition or other genetic processes.

Isotopic ratios (Sr, Nd, Hf, Pb) indicate that Mt. Erebus lavas are derived from a HIMU-like OIB mantle source at low degrees of partial melting (Sun and Hanson, 1975; Kyle et al., 1992; Sims et al., in prep.). While there is controversy over the use of IERs in ways similar to isotopic ratios (Halliday et al., 1995; Sims and DePaolo, 1997; Hofmann, 1997), selected IERs from the phonolite lavas support this conclusion. For example Zr/Rb (10.2 ± 2.4%; 2σ) and Nb/Ta (17.3 ± 2.2%; 2σ) are very similar to average primitive OIB basalts (Zr/Rb = 9.03, Nb/Ta = 17.8; Sun and McDonough, 1989) and show little variation during differentiation (Fig. 5). On the other hand, Nb/U shows considerable variation during magmatic evolution (Fig. 5) and Nb/U ratios in evolved rocks represent FC effects rather than source or melting characteristics. This highlights

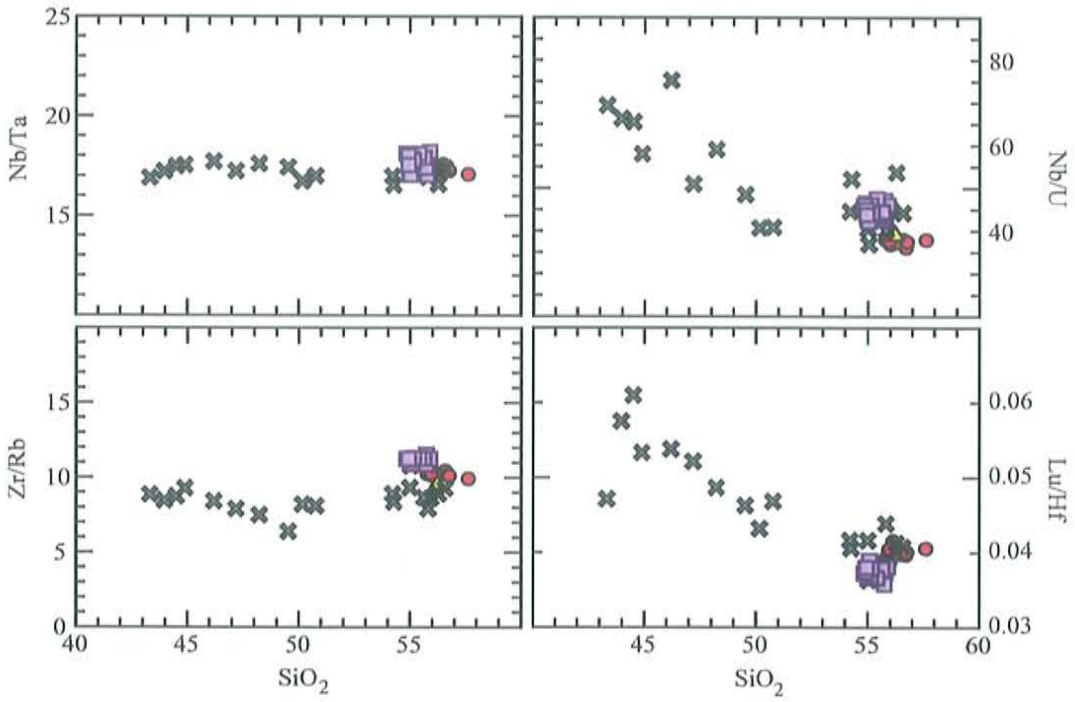

Figure 5. Selected incompatible element ratios vs. SiO_2. Symbols are the same as Figure 2.

the fundamental tenet that magmatic evolution must be well understood before IERs are used to infer source characteristics, and that radiogenic isotopes are in general a more robust tool for investigating source and melting parameters (Sims and DePaolo, 1997). More importantly, such ideal "isotope-like" behavior of some IERs in the EL reflects the relative simplicity of magmatic evolution at Mt. Erebus and should be taken as an exception rather than a rule.

4.3 Comparison of bulk lava and bulk tephra

Bulk analyses of tephra erupted between 1972 and 1986 (Caldwell and Kyle,1994) and an analysis of a bomb erupted in 1997 (Eschenbacher, 1998) show small compositional variations of the same magnitude and sense as the lavas that can be explained by anorthoclase content (Table 5). Some bulk tephra analyses have slightly higher concentrations of incompatible oxides (e.g. Na_2O) and lower concentrations of compatible oxides (e.g. FeO) than lavas but the differences are too small and inconsistent to be considered significant. Rare anorthoclase cumulates have been collected from the summit region (Moore, 1986; Kyle et al., 1992), which show that anorthoclase can be physically separated from the melt in the magma chamber, but this process is not reflected in the bulk analyses and must be relatively minor. The bulk tephra compositions are essentially indistinguishable from the bulk lavas and demonstrate that no significant change in bulk composition has occurred from ~17 ka to the present.

Finally, the bulk analyses indicate that the lavas and modern tephra achieved similar degrees of differentiation before anorthoclase were added or subtracted (Fig. 4). This implies that crystallization had proceeded to about the same point before each

eruption. Studies of other active steady state volcanoes have shown that nearly constant degrees of crystallization can be maintained over several decades (Landi et al., 2004; Streck et al., 2005), but our data suggest that Erebus has maintained a similar level of crystallization for thousands or tens of thousands of years. In order to directly test whether crystallization or any other process to modify the composition of magma in the lava lake is currently occurring, matrix glass and mineral compositions from modern bombs erupted from 1972 – 2004 were measured, and are discussed in the next section.

5. Mineralogy of tephra

5.1 Olivine

Olivine in bombs erupted between 1979 and 2004 were analyzed and recalculated into three end members: fayalite (Fa; Fe_2SiO_4), forsterite (Fo; Mg_2SiO_4), and tephroite (Te; Mn_2SiO_4) because of their high MnO content (~2.5 wt %). A representative olivine composition is given in Table 3. The olivine composition range is $Fa_{45.3\text{-}47.3}Fo_{49.6\text{-}51.9}Te_{2.8\text{-}3.2}$ with a mean composition of $Fa_{46.3}Fo_{50.7}Te_{3.0}$ (n = 67). The observed compositional variations are within limits expected due to analytical error. The crystals show no chemical zoning or significant systematic compositional variations. Our measurements are identical to olivine analyses from tephra erupted between 1972 and 1986 (Caldwell and Kyle, 1994), a 26 ± 4 ka old (Esser et al., 2004) phonolite lava (80020) (Moore, 1987), and olivine included in anorthoclase phenocrysts from older (~10's to 100's of years old) bombs scattered around the summit (Kyle,1977). There has been no significant change in olivine composition for at least 26 ± 4 ka.

5.2 Clinopyroxene

A small sample set of clinopyroxene phenocrysts from bombs erupted in 1979 and 1992, and one phenocryst of unknown age occurring as a synneusis intergrowth with anorthoclase from the summit crystal lag were analyzed. The analyses were recalculated to wollastonite (Wo; $Ca_2Si_2O_6$), ferrosilite (Fs; Fe_2SiO_6), and enstatite (En; $Mg_2Si_2O_6$) endmembers. A representative clinopyroxene composition is given in Table 3. The range of compositions ($Wo_{45.4\text{-}47.0}En_{35.0\text{-}37.7}Fs_{16.4\text{-}18.9}$) is within expected analytical uncertainty. The mean composition ($Wo_{46.1}En_{36.6}Fs_{17.3}$; n = 19) is similar to that obtained on a larger sample suite ($Wo_{47}En_{36}Fs_{17}$; n = 47) (Caldwell and Kyle,1994). The lack of Fe^{3+} and Na variation in the pyroxene crystals suggests that oxygen fugacity is constant during clinopyroxene crystallization (Caldwell and Kyle, 1994). A clinopyroxene in a 73 ± 10 ka (Esser et al., 2004) tephriphonolite lava (E83448) (Kyle et al. 1992) is similar in composition ($Wo_{45}En_{38}Fs_{17}$) to those in the tephra.

5.3 Titanomagnetite

Fe-Ti oxides reequilibrate quickly (days to weeks) to changes in temperature and oxygen fugacity under magmatic conditions (Venezky and Rutherford, 1999) and their utility in elucidating fine-scale thermal magmatic processes has been demonstrated by many studies (e.g. Nakamura, 1995; Devine et al., 2003). Caldwell and Kyle (1994) explained small (2 mol % ulvöspinel) variations in titanomagnetite compositions from Erebus tephra erupted between 1972 and 1986 as due to a 10° to 15°C progressive decrease in magmatic temperature. The result was based on a small number of analyses

(n = 64) and the authors suggested a more comprehensive study was needed to confirm their findings.

We made 624 analyses on 216 individual crystals from 32 bombs erupted between 1972 and 2003 (a representative composition is given in Table 3) including the same samples analyzed by Caldwell and Kyle (1994), and could not replicate their results. Rather, our data show titanomagnetite composition was constant from 1972 to 2003. The variations reported by Caldwell and Kyle (1994) are likely to be analytical. Furthermore, 22 rim-to-rim electron microprobe traverses across crystals ranging in size from 25μm to 400μm show no statistically significant compositional differences. Titanomagnetite grains found in matrix glass are compositionally indistinguishable from titanomagnetite inclusions in olivine, pyroxene, and anorthoclase crystals. Small (< 20 μm) crystals are also compositionally indistinguishable from larger crystals.

Finally, titanomagnetite analyses from a 26 ± 4 ka old (Esser et al., 2004) phonolite lava (80020) (Moore, 1986) agree with analyses of titanomagnetite from modern bombs. Titanomagnetite has maintained a similar composition for at least 26 ± 4 ka.

5.4 Fluor-apatite

Microphenocrysts of fluor-apatite are common as hexagonal, acicular crystals in matrix glass and also as inclusions in olivine, clinopyroxene, titanomagnetite, and anorthoclase. Analysis of crystals in tephra erupted from 1979 to 2003 occurring in groundmass and as inclusions in minerals shows fluor-apatite composition to be constant within analytical limits. A representative fluor-apatite composition is given in Table 3.

The fluor-apatites are notable for their high concentration of F (~ 3 wt %). Analyses of fluor-apatite from older lavas are not available.

5.5 Pyrrhotite

Small (< 50 μm) blebs of pyrrhotite, typically found contacting or within magnetite grains, are a very minor (< 1% mineral mode) though ubiquitous feature of tephra. Pyrrhotite analyses from phonolite lava 80200 (26 ± 4 ka; Esser et al., 2004) are indistinguishable from the analyses made on modern tephra.

5.6 Anorthoclase feldspar

Anorthoclase feldspar phenocrysts up to 10 cm in length are the most striking feature of Mt. Erebus lavas and tephra. Anorthoclase is also notable because it is the only mineral in historic tephra that shows compositional zoning (Kyle, 1977; Caldwell and Kyle, 1994; Dunbar et al., 1994). Results of EMP traverses made on 8 crystals are summarized in Figs. 6 & 7. For clarity, the major element traverse data are represented by An profiles because statistically Or is its inverse and Ab shows little variation, as discussed below. The observed compositional range in the 8 crystals is $An_{10.3\text{-}22.9}Ab_{62.8\text{-}68.1}Or_{11.4\text{-}27.2}$ (mean = $An_{16.2}Ab_{65.8}Or_{17.9}$; n = 756). An anorthoclase from lava 80020 (26 ± 4 ka; Esser et al., 2004) has a compositional range very similar to modern anorthoclase ($An_{10\text{-}18}Ab_{65\text{-}68}Or_{15\text{-}25}$; n = 5; Moore, 1986).

A single ternary feldspar is found in all tephra. The crystallization path is around the nose of the solvus (Fig. 6), which is indicative of the high temperature and very low H_2O activity in the Mt. Erebus magmatic system (Nekvasil, 1992). Compositional

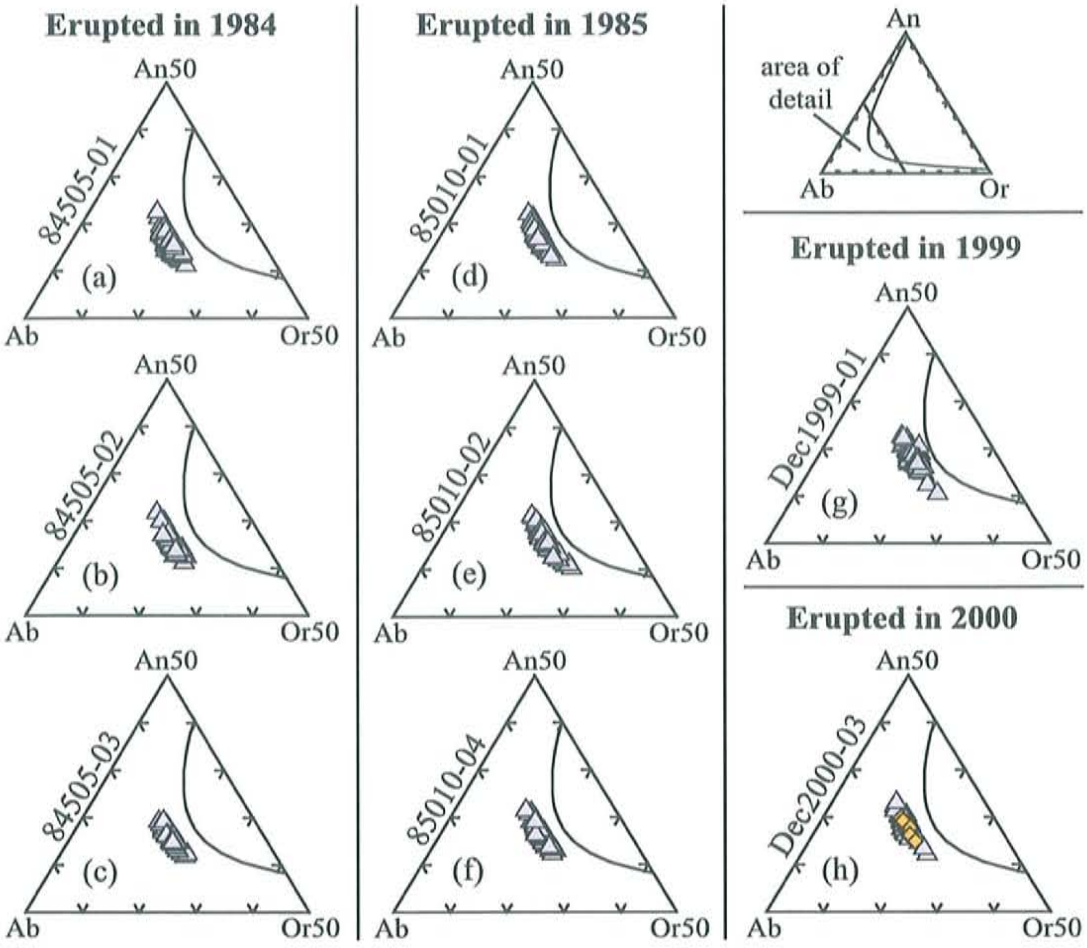

Figure 6a-h. Results of EMP traverses of eight anorthoclase crystals from bombs 84505, 85010, Dec1999, and Dec2000. An = anorthite, Ab = albite, Or = orthoclase. Isothermal solvus shown for reference calculated using the model of Elkins and Grove (1990) at 900°C and 1 bar and the computer program SOLVCALC (Wen and Nekvasil, 1994). Two traverses were made on crystal Dec2000-03 (Fig. 6h); one long traverse (triangles) and a second shorter traverse ("traverse 2"; diamonds) made parallel to and 500 μm from the first traverse. Ternary diagrams correspond to data shown in Fig. 7a-h.

Figure 7a-h. Selected major and trace element profiles of anorthoclase feldspar crystals from lava bombs erupted from Mt. Erebus volcano. X_{An} = mole fraction anorthite. Very Long Wavelength (VLW) model sine curve (λ = 5300 μm, A = 0.025 mol.) superimposed over measured X_{An} profiles. R-squared values (r^2) for X_{An} vs. BaO are shown for each crystal. Crystals were sectioned perpendicular to the c-axis and analyzed by EMP. Estimated analytical precision for X_{An} measurements (Table 4) are the same size as the symbols. BaO given in ppm with 2σ analytical precision envelope (Table 4). Average step size = 40 μm. Samples a (84505-01), b (84505-02), c (84505-03) from bomb 84505; d (85010-01), e (85010-02), f (85010-04) from bomb 85010; g (1999-01) from bomb Dec1999; h (Dec2000-03) from bomb Dec2000. Traverse "d" is a rim-to-rim traverse; all others are core to rim. Symbols for traverse "h" are the same as Fig. 6h. Analytical precision for "traverse 2" measurements are the same as other determinations but are not shown for clarity.

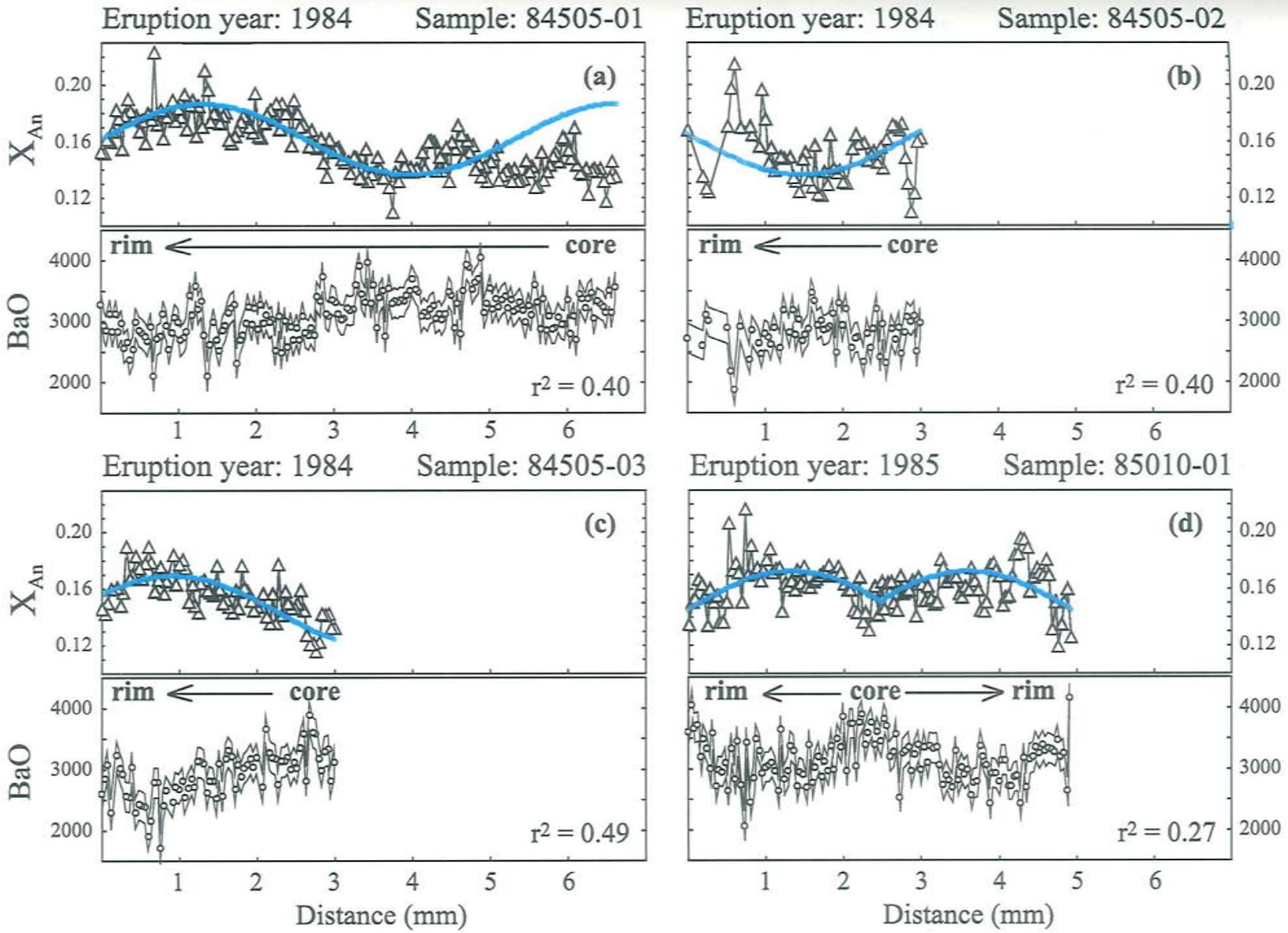
Eruption year: 1984 Sample: 84505-01
(a)
X_{An}
0.20
0.16
0.12
rim ← core
BaO
4000
3000
2000
$r^2 = 0.40$
1 2 3 4 5 6
Eruption year: 1984 Sample: 84505-02
(b)
rim ← core
$r^2 = 0.40$
Eruption year: 1984 Sample: 84505-03
(c)
rim ← core
$r^2 = 0.49$
Distance (mm)
Eruption year: 1985 Sample: 85010-01
(d)
rim ← core → rim
$r^2 = 0.27$
Distance (mm)

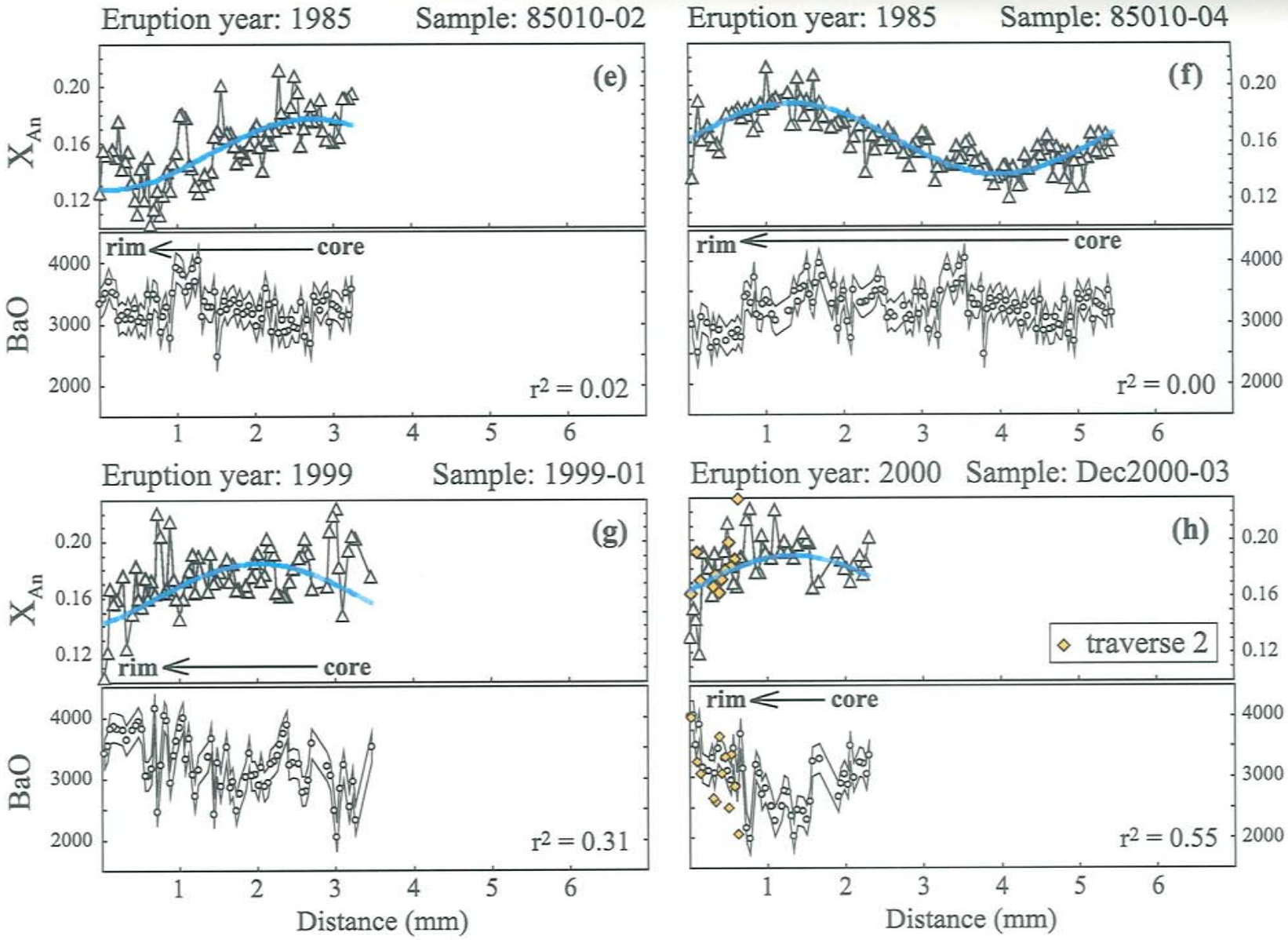
Eruption year: 1985 Sample: 85010-02
(e)
X_{An}
0.20
0.16
0.12
rim
core
BaO
4000
3000
2000
$r^2 = 0.02$
1 2 3 4 5 6
Eruption year: 1985 Sample: 85010-04
(f)
0.20
0.16
0.12
rim
core
4000
3000
2000
$r^2 = 0.00$
1 2 3 4 5 6
Eruption year: 1999 Sample: 1999-01
(g)
X_{An}
0.20
0.16
0.12
rim
core
BaO
4000
3000
2000
$r^2 = 0.31$
1 2 3 4 5 6
Distance (mm)
Eruption year: 2000 Sample: Dec2000-03
(h)
traverse 2
0.20
0.16
0.12
rim
core
4000
3000
2000
$r^2 = 0.55$
1 2 3 4 5 6
Distance (mm)

zoning in the anorthoclase is restricted to the An and Or components as Ab shows little variation. The compositional range in each crystal is similar (Figs. 6 & 7). Principle component analysis of the endmember data show that ~ 96% of the compositional variation in the crystals can be explained by the 1st principle component (PC), which is defined almost wholly by An and Or. The 2nd PC accounts for ~ 4% of the variation and is dominated by Ab. Thus, coupled inverse variations in An and Or account for ~ 96% of observed compositional variation and independent variations in Ab account for ~ 4%.

Two main types of compositional variation are observed in the crystals. The first is a sinusoidal very long wavelength (VLW) variation. The VLW variations are modeled with a sine curve with a wavelength of 5300 μm and an amplitude of 2.5 mol % An (Fig. 7). VLW variations are best exemplified by the two longest core – rim traverses (Figs. 7a & 7f). The VLW variation breaks down near the core of crystal 84505-01 (Fig. 7a), and is discussed in section 7.3.1. The same VLW variation is present in the smaller crystals, but only about half a wavelength is recorded. It is important to note that the same VLW signal is present in all the crystals, but that crystals erupted in the same bomb are not in phase and no systematic changes from year to year are apparent (Figs. 6 & 7).

Second, higher frequency (HF) variations < 1000 μm in wavelength and typically ≤ 2 mol % An in amplitude are superimposed upon the VLW signal. In rare cases An "spikes" deviate from the VLW signal by up to 7 mol %. Some periodic behavior including normal and reverse asymmetric ("sawtooth") 300 – 500 μm wavelength variations can be observed, but in general they lack the strong periodicity of the VLW signal. The shapes of other HF variations with wavelengths < 120 μm are aliased and

cannot be determined because of the relatively coarse step size of the traverses (avg. step size 40 - 45 μm).

In order to test the similarity of zoning within single crystals, a rim to rim traverse was made on crystal 85010-01 (Fig. 6d) and a short traverse ("traverse 2") was made parallel to the long traverse in crystal Dec2000-03 (Figs. 6h & 7h). The data show that HF variations are unique to each traverse whereas VLW variations are not. For example, the HF variations on the left side of 85010-01 do not match the HF variations on the right, yet the VLW variation is preserved in both sides of the crystal. This is evidence that the HF variations are driven mainly by local interactions at the crystal/melt interface on a sub-crystal scale during crystal growth and dissolution and do not relate to reservoir-scale changes in the magmatic system.

The trace elements BaO, SrO, and FeO were measured along with major elements. Analytical precision prevents detailed interpretation of the profiles, but general comments on the trends are justified. BaO shows the most variability and is anti-correlated with An in most crystals (Fig. 7). SrO is nearly constant and is decoupled from the major elements or may show weak positive correlation with An. FeO is also nearly constant or shows some minor variability that is decoupled from the other elements. There are no systematic crystal-scale trends in the TE profiles that suggest long-term changes in magma reservoir composition. However, BaO profiles in crystals erupted in 1984 are better correlated to major element compositions (Fig.7a-c) than BaO in crystals erupted in 1985 (Fig. 7d-f). The crystals erupted in 1999 and 2000 are also better correlated than the 1985 crystals (Fig. 7g-h). Given the similarity of the crystals'

major element profiles, the BaO traverses suggest intracrystalline diffusion may be affecting trace element profiles.

In summary, compositional zoning is defined mainly by variations in An and Or and the compositional range found within each crystal is similar to the total range observed in all 8 crystals. VLW compositional variations occur in each crystal, and are self-consistent within single crystals, but different crystals are not in phase. Finally, HF variations are unique to each traverse and cannot be correlated within single crystals or between different crystals and are likely controlled by local interactions at the crystal/melt interface on a sub-crystal scale during crystal growth. The origins and implications of VLW feldspar zoning are discussed in section 7.3.

5.7 Matrix glass

Matrix glass separates from tephra were analyzed to determine if any compositional changes due to injection of less differentiated magma, crystallization, or crystal fractionation had occurred from 1972 – 2004. Results are given in Table 2. Major element analyses of matrix glass by EMP show only analytical variability and the analyses are more a measure of analytical precision than compositional variations. Trace element analyses of matrix glass separates show minor variations that are greater than expected by analytical uncertainty, which is typically less than 3%. The variations are similar to those in the bulk lava analyses, where elements that are either highly anorthoclase-phyllic (e.g. Ba, Sr) or phobic (e.g Zr, Th) show the greatest variability. Replicate analyses show about as much variability as inter-sample comparisons and can be explained by a combination of analytical uncertainty and 0 – 3 wt.% contamination of

glass separates with anorthoclase. If the variations reflected real changes in glass composition due to crystallization, a slightly different but measurable compositional trend would result from crystallization of the remainder of the mineral suite. Analyses of samples Er2000 and 85010 feature the lowest Sr and Ba, and the highest Zr, and are considered the cleanest samples most representative of matrix glass composition. These samples were erupted in 1985 and 2000, which demonstrates that no measurable chemical change has occurred during this time period.

The matrix glass separates are slightly more differentiated than the bulk phonolite lavas (Fig. 8b). Major and trace element compositions are controlled mainly by anorthoclase fractionation, but continued crystallization of apatite results in depletions in the middle REE (Fig. 8a) and lower, very consistent Lu/Hf (0.0373 ± 3.53%) (Fig. 5). The consistency of IERs sensitive to differentiation demonstrates that no chemical changes have occurred from 1972-2004 (Fig. 5) and that crystallization is either progressing very slowly or perhaps not at all.

Matrix glass in tephra is modern residual melt remaining from parental basanite. Mass balance models (Table 5) indicate that matrix glass is about a 68% residual melt of bulk phonolite or about a 16% residual melt fraction of basanite assumed to be parental to the EL (DVDP-105.53; Kyle et al., 1992). As an independent check, the residual melt fraction (F) can also be calculated if an element is assumed to be perfectly incompatible using the Rayleigh distillation equation (Wilson, 1989):

$$C_L/C^0_L = F^{(D-1)}$$

where C^0_L is the original concentration, C_L is the final concentration, and D is the

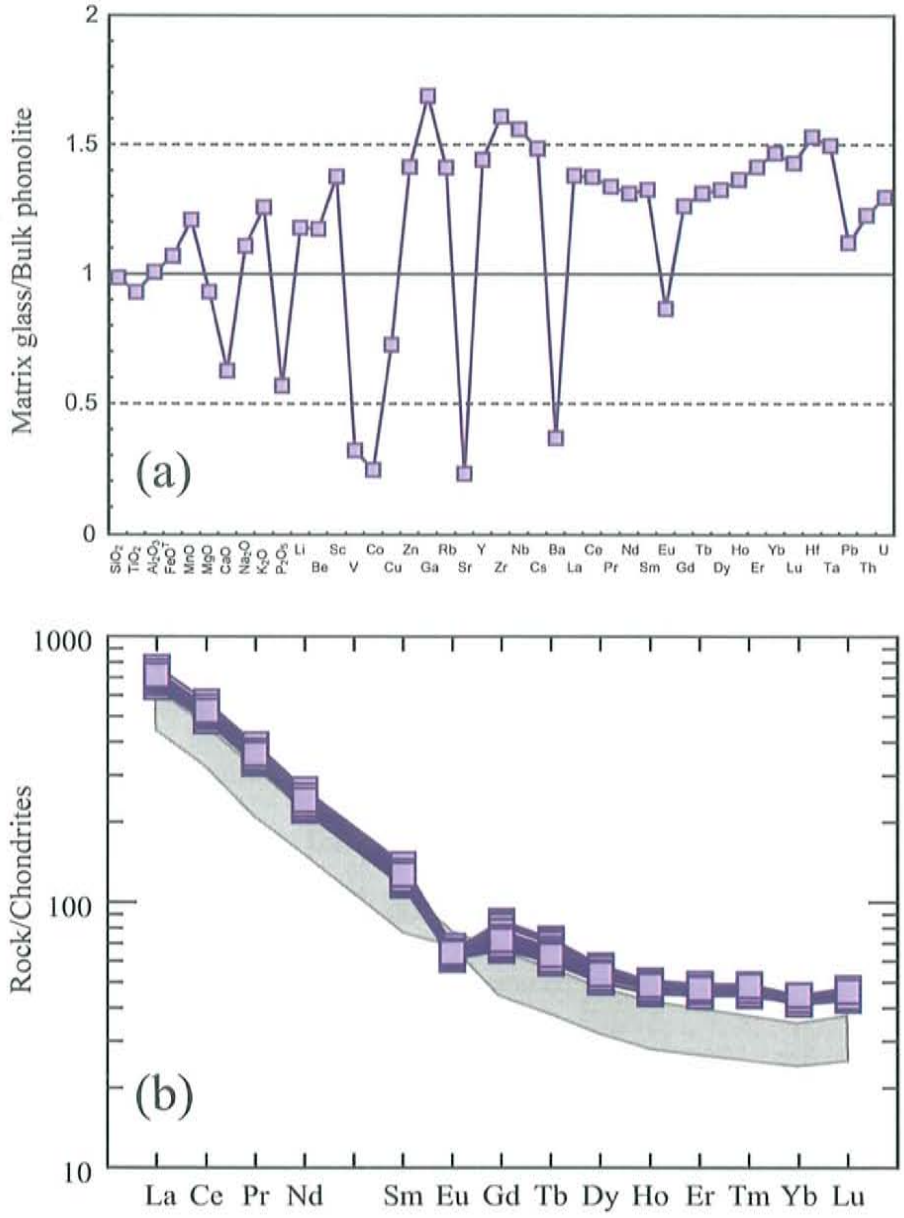

Figure 8a,b. (a) Representative matrix glass composition of tephra normalized against bulk phonolite composition. Note depletions in Ca, Sr, Ba, and Eu due to anorthoclase crystallization. Fe-Ti oxide crystallization depletes TiO_2, V, and Co. Crystallization of small amounts of apatite lead to strong depletions in P_2O_5, Lu relative to Hf, and overall depletion of middle rare earth elements (REE). (b) REE concentrations of matrix glass from tephra normalized to chrondrites (Sun and McDonough, 1989). Gray field represents range of bulk phonolite lava analyses. Note the negative Eu anomaly due to anorthoclase crystallization and general enrichment of REE in matrix glass.

partition coefficient because as $D \rightarrow 0$, C_L/C^0_L approaches 1/F. Uranium in modern matrix glass (C_L) is enriched by a factor of 7.6 over basanite taken to be parental for the EL (C^0_L; sample DVDP-105.53; [U] = 1.2 ppm; Kyle et al., 1992), which yields a residual melt fraction of 13% and is in good agreement with the mass balance models.

6. Intensive parameters and silica activity

Several independent empirical and experimental approaches have demonstrated that a T of 1000°C is a reasonable magmatic temperature for the lava lake (optical pyrometer, mineral thermometer, Kyle, 1977; melt inclusion homogenization, Dunbar et al., 1994; olivine-cpx thermometry, Caldwell and Kyle, 1994; Forward Looking InfraRed (FLIR), Calkins, in prep.). Using the olivine, titanomagnetite, and clinopyroxene data from Table 3, a temperature of 1000°C and pressure of 1 bar, the QUILF computer program (Anderson et al., 1993) returns an fO_2 of -11.86 ± 0.03 (ΔlogFMQ -0.88 ± 0.03) (Fig. 9) and a silica activity 0.461 ± 0.007 for magma in the lava lake. The presence of pyrrhotite in the tephra is consistent with reducing conditions.

7. Crystallization processes and magma chamber dynamics

A silicate melt may become supersaturated and crystallize in response to cooling or if the concentration of one of its components changes. Both of these factors could impose some control on crystallization and crystal composition at Mt. Erebus because magma cools as well as degasses at and near the lava lake surface. Magma that forms the crust of the lava lake is quickly cooled from ~1000°C to 500 - 600°C (Calkins, in prep.) before it is recycled back into the magma conduit and assimilated back into the melt.

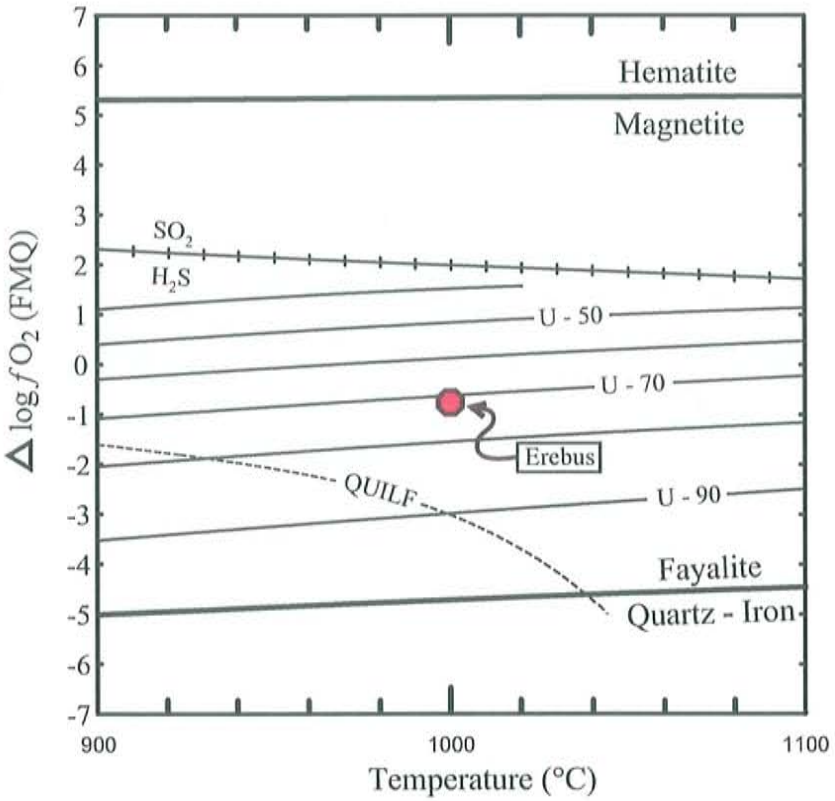

Figure 9. Oxygen fugacity relative to fayalite-magnetite-quartz buffer (FMQ) for magma in Mt. Erebus lava lake. Result given by QUILF computer program (Anderson et al., 1993) at T = 1000°C and P = 1 bar and the mineral assemblage olivine-magnetite-quartz-augite (values from Tables 2 & 3; symbol is larger than calculated errors). Ülvospinel and QUILF oxygen buffer curves reproduced after Anderson and Lindsley (1988). Fayalite-magnetite-quartz (FMQ), hematite–magnetite (HM) and quartz-iron-fayalite (QIF) buffer curves after Frost et al. (1988). SO_2–H_2S gas buffer curves from Goff et al. (2001).

Degassing decreases the concentrations of volatiles in the melt, notably water. Water has profound effects on many aspects of crystallization (e.g. Tuttle and Bowen, 1958). Anorthoclase is the dominant precipitating phase (~90 wt.% solid fraction; Table 5) and textural relationships indicate that it is the last major mineral phase to crystallize. Compositional zoning and low volatile contents of melt inclusions in anorthoclase suggest that they form in a dynamic environment shallow in the system (i.e. < 400 m; Dunbar et al., 1994; Eschenbacher, 1998; Seaman et al., 2006). Zoning in crystals, especially feldspar, has long been the subject of study because it is easily observable and offers potential for revealing the dynamics of magmatic processes. This is because feldspar compositions are sensitive to melt composition, pressure (P), temperature (T), and the concentration or partial pressure of water (P_{H_2O}) (e.g. Tuttle and Bowen, 1958; Pearce, 1994). For these reasons crystals are often viewed as Lagrangian particles that trace and record information about conditions within the magmatic system as they form (e.g Wallace and Bergantz, 2005). Their compositional profiles are treated as time-series and are interpreted in terms of dynamic processes thought to occur in magma chambers (magma recharge, differentiation, convection, changes in T, P_{H_2O} etc.)(e.g. Pearce, 1994).

First we conceptually take into account the effects cooling can have on crystallization and crystal composition versus changes in P_{H_2O} due to shallow degassing. Then we set about interpreting zoning in the anorthoclase in terms of magma dynamics. In the following discussion changes in P are not considered because P exerts small control on the composition of feldspar and the anorthoclase likely experience a limited P range (< 100 MPa). Strict changes in P are not likely to influence the composition of the anorthoclase inasmuch as intensive properties and P_{H_2O} vary with depth in the conduit.

7.1 Cooling-induced crystallization

Titanomagnetite compositions indicate that the temperature of the upper magmatic system is stable. However, large T changes are clearly occurring at the lake surface that are not reflected in magnetite compositions. This is probably because at lower pressure magnetite crystals take longer to reequilibrate to new T conditions (i.e. ~several weeks; Venezky and Rutherford, 1999), and cooled crust is rarely at the surface of the lava lake for more than 10 – 20 minutes before it sinks back into the conduit. Beneath the relatively thin crust (~1 m), magma cools little and is ~950 – 1000°C (Calkins, in prep.). Therefore, if cooling is driving crystallization it would most likely occur as the cold degassed slab sinks into the conduit and is reheated.

The effects of T on feldspar compositions are relatively well understood (e.g. Johannes, 1978; Loomis and Welber, 1982; Housh and Luhr, 1991) and experiments on plagioclase indicate that the slope of the solidus is around 1 mol.% An/5°C for intermediate compositions (Housh and Luhr, 1991). Assuming anorthoclase behave in roughly the same manner as plagioclase, we would expect large An variations in the anorthoclase because the temperature variations involved are very large. This is not the case; the total range of An variation observed is only 13 mol. %. Furthermore, if supercooling and large T variations were controlling crystallization, kinetic effects would influence crystal and MI compositions (Kirkpatrick, 1981; Cashman, 1990) because at such extreme degrees of undercooling melt viscosity would increase dramatically and replenishment of elements to the crystal/melt interface would be impeded. High crystal growth rates would further compound the effect and lead to the formation of a compositional boundary layer around the crystals (Marsh, 1989). Boundary layers are

not observed in quenched samples and the compositions of melt inclusions trapped during crystal growth show very small variations when compared to matrix glass (Kyle, 1977; Dunbar et al., 1994). This indicates that crystal growth rates are either less than or about equal to elemental diffusion rates in the melt, which implies large degrees of undercooling are not driving crystal growth.

Finally, at undercoolings on the order of 500°C the solvus would be intersected and a two-feldspar assemblage would precipitate. Rare sanidine overgrowths and microlites are found in older lavas from the flanks of Mt. Erebus (Moore, 1986; Kyle et al., 1992) but these probably formed as the lavas cooled after eruption. Quenched lava bombs provide no evidence that a two-feldspar assemblage has ever precipitated in the magma chamber. Therefore, while cooling is undisputedly occurring at the surface of the lava lake, it is not considered an important control on crystallization and hence crystal composition.

7.2 Degassing-induced crystallization

Decompression-induced crystallization is an old idea (Tuttle and Bowen, 1958) that has recently received attention from experimental petrologists (Geschwind and Rutherford, 1995; Hammer and Rutherford, 2002; Couch, 2003; Couch et al., 2003a,b). It has become recognized that syn-eruptive degassing and crystallization is a common phenomenon in shallow volcanic systems that can have important implications for eruption dynamics (e.g. Klug and Cashman, 1994; Hammer et al., 1999; Cashman and Blundy, 2000). Furthermore, the experimental studies have demonstrated that

information about the magnitude and history of decompression can be recorded in groundmass textures.

Water is very soluble in silicate melts, but ascent and decompression to low pressure will cause water to saturate and exsolve. Exsolution of water in turn raises the liquidus temperature and can drive groundmass microlite crystallization (Geschwind and Rutherford, 1995; Metrich and Rutherford, 1998; Hammer et al., 1999; Hammer et al., 2000), assuming there is sufficient time for crystallization to occur (Cashman and Blundy, 2000). The difference between the magmatic temperature and the (new) liquidus temperature that results from degassing is called the effective undercooling (ΔT_{eff}). Since the change in the liquidus drives crystallization there need be no actual change in temperature for crystallization to proceed. Indeed, the latent heat of crystallization can balance the heat lost from volatile exsolution and the entire process can be isothermal or nearly isothermal (Métrich and Rutherford, 1998; Couch et al., 2003a). Experimental studies have shown that high degrees of ΔT_{eff} lead to large numbers of microlite nucleation per unit area (N_A) and result in dense populations of small crystals (Hammer and Rutherford, 2002; Couch, 2003; Couch et al., 2003a; Couch et al., 2003b; Larsen, 2005). Conversely, lower degrees of ΔT_{eff} results in low N_A and fewer numbers of larger crystals. These two extremes are referred to as "nucleation dominated" and "growth dominated" regimes. In both cases the total mass crystallized can be similar, but in nucleation dominated cases the mass is spread over many sites growing at a slow rate and in growth dominated cases the mass is crystallized on few sites at a faster rate (Larsen, 2005).

Anorthoclase in historic tephra are large (up to 10 cm), crystal size distributions show that nucleation sites are extremely scarce ($N_A \approx 0$), and matrix glass is essentially microlite free (Dunbar et al., 1994). Nucleation sites are so scarce that titanomagnetite, olivine, clinopyroxene, and apatite crystals are commonly found as inclusions in anorthoclase and may serve as nucleation sites for some anorthoclase crystals (Kyle personal communication, 2006). The microlite-free matrix glass texture in tephra is consistent with growth dominated anorthoclase crystallization at low degrees of ΔT_{eff} (Hammer and Rutherford, 2002; Larsen, 2005). Low degrees of undercooling imply that relatively small amounts of water are exsolved from the melt as it ascends, degasses, and sinks back into the conduit. This is consistent with water contents in matrix glass and melt inclusions in anorthoclase which are similar and low (< 0.4 wt.%) (Dunbar et al., 1994; Eschenbacher, 1998; Seaman et al., 2006). Large amounts of water are not available to exsolve and drive the system to more extreme degrees of effective undercooling. The small compositional range of the anorthoclase and lack of disequilibrium textures in other minerals are consistent with small degrees of undercooling and fairly subtle changes in conditions during crystallization. However, unlike microlites that form during a single episode of ascent and eruption, there is abundant textural and chemical evidence to suggest that Erebus anorthoclase experience multiple episodes of decompression and rim growth during shallow convection in the lava lake (Dunbar et al., 1994; discussed in next section), which promotes the growth of large crystals. Ostwald ripening (e.g. Higgins, 1998), where small crystals dissolve and transfer their mass to larger ones, is sometimes invoked to explain the presence of very

large crystals but continuous CSD's (Dunbar et al., 1994) argue against this being an important process in the lava lake.

In summary, a model of crystallization driven by shallow exsolution of water is preferred over a cooling model. Isothermal decompression-induced crystallization is in accord with the homogeneous titanomagnetite compositions, the relatively subtle compositional zoning in the anorthoclase, and the microlite free matrix glass texture. The combination of a growth dominated crystallization regime controlled by shallow water exsolution and multiple episodes of crystallization due to shallow convection in the lava lake results in the extremely large anorthoclase crystals.

7.3 Anorthoclase zoning and magma chamber dynamics

7.3.1 Very Long Wavelength (VLW) variations

The strong periodicity of the VLW variation argues against reservoir-scale changes in bulk composition being a factor, and MI compositions, and TE profiles dismiss kinetic effects as an important consideration. Therefore the most likely explanation is that individual crystals record regular movement (convection) through either a P_{H2O} or T gradient over a relatively long period of time (100's – 1000's years; discussed below). Decreasing P_{H2O} and/or T will lead to decreases in An and increases in Or, and vice versa. While T variations on a century to millennial timescale would allow ample time for titanomagnetite to reequilibrate to new conditions, the homogeneity of the crystals within anorthoclase and other crystals and the lack of exsolution lamellae or other disequilibrium features suggest that T is fairly constant within the chamber. Furthermore, water concentrations in MI in anorthoclase are variable (0.12 wt.% - 0.39

wt.%; Seaman et al., 2006) and provide evidence for crystallization in an environment with variable P_{H2O}.

Dunbar et al., (1994) proposed a 2-stage growth process based on MI morphology and crystal compositions: (1) crystals undergo a rapid period of growth followed by; (2) convection and multiple episodes of rim growth and dissolution. They cited a distinct textural and compositional core/rim break as evidence for the 2-stage process. While we do not find evidence for this process in all the crystals, it can explain the compositional profile of 84505-01. We interpret the profile as representing initial rapid growth under fairly constant P_{H2O} conditions, possibly near a wall of the chamber, before being swept into a convection current in the magma chamber where it continued crystallizing while convection transported the crystal through a P_{H2O} gradient in the conduit.

A puzzling aspect of the VLW variation is that Normarski images and HF sawtooth zoning show evidence for resorption surfaces (Dunbar et al., 1994) and provide evidence that crystallization is episodic and marked by periods of dissolution, yet the VLW signal is preserved in all the crystals. This implies that the VLW signal is inherently aliased, but that the net growth rate and "sampling frequency" of the crystals are the same and that convection and degassing are extremely stable. If a constant growth rate of 1×10^{-10} (cm/s) with no resorption is assumed, anorthoclase 84505-01 would take about 220 years to form and one VLW (convective) cycle (5300 μm) would take about 170 years to complete. In reality, growth is likely episodic and followed by periods of no growth or resorption (Dunbar et al., 1994), and total crystallization and residence times are apt to be longer than times calculated under these unrealistic simplifying assumptions. Also, since the VLW signal is aliased and represents some

fraction of the true signal, convective timescales calculated based on its wavelength would be underestimates. Intracrystalline diffusion modeling (e.g. Morgan and Blake, 2006) has potential to better constrain anorthoclase residence times and crystallization timescales, and should be pursued in the future.

7.3.2 High Frequency (HF) variations

Many HF zones that show semi-continuous to continuous progressive An compositional changes are ~300 – 500 μm wide, which is in agreement with zoning widths observed in Normarski images of anorthoclase (e.g. 3.5 – 5 mm; Fig. 7d)(Dunbar et al., 1994). At a growth rate of 1×10^{-10} (cm/s), a 300 μm zone would grow in ~10 years. This precludes compositional changes being T-driven because titanomagnetite compositions would have ample time to reequilibrate to new T conditions. Therefore, the most plausible explanation is that small local changes in P_{H2O} are also responsible for HF zoning.

HF zoning types that can be resolved include normally zoned asymmetric (sawtooth) zones 200 – 500 μm wide (e.g. 1 – 3 mm; Fig. 7g) and quasi-periodic zoning with variable wavelengths (e.g. 2.2 – 3 mm; Fig. 7b & 4.5 – 5.1 mm; Fig. 7a). Since HF zoning is non-unique on a single-crystal scale and superimposed upon the VLW variation, it implies that flow in the conduit is irregular and that small-scale convective cells may operate within larger reservoir-scale cells.

8. Oxygen isotope geochemistry

Oxygen isotope measurements on anorthoclase and matrix glass mineral separates are very consistent and show no significant variation at the 1σ level. Anorthoclase feldspar phenocrysts from tephra samples and one prehistoric lava 6 ± 4 ka in age (Appendix F) have higher $\delta^{18}O$ than the matrix glass by ~0.2 ‰, as predicted by equilibrium isotope fractionation models (Fig. 9) (Zhao and Zheng, 2003). The O-isotope data suggest that the feldspars crystallized under equilibrium conditions from phonolite melt that has had a constant $\delta^{18}O$ composition of ~ 5.5 ‰ for at least 6 ± 4 ka.

Fractional crystallization can lead to small (~1 ‰), predictable changes in the stable isotope composition of evolving melts (Taylor & Sheppard, 1986). A forward model of oxygen isotope changes in melt due to Rayleigh crystallization (Fig. 10) predicts $\delta^{18}O$ enrichment of 1.1‰ in the most evolved melt (modern matrix glass; $F \approx 0.16$). The model result is comparable to $\delta^{18}O$ enrichments observed in other systems thought to have evolved primarily by high degrees of fractional crystallization (Matsuhisa, 1979; Muehlenbachs and Byerly, 1982; Sheppard and Harris, 1985; Wade et al, 2005). The oxygen isotope measurements are lower than predicted fractional crystallization model values by 0.64 ‰ to 1.26 ‰, taking into account analytical uncertainty (1σ), and yield primitive mantle-like values.

The observed $^{18}O/^{16}O$ ratios in the samples could be a singular or combined result of several factors: a mantle source with a very low $\delta^{18}O$ composition (i.e. ~ 4.1 to 4.6 ‰), post-eruption alteration, contamination of mineral separates with phenocrysts, addition of meteoric water in the magma chamber, or volatile exsolution (degassing). A global

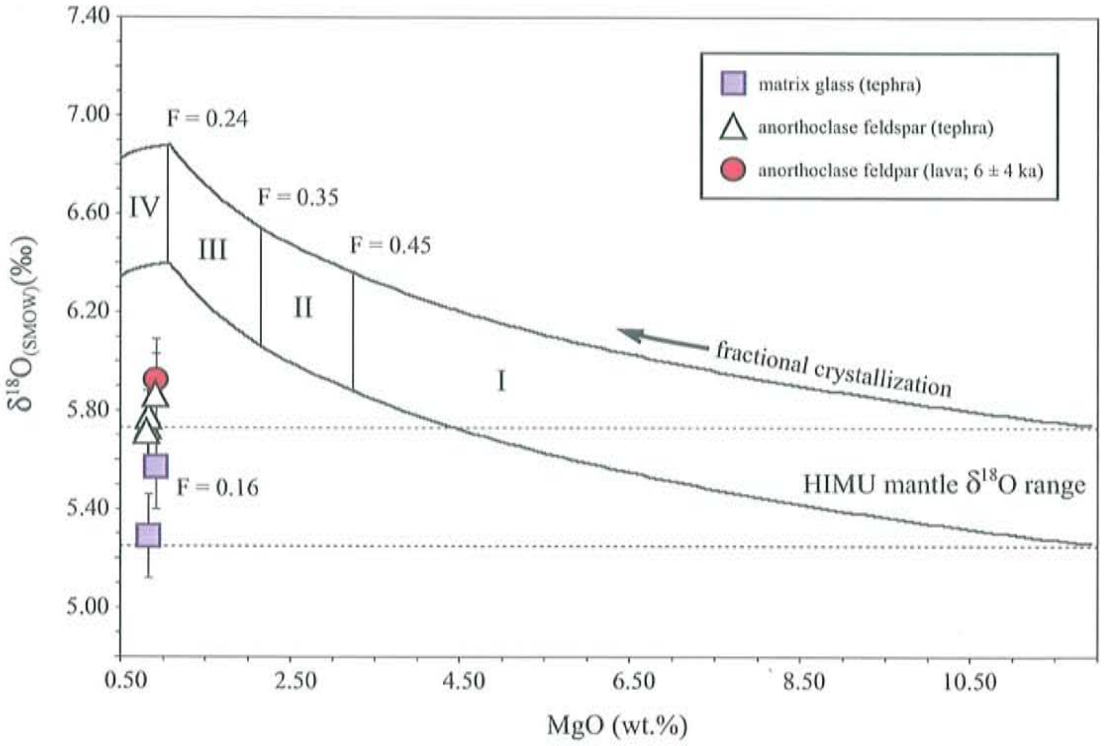

Figure 10. Forward model of $\delta^{18}O$ variation in melt due to fractionational crystallization during evolution from basanite to phonolite following the approach of Wade et al. (2005). Measured $\delta^{18}O$ in matrix glass and anorthoclase crystals from bombs and one older (6 ± 4 ka; Appendix F) anorthoclase crystal shown with 1σ errors (Table 6). X-axis errors are smaller than symbols. "F" is residual melt fraction of basanite assumed to be parental to EL (Kyle et al., 1992; this study). Initial $\delta^{18}O$ values are the range of HIMU mantle melt compositions presented by Eiler (2001). Equilibrium oxygen distribution between minerals and melt was modeled in four stages: (I) basanite→phonotephrite (II) phonotephrite→tephriphonolite (III) tephriphonolite→phonolite (IV) phonolite→ modern matrix glass. Mineral proportions and compositions from least-squares mass balance models of Kyle et al (1992; stages I - III) and this study (Tables 3, 4, 5; stage IV). Mineral-melt fractionation factors are from those summarized in Eiler (2001) and from Zhao and Zheng (2003) at 1200°C (Stage I), 1150°C (Stage II), 1100°C (Stage III), and 1000°C (Stage IV). Predicted anorthoclase – trachyandesite melt fractionation (1000lnα) at 1000°C is ~0.17‰ using fractionation factors of Zhao and Zheng (2003).

compilation of $\delta^{18}O$ compositions of melt derived from HIMU mantle sources shows a range from 5.25 to 5.73‰ (Eiler, 2001). Based on our data we cannot rule out the Erebus mantle source having a low $\delta^{18}O$ signature, but mantle with such a low oxygen isotopic composition has not been observed and it seems an unlikely explanation of the data. The samples are fresh and unaltered. Significant contamination of the matrix glass separates by isotopically light minerals (i.e. titanomagnetite) is also not probable based on trace element determinations performed on aliquots taken from the same bulk glass separates (Table 2). Age spectra from step-heating anorthoclase for $^{40}Ar/^{39}Ar$ age-determinations prepared in the same way as the anorthoclase analyzed here for $\delta^{18}O$ show that the mineral separates are greater than 99 % pure (Appendix F). Addition of meteoric water into the magma chamber is extremely doubtful because most water is frozen at Mt. Erebus and there is no known hydrothermal system on the mountain.

While it is generally recognized that degassing can deplete magma of ^{18}O, the range of depletions normally ascribed to this process is small, with depletions on the order of 0.2 ‰ to 0.3 ‰ considered extreme (Eiler, 2001). The reason for this is that models of degassing require large amounts (several wt.%) of volatiles to drive ^{18}O depletion (Eiler, 2001). If H_2O and CO_2 act as perfectly incompatible elements during magmatic evolution from basanite to the most evolved phonolite liquid ($F \approx 0.16$), we would expect ~10 wt.% H_2O and ~4 wt.% CO_2 to be degassed from the phonolite (Eschenbacher, 1998), which would yield only about a 0.3 ‰ depletion in ^{18}O. Even in water-rich arc volcanoes H_2O contents above 8 wt.% are rarely reported (Wallace, 2005), yet our data and other studies (e.g. Wade et al., 2005) suggest that in some cases $\delta^{18}O$ depletions on the order of ~0.5 ‰ or greater may be possible due to degassing, even

though they appear to require unreasonable amounts of volatiles. Many studies have shown that measured volatile fluxes are often many times or even an order of magnitude greater than those expected by petrologic estimates based on concentrations of pre-eruptive volatile contents in magmas (e.g. Rose et al, 1982; Andres et al., 1991; Allard et al., 1994; Eschenbacher, 1998). The "excess sulfur" or more aptly termed "excess volatile" mass-balance problem is well documented for many volcanoes of different eruptive styles (Rose et al., 1982; Andres et al., 1991; Westrich and Gerlach, 1992; Gerlach and McGee, 1994; Allard et al., 1994; Kazahaya et al., 1994; Allard, 1997; D'Alessandro et al., 1997; Eschenbacher, 1998; Wallace, 2005), and is especially pronounced in persistently degassing open-conduit systems like Erebus, Masaya, and Stromboli (Wallace, 2005). Eschenbacher (1998) calculated that if the phonolite at Erebus were producing the large observed CO_2 flux, it would have to contain ~50 wt.% CO_2, which is clearly not the case. Thus, it is reasonable to infer that CO_2 is saturating and exsolving from a deeper source within the magmatic system, possibly as deep as the mantle (Eschenbacher, 1998). These deep volatiles could play a larger than expected role in determining the oxygen-isotope composition of highly evolved melt and minerals at Mt. Erebus, as described below.

For example, if an infinite amount of CO_2 with a mantle-like $\delta^{18}O$ signature (e.g. 5.5 ‰) reached a single volume of evolved magma with $\delta^{18}O = 6.5$ ‰, partially or fully equilibrated and then degassed, the evolved magma would eventually come into equilibrium with the deep volatile phase and the effects of FC would be erased. Mass balance requires that if the phonolite magma degassed all of its H_2O and CO_2 resulting in a 0.3 ‰ $\delta^{18}O$ depletion, a minimum additional ~20 wt.% CO_2 would be needed to drive a

further 0.7 ‰ depletion. Once the upper level magma came into equilibrium with the deep volatile phase, no further $\delta^{18}O$ depletion would occur. This is not an unreasonable scenario because CO_2 saturates at ~300 to 400 MPa pressure (Eschenbacher, 1998) and the Mt. Erebus magma system is clearly very large, stable, long-lived, and CO_2 rich (Wardell et al., 2003, 2004).

9. Comparison with other persistently active volcanoes

Volcanoes that exhibit persistent activity are rare, and among those only a handful feature active lava lakes comparable to Mt. Erebus. Examples of persistently active volcanoes with petrologically well-studied eruption products include Stromboli, Italy (e.g. Francalanci et al., 2004; Cortés et al., 2005), Kilauea, Hawai'i (e.g. Garcia et al., 2003), and Arenal, Costa Rica (e.g. Reagan et al., 1986; Streck et al., 2004). Lava lakes have been observed at Kilauea in the last 200 years (e.g Tilling, 1987; Garcia et al., 2003) and other volcanoes with active lava lakes include Erta 'Ale, Ethiopia (e.g. Le Guern et al., 1979; Oppenheimer et al., 2004), Nyiragongo, Democratic Republic of Congo (e.g. Tazieff, 1984), Masaya, Nicaragua (e.g. Stoiber et al., 1986) and Villarrica, Chile (Witter et al., 2004).

The bulk composition of lava and tephra erupted from Mt. Erebus has not changed in ~17 ka and mineral compositions have also been nearly invariant. Bulk major and trace element compositions of material erupted from Stromboli and Kilauea have shown small variations in the last 100 – 200 years (Francalanci et al., 2004; Garcia et al., 2003), and much larger changes have occurred at Stromboli in the last 26 ka (Cortés et al., 2005). In both cases, multiple magma compositions, mixing, and complex

crystallization and differentiation histories have been invoked to explain small observed short (days) and long-term (ky's) compositional variations. Temporal chemical changes at volcanoes have been exploited to infer important parameters like residence time (Albarède, 1993) and mixing rates (Reagan et al., 1986), but at Mt. Erebus these approaches fail due to the extreme homogeneity of its lava and tephra. Eruption products from these classic persistently active volcanoes show greater bulk chemical, mineralogical, and isotopic variability than lavas and tephra erupted from Mt. Erebus in the last ~17 ka.

Arenal volcano has been continuously erupting since 1968, and there has been very little bulk compositional variation since 1970 (Streck et al., 2005). However, Streck et al.'s detailed mineralogic study of the seemingly "monotonous" lavas erupted since 1970 reveal the complex and diverse growth and mixing histories of the crystal assemblage. This contrasts with the "indolent" mineral assemblage found in lavas and tephra from Mt. Erebus which have not changed in composition for at least ~26 ka. The extreme homogeneity of the crystals, lack of disequilibrium features, and MI and oxygen isotope data indicate that the minerals found in lavas and tephra grew from magma with the composition of bulk phonolite. Unlike samples from Arenal, there is no evidence to suggest the crystals are xenocrystic in origin. Thus the differentiation process that creates the bulk phonolite composition at Mt. Erebus is older than the crystals found in the lavas and tephra.

It has been proposed that activity at persistently active volcanoes like Kilauea, Stromboli, and Arenal is sustained by a constant supply of fresh mantle-derived magma to upper levels of the volcanic system (e.g. Francis et al., 1993; Garcia et al., 2003;

Francalanci et al., 2004; Streck et al., 2005). There is no evidence to suggest this is the case at Mt. Erebus. While the lava lake has been constantly degassing, the net exogenous growth from 1972 to the present has been effectively zero, and campaign GPS surveys over the last five years show no evidence for endogenous growth of the volcanic edifice due to magma injection (P. Kyle, personal communication, 2006). Instead, observations over the last 30+ years indicate that lava lake activity at Mt. Erebus is sustained by convective exchange of magma from a deeper reservoir to the surface via an open conduit (Fig. 11) (e.g. Stevenson and Blake, 1998; Harris et al., 1999). Lava lakes at Erta 'Ale (Oppenheimer et al., 2004) and Villarrica (Witter et al., 2004) are thought to be sustained in the same way.

While it appears that the upper level magmatic system at Mt. Erebus is closed to continuous input of new magma, gas flux measurements and melt inclusion and oxygen isotope data suggest that volatiles are added to the upper level magma chamber from deeper in the system (Eschenbacher, 1998; Wardell et al., 2004), possibly on a continuous basis. Decoupled movement of volatiles and magma has been inferred to occur at many volcanoes (e.g. Stromboli, Allard et al., 1994; Mount Etna, D'Alessandro et al., 1997). If this is the case at Mt. Erebus, variations in the flux of volatiles from deep in the system may play a role in driving eruptive activity. It follows that the heightened eruptive activity observed in late-1984 could have been triggered by an episodic addition of a large amount of volatiles without concomitant addition of magma. On the other hand, it has also been proposed that physical changes in the conduit are responsible for the formation of the large gas slugs that result in strombolian eruptions (Aster et al., 2003; Grêt et al., 2005). Both processes may be important, and ongoing integrated gas

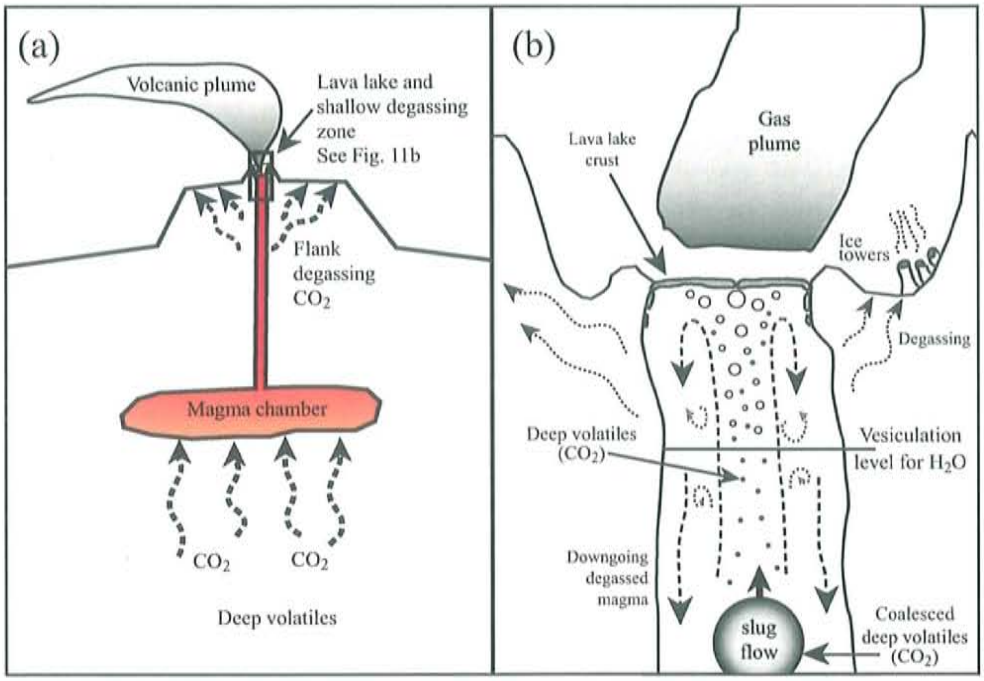

Figure 11. (a) Cartoon schematic showing conceptual structure of upper level magma chamber of Mt. Erebus volcano. Volatiles migrate from deep to an isolated chamber connected to the surface by a conduit. No scale is given and chamber shape is representational only. (b) Close up of summit-region/lava-lake conduit magma system. Arrows in conduit show movement of magma: volatile-rich magma rises in the conduit center, water bubbles form at shallow depths and degas at the surface, and dense degassed magma sinks back into the conduit. Smaller arrows show small eddies. Flank degassing is expressed on the surface by ice towers (described by Wardell et al., 2003). A large bubble of coalesced deep volatiles is shown rising in the conduit and will result in a strombolian expolsion at the surface (Aster et al., 2003). Figure after general model by Stevenson and Blake (1998).

monitoring and geophysical studies (Aster et al., 2004) should help elucidate what is driving activity at Mt. Erebus.

10. Conclusions

(1) Major and trace element analyses of summit lavas and modern bombs reveal that the bulk composition of material erupted from Erebus volcano has remained nearly constant for ~17 ka. Small bulk compositional variations result from inhomogenous distribution of anorthoclase feldspar in the samples, although it is unclear if this is a result of pre-, syn-, or post-eruptive processes.

(2) The compositions of matrix glasses from lava bombs erupted in the last 31 years indicate that no crystallization, assimilation, or mixing with magma of different composition has occurred during this time. Crystallization may be progressing slowly or not all, and the homogeneity of the mineral assemblage indicates that the system is at or close to equilibrium. Eruptive activity is decoupled from magma composition and is more likely controlled by conduit geometry and/or the flux of volatiles from deeper in the system.

(3) Bomb textures show that crystallization is largely controlled by shallow degassing of water. Anorthoclase phenocrysts feature complex compositional zoning that is interpreted to result from turbulent convection through a water gradient in the conduit.

(4) Oxygen isotope measurements on minerals erupted in 1982, 1984, 1985, 2000/2001 and 6 ± 4 ka ago are indistinguishable and lower than expected due to fractional crystallization. They are interpreted to show that the upper level magmatic system consists of an isolated chamber that is open to volatiles, mainly CO_2, from deeper in the system. It is unknown if volatiles are added to the upper level magma chamber on a continuous or episodic basis. An episodic influx of volatiles, decoupled from magma, may help explain the heightened eruptive activity observed in late-1984.

(5) Mineralogic and oxygen isotope data indicate the mineral assemblage found in lavas and bombs crystallizes from the bulk phonolite melt under closed system conditions. Thus, the differentiation process that creates the bulk phonolite melt is older than the crystals found in the bombs and the mineral assemblage crystallizes from the bulk phonolite melt under closed conditions. The recurrence interval of magma injections are not known, but if the 10 summit lava flows are assumed to have erupted in response to individual recharge events the recurrence interval is ~1.1 to 2.5 ka.

(6) The large size of Mt. Erebus volcano, its persistent activity, and the constant composition of material erupted over the past ~17 ka are broadly consistent with the Mt. Erebus magmatic system being very large and very stable. However, the residence time of magma, the volume of the upper level magma chamber, and the chamber's location in the crust are very poorly constrained at present. Placing

better estimates on these fundamental properties should be the focus of future research.

(7) Open-conduit conditions efficiently degas magma in the upper-level chamber, but if circumstances changed to allow accumulation of volatiles, the potential for explosive activity at Mt. Erebus is great. Tephra layers found up to ~180 km away indicate that explosive activity has occurred at Mt. Erebus throughout the Pleistocene and Holocene (Harpel et al., 2004), probably because of volatile build-up. The governing factors that lead to open or closed conduit conditions are hereto unknown.

References

Albarède, F., 1993. Residence time analysis of geochemical fluctuations in volcanic series. Geochim. Cosmochim. Acta. 57, 615-621.

Allard, P., 1997. Endogenous magma degassing and storage at Mount Etna. Geophysical Research Letters 24, 2219-2222.

Allard, P., Carbonnelle, J., Metrich, N., Loyer, H., Zetttwoog, P., 1994. Sulfur output and magma degassing budget of Stromboli volcano. Nature 368, 326-330.

Anderson, D. J., Lindsley, D.H., 1988. Internally consistent solution models for Fe-Mg-Mn-ti oxides: Fe-Ti oxides. American Mineralogist 73, 714-726.

Andersen D. J., Lindsley D. H., Davidson P. M., 1993. QUILF: A Pascal program to assess equilibria among Fe-Mg-Mn-Ti oxides, pyroxenes, olivine, and quartz. Comp. Geosc. 19, 1333–1350.

Andres, R.J., Rose, W.I., Kyle, P.R., deSilva, S., Francis, P., Gardeweg, M., Moreno Roa, H., 1991. Excessive sulfur dioxide emissions from Chilean volcanoes. J. Volcanol. Geotherm. Res. 46, 323–329.

Aster, R., Mah, S.Y., Kyle, P., McIntosh, W., Dunbar, N., Johnson, J., Ruiz, M., McNamara, S., 2003. Very long period oscillations of Mount Erebus volcano, J. Geophys. Res., 108 (B11), 2522, doi:10.1029/2002JB002101.

Aster, R., McIntosh, W., Kyle, P., Esser, R., Bartel, B., Dunbar, N., Johns, B., Johnson, J., Karstens, R., Kurnik, C., McGowan, M., McNamara, S., Meertens, C., Pauly, B., Richmond, M., Ruiz, M., 2004. New instrumentation delivers multidisciplinary real-time data from Mount Erebus, Antarctica. EOS trans. AGU., 85, no. 10, 9 March.

Bannister, S., Snieder, R.K., Passier, M.L., 2000. Shear-wave velocities under the Transantarctic Mountains and Terror Rift from surface wave inversion, Geophys. Res. Lett. 27, 281– 284.

Behrendt, J.C., LeMasurier, W.E., Cooper, A.K., Tessensohn, F., Trehu, A., Damaske, D., 1991. Geophysical studies of the West Antarctic rift system. Tectonics 10, 1257–1273.

Belkin, H. E., Kilburn, C.R.J., DeVivo, B., 1993. Sampling and major element chemistry of the Recent (A.D. 1631-1944) Vesuvius activity. J. Volcanol. Geotherm. Res. 58, 273–290.

Caldwell, D., Kyle, P.R., 1994. Mineralogy and geochemistry of ejecta erupted from Mount Erebus, Antarctica between 1972 and 1986, In: Kyle, P.R. (ed) Volcanological and Environmental Studies of Mount Erebus, Antarctica, Antarct. Res. Ser., vol. 66, Am Geophys Union, Washington, D.C. 147–162.

Cashman, K.V., 1990. Textural constraints on the kinetics of crystallization of igneous rocks. In: Nicholls, J., Russell, J.K. (eds) Reviews in mineralogy, vol. 24. Modern methods of igneous petrology, understanding magmatic processes. Mineral. Soc. Am., Washington, D.C. 259-314.

Cashman, K.V., Blundy, J., 2000. Degassing and crystallization of ascending andesite and dacite. Philos. Trans. R. Soc. London. Ser. A, 358, 1487-1513.

Chen, C.H., DePaolo, D.J., Nakada, S., Shieh, Y.N., 1993. Relationship between eruption volume and neodymium isotopic composition at Unzen volcano. Nature. 362, 831-834.

Cooper A.K., Davey F.J., Behrendt J.C., 1987. Seismic stratigraphy and structure of the Victoria Land basin, western Ross Sea, Antarctica. in: Cooper A.K., Davey F.J. (eds) The Antarctic Continental Margin: geology and geophysics of the western Ross Sea. Circum-Pacific Council for Energy and Resources, Houston, 27–65.

Cortés, J.A., Wilson, M., Condliffe, E., Francalanci, L., Chertkoff, D. G., 2005. The evolution of the magmatic system of Stromboli Volcano during the Vancori period (26 – 13.8 ky). J. Volcanol. Geotherm. Res. 147, 1-38.

Couch, S., 2003. Experimental investigation of crystallization kinetics in a haplogranite system. American Mineralogist. 88, 1471-1485.

Couch, S., Harford, C.L., Sparks, R.S.J., and Carroll, M.R., 2003a. Experimental constraints on andesite petrogenesis at the Soufrière Hills Volcano, Montserrat. Journal of Petrology. 44, 1455–1475.

Couch, S., Sparks, R.S.J., and Carroll, M.R., 2003b. The kinetics of degassing induced crystallization at Soufrière Hills Volcano, Montserrat. Journal of Petrology. 44, 1477–1502.

Craig, H., 1961. Standard for reporting concentrations of deuterium and oxygen-18 in natural waters. Science. 133, 1833-1834.

D'Alessandro, Giammanco, S., Parello, F., Valenza, 1997. CO_2 output and $\delta^{13}C(CO_2)$ from Mount Etna as indicators of degassing of shallow asthenosphere. Bull. Volcanol. 58, 455-458.

Devine, J.D., Rutherford, M.J., Norton, G.E., Young, S.R., 2003. Magma storage region processes inferred from geochemistry of Fe-Ti oxides in andesitic magma, Soufrière Hills Volcano, Montserrat, W.I. Journal of Petrology. 44, 1375-1400.

Dunbar, N., Cashman, K., Dupre, R., 1994. Crystallization processes of anorthoclase phenocrysts in the Mount Erebus magmatic system: Evidence from crystal composition, crystal size distributions and volatile contents of melt inclusions. In: Kyle, P.R. (ed.) Volcanological and Environmental Studies of Mount Erebus, Antarctica, Antarct. Res. Ser., 66, AGU, Washington, D. C. 129–146.

Eiler, J.M., 2001. Oxygen isotope variations of basaltic lavas and upper mantle rocks. In: Valley, J.W., Cole, D.R. (eds.), Stable Isotope Geochemistry, Reviews in mineralogy, 43. Min. Soc. Am., Washington, D.C. 319-364.

Elkins, L.T., Grove, T.L., 1990. Ternary feldspar experiments and thermodynamic models. American Mineralogist. 75, 544-559.

Eschenbacher, A. 1998. Open-system degassing of a fractionating, alkaline magma, Mount Erebus, Ross Island, Antarctica. Unpublished Master's Thesis, New Mexico Institute of Mining and Technology, Socorro.

Esser R.P., Kyle P.R., McIntosh W.C., 2004. $^{40}Ar/^{39}Ar$ dating of the eruptive history of Mount Erebus, Antarctica: Volcano evolution. Bull. Volcanol. 66, 671–686.

Esser R.P., McIntosh, W.C., Heizler, M.T., Kyle, P.R., 1997. Excess argon in melt inclusions in zero-age anorthoclase feldspar from Mt. Erebus, Antarctica, as revealed by the $^{40}Ar/^{39}Ar$ method. Geochim. Cosmochim. Acta. 61, 3789–3801.

Finn, C.A., Müller, R.D., Panter, K.S., 2005. A Cenozoic diffuse alkaline magmatic province (DAMP) in the southwest Pacific without rift or plume origin. Geochemistry Geophysics Geosystems. 6, Q02005, doi:10.1029/2004GC000723.

Francalanci, L., Tommasini, S., Conticelli, S., Davies, G. R., 1999. Sr isotope evidence for short magma residence time for the 20th century activity at Stromboli volcano, Italy. Earth. Planet. Sci. Lett. 167, 61-69.

Francalanci, L., Tommasini, S., Conticelli, S., 2004. The volcanic activity of Stromboli in the 1906-1998 AD period: mineralogical, geochemical and isotope data relevant to the understanding of the plumbing system. J. Volcanol. Geotherm. Res. 131, 179-211.

Francis, P., Oppenheimer, C., Stevenson, D., 1993. Endogenous growth of persistently active volcanoes. Nature. 366, 554-557.

Frost, R.B., Lindsley, D.H., Anderson, D.J., 1988. Fe-Ti oxide-silicate equilibria: Assemblages with fayalitic olivine. American Mineralogist, 73, 727-740.

Fujimaki, H., 1986. Partition coefficients of Hf, Zr, and REE between zircon, apatite, and liquid. Contrib. Min. Petrol. 94, 42-45.

Garcia, M.O., Pietruszka, A.J., Rhodes, J. M., 2003. A petrologic perspective of Kilauea Volcano's summit magma reservoir. Journal of Petrology. 44, 2313-2339.

Gerlach, T.M., McGee, K.A., 1994. Total sulfur dioxide emissions and pre-eruption vapor-saturated magma at Mt. St. Helens, 1980-99. Geophysical Research Letters 21, 2833-2836.

Geschwind, C., Rutherford, M.J., 1995. Crystallization of microlites during magma ascent; the fluid mechanics of 1980-1986 eruptions at Mount St. Helens. Bull. Volcanol. 57, 356-370.

Giggenbach, W., Kyle, P., Lyon, G., 1973. Present volcanic activity on Mt. Erebus, Ross Island, Antarctica. Geology. 1, 135– 156.

Goff, F., Love, S., Warren, R., Counce, d., Obenholzner, J., Seibe, C., and Schmidt, S., 2001. Passive infrared remote sensing evidence for large, intermittent CO_2 emissions at Popocatepetl volcano, Mexico. Chemical Geology. 177, 133-156.

Grêt, A., Snieder, R., Aster, R.C., Kyle, P.R., 2005. Monitoring rapid temporal change in a volcano with coda wave interferometry. Geophys Res Lett. 32, L06304, doi:10.1029/2004GL021143.

Hallett, R.B., 1994. Volcanic geology, paleomagnetism, geochronology and geochemistry of the Rio Puerco Necks, west-central New Mexico. Unpublished Ph.D thesis, New Mexico Institute of Mining and Technology, Socorro, New Mexico, U.S.A.

Hallett, R.B., Kyle, P.R., 1993. XRF and INAA determinations of major and trace elements in Geological Survey of Japan igneous and sedimentary rock standards. Geostandards Newsletter. 17, 127-133.

Halliday, A.N., Lee, D.-c., Tommasini, S., Davies, G.R., Paslick, C.R., Fitton, J.G., James, D.E. 1995. Incompatable trace elements in OIB and MORB and source enrichment in the sub-oceanic mantle. Earth. Plan. Sci, Lett. 133, 379-395.

Hammer, J.E., Cashman, K.V., Hoblitt, R.P., Newman, S., 1999. Degassing and microlite crystallization during pre-climatic events of the 1991 eruption of Mt. Pinitubo, Philippines. Bull. Volcanol. 60, 355-380.

Hammer, J.E., Cashman, K.V., Voight, B., 2000. Magmatic processes revealed by textural and compositional trends in Merapi dome lavas. J. Volcanol. Geotherm. Res. 100, 165-192.

Hammer, J.E., Rutherford, M.J., 2002. An experimental study of the kinetics of decompression-induced crystallization in silicic melt. J. Geophys. Res., DOI: 10.1029/2001JB000281.

Harpel, C.J., Kyle P.R., Caldwell, D.A., McIntosh W.C., Esser R.P., 2004. $^{40}Ar/^{39}Ar$ dating of the eruptive history of Mount Erebus, Antarctica: summit flows and caldera collapse. Bull. Volcanol. 66, 687–702.

Harris, A.J.L., Flynn, L.P., Rothery, D.A., Oppenheimer, C., Sherman, S.B., 1999. Mass flux measurements at active lava lakes: Implications for magma recycling. J. Geophys. Res. 104, 7117-7136.

Hawkesworth, C., Blake, S., Evans, P., Hughes, R., MacDonald, R., Thomas, L.E., Turner, S.P., Zellmer, G., 2000. Time scales of crystal fractionation in magma chambers – integrating physical, isotopic and geochemical perspectives. Journal of Petrology. 41, 991-1006.

Hawkesworth, C., Rhiannon, G., Turner, S., Zellmer, G., 2004. Time scales of magmatic processes. Earth. Planet. Sci. Lett. 218, 1-16.

Higgins, M., 1998. Origin of anorthosite by textural coarsening: Quantitative measurements of a natural sequence of textural development. Journal of Petrology. 39, 1307-1323.

Hofmann, A.W., 1997. Mantle geochemistry: the message from oceanic volcanism. Nature. 385, 219-229.

Housh, T.B., Luhr, J.F., 1991. Plagioclase – melt equilibria in hydrous systems. American Mineralogist. 76, 477-492

Johannes, W., 1978. Melting of plagioclase in the system Ab-An-H_2O at $P_{H2O} \leq 5$ kbars, an equilibrium problem. Contrib. Miner. Petrol. 66, 295-303.

Kazahaya, K., Shinohara, H., Saito, G., 1994. Excessive degassing of Izu-Oshima volcano: magma degassing in a conduit. Bulletin of Volcanology 56, 207-216.

Kelley, K.A., Plank, T., Ludden, J., Staudigel, H., 2003. Composition of altered oceanic crust at ODP sites 801 and 1149. Geochemistry, Geophysics, Geosystems 4 (6). Doi:10.1029/2002GC000435.

Kirkpatrick, R.J., 1981. Kinetics of crystallization of igneous rocks. In: Lasaga, A.C., Kirkpatrick, R.J. (eds), Kinetics of geological processes. Reviews in mineralogy, 8. Mineral. Soc. Am., Washington, D.C. 321-398.

Klug, C., Cashman, K.V., 1994. Vesiculation of May 18, 1980, Mount St. Helens magma. Geology. 22, 468-472.

Kyle, P.R., 1976. Geology, mineralogy, and geochemistry of the Late Cenozoic McMurdo Volcanic Group, Victoria Land, Antarctica. Unpublished Ph.D Thesis, Dept. of Geology, Victoria University of Wellington, New Zealand.

Kyle P.R., 1977. Mineralogy and glass chemistry of recent volcanic ejecta from Mt. Erebus, Ross Island, Antarctica. NZ J Geol Geophys. 20, 1123–1146.

Kyle, P., 1986. Volcanic activity of Mount Erebus, 1984 – 1986, Antarct. J. U.S., XXI, 7– 8.

Kyle, P.R., 1990a. McMurdo Volcanic Group-Western Ross Embayment: introduction. in: LeMasurier, W., Thomson, J. (eds) Volcanoes of the Antarctic Plate and Southern Oceans. Antarctic Research Series. Am Geophys Union, Washington, DC. 18–25.

Kyle, P.R., 1990b. Erebus Volcanic Province. in: LeMasurier, W., Thomson, J. (eds) Volcanoes of the Antarctic Plate and Southern Oceans. Antarctic Research Series. Am Geophys Union, Washington, DC

Kyle P.R., Cole, J.W., 1974. Structural control of volcanism in the McMurdo Volcanic Group, Antarctica. Bull Volcanol. 38, 16–25.

Kyle, P., Dibble, R., Giggenbach, W., Keys, J., 1982. Volcanic activity associated with the anorthoclase phonolite lava lake, Mt. Erebus, Antarctica, in: C. Craddock (ed), Antarctic Geosciences, Univ. Wisc. Press, Madison, 735–745.

Kyle P.R., Moore J.A., Thirlwall M.F., 1992. Petrologic evolution of anorthoclase phonolite lavas at Mount Erebus, Ross Island, Antarctica. J. Petrol. 33, 849–875.

Landi, P., Metrich, N., Bertagnini, A., Rosi, M., 2004. Dynamics of magma mixing and degassing recorded in plagioclase at Stromboli (Aeolian Archipelago, Italy). Contrib. Min. Petrol. 147, 213-227.

Larsen, J.F., 2005. Experimental study of plagioclase rim growth around anorthite seed crystals in rhyodacitic melt. American Mineralogist. 90, 417-427.

LeBas, M.J., LeMaitre, R.W., Streckeisen, A., and Zanettin, B., 1986. A chemical classification of volcanic rocks based on the total alkali silica diagram. Journal of Petrology. 27, 745-750.

Le Guern, F., Carbonelle, J., Tazieff, H., 1979. Erte 'Ale lava lake: Heat and gas transfer to the atmosphere, J. Volcanol. Geotherm. Res. 6, 27– 48.

Loomis, T.P., Welber, P.W., 1982. Crystallization processes in the Rocky Hill granodiorite pluton, California: an interpretation based on compositional zoning of plagioclase. Contrib. Mineral. Petrol. 81, 230-239.

Marsh, B.D., 1989. Magma chambers. Annu. Rev. Earth. Planet. Sci. 17, 439-474.

Matsushita, Y., 1973. Oxygen isotope variations in magmatic differentiation processes of the volcanic rocks in Japan. Contrib. Mineral. Petrol. 39, 277-288.

Metrich, N., Rutherford, M.J., 1998. Low pressure crystallization paths of H_2O-saturated basaltic-hawaiitic melts from Mt. Etna; implications for open-system degassing of basaltic volcanoes. Geochim. Cosmochim. Acta. 62, 1195-1205.

Moore J.A., 1986. Mineralogy, geochemistry and petrogenesis of the lavas of Mount Erebus, Antarctica. Unpublished Master's Thesis, New Mexico Institute of Mining and Technology, Socorro, U.S.A.

Morgan, D.J., Blake, S, 2006. Magmatic residence times of zoned phenocrysts: introduction and application of the binary element diffusion modelling (BEDM) technique. Contrib. Miner. Petrol. 151, 58-70.

Muehlenbachs, K., Byerly, G., 1982. ^{18}O-enrichment of silicic magmas caused by crystal fractionation at the Galapagos spreading center. Contrib. Miner. Petrol. 79, 76-79.

Nakamura, M., 1995. Continuous mixing of crystal mush and replenished magma in the ongoing Unzen eruption. Geology 23, 807–810.

Nekvasil, H., 1992. Tertiary feldspar crystallization in high-temperature felsic magmas. American Mineralogist. 77, 592-604.

Oppenheimer, C., McGonigle, A.J.S., Allard, P., Wooster, M.J., Tsanev, V., 2004. Sulfur, heat, and magma budget of Erta 'Ale lava lake, Ethiopia. Geology 32, 509-512.

Panter, K.S., Hart, S.R., Kyle, P., Blusztanjn, J., Wilch, T., 2000. Geochemistry of Late Cenozoic basalts from the Crary Mountains: characterization of mantle sources in Marie Byrd Land, Antarctica. Chemical Geology 165, 2000.

Panter, K.S., Blusztajn, J., Hart, S.R., Kyle, P.R., Esser, R., McIntosh, W.C., 2006. The Origin of HIMU in the SW Pacific: Evidence from Intraplate Volcanism in Southern New Zealand and Subantarctic Islands. Journal of Petrology (in press).

Pearce, T. H., 1994. Recent work on oscillatory zoning in plagioclase. In: Parsons, I (ed.) Feldspars and their reactions. NATO ASI Series. 421, 313-349.

Powers, H., 1955. Composition and origin of basaltic magma of the Hawaiian Islands. Geochim. Cosmochim. Acta. 7, 77-107.

Reagan, M., Gill, J., Malavassi, E., Garcia, M. O., 1987. Changes in magma composition at Arenal volcano, Costa Rica, 1968-1985: Real-time monitoring of open-system differentiation. Bull. Volcanol. 49, 415-434.

Rose Jr., W.I., Stoiber, R.E., Malinconico, L.L., 1982. Eruptive gas compositions and fluxes of explosive volcanoes: budget of S and Cl emitted from Fuego volcano, Guatemala. In: Thorpe, R.S. (Ed.), Andesites: Orogenic Andesites and Related Rocks. Wiley, New York, NY. 669– 676.

Seaman, S.J., Dyar, M.D., Marinkovic, N., Dunbar, N.W., 2006. An FTIR study of hydrogen in anorthoclase and associated melt inclusions. American Mineralogist. 91, 12-20.

Sheppard, S.M.F., Harris, C., 1985. Hydrogen and oxygen isotope geochemistry of Ascention Island lavas and granites: variation with crystal fractionation and interaction with sea water. Contrib. Mineral. Petrol. 91, 74 -81.

Sims, K.W.W., DePaolo, D.J., 1997. Inferences about mantle magma sources from incompatible element concentration ratios in oceanic basalts. Geochim. Cosmochim. Acta. 61, 765-784.

Sparks, R.S.J., 2003a. Forecasting volcanic eruptions. Earth Planet. Sci. Lett. 210, 1-15.

Sparks, R.S.J., 2003b. Dynamics of magma degassing. In: C. Oppenheimer, C., Barclay, J., Pyle, D. (Eds.), Origins, emissions and impacts of volcanic gases. Geol. Soc. London, Spec. Publ. 213, 5-22.

Stevenson, D.S., Blake, S., 1998. Modeling the dynamics and thermodynamics of volcanic degassing. Bull. Volcanol. 60, 307-317.

Stoiber, R., Williams, S., Huebert, B., 1986. Sulfur and halogen gases at Masaya caldera complex, Nicaragua: Total flux and variations with time. J. Geophys. Res. 91, 2215–2231.

Stormer, J.C., 1983. The effects of recalculation on estimates of temperature and oxygen fugacity from analyses of multicomponent iron-titanium oxides. American Mineralogist. 68, 586-594.

Streck, M.J., Dungan, M.A., Bussy, F., Malavassi, E., 2005. Mineral inventory of continuously erupting basaltic andesites at Arenal volcano, Costa Rica: implications for interpreting monotonous, crystal-rich, mafic arc stratigraphies. J. Volcanol. Geotherm. Res. 140, 133-155.

Sun, S.-S., Hanson, G.N., 1975. Origin of Ross Island basanitoids and limitations upon the heterogeneity of mantle sources for alkali basalts and nephelinites. Contrib. Miner. Petrol. 54, 139-55.

Sun, S.-S., Hanson, G.N., 1976. Rare earth element evidence for differentiation of McMurdo Volcanics, Ross Island, Antarctica. Contrib. Miner. Petrol. 54, 139-155.

Sun, S.-S., McDonough, W.F., 1989. Chemical and isotopic systematics of oceanic basalts: implications for mantle compositions and processes. In: Saunders, A.D., Norry, M.J. (Eds.), Magmatism in Ocean Basins. Geol. Soc. London, Spec. Publ. 42, 313–345.

Taylor, H.P., Sheppard, S.M.F., 1986. Igneous Rocks: I. Processes of Isotopic Fractionation and Isotope Systematics. In: Valley, J.W., Taylor, H.P., O'Neil, J.R. (eds.) Reviews in Mineralogy, 16. Stable Isotopes in High Temperature Geological Processes. Min. Soc. Am., Washington, D.C. 227-269.

Tazieff, H., 1984. Nyiragongo: Renewed activity of the lava lake. J. Volcanol. Geotherm. Res., 20, 267– 280.

Tilling, R.I., 1987. Fluctuations in surface height of active lava lakes during 1972-1974 Mauna Ulu eruption, Kilauea Volcano, Hawaii. J. Geophys. Res. 92, 13721-13730.

Tuttle, O.F., Bowen, N.L., 1958. Origin of granite in the light of experimental studies. Geological Society of America, Boulder, Colorado. 153 pp.

Venezky, D.Y., Rutherford, M.J., 1999. Petrology and Fe-Ti oxide reequilibration of the 1991 Mount Unzen mixed magma. J. Volcanol. Geotherm. Res. 89, 213-230.

Wade, J.A., Plank, T., Stern, R.J., Tollstrup, D.L, Gill, J.B., O'Leary, J.C., Eiler, J.M., Moore, R.B., Woodhead, J.D., Trusdell, F., Fischer, T.P., Hilton, D.R., 2005. The May 2003 eruption of Anatahan volcano, Mariana Islands: Geochemical evolution of a silicic island-arc volcano. J. Volcanol. Geotherm. Res. 146, 139-170.

Wallace, P.J., 2005. Volatiles in subduction zone magmas: concentrations and fluxes based on melt inclusion and volcanic gas data. J. Volcanol. Geotherm. Res. 140, 217–240.

Wallace, G.S., Bergantz, G.W., 2005. Reconciling heterogeneity in crystal zoning data: An application of shared characteristic diagrams at Chaos Crags, Lassen Volcanic Center, California. Contrib. Mineral. Petrol. 149, 98-112.

Wardell, L.J., Kyle, P.R., Campbell, A.R., 2003. Carbon dioxide emissions from fumarolic ice towers, Mount Erebus volcano, Antarctica. In: C. Oppenheimer, C., Barclay, J., Pyle, D. (Eds.), Origins, emissions and impacts of volcanic gases. Geol. Soc. London, Spec. Publ. 213, 231-246.

Wardell, L.J., Kyle, P.R., Chaffin, C., 2004. Carbon dioxide and carbon monoxide emission rates from an alkaline intra-plate volcano: Mt. Erebus, Antarctica. J. Volcanol. Geotherm. Res. 131, 109-121.

Wen, S., Nekvasil, H., 1994. SOLVCALC; an interactive graphics program package for calculating the ternary feldspar solvus and for two-feldspar geothermometry. Computers and Geosciences. 20, 1025-1040.

Westrich, H.R., Gerlach, T.M., 1992. Magmatic gas source for the stratospheric SO_2 cloud from the June 15, 1991, eruption of Mount Pinatubo. Geology. 20, 867-870.

Wilson, M., 1989. Igneous Petrogenesis. Unwin Hyman Ltd., London, England. 466 pp.

Witter, J.B., Kress, V.C., Delmelle, P., Stix, J., 2004. Volatile degassing, petrology, and magma dynamics of the Villarrica Lava Lake, Southern Chile. J. Volcanol. Geotherm. Res. 134, 303-337.

Wright, T. L., Fiske, R. S., 1971. Origin of differentiated and hybrid lavas of Kilauea Volcano, Hawaii. J. Petrol. 12, 1-65.

Zhao, Z., Zheng, Y., 2003. Calculation of oxygen isotope fractionation in magmatic rocks. Chemical Geology. 193, 59– 80.

Refinement of the younger geologic history of Mount Erebus volcano, Antarctica using $^{40}Ar/^{39}Ar$ age determinations.

Abstract

Six new $^{40}Ar/^{39}Ar$ age determinations provide a more complete record of the eruptive history of Mount Erebus volcano and development of the summit region. Furnace step-heating was used to analyze anorthoclase from 4 summit lava flows and a tephra and also a sanidine from a trachyte lava. The Northwest lava flow has an $^{40}Ar/^{39}Ar$ age of -3 ± 7 ka which is indistinguishable from 1 ± 5 ka previously reported and thus gives a weighted-mean age of 0 ± 4 ka. A sample from the southwestern caldera margin is 23 ±12 ka in agreement with ~25 ka lavas from the area. A pre-caldera lava sample from the north-northwestern caldera rim is 81 ± 3 ka and correlates with lavas from the northeastern caldera margin previously dated between 76 ± 4 ka and 95 ± 9 ka. A pre-caldera lava sample from the southeastern caldera margin has an age of 172 ± 10 ka which is significantly older than any previously dated sample from the summit region and greatly extends the age of lavas exposed in the caldera walls. The new dates support the presence of a second, younger, superimposed caldera near the southwestern margin of the summit plateau.

An anorthoclase-phyric bomb sample from "Bomb Peak" is 23 ± 3 ka, but the location of the vent that produced the bombs is unknown. Trachyte from "Ice Station" on the eastern flank is 159 ± 2 ka, similar to two other trachyte lavas found on Mount Erebus. Trachyte lavas were erupted from the eastern periphery of Mt. Erebus at ~160 ka, in close temporal and spatial proximity to Si-undersaturated lavas erupted from the modern-day summit region.

1. Introduction

Mount Erebus volcano (77°32'S, 167°10'E) is the southernmost active volcano in the world. It is a large (3794 m elevation, ~2000 km^3 volume), composite stratovolcano with an eruptive history spanning from ~1.3 Ma to the present (Esser et al., 2004; Harpel et al., 2004). Current activity includes up to ~6 strombolian eruptions per day from the persistent convecting anorthoclase phonolite lava lake located in the ~200-m-deep Inner Crater which is within and at the northern end of the ~500 m diameter Main Crater. There is a distinct break in slope of Erebus volcano at ~3500 m elevation that defines the rim of a broad, roughly circular ~4 km diameter summit plateau with the summit cone and Main Crater located south of the center (Fig. 1). The summit plateau has been interpreted to be a caldera formed between 80 and 24 ka and subsequently filled by post-collapse lava flows and pyroclastic deposits (Moore and Kyle, 1987; Harpel et al., 2004). Field relations, age determinations, and geochemical arguments support the presence of a second younger superimposed caldera that formed between 25 and 11 ka near the southwestern side of the summit plateau (Harpel, 2004). The eruptive history of young lava flows around the summit crater of Mount Erebus volcano has been examined by Harpel et al., (2004) using $^{40}Ar/^{39}Ar$ age determinations on anorthoclase phenocrysts. Here we report 3 new $^{40}Ar/^{39}Ar$ age determinations from key areas around the summit plateau, where age control was lacking, and these compliment the work of Harpel et al., (2004). The ages place better constraints on the temporal evolution of the north-northwest, southwest, and east-southeast margins of the summit plateau. We also report ages for a very young post-caldera collapse summit lava flow, a lava bomb from Bomb Peak, and a trachyte lava from high on the southeastern flank of Erebus. The new

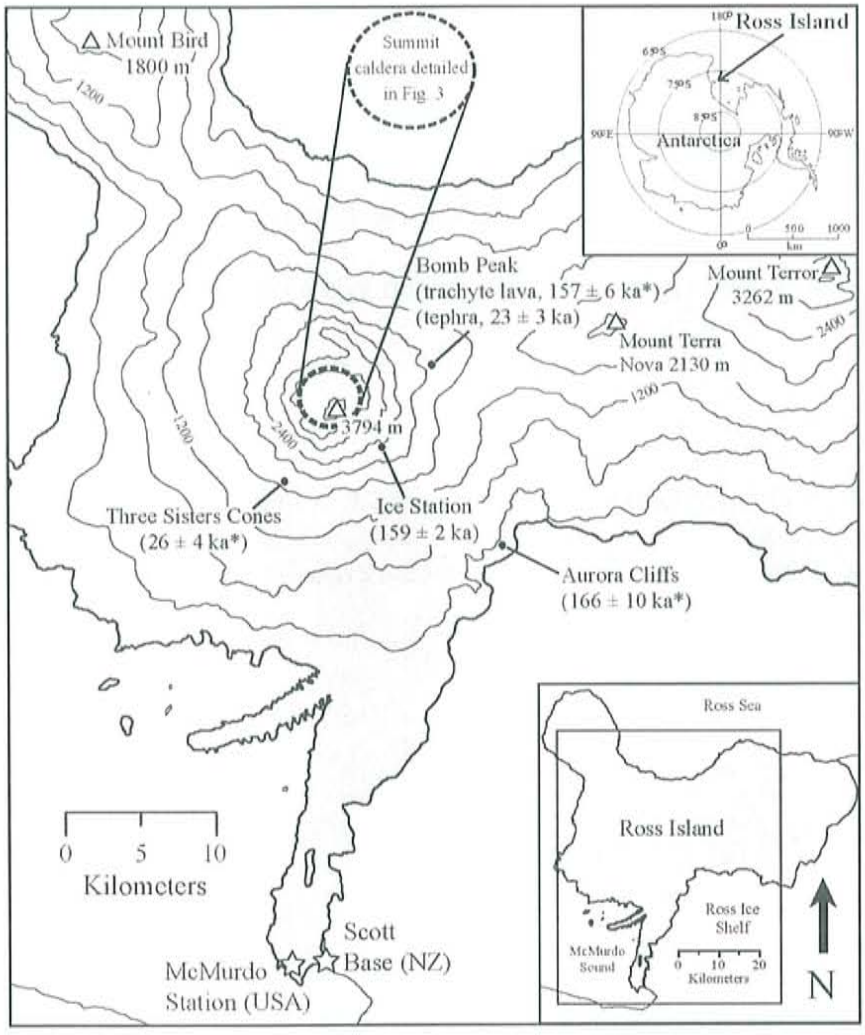

Figure 1. Topographic map showing part of Ross Island and selected sample localities with ages and 2σ uncertainty (in ka). * indicates age from Harpel et al. (2004). Contour interval is 400 meters. Inset maps show Ross Island and location in Antarctica.

age determinations provide a more complete history of Mount Erebus volcano and eruptions in the summit region over the last 170 ka.

Unraveling the eruptive history of the Erebus summit plateau region is difficult because many of the flows are covered in snow and ice which limits outcrop exposures and obscures important overlapping field relationships. The problem is compounded because the post-caldera phonolite lava flows are indistinguishable based on field appearance, mineralogy, mineral modes, bulk chemistry, and radiogenic isotope signatures (Moore, 1986; Kyle et al., 1992; Caldwell and Kyle, 1994; Harpel et al., 2004; Kelly, Part A; Sims et al., in prep.). Where geochemical characterization has failed the $^{40}Ar/^{39}Ar$ dating method is an effective method for investigating the eruptive history of Erebus volcano.

2. Methods

Excess argon ($^{40}Ar_E$) is present in matrix glass and melt inclusions in anorthoclase from Erebus volcano lavas and tephra (Esser et al., 1997). The anorthoclase can contain up to ~30% melt inclusions by volume (Kyle, 1977; Dunbar et al., 1994). It is therefore critical to remove melt inclusions and glass adhering to crystals to obtain accurate ages for the samples. Esser et al. (1997) developed a procedure where the anorthoclase was crushed to a small size (~500 μm) and etched in a 15% HF acid solution for about an hour. This selectively removes melt inclusions and adhered glass.

Anorthoclase from 4 lava flows and one lava bomb were prepared following the methods of Esser et al. (1997) except samples were crushed to a finer size (106 - 250 μm) to expose more melt inclusions. Glass and mafic minerals were removed using a Franz Isodynamic magnetic separator. The non-magnetic portions were then etched in a 15% hydrofluoric acid solution for 60 minutes in an ultrasonic bath to remove melt inclusions and adhering glass. The anorthoclase concentrates were checked for purity by petrographic microscope. Etched samples were then immersed in heavy liquid (D = 3.0 g/cm^3) and centrifuged to remove apatite. Any remaining impurities were removed by hand-picking. The final grain size for the anorthoclase concentrates was 20 - 70 μm.

Trachyte lava from "Ice Station," a seismic monitoring station located high on the southeastern flank of Mt. Erebus (Fig. 1; Aster et al., 2003), was crushed in a jaw crusher and sieved to a small size (106 - 250 μm). Sanidine crystals were then separated into a non-magnetic fraction using a Franz isodynamic magnetic separator. The sanidine were nearly melt-inclusion free when inspected microscopically and required no further preparation. All samples were greater than 99% pure when analyzed.

All samples were split into 3 to 5, 70 to 100 mg aliquots, encapsulated in copper foil, and sealed in evacuated quartz tubes for irradiation. Packets of Fish Canyon Tuff sanidine interlaboratory standard (FC-1, 28.02 Ma; Renne et al., 1998) were placed between the sample packets as flux monitors. Flux monitors were analyzed by single-crystal laser fusion using a CO_2 laser. The samples were first irradiated in Sept. 2004, but were not analyzed until Sept. 2005. Thus, the samples were re-irradiated in Sept 2005 so ^{37}Ar ($t_{1/2}$ = 35 days) could be analyzed for ^{36}Ar and ^{39}Ar corrections and for determination of K/Ca. The samples were irradiated for 15 minutes on 01 Sept 2004 at

the McMaster University research reactor under a fast neutron flux of ~12.5 x 10^{-5} J/h. The second irradiation was for 50 minutes on 09 September 2005 at the University of Texas under a fast neutron flux of ~10.5 x 10^{-5} J/h. The relative contribution of each irradiation to the total neutron flux was calculated for determination of J-factors and correction parameters.

$^{40}Ar/^{39}Ar$ analyses were made at the New Mexico Geochronology Research Laboratory (NMGRL) at the New Mexico Institute of Mining and Technology for this study. Analytical details are given in Table 1. 250 to 357 mg of anorthoclase or sanidine was used for each analysis. Argon extraction was accomplished by step-heating each sample in a double-vacuum resistance furnace capable of 1,750°C and fitted with a molybdenum crucible and liner. Step-heating began with an initial low-temperature step at 500 - 700°C and then incrementally progressed to 1700°C. Each temperature step was held for 10 minutes.

3. Results

Analytical data for the anorthoclase and sanidine samples are given in Table 1 and plotted as age spectra diagrams (Fig. 2). Full analytical data are available at Kelly et al., (in prep.). All uncertainities for age determinations are reported at the 2σ level.

The anorthoclase age spectra (Fig. 2a-f) have an imprecise low-temperature step due to degassing of atmospheric argon (Esser et al., 1997). Anorthoclase from Mount Erebus typically have anomalously high apparent ages and elevated Cl/K ratios in the

Table 1. $^{40}Ar/^{39}Ar$ ages for samples from the Mt. Erebus summit plateau and vicinity

Sample ID	Lab ID	Type	Summit Flow	Material	Steps (°C)	# Steps	^{39}Ar (%)	Age (ka)	± 2σ
E87037	55367	Lava	Pre-Caldera	anorthoclase	750-1000	4	46.5	**81**	**3**
E86031	55370	Lava	Pre-Caldera	anorthoclase	650-1000	6	64.4	**172**	**10**
E86003	55374	Lava	Pre-Caldera	anorthoclase	650-1000	6	64.9	**23**	**12**
E87025[Φ]	55347	Lava	Pre-Caldera	anorthoclase					
E87040	55363	Lava	Northwest	anorthoclase	800-1100	4	59.2	-3	7
E87040*	8855			anorthoclase	800-1100	4	79.8	1	5
Northwest Flow weighted-mean age, n = 2								**0**	**4**
Bomb Peak	55348	Tephra		anorthoclase	750-900	3	56.3	**23**	**3**
Ice Station	55359	Lava		sanidine	800-1700	6	97.5	**159**	**2**

Notes:

Lab ID is a unique laboratory identifier for each analysis

[Φ]E87025 did not yield an age

*Analysis from Harpel et al. (2004); effect of standard correction (FC-1 from 27.84 Ma to 28.02 Ma) is not significant

Analytical methods and parameters:

Mineral separation methods	magnetic (Franz), heavy liquid (lithium metatungstate), hand-picking
Irradiation geometry	alternating samples and monitors in sealed evacuated quartz tubes
Irradiation facilities	Irradiation 1: McMaster University, Toronto, Canada (15 minutes); Irradiation 2: Nuclear Science Center, College Station, TX (50 minutes)
Irradiation batch	NM-180
Neutron flux monitor	Fish Canyon Tuff sanidine (FC-1) @ 28.02 Ma (Renne et al., 1998)
Lab	New Mexico Geochronology Research Laboratory, New Mexico Tech, Socorro, NM
Spectrometer	Mass Analyzer Products 215-50
Extraction system	automated, all-metal
Laser	50 watt Synrad CO_2 laser
Furnace	double vacuum resistance, maximum temperature 1750°C
Heating procedures	anorthoclase and sanidine unknowns: furnace; sanidine flux monitors: single-crystal laser fusion
Gas cleanup, laser	two SAES GP-50 getters@ ~450°C and 20°C, W filament @ ~2000°C, cold finger @ -120°C
Gas cleanup times, laser	2 minutes
Electron multiplier sensitivity, laser	2.94×10^{-16} moles/pA
Total system blank average, laser	1740, 7.9, 3.1, 7.5, 1.5×10^{-18} moles @ masses 40, 39, 38, 37 and 36
Gas cleanup times, furnace	14 minutes
Gas cleanup, furnace	1st stage: SAES GP-50 getter @ ~450°C, 2nd stage: SAES GP-50 getter @ 20°C, W filament @ ~2000°C, cold finger @ -120°C
Electron multiplier sensitivity, furnace	5.2×10^{-16} moles/pA
Total system blank average, furnace	1513, 33.9, 1.8, 4.8, 4.7×10^{-18} moles @ masses 40, 39, 38, 37 and 36
J-factor determination	CO_2 laser-fusion of 4 single crystals from each of 4 radial positions around irradiation tray
J-factor precision	±0.25% (1σ)
Correction factor monitors	K-glass and CaF_2
Correction factors NM-180	$(^{40}Ar/^{39}Ar)_K = 0.0125 \pm 0.0015$; $(^{36}Ar/^{37}Ar)_{Ca} = 0.00028 \pm 0.00001$; $(^{39}Ar/^{37}Ar)_{Ca} = 0.0007 \pm 0.00005$; (38Ar/39Ar)K = 0.0125
Isotopic ratio corrections	blank, radioactive decay, mass discrimination (not corrected for interfering reactions)
Individual analysis errors	analytical error only (uncertainties in interfering reactions and J factors excluded)
Mean age	weighted mean age of Taylor (1982)
Mean age error calculation	weighted error of the mean (Taylor, 1982), multiplied by root of MSWD where MSWD>1
Mean age errors	uncertainties in interfering reactions and J factors included
Decay constants	Steiger and Jaeger (1977)

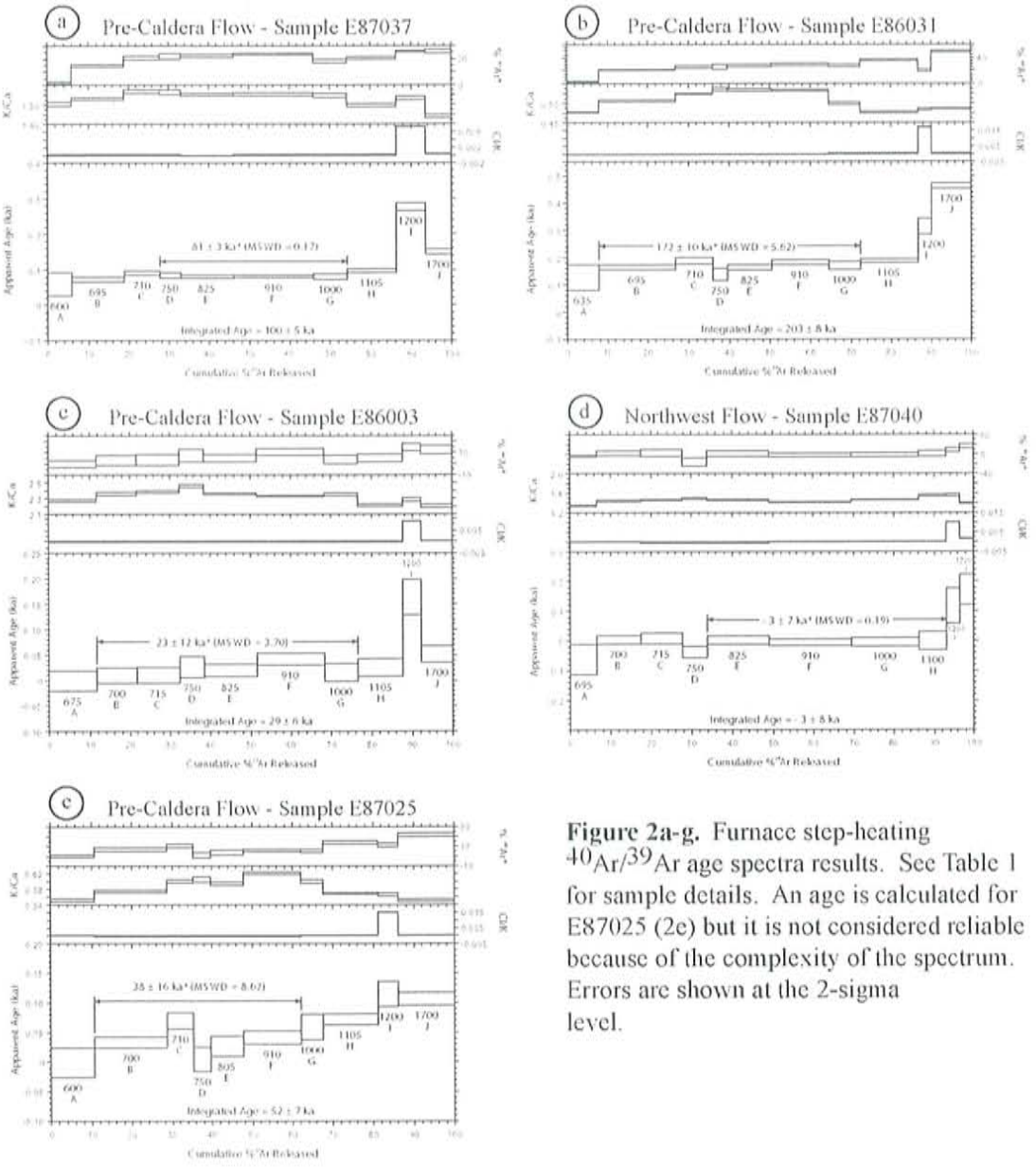

Figure 2a-g. Furnace step-heating $^{40}Ar/^{39}Ar$ age spectra results. See Table 1 for sample details. An age is calculated for E87025 (2e) but it is not considered reliable because of the complexity of the spectrum. Errors are shown at the 2-sigma level.

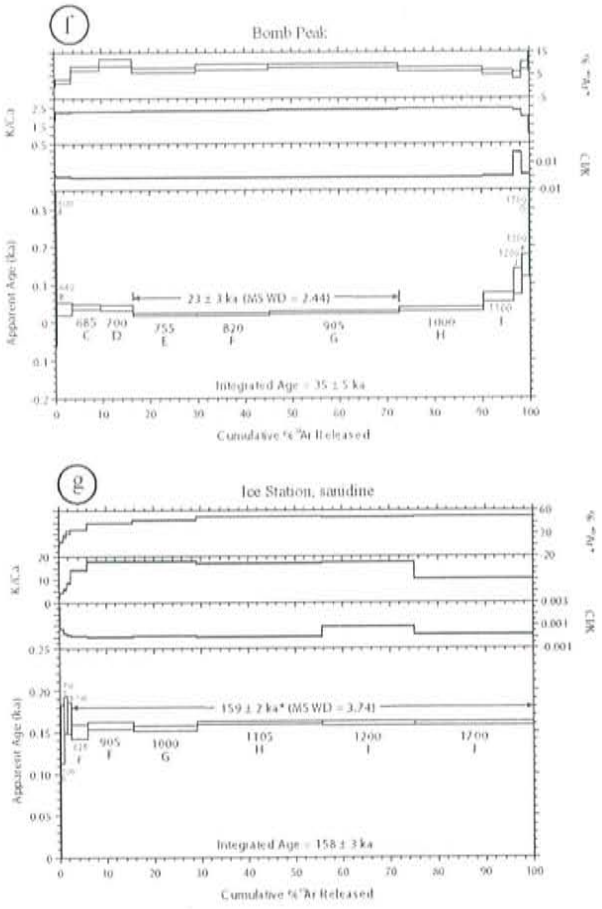

Figure 2. (continued)

initial low-temperature step (Esser et al., 1997; Esser et al., 2004; Harpel et al., 2004). This has been attributed to degassing melt inclusions near the surface of mineral grains that contain Cl and $^{40}Ar_E$. The analyses reported here have imprecise but concordant first heating steps, with near-constant Cl/K ratios and near-zero $^{40}Ar^*$ yields. This is evidence that our modified preparation procedure (i.e. crushing samples to a smaller size) removes a larger proportion of melt inclusions and yields samples of greater purity.

With one exception (E87025; Fig. 2e), the initial imprecise low-temperature step in each anorthoclase age spectrum is followed by generally concordant and relatively precise intermediate-temperature steps from 700 to 1100°C. These concordant intermediate-temperature step plateaus are used for calculation of weighted-mean ages (each step weighted by the inverse of the variance), as discussed later in this section.

The apparent age spectrum for sample E87025 features two discontinuous rising patterns with increasing temperature. The first rising pattern is comprised of the first three temperature steps (A – C; 600 to 710°C), with a minimum apparent age of -1 ± 12 ka (step A) and a maximum apparent age of 69 ± 7 ka (step C). The second rising pattern begins at step D (750°C; 4 ± 10 ka) and continues through the intermediate and high temperature steps (E – J; 805 to 1700°C). The last two steps (I & J; 1200 & 1700°C) are analytically indistinguishable and give the oldest apparent ages (step I, 114 ± 11 ka; step J, 107 ± 5 ka). The Cl/K ratio is nearly constant for all the temperature steps, but has an abrupt spike at 1200°C.

The E87025 spectrum is likely a result of $^{40}Ar_E$ interference due to incomplete removal of melt inclusions. Traces of melt inclusions that remain near the surface of the

sample crystal fragments will degas early (i.e. steps A - C), whereas melt inclusions from the interior of the crystal fragments may progressively degas as the temperature increases. This would result in the observed discordant spectra.

From 1100 to 1700°C the anorthoclase age-spectra steps are imprecise. These steps feature elevated radiogenic yields and apparent ages. The discordant high temperature steps are interpreted to result from melt inclusion degassing of $^{40}Ar_E$ and $^{38}Ar_{Cl}$, which leads to higher apparent ages, total gas ages, and Cl/K ratios (Esser et al., 1997).

An abrupt increase in the Cl/K ratio and apparent age at 1200°C is present in all the anorthoclase analyses and has been observed in other step-heating $^{40}Ar/^{39}Ar$ studies of Mt. Erebus anorthoclase (Esser et al., 1997; Esser et al., 2004; Harpel et al., 2004). This is because the anorthoclase begins to melt around 1200°C and the interior melt inclusions can more freely degas (Esser et al., 1997).

The Ice Station sanidine sample (Fig. 2g) has four small low-temperature (600 - 750°C) steps that have imprecise apparent ages, elevated Cl/K, low K/Ca, and low radiogenic yields. Otherwise, the apparent age spectrum is concordant and precise from 825 - 1700°C. At 1200°C there is a small jump in Cl/K from near-zero to 0.001 with no associated effect on apparent age. The amount of Cl and $^{40}Ar_E$ released when the crystal began to melt at ~1200°C was too small to affect total ^{40}Ar (i.e. apparent age) because sanidine were nearly melt inclusion free.

The steps selected for weighted-mean ages form quasi-linear isochron arrays, yet due to the small number of data points and low, consistent $^{40}Ar^*$ yields, the data typically

plot as clusters and the corresponding errors on the isochron diagrams are large. For example, the weighted-mean age of sample E87037 is 81 ± 3 ka and its isochron age is 80 ± 22 ka. Therefore the weighted mean age approach is favored for these samples, a conclusion also reached by Esser et al. (1997), Esser et al. (2004), and Harpel et al. (2004).

Weighted mean ages were calculated for the samples by choosing three or more contiguous, intermediate temperature heating steps that are relatively concordant. The chosen steps are mostly between 650 and 1000°C, typically comprise greater than 50% of $^{40}Ar^*$ released, and with one exception (Ice Station) yield apparent ages that are younger than the total gas (integrated) age (Table 1; Fig. 2a-g). An age was not calculated for sample E87025 because its spectrum did not yield any contiguous, concordant steps.

In a strict sense we must consider the ages to be maxima because $^{40}Ar_E$ is known to be present (Esser et al., 1997; Esser et al., 2004). However, the chosen plateaus for all the samples are fairly flat and have low Cl/K ratios, indicating that the effect of $^{40}Ar_E$ on the chosen steps is insignificant. Therefore it is reasonable to take the $^{40}Ar/^{39}Ar$ ages as eruption ages (Esser et al., 2004; Harpel et al., 2004).

4. Discussion

4.1 The summit plateau

Three lava samples from the caldera rim and one post-caldera lava were dated (Table 1). Sample E87037 from the north-northwestern caldera rim is 81 ± 3 ka and

indistinguishable in age from two other lava flows (86 ±15 ka & 76 ± 4 ka; Harpel et al., 2004) from the north-northeastern margin (Fig. 3), This shows that the north-northwestern and eastern segments of the rim have similar histories.

Harpel et al. (2004) found that the southwestern caldera rim (~25 ka) was younger than the northern and eastern rims (Fig. 3) (~80 – 90 ka). Using field relationships they inferred that a distinct ridge was correlated with the young portion of the southwest caldera rim, and that together they define the rim of a second, younger caldera ("Caldera Collapse B" from Harpel et al., 2004) superimposed within the larger, older caldera (Figs. 3 & 4) ("Caldera Collapse A" from Harpel et al., 2004). Sample E86003 is from the distinct ridge and its age (23 ± 12 ka) is indistinguishable from the two other lavas that define the young caldera rim (21 ± 4 & 27 ± 3), confirming the correlation. Analytical errors prevent us from further refining the age of the young caldera collapse (Caldera Collapse B).

Sample E86031 (172 ± 10 ka), from the eastern rim is significantly older than any other previously dated lava from the summit region (Fig. 3). The next oldest lava is also from the eastern rim and is 95 ± 9 ka (Harpel et al., 2004). The data suggest that the oldest part of the summit region is the southeastern side, and that eruptive activity has occurred in the summit area for at least ~170 ka, and probably longer.

We dated one post-caldera summit lava flow (E87040) previously dated by Harpel et al. (2004) to assess precision and to verify that the results of our study are directly comparable to Harpel et al. (2004). Harpel et al. reported an age of 1 ± 5 ka

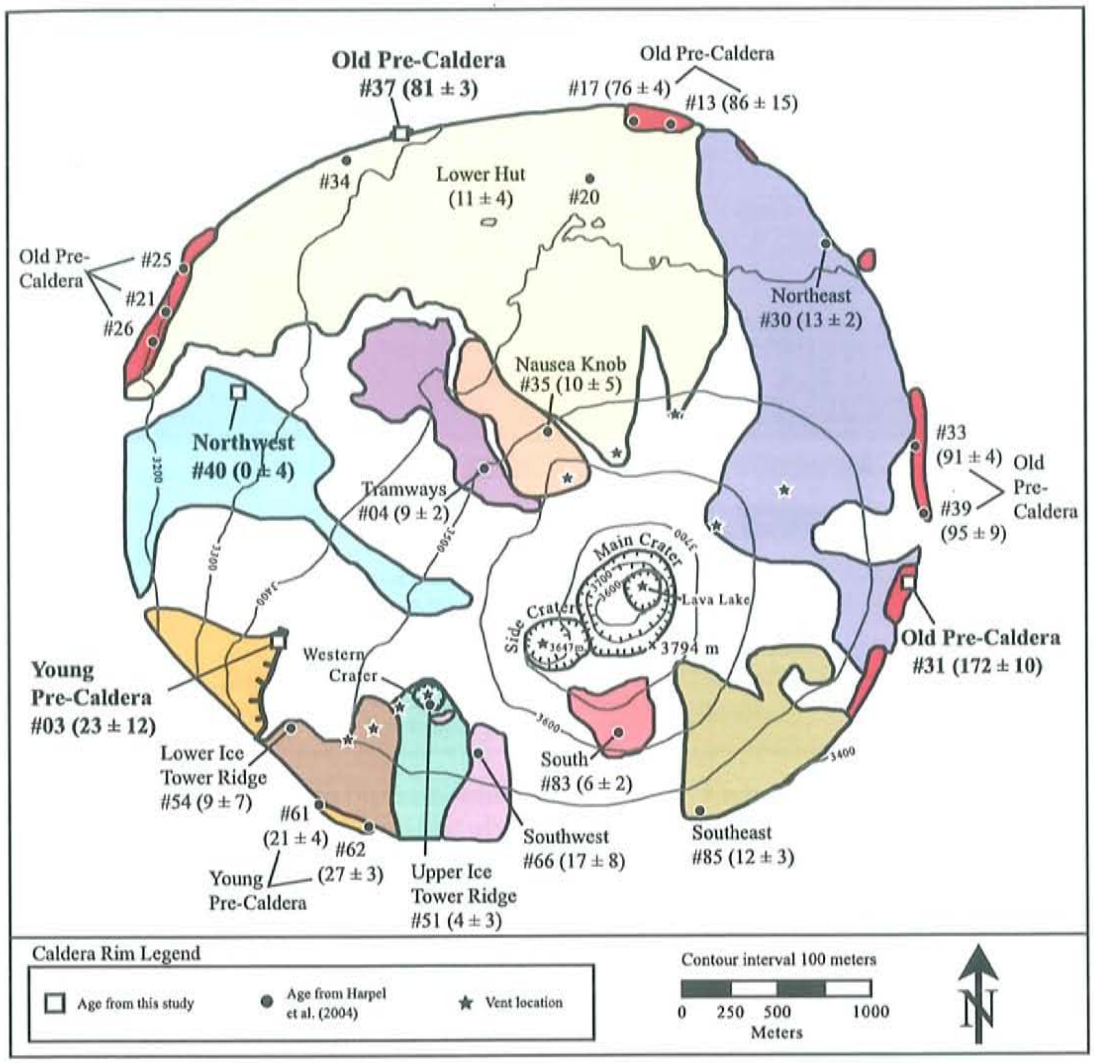

Figure 3. Geologic map of Mt. Erebus summit plateau showing topography, lava flows with ages and 2σ uncertainty (in ka), vent locations, and sample numbers and locations. Ages shown for Lower Hut and Northeast flows are weighted mean ages of three determinations each (Harpel et al., 2004). All sample numbers are prefixed by "E870" except #13 which is prefixed by "E930" and #03 and #31 which are prefixed by "E860." Map modified after Harpel et al. (2004).

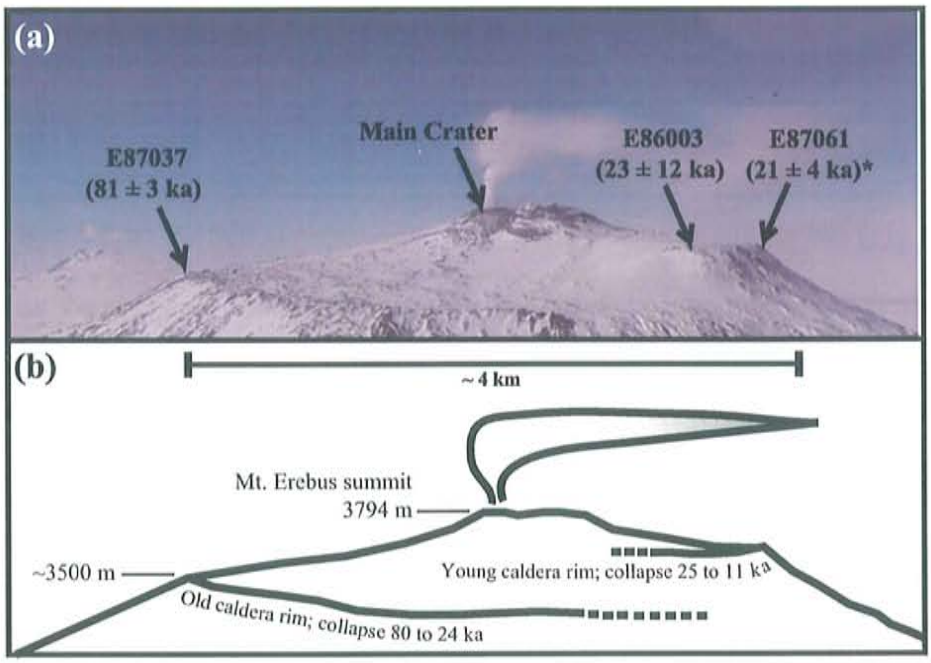

Figure 4. (a) Aerial view to the east-southeast of the Mt. Erebus summit region showing caldera collapse rims (photo modified after Harpel et al., 2004). Approximate sample locations and $^{40}Ar/^{39}Ar$ ages with 2σ uncertainty are labelled. * indicates age from Harpel et al. (2004). (b) Sketch of photo showing caldera rims and inferred collapse ages (Harpel et al., 2004).

for E87040. Our result is analytically indistinguishable (-3 ± 7 ka) and indicative of the very young age of this lava (i.e. < 4 ka). Since the two analyses are analytically indistinguishable, our preferred age for E87040 is a weighted mean of the two measurements (0 ± 4 ka; see Table 1 for details).

4.2 Bomb Peak

Bomb Peak (~1800 m elevation), on the eastern flank of Mt. Erebus (Fig. 1), is named for the abundant remnants of anorthoclase-phyric lava bombs that litter the area. The bomb remnants consist of small piles of anorthoclase crystals formed by in-situ disintegration of matrix glass that rest on trachyte lava dated to 157 ± 6 ka (Esser et al., 2004). An anorthoclase sample gave an age of 23 ± 3 ka.

The location of the vent that produced the bombs at Bomb Peak is not known. One possibility is that it originated from a flank eruption. Other flank eruptions have occurred around the same time at Three Sisters Cones (26 ± 4 ka), on the southwestern side of the volcano (Fig. 1) (Esser et al., 2004). Another possibility is that the tephra are related to an eruption from the summit region. Harpel et al. (2004) dated two local englacial ash layers to 71 ± 5 ka and 15 ± 4 ka that stratigraphically bracket 14 undated ashes and predate 19 others, showing that regular explosive activity has been occurring over the last several tens of thousands of years. Due to extensive snow and ice cover and the extreme chemical homogeneity of young (< 36 ka) Erebus eruptives (Harpel et al., 2004; Kelly, Part A; Sims et al., in prep.), it may not be possible to determine the location of the vent that produced the Bomb Peak tephra.

4.3 Ice Station

Sanidine from a trachyte lava at Ice Station (~2400 m elevation) yielded an age of 159 ± 2 ka (Table 1). Trachyte lavas on Mt. Erebus are rare compared to the basanite to phonolite Erebus Lineage lavas that comprise the vast majority of the Erebus edifice (Kyle et al., 1992). The trachyte lavas are more differentiated than those of the Erebus Lineage and have elevated $^{87}Sr/^{86}Sr$ ratios (Kyle et al., 1992). They are thought to have evolved by combined assimilation of crustal rocks and fractional crystallization (AFC), whereas the Erebus Lineage can be modeled as simple fractional crystallization sequence.

The age of the Ice Station trachyte is similar to the age of two other trachyte lavas from Bomb Peak (E82405; 157 ± 6 ka) and Aurora Cliffs (E83454; 166 ± 10 ka), as well as E86031 (172 ± 10 ka), a Pre-Caldera Erebus Lineage lava discussed above. This reinforces the point that flank volcanism and summit eruptive activity have occurred simultaneously throughout the history of Mt. Erebus (Esser et al., 2004; Harpel et al., 2004), and that lavas with vastly different petrogenetic histories have been erupted contemporaneously and within close proximity to each other (< 5 km). Why these lavas evolved by assimilating crust while Erebus Lineage lavas did not remains an open question.

5. Conclusions

Our refinement of the sample preparation procedure of Esser et al. (1997) is more effective at removing $^{40}Ar_E$-rich melt inclusions and typically results in samples of

greater purity with more concordant low-temperature age spectra steps. Careful removal of melt inclusions is critical to obtaining meaningful ages of Erebus anorthoclase.

New $^{40}Ar/^{39}Ar$ age determinations from the Erebus Volcano summit region reveal details of the area's development. One of our new dates (sample E86003, 23 ± 12 ka) confirms the correlation of and provides further evidence for the presence of a young superimposed caldera near the southwestern margin of the larger, older caldera. A sample from the north-northwestern margin of the older caldera (E87037, 81 ± 3 ka) agrees with age determinations from the northeastern quadrant of the older caldera rim (Harpel et al., 2004). Sample E86031 (172 ± 10 ka), from the east-southeastern caldera rim, is ~70 ka older than the next oldest caldera rim sample (E87039, 95 ± 9 ka; Harpel et al., 2004), which means summit area activity has been ongoing for at least 170 ka. Anorthoclase from tephra at Bomb Peak is 23 ± 3 ka, but no eruptive vent is known for the bombs. Sanidine from a trachyte at Ice Station on the southeastern flank is 159 ± 2 ka. The age is indistinguishable from trachytes at Bomb Peak (157 ± 6 ka) and Aurora Cliffs (166 ± 10 ka) (Esser et al., 2004). Trachytes may have been erupted in a single short pulse of activity at ~160ka. The trachyte lavas were erupted from the eastern periphery of Mt. Erebus at nearly the same time Si-undersaturated Erebus Lineage lava was erupted from the modern-day summit region (E86031; 172 ± 10 ka), less than 5 km away. This raises questions about how and why lavas with vastly different petrogenetic histories can be erupted in such close spatial and temporal proximity.

References

Aster, R., Mah, S.Y., Kyle, P., McIntosh, W., Dunbar, N., Johnson, J., Ruiz, M., McNamara, S., 2003. Very long period oscillations of Mount Erebus volcano, J. Geophys. Res., 108 (B11), 2522, doi:10.1029/2002JB002101.

Armstrong, R.L., 1978. K-Ar dating: Late Cenozoic McMurdo Volcanic Group and dry valley glacial history, Victoria Land, Antarctica. NZ J Geol Geophys 21, 685–698.

Caldwell, D., Kyle, P.R., 1994. Mineralogy and geochemistry of ejecta erupted from Mount Erebus, Antarctica between 1972 and 1986, In: Kyle, P.R. (ed) Volcanological and Environmental Studies of Mount Erebus, Antarctica, Antarct. Res. Ser., Am Geophys Union, Washington, D.C. 66, 147–162.

Dunbar N.W., Cashman K.V., Dupré, R., 1994. Crystallization processes of anorthoclase phenocrysts in the Mount Erebus magmatic system: evidence from crystal composition, crystal size distributions, and volatile contents of melt inclusions. In: Kyle P.R. (ed) Volcanological and environmental studies of Mount Erebus, Antarctica. Antarctic Research Series V. 66, American Geophysical Union, Washington, DC, 129–146.

Esser R.P., Kyle P.R., McIntosh W.C., 2004. $^{40}Ar/^{39}Ar$ dating of the eruptive history of Mount Erebus, Antarctica: Volcano evolution. Bull. Volcanol. 66, 671–686.

Esser R.P., McIntosh W.C., Heizler M.T., Kyle P.R., 1997. Excess argon in melt inclusions in zero-age anorthoclase feldspar from Mount Erebus, Antarctica, as revealed by the 40Ar/39Ar method Geochim Cosmochim Acta 61, 3789–3801.

Harpel, C.J., 2000. Late Quaternary eruptive history of Mount Erebus, Antarctica using $^{40}Ar/^{39}Ar$ geochronology and tephrostratigraphy. Master's Thesis, New Mexico Institute of Mining and Technology, Socorro

Harpel, C.J., Kyle, P.R., Caldwell, D.A., McIntosh, W.C., Esser, R.P., 2004. $^{40}Ar/^{39}Ar$ dating of the eruptive history of Mount Erebus, Antarctica: summit flows and caldera collapse. Bull. Volcanol. 66, 687–702.

Kelly, P., et al., in prep. Open file report, NMGRL.

Kyle P.R., 1977. Mineralogy and glass chemistry of recent volcanic ejecta from Mt. Erebus, Ross Island, Antarctica. NZ J Geol Geophys. 20, 1123–1146.

Kyle, P.R., Moore, J.A., Thirlwall, M.F., 1992. Petrologic evolution of anorthoclase phonolite lavas at Mount Erebus, Ross Island, Antarctica. J Petrol 33, 849–875.

Moore, J.A., 1986. Mineralogy, geochemistry and petrogenesis of the lavas of Mount Erebus, Antarctica. Unpublished Master's Thesis, New Mexico Institute of Mining and Technology

Moore, J.A., Kyle, P.R., 1987. Volcanic geology of Mount Erebus, Ross Island, Antarctica. Proceedings of the NIPR symposium on Antarctic Geosciences, Tokyo, Japan, Vol.1, 48–65.

Renne, P.R., Swisher, C.C., Deino, A.L., Karner, D.B., Owens, T.L., DePaolo, D.J., 1998. Intercalibration of standards, absolute ages and uncertainties in $^{40}Ar/^{39}Ar$ dating. Chemical Geology 145, 117-152.

Sims, K.W.W. et al., in prep. Radiogenic isotopic compositions of tephra from the Mount Erebus, Antarctica, lava lake from 1972 – 2004 and comparison with older lavas.

Steiger, R.H., Jaeger, E., 1977. Subcommission on geochronology: convention on the use of decay constants in geo- and cosmochronology. Earth Planet Sci Lett 36, 359–362.

Taylor, J.R., 1982. An introduction to error analysis: the study of uncertainties in physical measurements. University Science Books, Mill Valley, 1–269.

Appendix A. Sample Information

Tephra

Thirty-two phonolite volcanic bombs were selected for study. All of the bombs were erupted from the summit magma lake or associated vents between December 1972 and January 2004. All the bombs were collected from within the main summit crater or around the crater rim. All of the bombs were rapidly cooled during eruption and contain large (up to ~10 cm) anorthoclase feldspar crystals (up to ~30% by volume) and smaller (cm to sub-mm size), much less abundant pyroxene, olivine, titanomagnetite, fluoroapatite, and pyrrhotite crystals in a highly vesicular glass matrix.

The bomb samples had a fresh appearance and showed no signs of alteration or deposition of salts from exposure to the volcanic plume. The plume which is continuously emitted from the magma lake and surrounding fumaroles is acid and has been observed to alter materials (e.g. rocks, snow, clothing, equipment) on short timescales (< 1 – 2 weeks). Some bomb samples were collected immediately after eruption while still hot and the exact time and date of eruption are known. Other samples were collected based on their fresh appearance and an exact date of eruption is not known. These samples were erupted at most one month prior to collection based on their unaltered condition. The sample suite represents a temporally accurate, nearly complete annual quenched record of magma lake composition from December 1972 to December/January 2003/2004.

Table A.1. Tephra sample information

Field Sample #	Eruption date Year	Month	Day	Notes
25724	1972	DEC		26 Dec 72. Recent (< 2 weeks old)
25721	1974	DEC		Collected Dec 1974
2E2	1974	DEC	18	18 Dec 1974 ~1200 hot on crater floor
25723	1975	DEC		Collected Dec 1975
77016	1977	NOV		28 Nov 1977 <2 weeks old
78325	1977	OCT-NOV		Oct-Nov 1977 (collected 25 Dec 1978)
79302	1979	DEC	26	Erupt ~ 1138 26 Dec 1979
80300	1980	NOV		Collected Nov 1980
81401	1981	NOV-DEC		5 Dec 1981 (< 3 weeks old)
82416	1982	DEC		Collected 12/22/1982
83220	1983	DEC		15 Dec 1983 <2 weeks old
84505	1984	DEC		Collected Dec 1984 <3 weeks old
84501	1984	DEC		Collected Dec 1984 near old hut
85010	1985	DEC	17	Erupt am 17 Dec 1985
85009	1985	DEC		Dec-85
86022-1	1986	DEC	22	Erupt 22 Dec 1986
88104	1988	DEC		Collected Dec 88 - bomb from crater
89001	1989	DEC		Dec-89
91101	1990/91	DEC-JAN		Collected 14 Jan 1991 <2 months old
Er 92KS	1992			Collected by K.W.W. Sims
PK 92101	1992	OCT-DEC		Collected Dec 1992 Fresh (<3 months)
93102	1993	DEC		Collected 7 to 14th Dec 93
Er 96	1996			Collected by K.W.W. Sims
E96-01	1996	DEC		Collected Dec 1996
Er 97	1997			Collected by K.W.W. Sims
97018	1997	DEC	21	Erupt 12/21/1997
Er 99	1999			Collected by K.W.W. Sims
1999 bomb	1999	DEC		Collected Dec 1999
Y2K	2000			Collected by J. Crain
DEC 2000	2000	DEC		Collected Dec 2000
E2001	2001	DEC		Collected Dec 2001
Jan 2004	2003/04	DEC-JAN		Collected crtr rim 17 Jan 2004: erupt late Dec/early Jan

Lavas

Thirteen lava samples were examined for comparison with the historic tephra samples. Eleven of the lava samples are phonolites, were collected from the summit plateau, and are younger than 17±8 ka (Harpel et al, 2004)(Table A.2.). Two lava samples from other localities were also studied: a phonolite (83452) of unknown absolute age from Bomb Peak and one tephriphonolite (243±10 ka; Esser et al., 2004) from Turks Head.

Complete sample descriptions and details on the $^{40}Ar/^{39}Ar$ age-dating results of these samples are given by Esser (1996), Harpel (2001; NMT thesis), Esser et al. (2004), and Harpel et al (2004). See Moore (1986) and Kyle et al. (1992) for description and analysis of 83452.

Table A.2. Lava sample information

Sample #	$^{40}Ar/^{39}Ar$ Age (ka)	Rock Classification (TAS)	Flow
E87040	0±4[c]	phonolite	Northwest
E87051	4±3[a]	phonolite	Upper Ice Tower Ridge
E87083	6±2[a]	phonolite	South
E87054	9±7[a]	phonolite	Lower Ice Tower Ridge
E87004	9±2[a]	phonolite	Tramways
E87035	10±5[a]	phonolite	Nausea knob
E87034	11±8[a]	phonolite	Lower Hut
E87020	11±4[a]	phonolite	Lower Hut
E87085	12±3[a]	phonolite	Southeast
E87030	13±2[a]	phonolite	Northeast
E87066	17±8[a]	phonolite	Southwest
83452		phonolite	Bomb Peak
AW82015	243±10[b]	tephriphonolite	Turks Head

[a]Harpel et al, (2004) Bull of Volc 66: 687-702
[b]Esser et al, (2004) Bull of Volc 66: 671-686
[c]Kelly, Part B

Appendix B. Sample Preparation and Analytical Procedures

Sample Preparation

Lava Samples for X-ray Fluorescence Mass Spectrometry (XRF) Major-Element analysis and ICP-MS Trace Element Analysis

Lava samples prepared by Moore (1986) and Caldwell (1989) were used. The lavas contain abundant coarse phenocrysts, so to best approximate true bulk chemical composition 2 - 4 kg's of each sample were crushed in a jaw crusher to a size of ~10 microns. See Moore (1986) and Caldwell (1989; unpublished independent study, NMT) for full sample preparation details. All of the powders were vigorously shaken before aliquots were removed to assure homogeneity.

Tephra Samples for Inductively Coupled Plasma Mass Spectrometry (ICP-MS) Trace Element Analysis

Matrix glass from tephra was manually crushed in a cloth sample bag to a small size (~ 1mm); then a strong hand magnet was run over the shards several times to remove Fe-rich minerals. About 200mg of sample was then hand-picked under a binocular microscope to remove any remaining crystals.

Tephra samples for Electron Microprobe Analysis

Matrix glass and groundmass minerals were prepared by manually crushing tephra to a size suitable for analysis (~mm-sized shards) in a cloth sample bag. Titanomagnetite crystals were separated by covering a strong hand magnet with weighing paper and passing it over crushed tephra shards. The magnetic material was removed from the

magnet by removing the weighing paper. Anorthoclase megacrysts were sectioned perpendicular to the c-axis using a rock trim saw. All samples were then swathed in epoxy to make a disc, polished, and carbon-coated for analysis.

Anorthoclase Feldspar and Matrix Glass for Oxygen Isotope Analysis

Fifty milligram aliquots of tephra matrix glass were prepared for oxygen isotope analysis according to the same method used to prepare samples for trace element ICP-MS analyses. Anorthoclase feldspars from tephra and one lava were prepared in a method similar to that devised by Esser et al. (1996) for $^{40}Ar/^{39}Ar$ age dating. This method seeks to remove melt inclusions and other impurities from feldspars by crushing to a fine size and leaching in hydrofluoric acid. Anorthoclase from tephra were simply picked out of the matrix glass and then crushed. The lava containing anorthoclase was crushed and sieved to 60 – 150 mesh, separated from matrix using a Franz isodynamic magnetic separator (1° slide, 11° side, 0.85 – 0.90 A), and floated in heavy liquid (d = 3.0) to remove apatite and other minerals. The tephra anorthoclase samples were crushed using a ceramic mortar and pestle to 28 – 35 mesh (600 – 425 μm) to expose melt inclusions. Both the tephra and lava anorthoclase were then leached for one hour in a 15% reagent-grade solution of HF in an ultrasonic bath. Two grams of anorthoclase from tephra yielded ~50 – 200 mg of clean sample while ~250 g of crushed and sieved lava yielded ~2.5 g of clean anorthoclase.

Analytical Procedures

X-ray Fluorescence Spectrometry

Major element analyses of lavas were made with a Rigaku XRF spectrometer at New Mexico Tech. Approximately one gram of each sample was mixed with Li-tetraborate-Li metaborate flux, fused in a Pt-Au crucible, and poured into a mold to make a glass disc. Calibration was made using a large suite of international standards.

ICP-MS Trace Element Analysis

Trace element concentrations of matrix glass separates from tephra were measured on a VG PlasmaQuad Excell Inductively Coupled Plasma-Mass Spectrometer at Boston University by Dr. Terry Plank. Replicate analyses of samples were made to assess analytical precision (see Table D.8.3.).

Electron Microprobe Analysis

All electron microprobe analyses of phenocrysts, groundmass minerals, matrix glass, and melt inclusions were performed using the Cameca SX-100 3-spectrometer electron microprobe at New Mexico Tech. A 1 μm beam with 15.0 kV accelerating potential and 20 nA current was used for olivine, pyroxene, and pyrrhotite mineral analyses. A 5 μm beam was used for fluoroapatite analyses and a 10 μm beam was used for anorthoclase analyses at 15.0 kV and 20 nA. Matrix glass and melt inclusions were analyzed using 20 or 25-micron beams at 15.0 kV and 10 nA to avoid volatilization of Na. Natural mineral standards were used for instrument calibration and general precision assessment (see Table D.1.1.). Natural mineral reference materials were used when possible to assess precision of analyses of unknowns of similar composition. Precision of Sr, Ba, and Fe analyses in anorthoclase were determined by counting statistics. Replicate analyses were

made to assess analytical precision of titanomagnetite (Table D.4.1) and matrix glass (Table D.8.1). Analyses with totals less than 98 wt% and greater than 101% were rejected. Structure formulas were calculated using standard methods for titanomagnetites and feldspars to assure analysis quality.

Oxygen Isotope Measurements

Oxygen isotope measurements were made on a Thermo Finnigan Delta Plus XP isotope ratio mass spectrometer at New Mexico Tech. Calibration was made using reference gasses. An in-house standard, Capitan Quartz (Campbell, personal communication 2005), and NBS-28 were used for precision assessment (Table E.1). All samples were run in duplicate to assess precision (Table E.2).

Appendix C. Lava bulk rock analyses

Table C.1. Major element bulk lava analyses by XRF

Sample	AW82015	83452	E87066	E87030	E87085	E87020	E87034	E87035	E87004	E87054	E87083	E87051	E87040	97018*
age	243±10[6]		17±8[3]	13±2[4]	12±3[3]	11±4[4]	11±8[1]	10±5[3]	9±2[4]	9±7[1]	6±2[4]	4±3[3]	1±5[2]	21-Dec-97
TAS class.	tephriphon	phonolite	phonolite	phonolite	phonolite	phonolite	phonolite	phonolite	phonolite	phonolite	phonolite	phonolite	phonolite	phonolite
flow	Turks Head	Bomb Peak	Southwest	Northeast	Southeast	Lower Hut	Lower Hut	Nausea knob	Tramways ce	Tower Ridge	South ce	Tower Ridge	Northwest	
SiO_2	54.39	55.07	56.02	56.49	56.59	56.05	55.80	56.72	57.64	56.22	56.15	55.97	56.77	56.23
TiO_2	1.61	1.38	0.98	1.08	1.13	1.11	1.10	1.00	0.89	1.09	1.00	1.11	0.96	0.99
Al_2O_3	18.94	18.42	19.88	19.73	19.88	19.71	19.62	19.94	20.27	19.60	19.38	19.61	20.11	19.82
Fe_2O_3	7.60	7.19	5.22	5.81	6.19	5.92	5.87	5.27	4.68	5.76	5.82	5.98	4.97	5.35
MnO	0.24	0.27	0.21	0.24	0.26	0.24	0.24	0.23	0.19	0.23	0.24	0.24	0.20	0.23
MgO	1.55	1.39	0.91	1.03	1.03	0.99	0.98	0.94	0.83	0.89	0.97	1.03	0.85	0.88
CaO	4.17	3.28	2.86	2.90	2.74	2.79	2.78	2.93	3.00	2.86	2.75	2.82	2.91	2.68
K_2O	3.87	4.28	4.40	4.46	4.71	4.59	4.58	4.38	4.21	4.47	4.45	4.43	4.33	4.51
Na_2O	6.99	7.70	8.13	8.05	8.18	8.32	8.35	8.10	8.02	8.16	8.10	8.11	8.10	8.38
P_2O_5	0.72	0.56	0.42	0.47	0.48	0.47	0.48	0.43	0.39	0.46	0.44	0.48	0.41	0.41
L.O.I.	-0.05	-0.16	-0.15	-0.18	-0.08	0.10	0.33	-0.11	-0.12	-0.21	-0.14	-0.14	-0.09	-0.16
Total	100.03	99.38	98.88	100.08	101.10	100.29	100.13	99.83	100.00	99.53	98.96	99.65	99.52	99.61

L.O.I. = Loss on ignition

Table C.2. Trace element bulk lava analyses by ICP-MS

Sample	AW82015	83452	E87066	E87030	E87085	E87020	E87034	E87035	E87004	E87054	E87083	E87051	E87040	97018*
TiO_2 (%)	1.622	1.393	.997	1.219	1.063	1.115	1.313	1.111	.902	1.154	1.024	1.12	.991	
Li	19.89	22.23	17.82	23.21	26.3	27.61	30.58	26.43	19.92	24.22	20.24	22.68	21.11	
Be	6.73	8.18	8.66	9.64	9.35	9.5	10.8	9.24	7.07	8.7	8.29	8.82	7.78	
Sc	4.6	5.1	3.1	3.3	3.4	3.2	4.	3.1	2.5	3.6	3.5	3.1	3.1	
V	19.8	29.5	4.97	7.79	6.08	5.88	7.31	6.19	5.05	7.72	5.66	6.88	5.2	8.5
Cr		2.												
Co	18.2	21.	10.4	10.1	9.06	10.2	13.9	12.6	18.2	9.24	8.91	10.7	11.	
Ni	1.31	3.51	1.9	.612	.643	.803	.976	.88	.607	.58	.758	.543	.515	4.5
Cu	11.2	12.8	6.84	5.63	5.08	5.38	6.19	5.61	4.28	5.35	5.13	5.06	5.01	4.5
Zn	122.	150.	115.	138.	128.	129.	151.	136.	97.5	128.	128.	128.	107.	127.
Ga	17.9	20.6	21.9	25.6	22.5	22.1	27.1	24.3	22.9	22.7	22.6	22.	21.7	27.2
Rb	79.5	92.3	95.8	107.	104.	107.	119.	100.	80.8	99.2	96.3	100.	90.	107
Sr	1196.	764.	1028.	939.	726.	780.	917.	1145.	1234.	941.	886.	854.	1120.	914
Y	49.	63.8	52.9	62.4	62.2	60.5	67.3	57.2	44.9	58.2	58.7	59.3	50.4	55.9
Zr	791.	967.	969.	1092.	1083.	1084.	1216.	1018.	799.	1007.	983.	1024.	907.	1016
Nb	207.	250.	252.	286.	281.	284.	320.	266.	208.	264.	257.	267.	236.	261
Cs	1.12	1.25	1.29	1.47	1.44	1.48	1.62	1.35	1.08	1.35	1.31	1.39	1.23	
Ba	964.	1007.	1124.	1075.	881.	889.	1037.	1271.	1346.	1103.	1141.	989.	1224.	1129
La	108.	132.	118.	136.	133.	130.	147.	127.	103.	127.	128.	129.	114.	
Ce	212.	255.	226.	259.	255.	249.	279.	241.	193.	242.	246.	247.	215.	
Pr	23.24	28.78	23.84	28.32	28.02	26.61	29.82	25.52	19.71	26.37	26.49	26.6	22.6	
Nd	83.7	100.	82.5	96.3	93.5	90.9	102.	88.1	70.2	89.9	90.4	90.8	79.3	
Sm	14.23	17.27	13.72	16.08	15.77	15.27	17.08	14.72	11.69	15.14	15.17	15.34	13.12	
Eu	4.06	4.58	4.12	4.44	3.97	3.91	4.45	4.55	4.26	4.31	4.34	4.11	4.24	
Gd	11.3	13.7	10.8	12.7	12.5	12.	13.4	11.6	9.13	12.1	12.	12.	10.4	
Tb	1.67	2.07	1.67	1.94	1.92	1.86	2.07	1.79	1.41	1.85	1.85	1.84	1.6	
Dy	9.24	11.6	9.52	11.	10.8	10.7	11.9	10.2	8.09	10.5	10.4	10.6	9.07	
Ho	1.77	2.26	1.88	2.16	2.14	2.12	2.34	2.03	1.58	2.06	2.06	2.08	1.8	
Er	4.77	6.04	5.23	5.95	5.9	5.8	6.47	5.55	4.39	5.63	5.59	5.67	4.91	
Yb	4.31	5.36	4.86	5.52	5.45	5.39	5.96	5.23	4.07	5.15	5.09	5.25	4.56	
Lu	.685	.844	.757	.854	.859	.851	.937	.809	.64	.805	.805	.82	.716	
Hf	15.7	19.8	19.2	21.5	21.4	21.4	24.	20.4	15.8	20.2	19.4	20.3	17.9	
Ta	12.3	14.8	14.7	16.3	16.1	16.3	18.5	15.4	12.2	15.5	14.7	15.5	13.7	
Pb	4.7	5.14	4.91	5.29	5.2	5.28	5.95	5.36	4.2	5.08	4.86	4.99	4.75	5.8
Th	19.8	23.	24.	26.2	26.6	26.5	29.6	25.1	19.5	24.7	23.3	25.1	22.	26.4
U	5.68	6.54	6.85	7.55	7.42	7.52	8.45	7.39	5.5	7.11	6.66	7.11	6.32	6.7

*Average of two major and trace element whole-rock analyses of bomb 97018 by XRF (Eschenbacher, 1998). Replicate sample agreement is <1% for major elements and <2% for most trace elements

[6] $^{40}Ar/^{39}Ar$ ages with 2σ uncertainty by Harpel et al. (2004) Bull of Volc 66: 687-702

[1-4] $^{40}Ar/^{39}Ar$ ages with 2σ uncertainty by Esser et al. (2004) Bull of Volc 66: 671-686

Table C.3. Minor and trace element bulk rock analyses of summit lava suite by XRF (P. Kyle)

Sample	TIO2 (wt.%)	FE2O3	MNO	V (ppm)	Cr	Ni	Cu	Zn	Ga	As	Rb	Sr	Y	Zr	Nb	Mo	Ba	W	Pb	Th	U
E86001.1	0.92	6.16	0.262	3.5	6.8	5.4	8.7	151.8	29.7	2.3	111.3	677.2	67.7	1072.9	271.7	12.3	1101.4	56.4	5.0	26.5	7.1
E86001.2	0.92	6.15	0.262	3.2	5.8	4.9	3.3	151.1	29.3	3.1	111.0	682.0	66.6	1069.5	270.3	12.3	1099.2	55.3	5.3	26.6	6.6
E86002	0.91	5.25	0.206	7.9	27.8	5.8	4.9	122.4	27.7	2.9	98.5	984.3	54.9	938.3	238.3	11.9	1286.6	78.0	5.4	25.4	5.8
E86003	0.87	6.02	0.251	3.6	10.4	4.3	5.3	147.8	29.6	1.0	112.6	682.6	67.5	1071.1	268.5	11.2	1099.1	55.2	5.9	27.4	7.0
E86011	0.91	5.18	0.205	6.4	13.5	4.7	4.8	121.3	27.3	2.6	107.8	858.8	56.9	1019.8	260.1	12.2	1051.8	62.9	5.4	26.7	7.0
E86012	0.50	4.63	0.079	87.9	98.3	11.4	6.2	60.7	14.6	4.0	54.5	178.9	24.4	182.0	8.2	1.8	418.1	197.4	15.1	12.0	3.2
E86024	0.89	5.37	0.22	7.7	33.7	6.8	6.0	126.7	29.4	3.2	107.4	822.8	61.0	1019.3	256.5	10.8	1111.6	92.5	4.8	25.9	7.5
E86025	1.15	6.08	0.194	5.8	22.2	5.4	8.2	112.2	25.5	3.9	106.0	1034.1	48.6	937.1	226.8	11.4	932.5	90.6	5.9	26.0	7.2
E86026	0.96	5.53	0.223	9.4	11.3	4.7	3.3	128.3	27.7	2.5	110.0	841.9	58.2	1050.0	269.1	13.0	1050.0	131.9	6.2	27.1	6.9
E86029	1.09	5.45	0.185	15.6	10.3	5.0	5.0	102.2	27.3	2.5	103.7	922.9	52.4	921.8	233.4	11.5	1001.1	59.3	6.1	24.3	6.7
E86030	0.93	5.31	0.223	6.2	6.9	3.8	5.2	134.6	28.6	3.0	109.4	872.8	57.6	1038.9	265.7	12.4	1087.5	78.4	5.8	27.6	7.1
E86031.1	1.22	5.96	0.185	11.4	10.0	4.5	6.4	102.1	24.4	2.6	114.2	862.6	44.7	888.9	221.7	12.3	849.8	151.8	5.7	26.6	6.6
E86031.2	1.29	6.3	0.194	11.9	8.7	3.6	6.2	106.9	24.5	1.3	120.1	756.3	48.2	937.1	235.0	12.8	807.5	143.6	7.8	27.7	6.7
E87001	0.97	5.47	0.218	8.4	11.6	4.5	9.0	127.0	28.2	2.8	107.8	853.5	58.5	1040.2	267.6	13.6	1029.8	125.4	5.9	26.0	6.4
E87002	0.92	5.33	0.211	5.2	11.7	4.9	11.0	123.0	27.6	4.0	104.4	917.8	56.6	1004.2	256.8	12.8	1164.8	126.5	5.1	25.1	6.1
E87003	0.92	5.26	0.206	3.7	12.2	4.4	6.5	122.3	27.2	2.9	103.5	931.8	55.4	989.4	253.2	12.4	1205.3	127.5	5.6	24.5	6.3
E87004	0.78	4.46	0.171	7.1	13.2	4.5	5.6	102.0	26.2	3.5	87.1	1175.3	47.4	827.3	208.4	9.9	1464.5	104.4	4.1	20.3	6.7
E87005	0.93	5.35	0.211	8.4	10.9	5.0	12.3	133.8	27.4	3.4	103.9	926.6	56.1	993.4	253.0	12.3	1151.4	106.3	5.9	24.4	5.9
E87007	0.92	5.29	0.21	6.6	17.7	5.2	11.1	133.3	27.6	3.1	102.4	952.8	56.0	974.9	249.1	12.5	1206.9	124.5	5.1	24.0	6.7
E87008	0.89	5.1	0.201	3.4	7.2	4.8	27.5	119.7	27.4	3.9	99.7	997.9	53.6	950.0	242.3	12.0	1219.4	115.7	4.6	22.5	7.0
E87009	0.91	5.15	0.204	6.0	13.5	4.2	8.5	119.4	26.9	3.1	99.4	984.3	54.7	949.6	242.6	12.4	1220.9	94.8	5.4	23.2	6.1
E87010	0.91	5.17	0.202	6.8	11.1	5.1	6.8	120.6	26.7	3.9	100.4	964.1	55.3	964.4	246.6	12.1	1224.5	120.7	4.6	23.2	5.9
E87011	0.9	5.23	0.205	6.3	18.2	5.2	8.2	120.5	27.9	6.2	101.7	942.2	56.1	979.5	247.8	12.7	1208.3	98.0	4.9	24.0	6.6
E87012	0.92	5.32	0.214	7.3	12.7	4.3	6.8	127.1	27.6	3.1	104.0	914.5	57.4	1000.9	254.5	12.1	1160.9	86.4	5.9	25.3	6.3
E87013	0.91	5.2	0.201	8.0	21.9	5.9	10.8	118.9	27.5	3.8	100.1	973.5	54.6	956.8	243.3	11.2	1222.4	81.3	4.8	24.3	6.4
E87014	0.97	5.63	0.22	10.7	6.9	4.3	9.8	130.2	28.4	2.8	108.7	831.6	61.4	1039.3	265.1	11.7	1062.1	72.2	5.7	27.1	5.8
E87015	1.07	5.47	0.186	17.9	12.5	4.5	15.5	109.6	26.7	2.6	113.6	828.7	54.4	1000.7	254.0	11.3	875.0	59.4	6.6	26.6	6.7
E87016	0.88	5.04	0.196	10.0	7.4	4.5	4.7	116.5	27.3	4.1	101.7	984.3	54.5	964.1	245.0	11.4	1165.9	63.8	5.4	25.2	7.2
E87017	1.06	5.29	0.184	13.5	1.0	3.7	8.0	106.6	27.4	3.6	108.2	900.6	52.4	958.7	243.8	11.5	932.0	68.6	5.6	25.0	6.9
E87018	0.94	5.39	0.21	8.5	12.3	4.1	11.7	126.2	28.2	3.2	109.3	861.0	53.7	1043.7	266.5	12.2	1050.1	63.8	5.9	26.5	7.5
E87019	0.91	5.26	0.208	10.1	13.2	5.4	5.9	121.6	27.9	2.9	105.7	905.8	57.7	1008.9	258.6	11.4	1062.7	69.7	5.6	25.4	7.0
E87020	0.94	5.47	0.214	5.2	11.4	4.4	10.7	130.4	27.2	2.9	113.4	791.0	60.0	1083.1	277.7	12.5	911.9	63.0	5.0	26.9	7.6
E87021	1.1	5.97	0.198	11.9	4.5	4.5	8.6	115.8	26.1	2.9	108.6	992.8	50.9	955.6	234.5	9.3	922.4	71.4	6.9	25.8	5.9
E87022	0.99	5.65	0.226	10.2	12.4	3.9	6.8	131.1	28.2	2.6	110.8	841.3	60.8	1059.2	271.2	12.0	1013.6	75.0	5.3	27.0	7.9
E87023	1.13	5.99	0.188	9.8	10.4	5.0	9.2	108.7	26.9	3.0	105.9	1042.7	49.6	937.4	226.4	10.3	934.2	73.3	6.4	25.8	5.5
E87024	1.08	5.85	0.191	10.7	6.9	3.9	8.3	117.1	26.6	2.9	109.1	994.9	51.5	953.6	230.4	10.3	944.6	57.1	7.5	26.3	6.7
E87025	1.11	5.95	0.194	10.6	12.6	4.2	8.0	110.9	26.6	1.7	109.4	986.0	51.5	961.0	235.1	10.5	922.7	52.9	6.6	26.6	6.7
E87026	1.11	5.94	0.186	9.0	23.9	6.1	14.3	110.5	26.7	2.9	105.0	1042.0	49.7	936.4	226.9	9.5	909.1	57.4	6.0	25.3	6.4
E87027	0.9	5.17	0.205	8.6	18.3	4.8	16.2	120.4	27.8	3.2	103.8	952.8	55.2	985.7	251.7	11.4	1134.0	69.6	5.1	25.2	5.7
E87028	0.9	5.16	0.202	11.0	11.5	5.2	8.6	121.2	26.7	3.1	100.8	967.5	55.3	961.7	245.5	11.3	1214.6	69.4	5.9	24.8	7.0
E87029	0.88	5.18	0.203	7.7	21.7	4.6	7.8	118.1	27.2	3.6	98.2	1007.3	55.9	938.8	237.9	11.2	1271.4	64.4	5.0	22.3	6.9
E87030	0.95	5.47	0.217	7.9	18.9	5.7	7.2	124.3	28.7	3.0	105.1	896.9	59.9	1009.8	257.3	11.8	1065.1	51.5	4.3	24.8	6.4
E87031	1.01	5.11	0.176	13.5	8.6	4.3	8.0	101.0	26.9	3.6	108.8	885.3	51.5	962.5	243.6	11.6	908.4	55.5	5.3	24.1	7.2
E87032	0.9	5.16	0.201	8.3	10.8	5.5	9.8	118.1	27.4	3.5	99.0	981.0	56.8	947.6	240.8	11.2	1253.3	67.4	4.0	21.7	6.0
E87033	1.05	5.35	0.216	12.6	7.7	5.0	10.5	123.6	29.1	2.2	113.1	710.1	61.4	1032.8	267.1	11.4	903.0	68.2	6.2	24.4	6.3
E87034	0.93	5.47	0.213	8.6	7.8	5.0	10.1	130.5	28.3	3.4	112.4	795.7	60.2	1071.9	273.0	12.8	894.7	73.5	5.3	26.0	7.3
E87035	0.86	5	0.215	7.2	16.4	3.6	8.5	125.8	27.0	4.1	98.1	1019.4	53.9	939.2	237.1	10.8	1239.5	70.6	4.9	22.6	6.3

Table C.3. *continued*

Sample	TiO2 (wt.%)	FE2O3	MNO	V (ppm)	Cr	Ni	Cu	Zn	Ga	As	Rb	Sr	Y	Zr	Nb	Mo	Ba	W	Pb	Th	U
E87036	0.95	5.39	0.218	90	74	47	75	130 4	27 9	3 9	107 3	881 6	58 0	1028 7	262 3	12 1	1064 9	59 5	4 3	23 8	6 8
E87037	1 05	5 97	0 231	139	70	4 4	6 8	138 9	28 4	3 0	116 2	678 6	63 9	1047 3	270 5	11 7	881 2	51 3	6 1	24 6	6 5
E87038	0 96	5 76	0 232	64	9 5	4 9	6 7	136 8	28 3	2 5	110 4	785 8	65 0	1066 4	270 9	11 9	1098 0	59 0	6 8	25 3	7 5
E87039	1 02	5 25	0 186	169	1 8	4 5	6 6	110 3	27 9	3 9	114 8	815 4	54 3	1000 8	256 6	10 7	854 8	51 8	6 7	26 2	6 8
E87040	0 86	4 85	0 189	10 6	8 4	4 2	8 3	110 6	26 4	4 3	95 7	1074 9	51 3	905 6	229 7	11 2	1268 4	52 0	4 4	22 0	6 6
E87041	0 93	5 39	0 212	130	9 1	4 5	4 2	124 9	27 9	3 6	101 4	933 0	57 9	982 0	250 0	11 5	1197 7	55 4	4 6	23 4	8 2
E87042	0 93	5 26	0 206	6 5	4 4	4 1	5 1	122 4	26 6	2 5	104 6	932 6	57 0	1002 3	255 6	11 8	1133 8	59 2	5 5	23 7	7 2
E87043	1 54	8 23	0 225	19 4	8 3	4 4	15 5	135 1	27 5	3 7	105 1	817 3	61 7	844 8	199 3	9 4	982 2	47 6	7 6	22 5	6 1
E87044	1 57	8 88	0 212	61 2	23 3	7 2	11 2	100 2	25 2	4 0	83 9	945 6	53 5	572 5	134 5	5 0	953 8	42 6	5 8	16 5	4 6
E87045	1 61	8 39	0 233	22 1	9 0	4 2	13 1	137 4	26 7	3 6	101 8	855 4	62 1	837 3	199 6	9 6	979 4	49 2	7 5	21 4	5 4
E87046	0 97	5 66	0 225	8 2	4 0	4 2	3 5	132 4	28 5	2 4	108 8	841 9	61 4	1041 6	266 3	12 4	1038 6	57 9	4 6	24 4	7 2
E87047	0 92	5 22	0 206	9 2	6 2	3 9	3 0	122 5	28 5	3 7	103 5	948 7	55 9	996 2	253 3	11 9	1160 1	71 8	4 9	22 9	6 8
E87048	0 9	5 08	0 2	12 5	7 5	4 0	4 1	116 8	27 4	4 1	100 7	1000 2	54 6	959 9	244 8	11 7	1182 8	53 0	4 5	23 2	6 5
E87049	0 99	5 66	0 228	10 4	9 8	4 1	6 0	132 8	28 3	3 8	113 7	794 6	61 7	1091 8	279 9	11 6	936 0	48 2	4 6	26 1	6 7
E87050	0 82	5 1	0 212	9 8	8 6	5 1	4 5	129 1	28 5	3 0	104 9	852 3	59 8	1010 8	255 7	12 0	1227 2	55 8	5 8	23 6	6 7
E87051	0 95	5 56	0 22	11 8	6 1	3 1	6 8	127 9	28 2	2 9	108 2	845 7	60 6	1038 7	264 8	12 0	1042 1	53 2	4 3	25 6	7 2
E87052	0 97	5 64	0 221	8 7	8 2	4 9	4 7	128 6	28 6	2 8	110 7	833 1	63 4	1061 9	270 5	12 3	1015 8	49 0	5 7	25 7	7 1
E87053	0 86	4 89	0 191	9 3	4 8	3 2	6 8	112 6	27 5	3 6	97 0	1067 5	52 0	912 9	231 9	10 7	1256 3	55 0	4 6	22 9	6 4
E87054	0 91	5 27	0 206	9 3	5 1	3 9	8 2	122 3	27 8	3 8	102 4	941 7	56 7	974 8	247 8	11 7	1232 1	56 2	3 7	22 7	7 1
E87055	0 98	5 84	0 233	4 0	3 4	3 3	5 8	137 4	28 6	2 9	117 1	709 2	63 1	1121 6	287 5	13 0	879 8	52 2	6 4	26 5	7 5
E87056	0 92	5 42	0 214	10 6	7 2	3 9	4 0	125 1	27 9	3 1	105 9	878 2	58 8	1015 1	258 2	12 3	1182 8	55 4	4 9	23 8	7 4
E87057	1	5 77	0 232	8 3	6 1	4 5	5 6	131 5	28 2	2 8	111 1	800 4	61 5	1060 7	272 2	12 2	944 7	46 1	4 8	23 7	6 0
E87058	0 89	5 25	0 208	11 4	10 0	4 1	5 1	122 6	27 6	2 9	103 1	911 0	56 3	986 3	251 9	12 3	1207 5	57 9	5 3	22 2	6 6
E87059	0 93	5 36	0 21	7 0	5 7	5 1	5 8	123 7	28 2	2 4	101 9	936 0	56 1	973 6	248 2	11 7	1213 4	56 6	5 0	22 0	7 1
E87060	0 95	5 55	0 221	6 8	4 6	3 9	4 8	129 4	29 1	2 7	110 7	807 3	60 7	1065 1	271 3	12 1	1067 0	47 2	5 6	24 3	6 3
E87061	0 78	5 23	0 219	2 4	4 4	4 1	3 2	126 7	27 5	2 4	96 1	869 2	57 9	913 8	228 9	10 9	1457 0	49 5	5 6	21 1	6 2
E87062	0 82	5 53	0 234	5 3	12 3	4 5	4 5	134 2	28 4	2 6	101 4	820 5	60 1	968 0	243 2	11 7	1311 1	50 0	5 4	21 7	6 2
87062#2	0 85	5 68	0 238	6 7	8 2	5 0	12 9	138 3	27 8	3 1	102 8	791 1	61 8	968 7	248 7	11 9	1287 5	63 2	4 6	21 6	6 7
E87063	0 89	5 29	0 209	11 7	7 1	5 1	4 2	124 5	28 3	2 2	104 6	892 8	57 3	1002 0	254 9	11 3	1181 5	49 3	5 4	22 2	6 8
E87064	0 95	5 55	0 22	8 6	7 7	3 9	5 2	130 2	28 8	1 7	112 7	783 1	61 3	1088 6	278 0	11 9	968 5	50 2	6 2	25 2	7 2
E87065	0 93	5 52	0 218	5 9	12 7	5 2	6 7	128 5	28 3	1 5	111 4	793 1	60 9	1075 9	274 1	12 3	1020 4	41 8	6 2	24 0	7 8
E87066	0 89	5 07	0 2	8 6	3 7	4 1	5 5	119 0	26 7	3 6	100 6	997 2	53 7	959 9	244 2	10 9	1190 5	60 3	4 2	21 7	5 7
E87067	0 81	4 55	0 178	9 1	4 6	4 1	9 2	104 4	25 8	3 1	89 8	1166 4	47 9	841 8	212 8	9 9	1361 9	52 4	4 7	19 5	5 0
E87068	0 82	4 77	0 187	3 3	9 0	4 5	6 3	110 3	27 3	3 6	93 0	1056 6	51 3	876 9	221 3	10 7	1368 2	52 3	5 1	19 8	6 5
E87069	0 91	5 46	0 215	10 4	5 3	4 3	6 5	128 2	29 3	2 0	110 7	814 9	60 9	1064 4	270 6	11 7	1045 7	40 8	5 5	24 0	7 8
E87070	0 91	5 24	0 206	6 9	12 8	5 3	9 6	121 3	28 0	3 3	102 2	963 2	56 4	975 0	248 0	11 1	1172 1	54 5	4 6	21 8	6 5
E87071	0 92	5 43	0 231	4 7	7 7	4 5	10 7	138 4	27 8	3 0	114 0	802 6	59 5	1086 4	279 7	12 5	981 3	50 3	5 9	24 6	8 3
E87072	0 92	5 36	0 21	10 9	10 9	4 5	7 4	121 5	27 3	3 1	102 6	934 2	56 4	975 7	247 8	11 7	1181 8	50 1	6 2	23 5	6 9
E87074	0 86	5 12	0 213	9 0	6 9	3 5	9 8	122 8	27 7	3 1	103 5	953 0	55 7	984 7	252 7	12 3	1149 3	63 5	6 4	22 7	6 6
E87075	0 73	4 23	0 17	5 0	3 9	3 4	11 7	100 5	26 3	3 5	85 3	1254 4	44 6	790 7	199 1	8 9	1455 4	47 9	4 7	19 2	4 6
E87076	0 76	4 54	0 186	6 9	3 2	3 8	6 6	108 3	27 8	3 1	91 8	1126 5	48 8	862 6	219 8	10 4	1316 0	45 6	4 7	18 8	6 4
E87077	0 9	5 43	0 217	7 8	11 8	4 9	9 1	127 6	28 4	2 1	106 8	871 3	58 5	1024 1	261 5	12 0	1175 5	49 6	6 2	23 5	7 0
E87078	0 91	5 44	0 215	7 8	4 6	4 3	5 2	126 1	28 1	3 0	110 1	821 6	59 5	1055 3	268 2	11 3	1002 1	39 7	5 1	23 1	7 1
E87079	0 95	5 33	0 211	6 8	12 2	5 1	7 9	122 8	27 9	2 5	110 2	870 9	59 0	1044 1	266 3	11 9	988 3	42 8	6 1	24 0	7 3
E87080	0 82	4 6	0 18	8 2	3 9	4 1	4 5	106 8	26 3	3 8	89 7	1173 5	48 4	844 1	214 1	10 5	1358 4	48 2	4 8	20 2	5 5
E87081	0 9	5 29	0 208	6 6	7 4	4 2	6 7	122 4	28 1	3 5	104 4	911 2	58 2	1000 1	255 4	11 9	1186 3	44 9	4 9	23 2	6 0
E87082	0 91	5 73	0 236	10 8	10 0	4 1	4 6	142 8	29 2	1 9	114 2	736 2	64 4	1105 2	282 0	12 5	1055 0	42 5	5 9	25 3	7 5
E87083	0 85	5 16	0 212	8 1	9 2	4 4	5 6	126 0	27 4	2 9	99 3	907 7	57 3	954 2	241 6	11 0	1265 2	52 5	4 5	20 1	5 6
E87084	0 89	5 35	0 218	8 9	13 2	5 9	12 3	128 9	28 0	3 6	101 8	883 0	59 3	982 2	248 8	11 8	1222 5	65 9	4 7	21 7	7 2
E87085	0 96	5 71	0 231	7 6	4 7	4 3	7 4	137 1	29 3	2 5	116 7	733 4	62 1	1116 9	285 3	12 3	925 2	50 0	5 6	25 9	7 2

Appendix D. Mineral analyses

D.1. Electron Microprobe Standards

D.2. Olivine

D.3. Pyroxene

D.4. Titanomagnetite

D.5. Fluoroapatite

D.6. Anorthoclase Feldspar

D.7. Pyrrhotite

D.8. Glass

Table D.1. Electron microprobe standard analyses

Table D.1.1. Electron Microprobe Standard Analyses

	Accepted Measured		Accepted Measured			Accepted Measured			Accepted	Accepted Measured			Accepted Measured			Accepted Measured			Accepted Measured			Accepted Measured		
	VG-568		VG-568			KN-18			Benson Apatite	Bee-Ajax			NMGN			Ilmenite			Feld-dlkr			USNM-OI			Orthoclase			Albite		
n	20	1σ		19	1σ		14	1σ					35	1σ			6	1σ		6	1σ		10	1σ		21	1σ		21	1σ
SiO_2	76.71	76.06	0.54	74.60	74.23	0.84	0.11	0.08	0.05	0.69			0.15	0.02					42.78	42.62	0.12	40.81	40.96	0.38	64.39	64.50	0.52	68.24	68.72	1.00
TiO_2	0.12	0.09	0.03	0.18	0.16	0.03				0.02			0.05	0.02		45.70	46.42	0.70												
Al_2O_3	12.06	12.16	0.21	10.53	10.66	0.15				0.38			0.49	0.37											16.72	16.54	0.06	19.9	20.03	0.21
Fe_2O_3							8.84									11.60	10.69	1.24												
FeO	1.23	1.11	0.07	3.45	3.50	0.06		0.01	0.01	92.73			91.84	0.77		36.10	36.65	0.65				9.55	9.65	0.16	1.88	1.76	0.04			
MnO	0.03	0.04	0.02	0.06	0.06	0.02		0.04	0.01	0.07			0.02	0.03		4.77	4.50	0.07				0.14	0.14	0.04						
MgO		0.02	0.01	0.01	0.00	0.00				0.12			0.13	0.11		0.31	0.32	0.02	97.30	57.01	0.11	49.42	48.46	0.14						
CaO	0.50	0.42	0.03	8.15	0.16	0.04	54.31	54.22	0.42																			0.03	0.01	0.01
Na_2O	3.75	3.92	0.42	5.68	5.16	0.98																			8.91	0.94	0.03	11.54	11.46	1.02
K_2O	4.89	5.03	0.09	4.39	4.59	0.06																			15.49	15.52	0.10	0.04	0.00	0.01
P_2O_5		0.02	0.02		0.01	0.01	40.93	41.09	0.26																					
Cr_2O_3										0.01			0.01	0.01																
BaO																									0.85	0.06	0.02			
SO_3		0.02	0.02		0.03	0.02	0.59	0.37	0.02																					
SrO							0.20	0.44	0.03																					
F		0.17	0.06		0.58	0.11	3.67	3.27	0.39																					
Cl		0.10	0.02		0.31	0.02																								

Table D.2.1. Electron Microprobe Analyses of Olivine in Tephra

Sample	79302	79302	79302	79302	79302	79302	79302	85010	85010	85010	85010	85010	91101
Host	gl	gl	gl	gl	gl	gl	pyx	gl	gl	gl	gl	gl	gl
xtyl-anal.	1-1	1-2	1-3	1-4	1-5	1-6	2-1	1-1	1-2	1-3	1-4	1-5	1-1
Location*	r	c	r	c	r	r	c	c	c	c	c	c	r
SiO2	34.66	34.88	34.72	34.88	34.89	34.61	34.73	34.69	34.84	34.69	34.89	34.86	34.89
Al2O3	0.02	0.01	0.01	0.00	0.02	0.01	0.01	0.01	0.02	0.01	0.01	0.01	0.01
FeO	38.84	38.80	38.42	38.95	39.05	38.99	38.35	38.94	39.32	39.17	39.18	39.37	38.94
MnO	2.52	2.56	2.55	2.58	2.64	2.54	2.43	2.63	2.53	2.60	2.51	2.57	2.60
MgO	23.66	23.58	23.88	23.75	23.73	23.88	23.95	23.67	23.57	23.42	23.69	23.53	23.86
CaO	0.50	0.53	0.59	0.52	0.52	0.51	0.57	0.49	0.49	0.49	0.48	0.49	0.52
Total	100.20	100.34	100.15	100.64	100.85	100.35	100.04	100.42	100.56	100.38	100.56	100.82	100.83
Fo	50.47	50.39	50.92	50.48	50.35	50.39	51.14	50.36	50.08	49.97	50.30	49.99	50.57
Fa	46.47	46.51	45.99	46.43	46.47	46.54	45.92	46.46	46.86	46.88	46.67	46.91	46.30
Te	3.06	3.10	3.09	3.09	3.18	3.07	2.94	3.18	3.06	3.16	3.03	3.10	3.14

*r = rim, c = core, i = intermediate

Table D.2.1. Electron Microprobe Analyses of Olivine in Tephra, Continued

Sample	Y2K	Y2K	Y2K	Y2K	E2001	E2001	E2001	E2001	E2001	E2001	E2001	E2001	E2001
Host	gl	gl	gl	gl	gl	gl	gl	gl	gl	gl	gl	gl	gl
xtyl-anal.	3-1	3-2	3-3	3-4	1-1	1-2	1-3	1-4	2-1	3-1	3-2	4-1	5-1
Location*	r	c	c	r	r	i	i	c	c	r	c	r	c
SiO2	34.36	34.66	34.85	34.90	34.75	35.12	35.18	35.05	34.84	35.05	34.80	34.76	34.53
Al2O3	0.00	0.01	0.00	0.00	0.00	0.01	0.00	0.02	0.02	0.00	0.04	0.02	0.00
FeO	37.91	37.81	37.63	37.69	37.20	37.16	37.22	37.16	37.58	37.09	37.17	37.37	37.33
MnO	2.45	2.52	2.37	2.30	2.43	2.44	2.32	2.36	2.27	2.30	2.35	2.38	2.31
MgO	23.08	23.01	23.02	23.09	23.59	23.44	23.57	23.46	23.55	23.35	23.48	23.46	23.36
CaO	0.51	0.56	0.54	0.56	0.51	0.50	0.48	0.50	0.49	0.47	0.49	0.49	0.49
Total	98.40	98.43	98.45	98.64	98.55	98.78	98.85	98.68	98.77	98.29	98.38	98.53	98.08
Fo	50.44	50.53	50.62	50.70	51.47	51.32	51.50	51.39	51.29	51.37	51.40	51.26	51.22
Fa	46.51	46.33	46.41	46.43	45.52	45.64	45.62	45.67	45.91	45.76	45.67	45.79	45.90
Te	3.04	3.15	2.97	2.87	3.01	3.04	2.88	2.94	2.81	2.87	2.93	2.95	2.88

*r = rim, c = core, i = intermediate

Table D.2.1. Electron Microprobe Analyses of Olivine in Tephra, Continued

Sample	91101	91101	91101	91101	91101	91101	91101	91101	91101	91101	92101	92101	92101
Host	gl	gl	gl	gl	gl	gl	gl	gl	gl	gl	gl	gl	gl
xtyl-anal.	1-2	1-3	1-4	1-5	1-6	2-1	3-1	3-2	4-1	4-2	1-1	1-2	2-1
Location*	r	r	i	c	i	r	r	c	r	r	c	c	r
SiO2	34.90	34.93	34.74	34.83	34.88	34.98	34.66	34.77	34.80	35.03	34.99	35.04	34.76
Al2O3	0.02	0.01	0.03	0.02	0.02	0.02	0.02	0.02	0.02	0.02	0.00	0.00	0.01
FeO	39.06	38.64	38.83	38.86	39.12	38.91	39.18	38.86	39.09	38.71	39.07	38.92	38.99
MnO	2.60	2.43	2.55	2.55	2.41	2.47	2.55	2.53	2.52	2.44	2.58	2.49	2.53
MgO	23.52	23.78	23.64	23.91	23.62	23.64	23.67	23.53	23.64	23.42	23.79	23.60	23.68
CaO	0.52	0.52	0.49	0.50	0.51	0.52	0.50	0.52	0.53	0.52	0.48	0.50	0.50
Total	100.60	100.31	100.28	100.66	100.56	100.54	100.59	100.21	100.60	100.15	100.90	100.56	100.46
Fo	50.14	50.77	50.44	50.71	50.32	50.44	50.26	50.32	50.30	50.35	50.44	50.38	50.40
Fa	46.71	46.28	46.47	46.22	46.76	46.57	46.66	46.81	46.65	46.67	46.46	46.60	46.55
Te	3.14	2.95	3.09	3.07	2.92	3.00	3.08	3.07	3.05	2.98	3.10	3.02	3.05

*r = rim, c = core, I = intermediate

Table D.2.1. Electron Microprobe Analyses of Olivine in Tephra, Continued

Sample	82101	82101	Er92KS	93102	93102	93102	Er96	Er96	Er96	Er96	Er96	Er96	Er96
Host	gl	gl	gl	gl	gl	gl	gl	gl	gl	gl	gl	gl	gl
xtyl-anal.	2-2	2-3	1-1	1-1	1-2	1-3	1-1	1-2	1-3	1-4	2-1	2-2	2-3
Location*	c	r	c	r	c	c	r	c	c	r	c	c	r
SiO2	34.78	34.87	34.86	34.83	34.90	34.82	34.87	34.94	34.85	34.50	34.78	34.91	34.48
Al2O3	0.01	0.00	0.01	0.03	0.03	0.02	0.03	0.03	0.03	0.03	0.03	0.02	0.03
FeO	39.35	39.26	39.08	38.87	38.85	39.08	38.99	38.81	38.75	38.86	39.65	39.49	39.03
MnO	2.56	2.52	2.54	2.53	2.60	2.59	2.61	2.48	2.47	2.58	2.52	2.51	2.60
MgO	23.73	23.53	24.01	23.84	23.89	23.88	23.76	23.75	23.77	23.91	23.28	23.53	23.70
CaO	0.49	0.52	0.48	0.51	0.49	0.49	0.47	0.49	0.52	0.51	0.44	0.45	0.45
Total	100.89	100.71	100.98	100.60	100.75	100.90	100.43	100.49	100.38	100.18	100.69	100.91	100.26
Fo	50.21	50.08	50.68	50.65	50.66	50.51	50.50	50.61	50.68	50.82	49.59	49.95	50.36
Fa	46.71	46.87	46.27	46.30	46.21	46.37	46.47	46.36	46.33	46.08	47.37	47.02	46.51
Te	3.08	3.05	3.05	3.05	3.13	3.12	3.03	3.00	2.99	3.11	3.05	3.03	3.13

*r = rim, c = core, I = intermediate

Table D.2.1. Electron Microprobe Analyses of Olivine in Tephra, Continued

Sample	1999	1999	1999	1999	DEC2000	DEC2000	DEC2000	DEC2000	Y2K	Y2K	Y2K	Y2K	Y2K
Host					gl	gl	gl	gl	gl	gl	gl	gl	gl
xtyl-anal.					1-1	1-2	1-3	1-4	1-1	1-2	1-3	1-4	2-1
Location*					r	c	c	r	r	i	i	c	r
SiO2	35.02	34.89	35.02	34.73	34.96	34.74	34.78	34.82	34.54	34.61	34.83	34.23	34.81
Al2O3	0.00	0.00	0.01	0.04	0.01	0.00	0.01	0.00	0.01	0.00	0.00	0.00	0.00
FeO	37.29	37.25	37.25	37.36	36.96	37.68	37.55	37.36	37.84	37.85	37.94	38.06	37.28
MnO	2.28	2.28	2.27	2.31	2.32	2.40	2.33	2.27	2.35	2.43	2.27	2.33	2.28
MgO	23.47	23.28	23.46	23.32	23.33	23.30	23.25	23.54	23.17	23.04	22.95	23.13	23.25
CaO	0.47	0.45	0.47	0.48	0.50	0.45	0.48	0.55	0.48	0.46	0.46	0.45	0.48
Total	98.61	98.19	98.55	98.64	98.24	98.64	98.44	98.60	98.40	98.46	98.52	98.29	98.17
Fo	51.38	51.20	51.40	51.15	51.41	50.88	50.95	51.41	50.87	50.47	50.41	50.50	51.14
Fa	45.79	45.95	45.78	45.97	45.68	46.15	46.15	45.78	46.41	46.51	46.76	46.61	46.01
Te	2.83	2.85	2.82	2.87	2.91	2.97	2.90	2.81	2.92	3.02	2.83	2.89	2.85

*r = rim, c = core, I = intermediate

Table D.2.1. Electron Microprobe Analyses of Olivine in Tephra, Continued

Sample	JAN2004	JAN2004
Host	gl	gl
xtyl-anal.	1-1	1-2
Location*	r	c
SiO2	34.78	35.18
Al2O3	0.00	0.00
FeO	37.34	36.62
MnO	2.34	2.26
MgO	23.45	23.51
CaO	0.47	0.46
Total	98.41	98.09
Fo	51.29	51.66
Fa	45.80	45.30
Te	2.91	2.84

*r = rim, c = core, I = intermediate

Table D.3.1. Electron Microprobe Analyses of Pyroxene in Tephra and from Summit Crystal Lag

Sample	Er-pyx-01	Er-pyx-01	Er-pyx-01	Er-pyx-01	Er-pyx-01	Er-pyx-01	Er-pyx-01	Er-pyx-01	Er-pyx-01	Er-pyx-01	Er-pyx-01	79302	79302
host[A]	gl/fel	gl/fel	gl/fel	gl/fel	gl/fel	gl/fel	gl/fel	gl/fel	gl/fel	gl/fel	gl/fel	gl	gl
xtyl-anal.	1-1	1-2	1-3	1-4	1-5	1-6	1-7	1-8	1-9	1-10	1-11	1-1	1-2
location	r	I	I	I	I	c	I	I	I	I	r	c	c
SiO2	50.08	50.10	50.36	50.98	50.81	50.39	50.76	50.42	50.89	51.03	51.73	51.11	50.41
Al2O3	3.35	3.29	2.91	2.96	2.93	3.30	2.78	3.27	2.95	2.92	2.35	2.99	2.81
TiO2	1.59	1.47	1.40	1.42	1.39	1.46	1.35	1.58	1.42	1.46	1.21	1.33	1.25
FeO	10.24	10.03	9.45	9.64	9.48	9.53	9.43	9.75	9.36	9.66	9.65	9.95	9.69
MnO	0.68	0.67	0.63	0.66	0.63	0.66	0.63	0.66	0.63	0.66	0.69	0.69	0.61
MgO	11.31	11.67	12.13	12.10	12.24	11.95	12.24	12.00	12.07	12.09	12.46	12.03	12.16
CaO	20.68	20.75	21.80	21.59	21.21	20.96	21.51	21.37	21.80	21.37	21.88	20.89	21.26
Na2O	1.16	1.16	0.89	1.00	0.95	1.06	0.91	1.05	0.85	1.00	0.66	1.00	0.87
Total	99.13	99.18	99.37	100.36	99.64	99.35	99.60	100.10	99.98	100.18	100.82	99.91	99.18
Wo	46.05	45.79	46.83	46.49	46.01	46.03	46.39	46.29	47.02	46.25	46.30	45.57	46.03
En	35.04	35.84	36.45	36.27	36.94	36.52	36.73	36.17	36.23	36.39	36.70	36.53	36.83
Fs	18.92	18.37	16.92	17.25	17.05	17.45	16.87	17.54	16.74	17.36	17.00	17.90	17.34

[T]r = rim, c = core, I = intermediate

[A]gl/fel = attached to feldspar megacryst, surrounded by glass

Table D.3.1. Electron Microprobe Analyses of Pyroxene in Tephra and from Summit Crystal Lag, Continued

Sample	79302	79302	92101	92101	92101	92101
host	gl	gl	gl	gl	gl	gl
xtyl-anal.	1-3	1-4	1-1	1-2	1-3	2-1
location	c	c	r	c	r	c
SiO2	50.86	50.50	51.17	50.62	51.25	51.20
Al2O3	2.90	2.57	2.47	2.84	3.09	2.85
TiO2	1.45	1.24	1.28	1.47	1.48	1.25
FeO	9.81	9.74	9.22	9.16	9.51	9.36
MnO	0.66	0.70	0.61	0.60	0.65	0.66
MgO	11.98	12.15	12.64	12.44	12.16	12.30
CaO	21.14	21.01	21.48	21.35	21.20	20.73
Na2O	0.84	0.84	0.80	0.88	1.00	0.90
Total	99.74	98.85	99.67	99.35	100.34	99.25
Wo	45.99	45.64	45.99	46.16	46.06	45.42
En	36.28	36.71	37.65	37.44	36.77	37.50
Fs	17.72	17.64	16.35	16.40	17.16	17.08

[T]r = rim, c = core, I = intermediate

[A]gl/fel = attached to feldspar megacryst, surrounded by glass

Appendix D.4. Electron Microprobe Analysis of Titanomagnetite

Over six hundred analyses were performed on titanomagnetites from twenty-eight volcanic bombs erupted from 1972 to 2004 (Figure D.4.23.) and one pyroxene megacryst of unknown age. Twenty-two traverses were made on grains ranging from 30μm to 400μm across to assess intracrystalline homogeneity (Figures D.3.1. to D.3.22.). Analyses were checked for quality three ways: (1) those with totals less than 98 wt% or greater than 101 wt% were rejected (2) SiO_2 was used as a monitor for edge effects for analyses close to crystal rims; analyses with elevated SiO_2 were rejected (3) All analyses were recalculated into cation proportions to assure stoichiometry using the method of Carmichael (1967). Ülvospinel endmember molar percentages were calculated according to the method of Stormer (1983). Analytical errors were assessed by repeat analysis of cores of titanomagnetites over several analytical sessions (Table D.4.1.). This approach is favorable here because there are no standards of similar composition available.

Table D.4.1. Analytical error estimate from repeat analysis of titanomagnetites over several analytical sessions. The pooled mean composition and two standard deviations of the mean for the entire data set are given for comparison.

	Analytical error estimate: repeat analyses	Whole dataset: pooled average and two standard deviations	
	2σ	mean	2σ
n	47	634	
TiO_2 (wt.%)	0.51	24.52	0.62
Al_2O_3	0.17	2.27	0.26
Fe_2O_3	0.73	20.07	1.17
FeO	0.63	47.80	0.85
MnO	0.11	1.76	0.14
MgO	0.08	2.89	0.15
Mol% ülvospinel Stormer (1983)	1.3	71.5	1.9

Table D.4.2. Mean and One Standard Deviation of the Mean of EMP Titanomagnetite Analyses

Sample	25724	1σ	2E2	1σ	25723	1σ	78325	1σ	79302	1σ	81003	1σ
n	15		16		15		12		20		17	
TiO_2	24.68	0.12	24.66	0.28	24.67	0.27	24.66	0.17	24.34	0.28	24.42	0.23
Al_2O_3	2.28	0.07	2.21	0.03	2.27	0.03	2.20	0.02	2.27	0.02	2.27	0.04
Fe_2O_3	19.78	0.21	19.86	0.28	19.76	0.38	19.87	0.22	20.52	0.42	20.34	0.36
FeO	47.90	0.20	47.84	0.39	47.82	0.36	47.87	0.21	47.59	0.29	47.61	0.31
MnO	1.76	0.04	1.80	0.06	1.77	0.04	1.78	0.04	1.87	0.04	1.85	0.04
MgO	2.92	0.04	2.90	0.05	2.94	0.03	2.90	0.03	2.88	0.08	2.92	0.04
Total	99.31	0.31	99.28	0.47	99.22	0.45	99.28	0.24	99.48	0.31	99.41	0.34
Mol % Usp												
Stormer (1983)	72.0	0.3	71.8	0.6	72.0	0.7	71.8	0.4	70.8	0.7	71.1	0.6

Table D.4.2. Mean and One Standard Deviation of the Mean of EMP Titanomagnetite Analyses, Continued

Sample	81410	1σ	82418	1σ	83207	1σ	84500	1σ	84505	1σ	85009	1σ
n	43		37		39		17		22		21	
TiO_2	24.35	0.24	24.65	0.20	24.63	0.28	24.70	0.22	24.43	0.36	24.58	0.22
Al_2O_3	2.24	0.12	2.27	0.12	2.27	0.03	2.26	0.03	2.25	0.04	2.24	0.03
Fe_2O_3	20.30	0.37	19.83	0.33	19.50	0.45	20.24	0.34	20.75	0.54	20.43	0.44
FeO	47.51	0.32	47.79	0.28	47.60	0.38	48.21	0.28	47.99	0.42	48.08	0.28
MnO	1.86	0.05	1.84	0.04	1.85	0.03	1.74	0.05	1.70	0.05	1.72	0.04
MgO	2.88	0.05	2.91	0.04	2.92	0.03	2.89	0.05	2.89	0.03	2.89	0.04
Total	99.14	0.46	99.29	0.42	98.77	0.49	100.02	0.30	100.01	0.45	99.95	0.36
Mol % Usp												
Stormer (1983)	71.0	0.7	71.9	0.6	72.2	0.8	71.5	0.6	70.7	0.9	71.1	0.7

Table D.4.2. Mean and One Standard Deviation of the Mean of EMP Titanomagnetite Analyses, Continued

Sample	85010	1σ	86022	1σ	88104	1σ	91101	1σ	92101	1σ	Er92	1σ
n	12		19		14		10		14		7	
TiO_2	24.31	0.28	24.86	0.18	24.59	0.23	24.57	0.13	24.37	0.27	24.51	0.24
Al_2O_3	2.24	0.05	2.27	0.04	2.27	0.10	2.23	0.03	2.24	0.04	2.27	0.04
Fe_2O_3	20.33	0.54	19.77	0.26	19.78	0.26	19.99	0.27	20.47	0.41	20.25	0.35
FeO	47.62	0.30	48.35	0.29	47.90	0.35	47.92	0.20	47.73	0.38	47.96	0.34
MnO	1.73	0.05	1.71	0.05	1.73	0.04	1.73	0.05	1.74	0.05	1.72	0.03
MgO	2.84	0.03	2.88	0.04	2.84	0.04	2.85	0.03	2.88	0.04	2.86	0.03
Total	99.07	0.34	99.85	0.38	99.11	0.45	99.29	0.38	99.43	0.34	99.56	0.41
Mol % Usp												
Stormer (1983)	71.0	0.8	72.2	0.5	72.0	0.6	71.6	0.4	70.9	0.7	71.3	0.6

Table D.4.2. Mean and One Standard Deviation of the Mean of EMP Titanomagnetite Analyses, Continued

Sample	93102	1σ	Er96	1σ	97018	1σ	Er-97	1σ	1999	1σ	Er99	1σ
n	15		63		32		29		15		14	
TiO_2	24.36	0.28	24.39	0.33	24.73	0.23	24.39	0.29	24.08	0.28	24.08	0.28
Al_2O_3	2.23	0.04	2.23	0.05	2.23	0.03	2.24	0.04	2.33	0.09	2.33	0.15
Fe_2O_3	20.50	0.34	20.51	0.64	19.06	0.31	19.91	0.29	20.10	0.24	20.10	0.51
FeO	47.80	0.41	47.86	0.43	47.76	0.29	47.54	0.44	47.16	0.17	47.16	0.27
MnO	1.72	0.05	1.73	0.04	1.73	0.05	1.71	0.05	1.74	0.04	1.74	0.05
MgO	2.84	0.05	2.83	0.05	2.87	0.03	2.87	0.04	2.85	0.03	2.85	0.04
Total	99.45	0.45	99.55	0.69	98.39	0.33	98.66	0.57	98.26	0.22	98.26	0.24
Mol % Usp												
Stormer (1983)	70.9	0.6	70.9	1.0	72.9	0.6	71.6	0.6	71.2	0.4	71.2	0.8

Table D.4.2. Mean and One Standard Deviation of the Mean of EMP Titanomagnetite Analyses, Continued

Sample	Dec2000	1σ	Y2K	1σ	E2001	1σ	2004	1σ	Er-pyx-01	1σ
n	10		7		10		10		22	
TiO_2	24.45	0.21	24.26	0.36	24.79	0.13	24.44	0.19	24.65	0.33
Al_2O_3	2.29	0.03	2.73	0.71	2.25	0.05	2.32	0.14	2.48	0.17
Fe_2O_3	19.94	0.29	19.88	0.63	20.27	0.23	19.63	0.34	19.83	0.60
FeO	47.72	0.25	47.63	0.42	48.26	0.20	47.57	0.25	47.76	0.57
MnO	1.76	0.05	1.75	0.03	1.77	0.06	1.75	0.03	1.69	0.06
MgO	2.84	0.04	2.86	0.04	2.94	0.04	2.85	0.05	3.10	0.20
Total	98.99	0.23	99.11	0.72	100.28	0.24	98.56	0.37	99.50	0.46
Mol % Usp										
Stormer (1983)	71.7	0.5	72.1	1.4	71.5	0.4	72.1	0.6	72.1	1.2

Table D.4.3. Mean and Two Standard Deviations of the Mean of EMP Analyses of Titanomagnetites in different host materials

host	olivine		pyroxene		feldspar		matrix glass	
n	40	2σ	22	2σ	5	2σ	567	2σ
TiO_2	24.28	0.60	24.65	0.66	24.58	0.32	24.54	0.60
Al_2O_3	2.23	0.09	2.48	0.34	2.58	0.31	2.26	0.25
Fe_2O_3	20.77	0.97	19.83	1.20	20.17	0.47	20.03	1.11
FeO	47.78	0.87	47.76	1.14	48.08	0.24	47.81	0.83
MnO	1.74	0.09	1.69	0.13	1.72	0.17	1.77	0.14
MgO	2.83	0.11	3.10	0.40	2.94	0.12	2.88	0.10
Total	99.63	1.52	99.50	0.91	100.05	0.34	99.29	1.30
Mol % Usp								
Stormer (1983)	70.5	1.4	72.1	2.4	71.8	0.9	71.6	1.7

Figures D.4.1 – D.4.22.: EMP traverses of titanomagnetite (error bars represent 2σ analytical uncertainty)

Figure D.4.1. Electron Microprobe Traverse of Titanomagnetite 79302-1

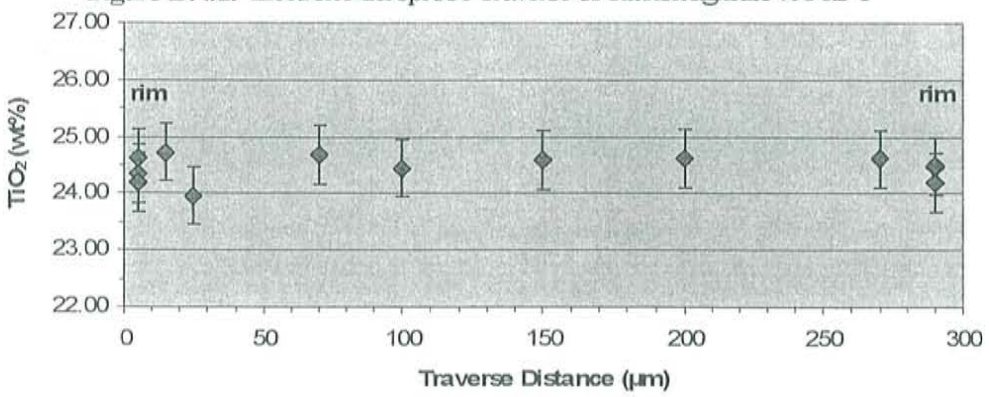

Figure D.4.2. Electron Microprobe Traverse of Titanomagnetite 81003-1

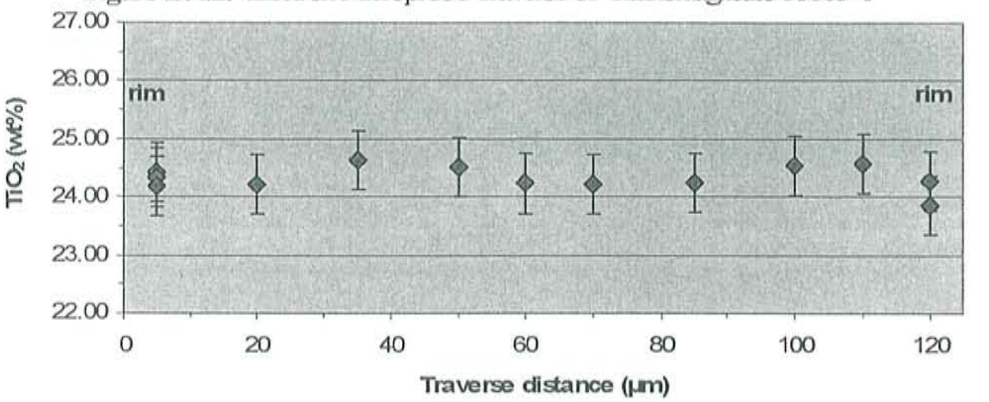

Figure D.4.3. Electron Microprobe Traverse of Titanomagnetite 81410-1

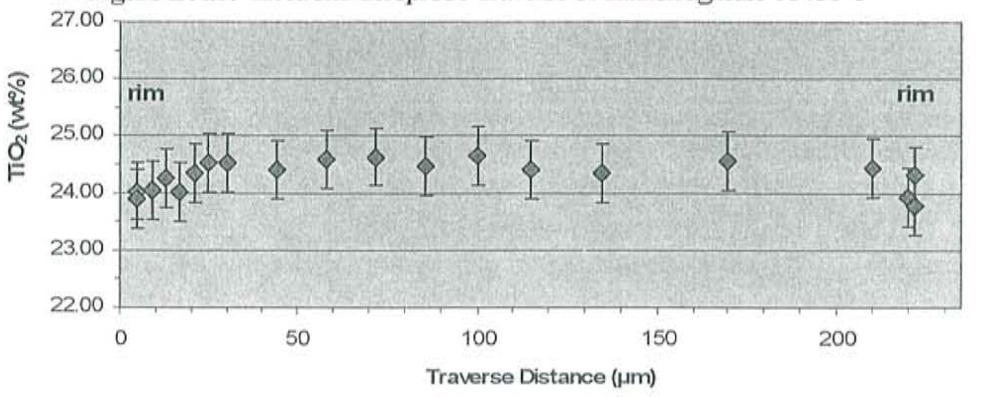

Figure D.4.4. Electron Microprobe Traverse of Titanomagnetite 82418-1

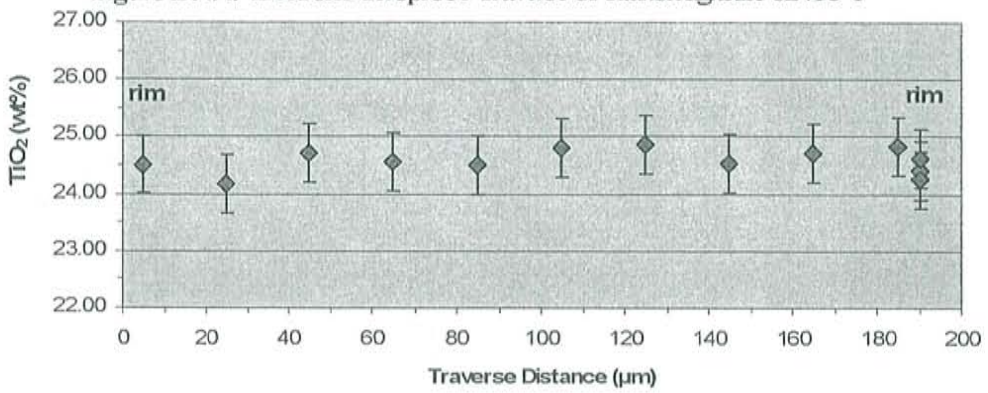

Figure D.4.5. Electron Microprobe Traverse of Titanomagnetite 82418-2

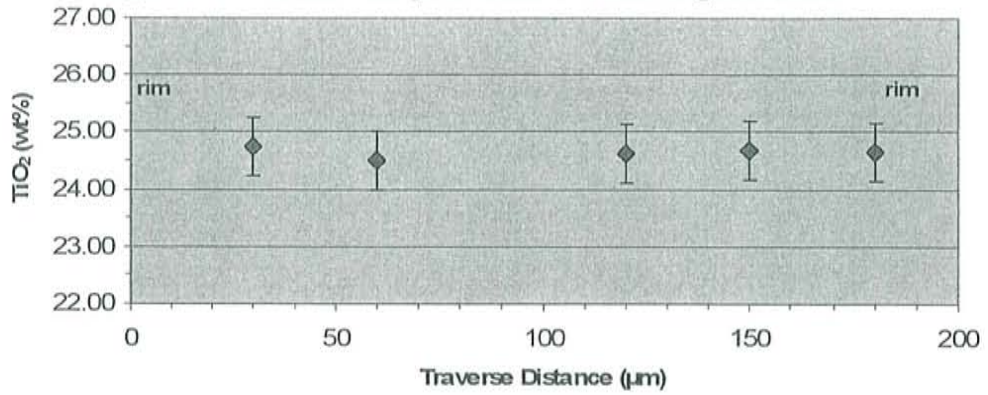

Figure D.4.6. Electron Microprobe Traverse of Titanomagnetite 82418-3

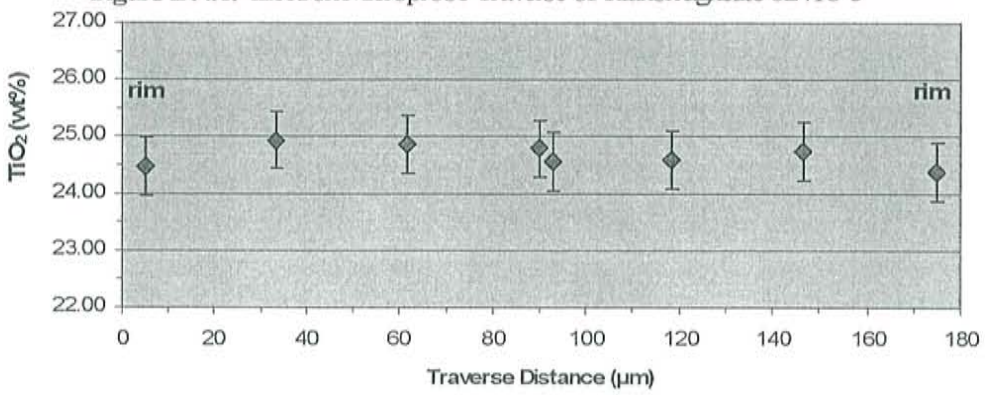

Figure D.4.7. Electron Microprobe Traverse of Titanomagnetite 83207-1

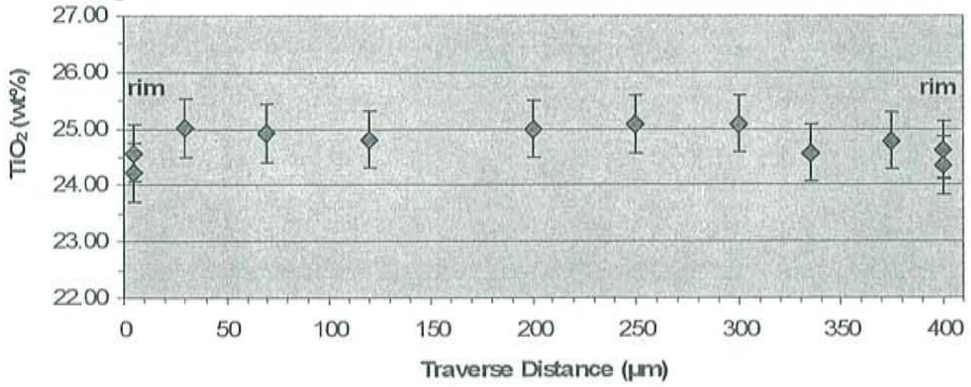

Figure D.4.8. Electron Microprobe Traverse of Titanomagnetite 83207-2

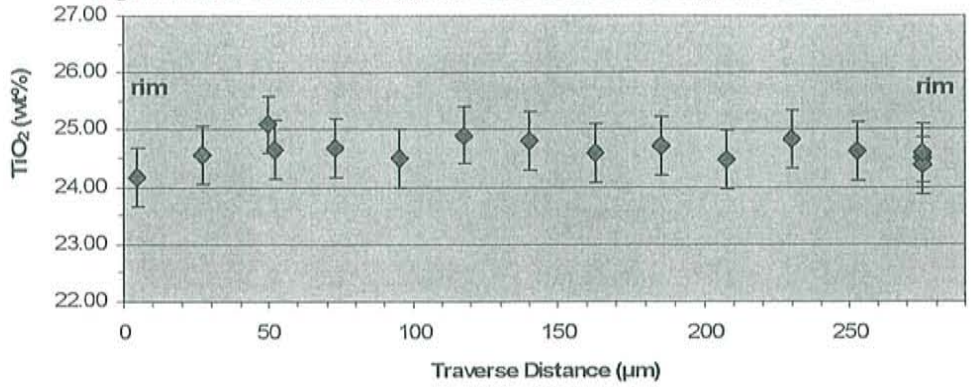

Figure D.4.9. Electron Microprobe Traverse of Titanomagnetite 84500-1

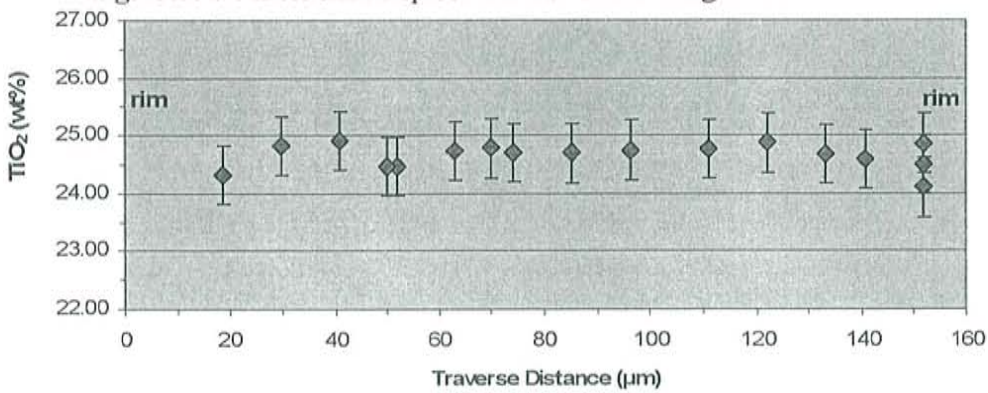

Figure D.4.10. Electron Microprobe Traverse of Titanomagnetite 84500-2

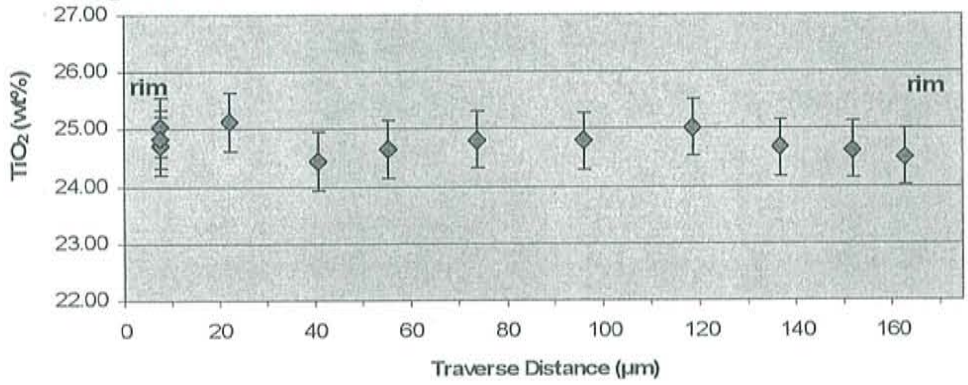

Figure D.4.11. Electron Microprobe Traverse of Titanomagnetite 84505-1

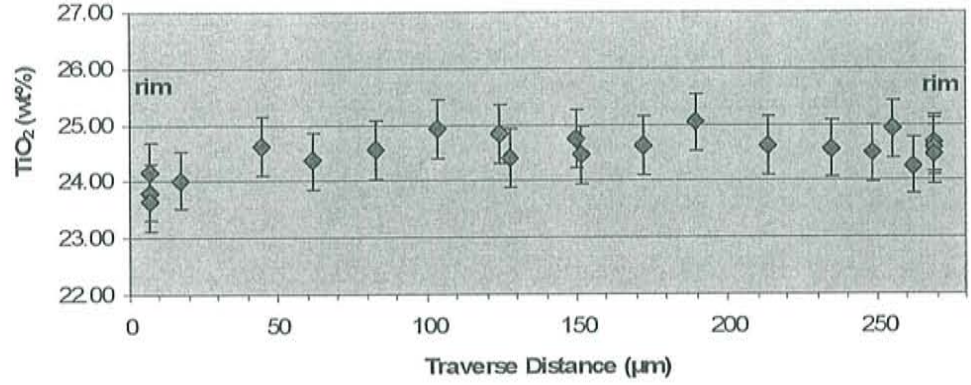

Figure D.4.12. Electron Microprobe Traverse of Titanomagnetite 85009-1

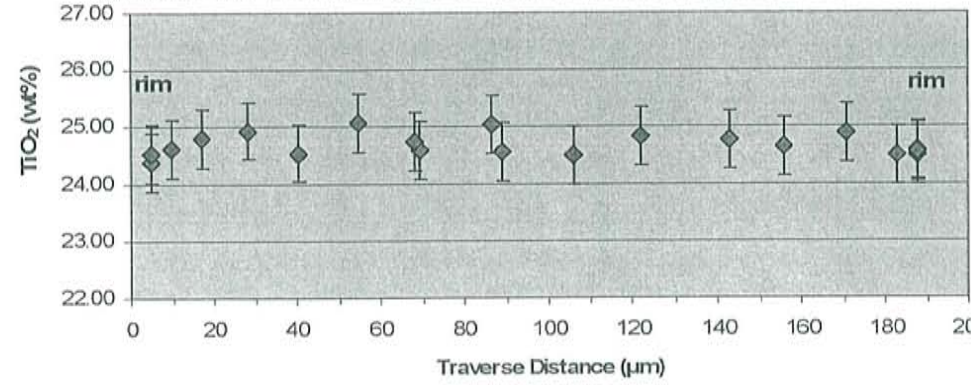

Figure D.4.13. Electron Microprobe Traverse of Titanomagnetite 86022-1

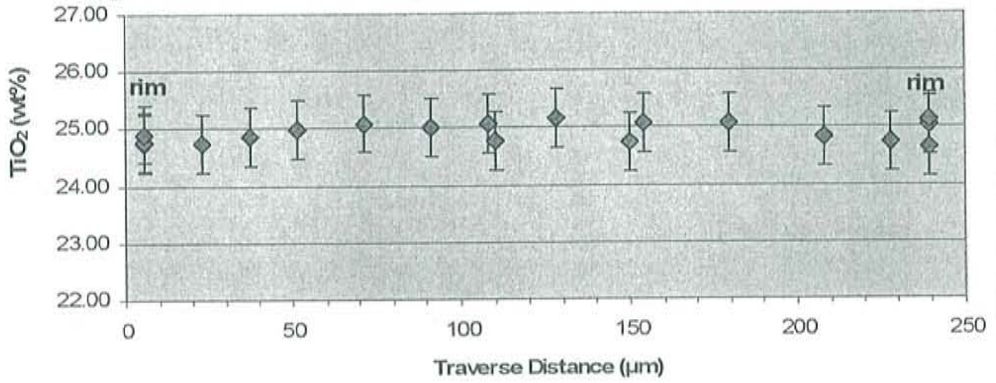

Figure D.4.14. Electron Microprobe Traverse of Titanomagnetite 86022-2

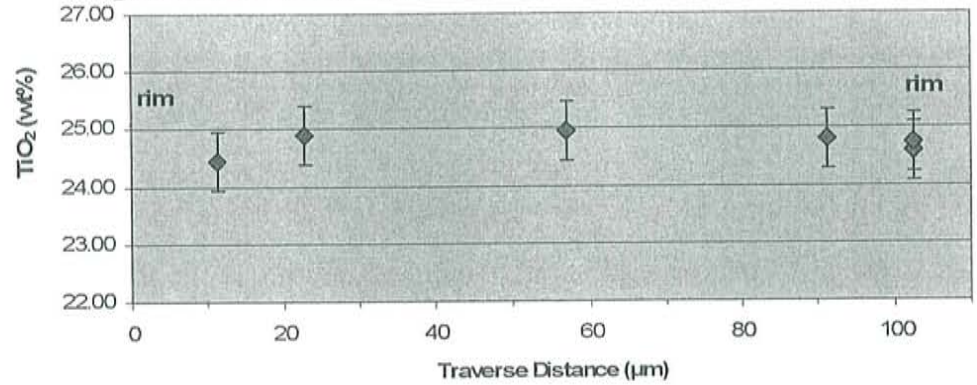

Figure D.4.15. Electron Microprobe Traverse of Titanomagnetite Er96-1

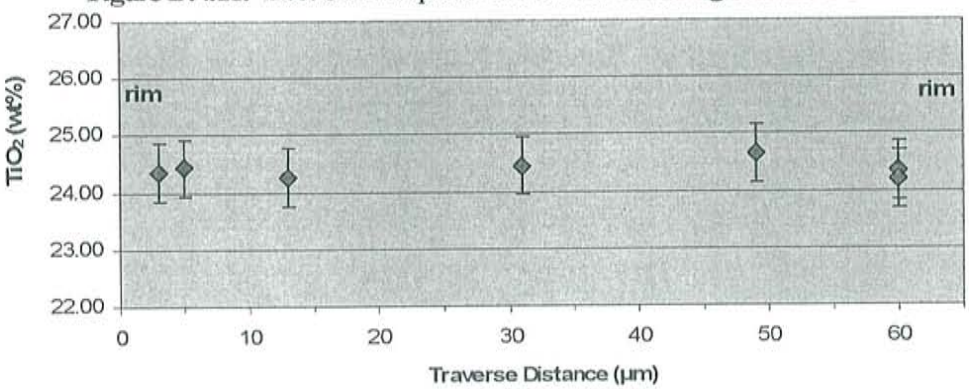

Figure D.4.16. Electron Microprobe Traverse of Titanomagnetite Er-96-2

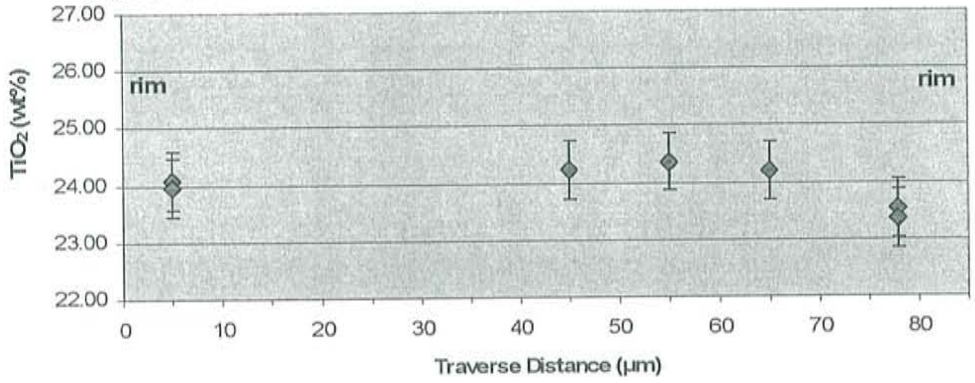

Figure D.4.17. Electron Microprobe Traverse of Olivine-Hosted Titanomagnetite Er-96-13

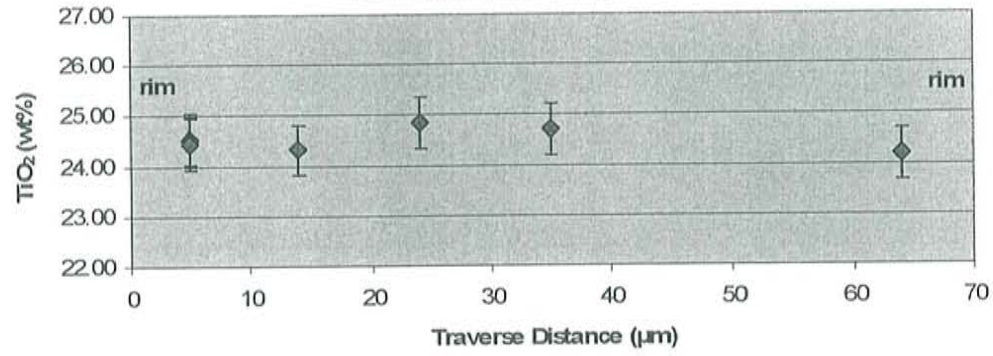

Figure D.4.18. Electron Microprobe Traverse of Olivine-Hosted Titanomagnetite Er-96-14

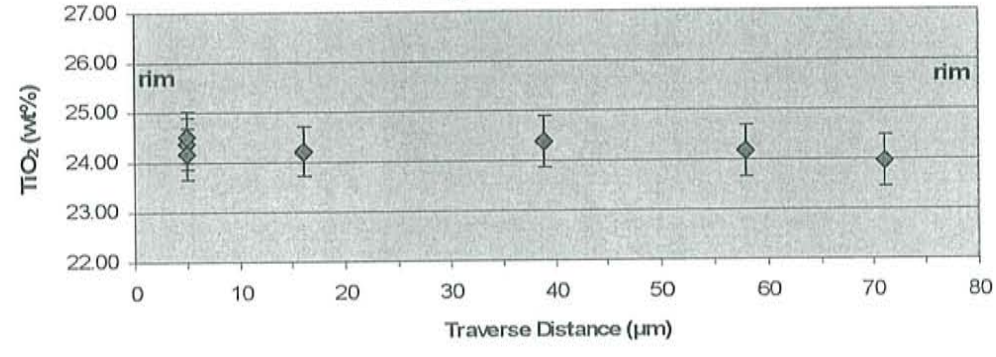

Figure D.4.19. Electron Microprobe Traverse of Olivine-Hosted Titanomagnetite Er96-16

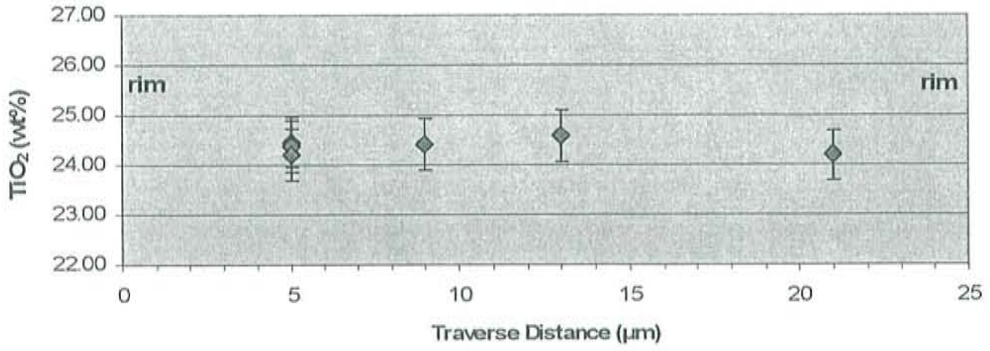

Figure D.4.20. Electron Microprobe Traverse of Titanomagnetite 97018-7

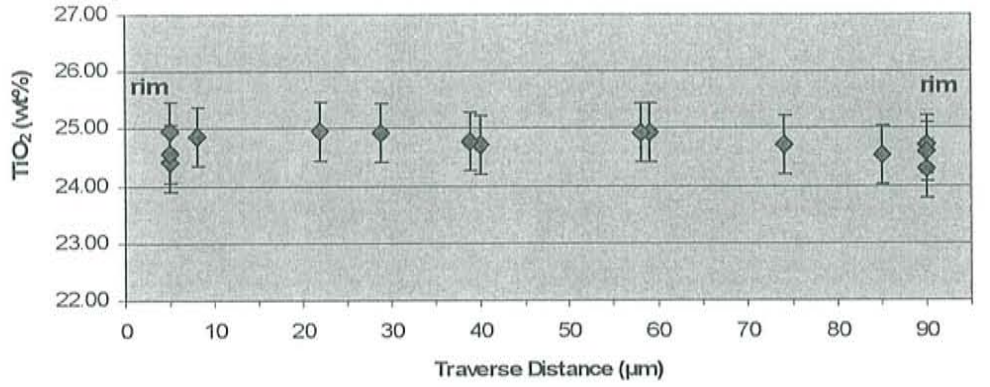

Figure D.4.21. Electron Microprobe Traverse of Titanomagnetite Er97-4

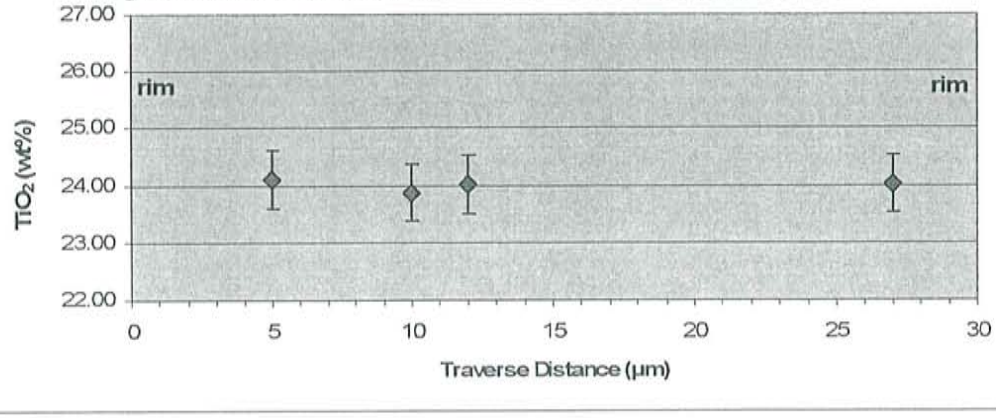

Figure D.4.22. Electron Microprobe Traverse of Titanomagnetite Er97-5

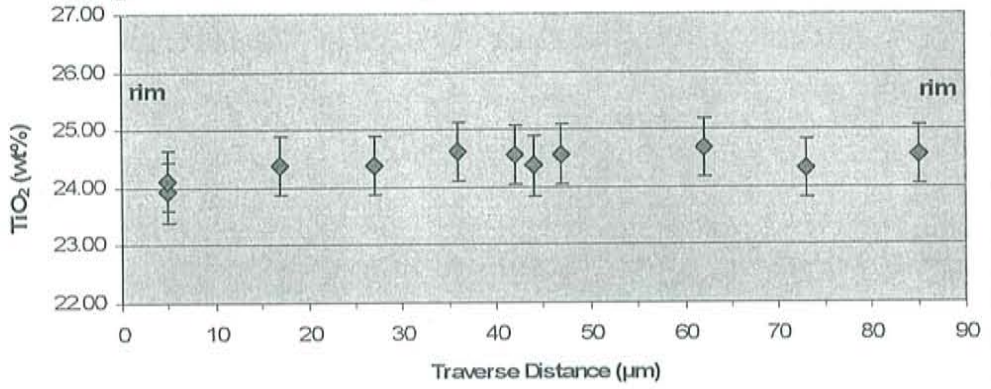

Figure D.4.23. Average composition of titanomagnetites in Tephra erupted from 1972 – 2004 (error bars represent 2σ analytical error; see Table D.4.2 for data)

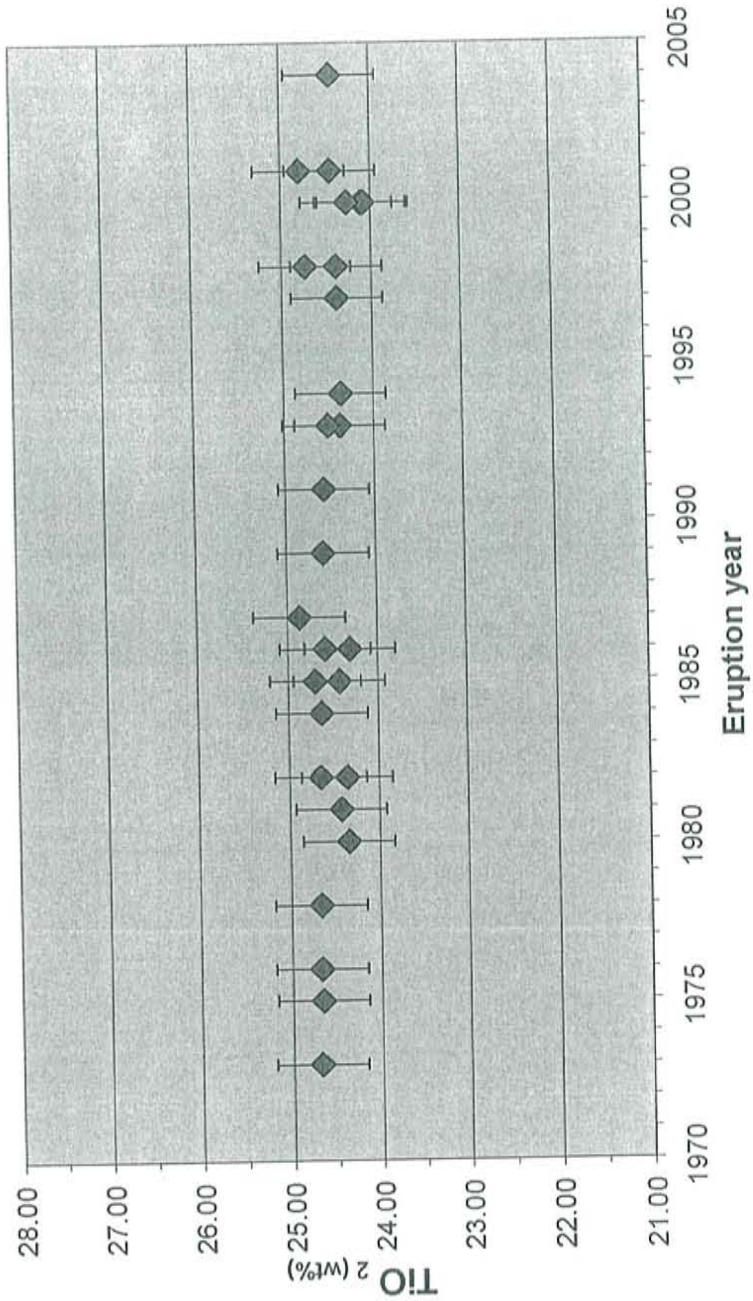

Figure D.4.24. Comparison of average TiO_2 (wt%) concetrations of titanomagnetites with different host minerals (error bars represent 2σ analytical error; 2σ of pooled analyses are similar: see Table D.4.3 for data)

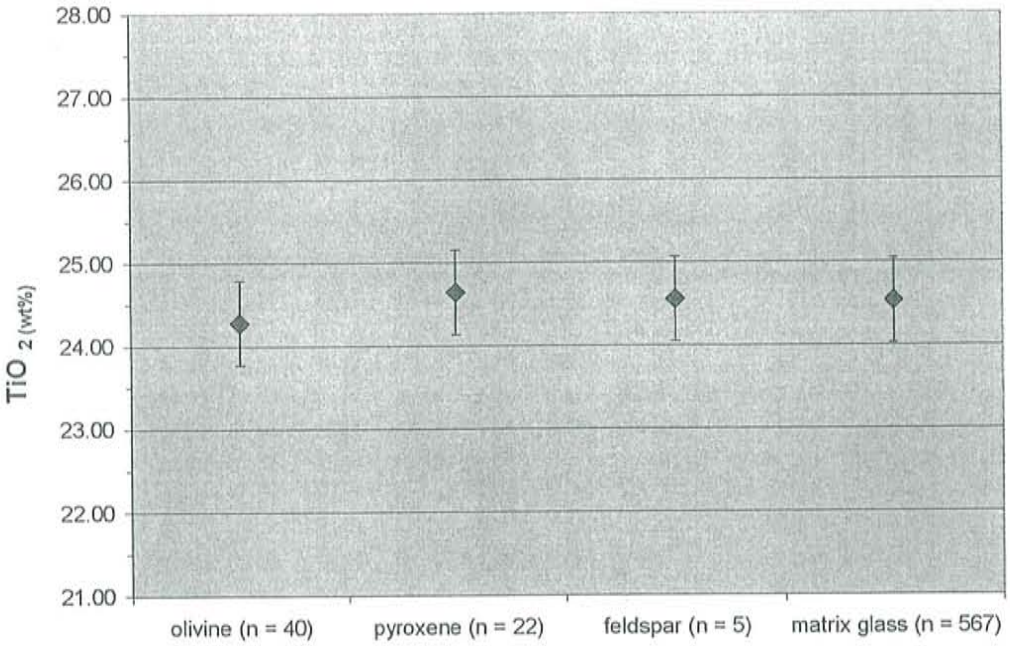

Table D.4.3 Electron Microprobe Analyses of Titanomagnetite in Tephra

r = rim, I = intermediate, c = core
* = small crystal (< 20µm)
$ = crystal number & analysis number (e.g. 3-2 = crystal #3, analysis #2)
^host is matrix glass unless otherwise noted (ol = olivine, pyx = pyroxene, fel = feldspar)

Sample	*n*	TiO_2	Al_2O_3	Fe_2O_3	FeO	MnO	MgO	Total	mol% ülvospinel *Stormer (1983)*	traverse coord. (µm)	location*	crystal-analysis$	host^
25724	1	24.41	2.25	20.29	47.49	1.81	2.96	99.21	71.1		c	1-1	
25724	2	24.64	2.31	19.84	47.89	1.77	2.92	99.36	71.9		c	1-2	
25724	3	24.56	2.22	19.87	47.70	1.77	2.91	99.02	71.7		c	2-1	
25724	4	24.73	2.35	19.74	48.16	1.71	2.87	99.55	72.2		c	3-1	
25724	5	24.80	2.24	19.64	48.13	1.74	2.88	99.42	72.2		c	4-1	
25724	6	24.58	2.46	19.81	47.85	1.73	2.94	99.36	72.1		c	5-1	
25724	7	24.58	2.25	19.82	47.78	1.81	2.85	99.08	71.8		c	6-1	
25724	8	24.73	2.30	19.51	47.83	1.75	2.96	99.09	72.4		c	7-1	
25724	9	24.79	2.33	19.74	48.02	1.79	2.96	99.63	72.2		c	7-2	
25724	10	24.63	2.27	20.01	47.98	1.68	2.93	99.49	71.7		c	8-1	
25724	11	24.72	2.30	19.72	47.97	1.80	2.89	99.40	72.1		c	9-1	
25724	12	24.75	2.25	19.94	47.89	1.77	3.01	99.61	71.7		c	10-1	
25724	13	24.63	2.18	19.43	47.61	1.78	2.89	98.52	72.2		c	11-1	
25724	14	24.85	2.29	19.75	48.21	1.72	2.94	99.74	72.2		c	12-1	
25724	15	24.77	2.20	19.62	47.95	1.79	2.90	99.23	72.1		c	13-1	
2E2	1	24.57	2.26	19.94	47.69	1.89	2.89	99.24	71.7		c	1-1	
2E2	2	24.80	2.22	19.84	47.94	1.90	2.93	99.61	71.9		c	1-2	
2E2	3	24.21	2.17	20.21	47.26	1.73	2.90	98.48	70.9		c	2-1	
2E2	4	24.50	2.21	20.10	47.65	1.86	2.88	99.19	71.4		r	3-1	
2E2	5	24.83	2.18	19.82	48.02	1.85	2.93	99.64	71.9		r	3-2	
2E2	6	24.84	2.24	19.43	48.24	1.75	2.80	99.30	72.6		c	3-3	
2E2	7	24.81	2.21	19.71	48.10	1.76	2.89	99.47	72.1		r	3-4	
2E2	8	24.81	2.20	19.56	48.19	1.71	2.84	99.31	72.3		c	4-1	
2E2	9	24.83	2.22	19.71	48.15	1.78	2.88	99.57	72.1		c	4-2	
2E2	10	24.88	2.19	19.52	48.10	1.77	2.91	99.36	72.4		c	4-3	
2E2	11	24.21	2.22	20.32	47.12	1.78	2.98	98.63	70.8		c	5-1	
2E2	12	24.05	2.18	20.25	47.03	1.75	2.86	98.12	70.8		r	5-2	
2E2	13	24.64	2.25	20.04	47.92	1.82	2.89	99.57	71.6		c	6-1	
2E2	14	24.68	2.21	20.04	47.88	1.81	2.94	99.56	71.5		c	6-2	
2E2	15	24.77	2.24	19.77	47.96	1.75	2.96	99.45	72.0		c	6-3	
2E2	16	25.05	2.24	19.54	48.26	1.87	2.96	99.92	72.5		c	7-1	
25723	1	24.43	2.24	20.14	47.64	1.73	2.91	99.10	71.3		c	1-1	
25723	2	24.84	2.27	19.44	47.97	1.77	2.95	99.23	72.5		c	1-2	
25723	3	24.22	2.25	20.38	47.23	1.81	2.94	98.84	70.8		c	2-1	
25723	4	24.68	2.29	19.72	47.92	1.69	2.95	99.26	72.1		c	3-1	

Table D.4.3 Electron Microprobe Analyses of Titanomagnetite in Tephra

r = rim, I = intermediate, c = core
* = small crystal (< 20μm)
$ = crystal number & analysis number (e.g. 3-2 = crystal #3, analysis #2)
^host is matrix glass unless otherwise noted (ol = olivine, pyx = pyroxene, fel = feldspar)

Sample	*n*	TiO_2	Al_2O_3	Fe_2O_3	FeO	MnO	MgO	Total	mol% ülvospinel *Stormer (1983)*	traverse coord. (μm)	location*	crystal-analysis$	host^
25723	5	25.02	2.28	19.18	48.23	1.78	2.92	99.41	73.0		c	4-1	
25723	6	24.70	2.29	19.27	47.82	1.74	2.87	98.69	72.7		c	4-2	
25723	7	24.82	2.25	19.76	48.04	1.76	2.97	99.60	72.1		c	5-1	
25723	8	24.49	2.29	20.18	47.71	1.77	2.93	99.37	71.4		c	6-1	
25723	9	24.52	2.24	20.06	47.73	1.77	2.91	99.23	71.5		r	6-2	
25723	10	24.28	2.21	19.72	47.11	1.75	2.93	98.00	71.6		c	7-1	
25723	11	24.95	2.31	19.47	48.28	1.73	2.93	99.67	72.6		c	8-1	
25723	12	24.33	2.24	20.38	47.37	1.85	2.95	99.10	70.9		c	9-1	
25723	13	24.87	2.27	19.60	48.09	1.80	2.94	99.56	72.3		c	10-1	
25723	14	24.99	2.27	19.58	48.23	1.74	3.00	99.81	72.4		c	11-1	
25723	15	24.87	2.30	19.54	47.97	1.85	2.97	99.50	72.4		c	12-1	
78325	1	24.96	2.18	19.41	48.22	1.79	2.88	99.43	72.6		c	1-1	
78325	2	24.53	2.20	19.99	47.74	1.76	2.89	99.10	71.5		c	2-1	
78325	3	24.81	2.16	19.72	48.08	1.74	2.90	99.41	72.0		c	2-2	
78325	4	24.45	2.18	20.04	47.76	1.72	2.82	98.98	71.4		c	3-1	
78325	5	24.80	2.19	19.79	48.15	1.72	2.89	99.54	72.0		c	4-1	
78325	6	24.59	2.19	20.15	47.83	1.84	2.88	99.48	71.4		c	4-2	
78325	7	24.53	2.21	20.06	47.67	1.81	2.92	99.19	71.4		c	5-1	
78325	8	24.87	2.24	19.77	48.06	1.85	2.96	99.75	72.1		c	6-1	
78325	9	24.76	2.24	19.61	47.97	1.76	2.91	99.23	72.2		c	6-2	
78325	10	24.53	2.20	20.08	47.74	1.77	2.91	99.22	71.4		c	7-1	
78325	11	24.50	2.19	19.97	47.55	1.79	2.94	98.95	71.5		c*	8-1	
78325	12	24.61	2.19	19.86	47.73	1.78	2.92	99.10	71.7		c*	8-2	
79302	1	24.63	2.24	20.02	47.97	1.86	2.83	99.56	71.6	5	r	1-1	
79302	2	24.35	2.29	20.51	47.63	1.89	2.86	99.52	70.8	5	r	1-2	
79302	3	24.20	2.26	20.69	47.38	1.92	2.86	99.32	70.5	5	r	1-3	
79302	4	24.72	2.25	20.06	48.16	1.83	2.84	99.86	71.7	15	i	1-4	
79302	5	23.96	2.29	20.56	47.42	1.86	2.61	98.71	70.6	25	i	1-5	
79302	6	24.68	2.26	20.03	47.76	1.98	2.94	99.65	71.6	70	i	1-6	
79302	7	24.45	2.33	20.16	47.56	1.87	2.95	99.31	71.3	100	i	1-7	
79302	8	24.59	2.28	20.34	47.93	1.86	2.90	99.89	71.2	150	c	1-8	
79302	9	24.62	2.27	20.23	47.92	1.90	2.89	99.83	71.4	200	i	1-9	
79302	10	24.61	2.26	20.35	47.82	1.92	2.94	99.89	71.2	270	i	1-10	
79302	11	24.19	2.30	20.74	47.34	1.88	2.94	99.39	70.4	290	r	1-11	
79302	12	24.48	2.29	20.03	47.74	1.81	2.85	99.19	71.6	290	r	1-12	
79302	13	24.49	2.28	20.15	47.70	1.86	2.88	99.35	71.4	290	r	1-13	

Table D.4.3 Electron Microprobe Analyses of Titanomagnetite in Tephra

r = rim, I = intermediate, c = core
* = small crystal (< 20µm)
$ = crystal number & analysis number (e.g. 3-2 = crystal #3, analysis #2)
^host is matrix glass unless otherwise noted (ol = olivine, pyx = pyroxene, fel = feldspar)

Sample	*n*	TiO_2	Al_2O_3	Fe_2O_3	FeO	MnO	MgO	Total	mol% ülvospinel *Stormer (1983)*	traverse coord. (µm)	location*	crystal-analysis$	host^
79302	14	24.08	2.29	20.89	47.31	1.87	2.87	99.31	70.2		c	2-1	
79302	15	23.71	2.26	21.42	46.95	1.87	2.82	99.01	69.2		c	2-2	
79302	16	24.13	2.28	21.02	47.47	1.80	2.90	99.60	70.1		c	2-3	
79302	17	24.17	2.29	20.83	47.27	1.90	2.95	99.40	70.2		r	3-1	
79302	18	24.12	2.27	20.93	47.45	1.80	2.88	99.45	70.2		r	3-2	
79302	19	24.16	2.24	21.20	47.43	1.86	2.95	99.84	69.8		c	4-1	
79302	20	24.53	2.25	20.30	47.70	1.92	2.92	99.60	71.2		c	4-2	
81003	1	24.44	2.26	19.99	47.50	1.82	2.92	98.92	71.5	5	r	1-1	
81003	2	24.33	2.24	20.46	47.44	1.89	2.91	99.26	70.8	5	r	1-2	
81003	3	24.18	2.20	20.72	47.32	1.83	2.92	99.17	70.3	5	r	1-3	
81003	4	24.20	2.26	20.94	47.44	1.90	2.91	99.66	70.1	20	i	1-4	
81003	5	24.64	2.24	20.06	47.85	1.85	2.92	99.56	71.5	35	i	1-5	
81003	6	24.51	2.29	20.19	47.66	1.84	2.95	99.43	71.3	50	i	1-6	
81003	7	24.22	2.27	20.73	47.43	1.80	2.94	99.39	70.4	70	c	1-7	
81003	8	24.25	2.32	20.64	47.48	1.82	2.92	99.44	70.6	85	i	1-8	
81003	9	24.53	2.31	20.29	47.78	1.89	2.91	99.70	71.3	100	i	1-9	
81003	10	24.57	2.30	19.84	47.69	1.73	2.97	99.10	71.8	110	i	1-10	
81003	11	24.28	2.31	20.38	47.42	1.88	2.88	99.15	70.9	120	r	1-11	
81003	12	23.86	2.35	20.81	46.76	1.86	2.98	98.62	70.1	120	r	1-12	
81003	13	24.23	2.24	20.72	47.39	1.88	2.91	99.37	70.4	60	c	1-13	
81003	14	24.52	2.27	20.06	47.55	1.94	2.93	99.27	71.4		r	2-1	
81003	15	24.70	2.26	20.12	47.92	1.85	2.96	99.82	71.5		c	2-2	
81003	16	24.86	2.29	19.89	48.24	1.84	2.90	100.01	72.0		r	2-3	
81003	17	24.27	2.29	20.63	47.59	1.82	2.87	99.46	70.7		c	2-4	
81003	18	24.68	2.25	20.19	47.96	1.84	2.93	99.85	71.4		r	3-1	
81003	19	24.56	2.28	19.80	47.74	1.81	2.86	99.05	71.9		r	3-2	
81003	20	24.42	2.21	20.67	47.64	1.83	2.96	99.73	70.6		c	4-1	
81003	21	24.65	2.24	20.00	47.98	1.86	2.84	99.56	71.7		c	4-2	
81410	1	24.03	2.19	20.42	47.13	1.79	2.81	98.37	70.6	5	r	1-1	
81410	2	23.90	2.27	20.52	46.89	1.86	2.83	98.26	70.4	5	r	1-2	
81410	3	24.06	1.61	20.84	46.63	1.92	2.92	97.98	69.2	9	i	1-3	
81410	4	24.26	2.22	20.24	47.42	1.87	2.80	98.82	71.0	13	i	1-4	
81410	5	24.02	2.21	20.45	47.06	1.80	2.84	98.39	70.6	17	i	1-5	
81410	6	24.34	2.22	20.44	47.51	1.86	2.89	99.25	70.8	21	i	1-6	
81410	7	24.52	2.24	20.06	47.70	1.96	2.81	99.30	71.5	25	i	1-7	
81410	8	24.53	2.24	19.78	47.52	1.90	2.89	98.86	71.8	30	i	1-8	

Table D.4.3 Electron Microprobe Analyses of Titanomagnetite in Tephra

r = rim, I = intermediate, c = core
* = small crystal (< 20μm)
$ = crystal number & analysis number (e.g. 3-2 = crystal #3, analysis #2)
^host is matrix glass unless otherwise noted (ol = olivine, pyx = pyroxene, fel = feldspar)

Sample	*n*	TiO_2	Al_2O_3	Fe_2O_3	FeO	MnO	MgO	Total	mol% ülvospinel *Stormer (1983)*	traverse coord. (μm)	location*	crystal-analysis$	host^
81410	9	24.42	2.27	20.40	47.61	1.89	2.90	99.48	71.0	44	i	1-9	
81410	10	24.59	2.28	20.03	47.76	1.89	2.90	99.45	71.6	58	c	1-10	
81410	11	24.63	2.29	19.83	47.87	1.85	2.87	99.34	71.9	72	i	1-11	
81410	12	24.48	2.31	20.09	47.66	1.86	2.89	99.28	71.5	86	i	1-12	
81410	13	24.64	2.26	19.86	47.80	1.85	2.90	99.31	71.8	100	i	1-13	
81410	14	24.35	2.28	20.46	47.60	1.79	2.92	99.40	70.9	135	i	1-14	
81410	15	24.56	2.31	19.84	47.64	1.91	2.89	99.14	71.8	170	i	1-15	
81410	16	24.43	2.27	20.09	47.58	1.81	2.90	99.08	71.4	210	i	1-16	
81410	17	23.94	2.26	21.24	47.14	1.85	2.91	99.34	69.6	220	r	1-17	
81410	18	23.77	2.26	20.92	46.82	1.81	2.86	98.45	69.8	222	r	1-18	
81410	19	24.31	2.26	20.90	47.50	1.90	2.97	99.83	70.2	222	r	1-19	
81410	20	24.42	2.32	20.51	47.58	1.91	2.96	99.69	70.9	115	c	1-24	
81410	21	24.43	2.18	20.24	47.83	1.83	2.75	99.26	71.2		r	1-20	
81410	22	24.36	2.17	20.42	47.61	1.84	2.84	99.22	70.8		r	1-21	
81410	23	24.09	2.26	20.64	47.23	1.82	2.87	98.91	70.4		r	1-22	
81410	24	24.12	2.24	20.77	47.40	1.83	2.83	99.18	70.3		i	1-23	
81410	25	24.49	2.28	20.07	47.70	1.89	2.85	99.29	71.5		r	2-1	
81410	26	24.50	2.33	20.03	47.63	1.92	2.89	99.29	71.6		c	2-2	
81410	27	24.15	2.25	20.78	47.44	1.77	2.89	99.27	70.3		r	2-3	
81410	28	24.57	2.28	19.85	47.70	1.82	2.91	99.13	71.8		c	3-1	
81410	29	24.33	2.28	19.95	47.44	1.82	2.84	98.66	71.5		c	3-2	
81410	30	24.63	2.26	20.14	47.84	1.90	2.91	99.68	71.5		c	4-1	
81410	31	24.59	2.28	20.35	47.89	1.93	2.89	99.93	71.2		c	4-2	
81410	32	24.69	2.27	20.11	48.07	1.88	2.84	99.86	71.6		c	4-3	
81410	33	24.48	2.24	19.89	47.53	1.87	2.88	98.88	71.6		c	5-1	
81410	34	24.43	2.30	20.11	47.46	1.85	2.96	99.11	71.3		c	5-2	
81410	35	24.81	2.18	19.64	48.19	1.77	2.81	99.39	72.2		c	6-1	
81410	36	24.53	2.17	20.20	47.89	1.80	2.81	99.41	71.3		r	6-2	
81410	37	24.58	2.21	20.32	47.83	1.83	2.93	99.70	71.1		r	7-1	
81410	38	24.30	2.15	20.60	47.62	1.80	2.83	99.30	70.6		c	8-1	
81410	39	24.30	2.21	20.46	47.40	1.78	2.95	99.08	70.7		c	9-1	
81410	40	24.37	2.19	20.37	47.62	1.78	2.87	99.20	70.9		c	10-1	
81410	41	24.41	2.14	20.10	47.61	1.71	2.86	98.83	71.2		c	11-1	
81410	42	24.65	2.19	19.69	47.89	1.75	2.85	99.02	72.0		r	12-1	
81410	43	24.74	2.21	19.77	47.80	1.84	2.96	99.32	71.9		c	12-2	

Table D.4.3 Electron Microprobe Analyses of Titanomagnetite in Tephra

r = rim, I = intermediate, c = core
* = small crystal (< 20μm)
$ = crystal number & analysis number (e.g. 3-2 = crystal #3, analysis #2)
^host is matrix glass unless otherwise noted (ol = olivine, pyx = pyroxene, fel = feldspar)

Sample	*n*	TiO_2	Al_2O_3	Fe_2O_3	FeO	MnO	MgO	Total	mol% ülvospinel *Stormer (1983)*	traverse coord. (μm)	location*	crystal-analysis$	host^
82418	1	24.51	2.30	19.38	47.46	1.78	2.90	98.33	72.4	5	r	1-1	
82418	2	24.17	2.33	20.13	47.14	1.78	2.93	98.49	71.2	25	i	1-2	
82418	3	24.70	2.27	19.85	47.84	1.84	2.94	99.44	71.9	45	i	1-3	
82418	4	24.57	2.26	19.73	47.61	1.83	2.91	98.91	71.9	65	i	1-4	
82418	5	24.51	2.31	20.16	47.65	1.89	2.93	99.44	71.4	85	i	1-5	
82418	6	24.79	2.30	19.65	48.04	1.81	2.92	99.52	72.3	105	c	1-6	
82418	7	24.85	2.25	19.69	48.11	1.84	2.89	99.63	72.2	125	c	1-7	
82418	8	24.52	2.29	19.84	47.63	1.81	2.90	98.99	71.8	145	i	1-8	
82418	9	24.70	2.29	19.76	47.92	1.83	2.89	99.38	72.0	165	i	1-9	
82418	10	24.83	2.32	19.16	47.77	1.81	2.97	98.86	72.8	185	i	1-10	
82418	11	24.41	2.30	19.68	47.42	1.86	2.84	98.52	71.9	190	r	1-11	
82418	12	24.24	2.26	20.16	47.24	1.80	2.93	98.63	71.1	190	r	1-12	
82418	13	24.61	2.31	20.09	47.77	1.97	2.90	99.65	71.5	190	r	1-13	
82418	14	24.74	1.78	19.70	47.47	1.85	2.95	98.48	71.4	30	i	2-1	
82418	15	24.49	1.77	20.53	47.40	1.84	2.95	99.00	70.2	60	c	2-2	
82418	16	24.61	2.23	20.24	48.02	1.88	2.82	99.80	71.4	120	c	2-3	
82418	17	24.69	2.26	20.11	47.91	1.82	2.97	99.75	71.5	150	i	2-4	
82418	18	24.65	2.24	19.87	47.72	1.88	2.93	99.29	71.7	180	r	2-5	
82418	19	24.46	2.31	19.75	47.56	1.83	2.87	98.79	71.9	5	r	3-1	
82418	20	24.94	2.37	19.38	48.29	1.78	2.88	99.63	72.8	33	i	3-2	
82418	21	24.85	2.30	19.52	48.04	1.87	2.90	99.48	72.5	62	i	3-3	
82418	22	24.79	2.28	19.57	47.97	1.85	2.89	99.36	72.3	90	c	3-4	
82418	23	24.58	2.29	20.09	47.72	1.86	2.94	99.48	71.5	118	i	3-5	
82418	24	24.74	2.34	19.61	48.04	1.85	2.84	99.42	72.3	147	i	3-6	
82418	25	24.38	2.28	20.11	47.44	1.79	2.95	98.95	71.3	175	r	3-7	
82418	26	24.57	2.38	20.01	47.84	1.85	2.89	99.54	71.7	93	c	3-8	
82418	27	24.69	2.25	19.72	47.74	1.86	2.94	99.20	72.0		r	4-1	
82418	28	24.47	2.31	20.32	47.75	1.87	2.88	99.59	71.2		r	4-2	
82418	29	24.54	2.24	20.28	47.87	1.83	2.87	99.63	71.2		r	4-3	
82418	30	24.94	2.30	19.42	48.24	1.92	2.82	99.64	72.7		c	4-4	
82418	31	24.99	2.29	19.41	48.16	1.85	2.94	99.64	72.6		c	4-5	
82418	32	25.04	2.37	19.18	48.23	1.81	2.96	99.60	73.1		c	4-6	
82418	33	24.96	2.32	19.50	48.15	1.86	2.95	99.73	72.5		c	4-7	
82418	34	24.52	2.31	20.13	47.77	1.81	2.91	99.44	71.5		r	4-8	
82418	35	24.58	2.27	19.85	47.74	1.81	2.90	99.16	71.8		r	4-9	
82418	36	24.75	2.25	19.88	47.88	1.83	2.98	99.57	71.8		r	4-10	

Table D.4.3 Electron Microprobe Analyses of Titanomagnetite in Tephra

r = rim, I = intermediate, c = core
* = small crystal (< 20μm)
$ = crystal number & analysis number (e.g. 3-2 = crystal #3, analysis #2)
^host is matrix glass unless otherwise noted (ol = olivine, pyx = pyroxene, fel = feldspar)

Sample	*n*	TiO_2	Al_2O_3	Fe_2O_3	FeO	MnO	MgO	Total	mol% ülvospinel *Stormer (1983)*	traverse coord. (μm)	location*	crystal-analysis$	host^
82418	37	24.62	2.32	20.09	47.82	1.85	2.96	99.66	71.6		c	4-11	
83207	1	24.23	2.22	19.79	46.98	1.84	2.92	97.98	71.4	5	r	1-1	
83207	2	24.57	2.25	19.05	47.31	1.83	2.91	97.92	72.7	5	i	1-2	
83207	3	25.02	2.28	18.73	47.90	1.88	2.93	98.73	73.5	30	i	1-3	
83207	4	24.92	2.29	18.84	47.82	1.88	2.92	98.67	73.3	70	i	1-4	
83207	5	24.81	2.29	19.13	47.73	1.82	2.96	98.74	72.8	120	i	1-5	
83207	6	25.00	2.28	18.85	48.08	1.79	2.90	98.90	73.4	200	c	1-6	
83207	7	25.08	2.23	18.49	47.96	1.83	2.91	98.49	73.8	250	i	1-7	
83207	8	25.09	2.28	18.55	48.10	1.83	2.87	98.72	73.8	300	i	1-8	
83207	9	24.58	2.31	19.24	47.41	1.86	2.91	98.30	72.5	335	i	1-9	
83207	10	24.78	2.29	19.56	47.92	1.80	2.94	99.30	72.3	375	i	1-10	
83207	11	24.62	2.23	19.14	47.27	1.88	2.98	98.13	72.5	400	i	1-11	
83207	12	24.63	2.30	19.60	47.53	1.85	2.99	98.90	72.1	400	i	1-11	
83207	13	24.35	2.22	19.50	46.97	1.86	2.96	97.84	71.9	400	r	1-11	
83207	14	24.18	2.31	20.22	47.04	1.86	2.96	98.57	71.0	5	r	2-1	
83207	15	24.56	2.31	19.64	47.47	1.86	2.96	98.79	72.0	28	i	2-2	
83207	16	25.09	2.28	19.26	48.24	1.86	2.96	99.68	72.9	50	i	2-3	
83207	17	24.69	2.30	19.36	47.80	1.82	2.86	98.84	72.5	73	i	2-4	
83207	18	24.50	2.29	19.77	47.56	1.84	2.90	98.87	71.8	95	i	2-5	
83207	19	24.91	2.34	19.23	48.07	1.83	2.91	99.27	72.9	118	i	2-6	
83207	20	24.80	2.29	19.35	47.76	1.88	2.96	99.04	72.5	140	c	2-7	
83207	21	24.58	2.33	19.72	47.61	1.89	2.93	99.05	72.0	163	i	2-8	
83207	22	24.70	2.29	19.59	47.81	1.82	2.92	99.13	72.2	185	i	2-9	
83207	23	24.47	2.29	19.82	47.44	1.84	2.93	98.79	71.7	208	i	2-10	
83207	24	24.84	2.28	19.15	47.94	1.76	2.90	98.88	72.9	230	i	2-11	
83207	25	24.63	2.25	19.77	47.72	1.89	2.89	99.15	71.9	253	i	2-12	
83207	26	24.49	2.22	19.62	47.24	1.87	2.98	98.40	71.8	275	r	2-13	
83207	27	24.37	2.28	19.76	47.20	1.84	2.95	98.39	71.7	275	r	2-14	
83207	28	24.58	2.29	19.31	47.39	1.85	2.94	98.36	72.4	275	r	2-15	
83207	39	24.66	2.29	19.90	47.95	1.87	2.85	99.52	71.9	52	c	2-16	
83207	29	24.15	2.28	19.97	47.03	1.84	2.88	98.15	71.3		r	3-1	
83207	30	24.36	2.27	19.97	47.38	1.76	2.94	98.67	71.4		r	3-2	
83207	31	24.28	2.26	19.93	47.14	1.83	2.94	98.36	71.4		r	3-3	
83207	32	24.98	2.23	19.24	48.04	1.81	2.95	99.26	72.8		i	3-4	
83207	33	24.91	2.26	19.47	48.05	1.84	2.93	99.45	72.5		i	3-5	
83207	34	24.45	2.24	20.17	47.55	1.90	2.90	99.21	71.2		i	3-6	

Table D.4.3 Electron Microprobe Analyses of Titanomagnetite in Tephra

r = rim, I = intermediate, c = core
* = small crystal (< 20μm)
$ = crystal number & analysis number (e.g. 3-2 = crystal #3, analysis #2)
^host is matrix glass unless otherwise noted (ol = olivine, pyx = pyroxene, fel = feldspar)

Sample	*n*	TiO_2	Al_2O_3	Fe_2O_3	FeO	MnO	MgO	Total	mol% ülvospinel *Stormer (1983)*	traverse coord. (μm)	location*	crystal-analysis$	host^
83207	35	24.80	2.26	19.67	47.93	1.85	2.94	99.46	72.1		r	3-7	
83207	36	24.39	2.22	19.71	47.33	1.84	2.87	98.36	71.7		r	3-8	
83207	37	23.95	2.28	20.37	46.82	1.87	2.90	98.19	70.6		r	3-9	
83207	38	24.66	2.23	20.14	47.82	1.91	2.93	99.69	71.4		c	3-10	
84500	1	24.32	2.22	20.86	47.66	1.76	2.94	99.75	70.3	19	i	1-1	
84500	2	24.82	2.26	19.89	48.40	1.61	2.90	99.87	72.1	30	i	1-2	
84500	3	24.93	2.27	20.10	48.45	1.68	2.98	100.40	71.8	41	i	1-3	
84500	4	24.46	2.26	20.76	48.11	1.69	2.87	100.15	70.7	52	i	1-4	
84500	5	24.73	2.24	20.14	48.14	1.76	2.91	99.92	71.6	63	i	1-5	
84500	6	24.71	2.29	20.05	48.18	1.75	2.87	99.85	71.8	74	c	1-6	
84500	7	24.70	2.27	20.32	48.26	1.81	2.85	100.19	71.4	85	i	1-7	
84500	8	24.75	2.29	20.17	48.28	1.73	2.90	100.12	71.7	96	i	1-8	
84500	9	24.77	2.27	20.33	48.27	1.75	2.95	100.34	71.4	111	i	1-9	
84500	10	24.87	2.18	20.21	48.53	1.77	2.83	100.39	71.6	122	i	1-10	
84500	11	24.69	2.23	20.53	48.12	1.72	2.99	100.29	71.0	133	i	1-11	
84500	12	24.59	2.26	20.44	48.05	1.70	2.94	99.99	71.1	141	i	1-12	
84500	13	24.10	2.27	20.96	47.43	1.75	2.91	99.41	70.1	152	r	1-13	
84500	14	24.50	2.25	20.55	47.84	1.78	2.94	99.87	70.9	152	r	1-14	
84500	15	24.87	2.25	19.68	48.19	1.76	2.91	99.66	72.2	152	r	1-15	
84500	16	24.79	2.25	20.29	48.28	1.79	2.91	100.32	71.4	70	c	1-16	
84500	17	24.48	2.24	20.65	47.93	1.73	2.92	99.94	70.8	50	i	1-17	
84500	18	25.03	2.27	20.21	48.61	1.81	2.96	100.88	71.8	7	r	2-1	
84500	19	24.71	2.27	20.16	48.28	1.75	2.84	100.01	71.6	7	r	2-2	
84500	20	24.84	2.21	19.91	48.36	1.73	2.85	99.90	72.0	7	r	2-3	
84500	21	25.13	2.27	19.73	48.71	1.81	2.88	100.52	72.5	22	i	2-4	
84500	22	24.45	2.29	20.53	47.92	1.83	2.84	99.85	71.0	41	i	2-5	
84500	23	24.64	2.27	20.32	48.30	1.68	2.84	100.05	71.4	56	i	2-6	
84500	24	24.82	2.27	20.02	48.39	1.68	2.88	100.06	71.9	74	c	2-7	
84500	25	24.79	2.26	19.83	48.35	1.67	2.84	99.74	72.1	96	c	2-8	
84500	26	25.03	2.31	19.60	48.61	1.75	2.84	100.15	72.6	118	i	2-9	
84500	27	24.67	2.27	19.86	48.04	1.73	2.86	99.44	71.9	137	i	2-10	
84500	28	24.63	2.26	20.19	48.08	1.82	2.84	99.82	71.5	152	i	2-11	
84500	29	24.52	2.24	20.53	47.97	1.77	2.89	99.91	70.9	163	r	2-12	
84500	30	24.53	2.25	20.55	48.07	1.72	2.88	99.99	71.0		c	3-1	
84500	31	24.81	2.26	19.97	48.39	1.70	2.85	99.98	71.9		c	3-2	
84500	32	24.97	2.22	19.98	48.65	1.74	2.84	100.40	72.0		c	3-3	

Table D.4.3 Electron Microprobe Analyses of Titanomagnetite in Tephra

r = rim, I = intermediate, c = core
* = small crystal (< 20μm)
$ = crystal number & analysis number (e.g. 3-2 = crystal #3, analysis #2)
^host is matrix glass unless otherwise noted (ol = olivine, pyx = pyroxene, fel = feldspar)

Sample	*n*	TiO_2	Al_2O_3	Fe_2O_3	FeO	MnO	MgO	Total	mol% ülvospinel *Stormer (1983)*	traverse coord. (μm)	location*	crystal-analysis$	host^
84500	33	24.74	2.22	20.09	48.31	1.69	2.85	99.90	71.7		c	3-4	
84500	34	24.39	2.21	20.56	47.76	1.73	2.90	99.55	70.8		r	4-1	
84500	35	24.48	2.27	20.57	48.08	1.67	2.88	99.94	71.0		c	4-2	
84500	36	24.85	2.33	19.94	48.47	1.76	2.84	100.19	72.1		c	4-3	
84505	1	24.18	2.26	21.73	48.00	1.67	2.89	100.73	69.4	7	r	1-1	
84505	2	23.81	2.25	21.78	47.61	1.57	2.81	99.84	69.0	7	r	1-2	
84505	3	23.64	2.26	22.10	47.27	1.64	2.87	99.77	68.5	7	r	1-3	
84505	4	24.02	2.20	21.36	47.58	1.63	2.88	99.67	69.6	17	i	1-4	
84505	5	24.63	2.27	20.35	48.18	1.67	2.90	100.00	71.3	45	i	1-5	
84505	6	24.36	2.28	20.89	47.87	1.74	2.91	100.06	70.5	62	i	1-6	
84505	7	24.56	2.27	20.83	48.27	1.73	2.87	100.52	70.7	83	i	1-7	
84505	8	24.92	2.29	20.26	48.60	1.71	2.93	100.70	71.7	103	i	1-8	
84505	9	24.41	2.29	20.96	48.08	1.69	2.89	100.31	70.5	128	i	1-9	
84505	10	24.46	2.28	20.69	47.96	1.73	2.91	100.02	70.8	152	c	1-10	
84505	11	24.62	2.27	20.62	48.27	1.72	2.89	100.40	71.0	172	i	1-11	
84505	12	25.04	2.25	19.94	48.70	1.73	2.88	100.54	72.1	190	i	1-12	
84505	13	24.62	2.25	20.75	48.31	1.65	2.93	100.50	70.8	214	i	1-13	
84505	14	24.57	2.26	20.60	48.12	1.70	2.92	100.18	70.9	234	i	1-14	
84505	15	24.49	2.30	20.53	48.09	1.63	2.90	99.94	71.1	248	i	1-15	
84505	16	24.92	2.21	20.18	48.59	1.69	2.89	100.47	71.7	255	i	1-16	
84505	17	24.27	2.24	21.14	47.74	1.73	2.95	100.06	70.0	262	i	1-17	
84505	18	24.67	2.26	20.38	48.30	1.64	2.91	100.16	71.3	269	r	1-18	
84505	19	24.60	2.29	20.53	48.12	1.77	2.91	100.21	71.1	269	r	1-19	
84505	20	24.47	2.23	20.71	48.00	1.67	2.92	100.00	70.7	269	r	1-20	
84505	21	24.84	2.27	20.06	48.34	1.79	2.89	100.18	71.8	124	c	1-21	
84505	22	24.75	2.26	20.22	48.25	1.80	2.87	100.15	71.5	150	c	1-22	
84505	23	23.72	2.11	21.42	46.95	1.74	2.85	98.79	69.0		r*	2-1	
84505	24	24.22	2.20	20.78	47.50	1.73	2.92	99.34	70.3		r*	2-2	
84505	25	24.32	2.21	20.93	47.84	1.74	2.86	99.89	70.3		c*	2-3	
84505	26	24.20	2.17	21.01	47.66	1.74	2.86	99.64	70.1		c*	2-4	
84505	27	23.66	2.19	21.52	46.96	1.72	2.85	98.89	69.0		c*	2-5	
84505	28	24.39	2.29	20.52	48.02	1.65	2.82	99.69	71.0		c	3-1	
84505	29	24.66	2.30	20.31	48.29	1.65	2.89	100.09	71.5		c	3-2	
84505	30	24.82	2.29	20.08	48.36	1.69	2.93	100.16	71.8		c	3-3	
84505	31	24.33	2.29	20.76	47.78	1.78	2.88	99.80	70.6		c	4-1	
84505	32	24.57	2.28	20.21	48.11	1.64	2.88	99.69	71.5		c	5-1	

Table D.4.3 Electron Microprobe Analyses of Titanomagnetite in Tephra

r = rim, I = intermediate, c = core
* = small crystal (< 20μm)
[$] = crystal number & analysis number (e.g. 3-2 = crystal #3, analysis #2)
^host is matrix glass unless otherwise noted (ol = olivine, pyx = pyroxene, fel = feldspar)

Sample	*n*	TiO_2	Al_2O_3	Fe_2O_3	FeO	MnO	MgO	Total	mol% ülvospinel *Stormer (1983)*	traverse coord. (μm)	location*	crystal-analysis[$]	host^
85009	1	24.52	2.20	20.41	47.95	1.66	2.92	99.66	71.1	5	r	1-1	
85009	2	24.39	2.22	20.40	47.68	1.69	2.92	99.31	71.0	5	r	1-2	
85009	3	24.53	2.19	19.94	47.83	1.72	2.84	99.05	71.6	5	r	1-3	
85009	4	24.63	2.25	20.42	48.12	1.75	2.90	100.07	71.2	10	i	1-4	
85009	5	24.81	2.20	19.91	48.29	1.68	2.88	99.77	71.9	17	i	1-5	
85009	6	24.94	2.21	19.75	48.41	1.73	2.88	99.91	72.2	28	i	1-6	
85009	7	24.55	2.27	20.42	47.95	1.73	2.93	99.85	71.1	40	i	1-7	
85009	8	25.06	2.26	19.60	48.55	1.71	2.92	100.12	72.5	55	i	1-8	
85009	9	24.59	2.21	20.06	47.90	1.68	2.92	99.36	71.5	70	i	1-9	
85009	10	25.03	2.22	19.64	48.59	1.68	2.88	100.03	72.4	87	c	1-10	
85009	11	24.49	2.27	20.40	47.95	1.78	2.84	99.73	71.1	106	i	1-11	
85009	12	24.84	2.21	20.16	48.33	1.72	2.93	100.19	71.6	122	i	1-12	
85009	13	24.77	2.25	20.33	48.34	1.74	2.91	100.34	71.4	143	i	1-13	
85009	14	24.66	2.20	20.44	48.24	1.63	2.92	100.09	71.2	156	i	1-14	
85009	15	24.89	2.23	20.12	48.53	1.76	2.85	100.37	71.8	171	i	1-15	
85009	16	24.51	2.22	20.92	48.01	1.74	2.96	100.35	70.4	183	i	1-16	
85009	17	24.60	2.22	20.10	47.91	1.74	2.91	99.46	71.5	188	r	1-17	
85009	18	24.49	2.25	20.56	47.97	1.71	2.90	99.87	70.9	188	r	1-18	
85009	19	24.57	2.25	20.46	48.18	1.71	2.85	100.02	71.2	188	r	1-19	
85009	20	24.75	2.19	19.99	48.20	1.79	2.83	99.75	71.7	68		1-20	
85009	21	24.56	2.31	20.21	48.03	1.69	2.89	99.69	71.5	89		1-21	
85009	22	24.66	2.26	20.43	48.40	1.70	2.82	100.27	71.3		c	2-1	
85009	23	24.49	2.21	20.70	47.87	1.75	2.96	99.98	70.6		c	2-2	
85009	24	24.47	2.27	20.51	48.11	1.64	2.85	99.86	71.1		c	2-3	
85009	25	24.54	2.26	20.77	48.07	1.77	2.92	100.34	70.7		c	3-1	
85009	26	24.72	2.27	20.46	48.36	1.74	2.88	100.43	71.3		c	3-2	
85009	27	24.22	2.27	20.98	47.70	1.66	2.93	99.77	70.2		r	3-3	
85009	28	24.30	2.25	20.97	47.74	1.80	2.89	99.95	70.2		r	3-4	
85009	29	24.11	2.16	21.11	47.40	1.77	2.91	99.45	69.8		r	3-5	
85009	30	24.46	2.24	21.09	48.18	1.74	2.86	100.57	70.3		c	4-1	
85009	31	24.56	2.24	20.80	48.19	1.75	2.88	100.42	70.7		c	4-2	
85009	32	24.22	2.26	21.15	47.77	1.70	2.91	100.01	70.0		c	5-1	
85009	33	24.31	2.27	21.16	47.94	1.76	2.87	100.32	70.1		c	5-2	
85010	1	24.05	2.32	20.84	47.37	1.78	2.85	99.22	70.3		c	1-1	
85010	2	23.98	2.26	21.00	47.36	1.77	2.81	99.18	70.0		c	1-2	
85010	3	24.39	2.25	20.01	47.58	1.80	2.83	98.85	71.5		c	2-1	

Table D.4.3 Electron Microprobe Analyses of Titanomagnetite in Tephra

r = rim, I = intermediate, c = core
* = small crystal (< 20μm)
$ = crystal number & analysis number (e.g. 3-2 = crystal #3, analysis #2)
^host is matrix glass unless otherwise noted (ol = olivine, pyx = pyroxene, fel = feldspar)

Sample	*n*	TiO_2	Al_2O_3	Fe_2O_3	FeO	MnO	MgO	Total	mol% ülvospinel *Stormer (1983)*	traverse coord. (μm)	location*	crystal-analysis$	host^
85010	4	24.40	2.17	20.06	47.52	1.77	2.88	98.79	71.3		c	3-1	
85010	5	24.75	2.22	19.69	48.24	1.71	2.79	99.40	72.2		c	4-1	
85010	6	24.58	2.19	19.82	47.81	1.80	2.82	99.03	71.8		c	4-2	
85010	7	23.98	2.28	20.83	47.35	1.68	2.84	98.95	70.2		c	5-1	
85010	8	24.09	2.24	20.37	47.17	1.69	2.91	98.46	70.8		c	5-2	
85010	9	24.22	2.31	20.68	47.75	1.65	2.85	99.46	70.7		c	6-1	
85010	10	24.04	2.31	21.09	47.54	1.70	2.86	99.54	70.0		c	6-2	
85010	11	24.59	2.18	19.54	47.81	1.72	2.81	98.64	72.1		c	7-1	
85010	12	24.60	2.20	20.00	47.93	1.72	2.88	99.32	71.6		c	7-2	
86022	1	24.75	2.27	19.74	48.09	1.74	2.88	99.47	72.1	6	r	1-1	
86022	2	24.76	2.26	19.75	48.00	1.77	2.93	99.46	72.1	6	r	1-2	
86022	3	24.91	2.30	19.41	48.29	1.67	2.90	99.46	72.7	6	r	1-3	
86022	4	24.75	2.26	19.81	48.20	1.73	2.85	99.60	72.1	23	i	1-4	
86022	5	24.85	2.24	19.85	48.20	1.81	2.90	99.86	72.0	37	i	1-5	
86022	6	24.99	2.25	19.80	48.63	1.69	2.86	100.21	72.3	51	i	1-6	
86022	7	25.09	2.23	19.65	48.80	1.71	2.81	100.28	72.5	71	i	1-7	
86022	8	25.02	2.31	19.36	48.45	1.75	2.87	99.76	72.9	91	i	1-8	
86022	9	25.06	2.29	19.73	48.77	1.70	2.85	100.40	72.5	108	c	1-9	
86022	10	25.15	2.34	19.14	48.67	1.70	2.86	99.86	73.3	128	i	1-10	
86022	11	25.08	2.21	19.27	48.54	1.72	2.83	99.64	72.9	154	i	1-11	
86022	12	25.07	2.33	19.43	48.72	1.65	2.86	100.05	72.9	180	i	1-12	
86022	13	24.82	2.26	19.84	48.38	1.67	2.86	99.83	72.1	208	i	1-13	
86022	14	24.74	2.20	19.57	48.09	1.69	2.83	99.11	72.3	228	i	1-14	
86022	15	24.66	2.24	19.90	47.96	1.76	2.88	99.40	71.8	239	r	1-15	
86022	16	25.05	2.21	20.05	48.72	1.79	2.86	100.67	72.0	239	r	1-16	
86022	17	25.12	2.30	19.61	48.93	1.67	2.81	100.44	72.7	239	r	1-17	
86022	18	24.76	2.31	20.23	48.29	1.73	2.93	100.24	71.6	110	c	1-18	
86022	19	24.74	2.30	20.14	48.33	1.68	2.89	100.08	71.7	150	c	1-19	
86022	20	24.43	2.21	20.18	47.81	1.69	2.84	99.16	71.3	11	r	2-1	
86022	21	24.90	2.24	19.86	48.37	1.79	2.87	100.03	72.1	23	i	2-2	
86022	22	24.94	2.23	19.74	48.43	1.69	2.90	99.93	72.2	57	c	2-3	
86022	23	24.80	2.31	19.93	48.31	1.77	2.86	99.98	72.0	91	i	2-4	
86022	24	24.60	2.27	20.06	47.91	1.65	2.97	99.45	71.6	103	i	2-5	
86022	25	24.74	2.27	19.84	48.18	1.69	2.88	99.61	72.0	103	r	2-6	
86022	26	24.89	2.34	19.58	48.33	1.64	2.93	99.71	72.5		c	3-1	
86022	27	24.83	2.29	19.95	48.26	1.72	2.95	100.01	71.9		c	3-2	

Table D.4.3 Electron Microprobe Analyses of Titanomagnetite in Tephra

r = rim, I = intermediate, c = core
* = small crystal (< 20µm)
$ = crystal number & analysis number (e.g. 3-2 = crystal #3, analysis #2)
^host is matrix glass unless otherwise noted (ol = olivine, pyx = pyroxene, fel = feldspar)

Sample	*n*	TiO_2	Al_2O_3	Fe_2O_3	FeO	MnO	MgO	Total	mol% ülvospinel *Stormer (1983)*	traverse coord. (µm)	location*	crystal-analysis$	host^
86022	28	24.64	2.27	20.29	48.10	1.66	2.95	99.91	71.4		c	4-1	
86022	29	24.93	2.29	19.73	48.39	1.75	2.89	99.97	72.3		c	4-2	
88104	1	23.98	2.21	20.28	46.94	1.81	2.82	98.04	70.7		c*	1-1	
88104	2	24.67	2.25	19.59	47.92	1.69	2.89	99.00	72.2		r	2-1	
88104	3	24.64	2.50	19.82	48.23	1.73	2.81	99.72	72.3		c	2-2	
88104	4	24.62	2.26	20.02	48.05	1.68	2.88	99.51	71.7		c	2-3	
88104	5	24.73	2.48	19.42	48.07	1.76	2.87	99.33	72.8		c	3-1	
88104	6	24.52	2.19	20.04	47.79	1.72	2.88	99.15	71.5		c	3-2	
88104	7	24.74	2.23	19.68	48.09	1.75	2.84	99.31	72.2		c	4-1	
88104	8	24.57	2.23	19.86	47.84	1.74	2.86	99.10	71.8		c	4-2	
88104	9	24.70	2.25	19.54	48.16	1.70	2.75	99.10	72.4		c	5-1	
88104	10	24.97	2.21	19.37	48.34	1.72	2.86	99.47	72.7		c	5-2	
88104	11	24.32	2.23	20.21	47.60	1.77	2.82	98.95	71.2		c	6-1	
88104	12	24.49	2.18	19.59	47.66	1.66	2.84	98.43	72.0		c*	7-1	
88104	13	24.59	2.20	19.76	47.78	1.77	2.85	98.95	71.9		c*	7-2	
88104	14	24.68	2.39	19.75	48.18	1.70	2.84	99.54	72.3		c	8-1	
91101	1	24.78	2.25	19.72	48.20	1.71	2.86	99.51	72.2		c	1-1	
91101	2	24.55	2.22	20.11	47.84	1.79	2.87	99.38	71.4		c	1-2	
91101	3	24.39	2.20	20.40	47.80	1.76	2.81	99.36	71.0		c	2-1	
91101	4	24.56	2.20	20.28	47.96	1.70	2.91	99.60	71.2		c	3-1	
91101	5	24.62	2.22	20.06	48.16	1.64	2.84	99.52	71.6		c	4-1	
91101	6	24.70	2.27	19.87	48.10	1.73	2.86	99.53	72.0		c	4-2	
91101	7	24.38	2.26	19.83	47.58	1.69	2.84	98.57	71.7		c	5-1	
91101	8	24.68	2.24	19.85	47.99	1.82	2.84	99.42	71.9		c	6-1	
91101	9	24.48	2.24	20.25	47.88	1.76	2.83	99.43	71.3		c	6-2	
91101	10	24.55	2.21	19.57	47.68	1.76	2.83	98.60	72.1		c	7-1	
92101	1	24.17	2.23	20.83	47.53	1.76	2.86	99.38	70.3		r	1-1	
92101	2	24.47	2.19	20.15	47.65	1.82	2.87	99.15	71.3		r	1-2	
92101	3	24.22	2.24	20.82	47.59	1.70	2.91	99.48	70.3		c	2-1	
92101	4	24.67	2.25	19.96	48.07	1.77	2.85	99.57	71.8		r	3-1	
92101	5	24.32	2.27	20.94	47.81	1.74	2.92	99.99	70.3		c	3-2	
92101	6	23.73	2.27	21.30	46.73	1.79	2.98	98.79	69.3		c*	4-1	
92101	7	24.42	2.29	20.12	47.73	1.73	2.87	99.16	71.4		c	5-1	
92101	8	24.29	2.25	20.37	47.70	1.74	2.80	99.13	71.0		c	6-1	
92101	9	24.18	2.17	20.74	47.45	1.74	2.88	99.15	70.3		c	6-2	
92101	10	24.26	2.19	20.68	47.59	1.74	2.88	99.34	70.5		c*	7-1	
92101	11	24.71	2.21	20.07	48.10	1.81	2.86	99.76	71.6		c	8-1	

Table D.4.3 Electron Microprobe Analyses of Titanomagnetite in Tephra

r = rim, I = intermediate, c = core
* = small crystal (< 20μm)
$ = crystal number & analysis number (e.g. 3-2 = crystal #3, analysis #2)
^host is matrix glass unless otherwise noted (ol = olivine, pyx = pyroxene, fel = feldspar)

Sample	*n*	TiO_2	Al_2O_3	Fe_2O_3	FeO	MnO	MgO	Total	mol% ülvospinel *Stormer (1983)*	traverse coord. (μm)	location*	crystal-analysis$	host^
92101	12	24.63	2.29	20.17	48.22	1.62	2.87	99.80	71.6		c	8-2	
92101	13	24.62	2.27	20.07	48.02	1.70	2.90	99.58	71.6		c	9-1	
92101	14	24.55	2.28	20.34	48.05	1.70	2.88	99.81	71.3		c	9-2	
Er92KS	1	24.68	2.24	19.93	48.17	1.71	2.82	99.55	71.9		c	1-1	
Er92KS	2	24.39	2.30	20.42	47.77	1.74	2.89	99.51	71.1		r	1-2	
Er92KS	3	24.27	2.21	20.76	47.81	1.66	2.83	99.54	70.5		c	1-3	
Er92KS	4	24.25	2.23	20.25	47.39	1.71	2.91	98.74	71.0		c	2-1	
Er92KS	5	24.43	2.30	20.48	47.93	1.77	2.83	99.74	71.1		c	3-1	
Er92KS	6	24.88	2.27	19.71	48.34	1.73	2.87	99.79	72.3		c	3-2	
Er92KS	7	24.66	2.32	20.24	48.31	1.69	2.84	100.07	71.6		c	3-3	
93102	1	24.30	2.19	20.91	47.86	1.73	2.83	99.81	70.3		r	1-1	
93102	2	24.57	2.27	20.36	47.96	1.76	2.92	99.83	71.2		c	1-2	
93102	3	24.44	2.16	20.70	47.95	1.79	2.83	99.87	70.6		r	2-1	
93102	4	24.24	2.24	20.58	47.73	1.73	2.78	99.29	70.7		c	2-2	
93102	5	24.48	2.17	20.39	47.86	1.73	2.88	99.50	71.0		c*	3-1	
93102	6	24.04	2.20	20.77	47.22	1.77	2.87	98.87	70.2		c*	4-1	
93102	7	24.60	2.24	19.99	48.03	1.73	2.82	99.41	71.7		c	5-1	
93102	8	24.35	2.25	20.29	47.70	1.71	2.85	99.14	71.1		c	6-1	
93102	9	24.47	2.21	20.66	48.07	1.65	2.87	99.91	70.8		c	6-2	
93102	10	24.64	2.22	20.03	48.28	1.70	2.74	99.63	71.7		c	7-1	
93102	11	24.69	2.25	20.13	48.30	1.67	2.85	99.89	71.7		c	7-2	
93102	12	24.41	2.28	20.33	47.94	1.81	2.74	99.50	71.2		c	8-1	
93102	13	24.05	2.24	21.07	47.46	1.67	2.89	99.37	69.9		c	8-2	
93102	14	24.47	2.24	20.33	47.94	1.70	2.85	99.53	71.2		c	9-1	
93102	15	23.65	2.27	21.03	46.71	1.69	2.90	98.26	69.6		c*	10-1	
Er96KS	1	24.34	2.16	19.95	47.47	1.70	2.85	98.47	71.4	60	r	1-1	ol
Er96KS	2	24.20	2.25	20.21	47.38	1.71	2.86	98.62	71.1	60	r	1-2	ol
Er96KS	3	24.64	2.17	19.50	47.73	1.73	2.88	98.66	72.2	49	i	1-3	ol
Er96KS	4	24.45	2.22	20.10	47.64	1.72	2.92	99.05	71.3	31	c	1-4	ol
Er96KS	5	24.27	2.20	20.49	47.50	1.68	2.92	99.06	70.7	13	i	1-5	ol
Er96KS	6	24.34	2.22	20.28	47.59	1.77	2.85	99.05	71.1	3	r	1-6	ol
Er96KS	7	24.43	2.19	20.15	47.70	1.80	2.81	99.08	71.3	5	r	1-7	ol
Er96KS	8	23.53	2.16	21.31	46.71	1.67	2.83	98.20	69.1	78	r	2-1	ol
Er96KS	9	23.34	2.23	21.54	46.38	1.76	2.85	98.10	68.7	78	r	2-2	ol
Er96KS	10	24.20	2.17	20.38	47.58	1.73	2.75	98.80	70.8	65	i	2-3	ol
Er96KS	11	24.36	2.29	20.29	47.90	1.71	2.77	99.33	71.3	55	c	2-4	ol
Er96KS	12	24.23	2.20	20.27	47.63	1.75	2.72	98.79	71.1	45	i	2-5	ol

Table D.4.3 Electron Microprobe Analyses of Titanomagnetite in Tephra

r = rim, I = intermediate, c = core
* = small crystal (< 20µm)
$ = crystal number & analysis number (e.g. 3-2 = crystal #3, analysis #2)
^host is matrix glass unless otherwise noted (ol = olivine, pyx = pyroxene, fel = feldspar)

Sample	*n*	TiO_2	Al_2O_3	Fe_2O_3	FeO	MnO	MgO	Total	mol% ülvospinel *Stormer (1983)*	traverse coord. (µm)	location*	crystal-analysis$	host^
Er96KS	13	24.07	2.23	20.49	47.50	1.71	2.73	98.73	70.7	5	r	2-6	ol
Er96KS	14	23.96	2.24	20.87	47.46	1.71	2.73	98.96	70.2	5	r	2-7	ol
Er96KS	15	24.37	2.21	20.19	47.66	1.67	2.87	98.96	71.2		c	3-1	
Er96KS	16	24.49	2.19	19.99	47.83	1.71	2.82	99.03	71.5		c	3-2	
Er96KS	17	24.53	2.29	19.82	47.88	1.69	2.84	99.04	71.9		r	3-3	
Er96KS	18	24.84	2.18	19.66	48.22	1.63	2.90	99.43	72.2		c	3-4	
Er96KS	19	24.20	2.20	20.54	47.29	1.77	2.94	98.93	70.6		c	4-1	
Er96KS	20	24.30	2.26	20.04	47.52	1.78	2.80	98.71	71.4		c	4-2	
Er96KS	21	24.23	2.21	20.24	47.36	1.73	2.88	98.65	71.0		c	5-1	
Er96KS	22	24.43	2.21	20.10	47.87	1.70	2.78	99.07	71.4		c	5-2	
Er96KS	23	23.84	2.27	21.14	47.42	1.63	2.76	99.06	69.8		c	6-1	ol
Er96KS	24	23.74	2.32	21.02	47.08	1.72	2.79	98.67	69.9		c	7-1	ol
Er96KS	25	24.70	2.26	19.81	48.14	1.71	2.83	99.45	72.0		c	8-1	
Er96KS	26	24.79	2.18	19.73	48.08	1.78	2.87	99.44	72.0		c	8-2	
Er96KS	27	24.34	2.13	19.66	47.53	1.71	2.73	98.10	71.8				
Er96KS	28	24.83	2.28	19.44	48.19	1.77	2.82	99.33	72.6		c	9-1	
Er96KS	29	25.01	2.22	19.48	48.52	1.74	2.82	99.78	72.6		c	9-2	
Er96KS	30	24.48	2.22	20.30	47.99	1.70	2.81	99.52	71.2		c	10-1	
Er96KS	31	24.76	2.21	20.10	48.22	1.75	2.89	99.91	71.6		c	11-1	
Er96KS	32	25.20	2.46	18.85	48.77	1.74	2.81	99.83	73.9		c	11-2	
Er96KS	33	24.72	2.25	19.66	48.06	1.73	2.85	99.26	72.2		c	11-3	
Er96KS	34	25.13	2.24	19.29	48.70	1.74	2.80	99.90	73.0		c	12-1	
Er96KS	35	24.76	2.25	20.01	48.36	1.67	2.84	99.90	71.9		c	12-2	
Er96KS	36	24.54	2.27	20.45	48.08	1.81	2.82	99.99	71.1	5	r	13-1	ol
Er96KS	37	24.48	2.20	20.78	47.94	1.85	2.87	100.12	70.6	5	r	13-2	ol
Er96KS	38	24.43	2.27	20.67	47.93	1.76	2.87	99.94	70.8	5	r	13-3	ol
Er96KS	39	24.31	2.25	20.89	47.86	1.74	2.86	99.91	70.4	14	i	13-4	ol
Er96KS	40	24.84	2.21	20.21	48.54	1.76	2.80	100.35	71.6	24	i	13-5	ol
Er96KS	41	24.71	2.26	20.42	48.44	1.77	2.81	100.42	71.3	35	c	13-6	ol
Er96KS	42	24.19	2.22	20.91	47.57	1.77	2.87	99.53	70.2	64	i	13-7	ol
Er96KS	43	23.97	2.27	21.55	47.75	1.68	2.79	99.99	69.4	71	i	14-1	ol
Er96KS	44	24.18	2.32	21.39	48.00	1.72	2.81	100.43	69.9	58	c	14-2	ol
Er96KS	45	24.38	2.30	21.18	48.19	1.72	2.85	100.60	70.2	39	c	14-3	ol
Er96KS	46	24.22	2.32	21.49	47.94	1.77	2.89	100.62	69.7	16	i	14-4	ol
Er96KS	47	24.37	2.28	20.89	48.17	1.74	2.75	100.20	70.6	5	r	14-5	ol

Table D.4.3 Electron Microprobe Analyses of Titanomagnetite in Tephra

r = rim, I = intermediate, c = core
* = small crystal (< 20µm)
$ = crystal number & analysis number (e.g. 3-2 = crystal #3, analysis #2)
^host is matrix glass unless otherwise noted (ol = olivine, pyx = pyroxene, fel = feldspar)

Sample	*n*	TiO_2	Al_2O_3	Fe_2O_3	FeO	MnO	MgO	Total	mol% ülvospinel *Stormer (1983)*	traverse coord. (µm)	location*	crystal-analysis$	host^
Er96KS	48	24.18	2.26	21.49	48.01	1.76	2.78	100.47	69.7	5	r	14-6	ol
Er96KS	49	24.52	2.27	20.95	48.44	1.72	2.78	100.68	70.6	5	r	14-7	ol
Er96KS	50	24.23	2.28	21.22	47.91	1.75	2.83	100.22	70.0		c*	15-1	ol
Er96KS	51	24.46	2.17	20.92	47.90	1.83	2.91	100.19	70.3	5	r	16-1	ol
Er96KS	52	24.38	2.22	20.89	47.88	1.76	2.88	100.01	70.4	5	r	16-2	ol
Er96KS	53	24.20	2.21	21.29	47.69	1.74	2.92	100.04	69.7	5	r	16-3	ol
Er96KS	54	24.42	2.18	20.80	48.03	1.76	2.81	100.01	70.5	9	i	16-4	ol
Er96KS	55	24.59	2.22	20.70	48.29	1.75	2.82	100.37	70.9	13	c	16-5	ol
Er96KS	56	24.20	2.19	21.14	47.69	1.74	2.88	99.83	69.9	21	i	16-6	ol
Er96KS	57	24.65	2.27	20.68	48.35	1.75	2.86	100.55	71.0		c	17-1	ol
Er96KS	58	24.23	2.22	21.10	47.83	1.73	2.83	99.93	70.1		c	17-2	ol
Er96KS	59	24.50	2.25	20.65	48.18	1.71	2.83	100.12	70.9		c	17-3	ol
Er96KS	60	23.92	2.23	21.56	47.39	1.72	2.89	99.71	69.2		c	18-1	
Er96KS	61	24.26	2.22	21.16	47.84	1.71	2.89	100.08	70.0		c	18-2	
Er96KS	62	24.37	2.26	20.95	48.12	1.66	2.83	100.18	70.5		c	18-3	
Er96KS	63	24.49	2.22	20.94	48.29	1.74	2.79	100.46	70.5		c	18-4	
97018	1	24.72	2.23	18.92	47.71	1.78	2.82	98.18	73.0		c	1-1	
97018	2	25.10	2.25	18.22	48.05	1.77	2.85	98.23	74.2		c	1-2	
97018	3	24.96	2.22	18.68	47.96	1.73	2.89	98.44	73.5		r	1-3	
97018	4	24.94	2.27	18.72	47.89	1.78	2.91	98.52	73.4		r	2-1	
97018	5	24.92	2.24	18.83	48.08	1.67	2.86	98.59	73.3		c	2-2	
97018	6	24.97	2.28	18.86	48.11	1.64	2.93	98.78	73.4		r	2-3	
97018	7	24.73	2.27	18.93	47.68	1.85	2.83	98.31	73.0		c	3-1	
97018	8	24.81	2.22	19.05	47.89	1.75	2.86	98.57	72.9		c	3-2	
97018	9	24.84	2.26	18.93	47.88	1.72	2.89	98.52	73.1		r*	4-1	
97018	10	24.89	2.21	18.96	47.87	1.76	2.92	98.62	73.0		c*	4-2	
97018	11	24.87	2.24	18.73	47.93	1.68	2.86	98.31	73.4		r*	4-3	
97018	12	24.73	2.17	18.96	47.66	1.78	2.85	98.15	72.9		c*	5-1	
97018	13	24.86	2.22	18.71	47.79	1.67	2.92	98.18	73.4		c*	5-2	
97018	14	24.45	2.26	19.27	47.36	1.74	2.86	97.94	72.4		c*	5-3	
97018	15	24.15	2.25	19.82	47.12	1.71	2.86	97.90	71.5		r	6-1	
97018	16	24.42	2.24	19.33	47.38	1.72	2.85	97.95	72.3		c	6-2	
97018	17	24.35	2.24	19.46	47.31	1.76	2.83	97.97	72.1		c	6-3	
97018	18	24.41	2.26	19.60	47.53	1.67	2.86	98.33	72.0	5	r	7-1	
97018	19	24.95	2.24	18.77	47.97	1.74	2.89	98.56	73.4	5	r	7-2	

Table D.4.3 Electron Microprobe Analyses of Titanomagnetite in Tephra

r = rim, I = intermediate, c = core
* = small crystal (< 20µm)
$ = crystal number & analysis number (e.g. 3-2 = crystal #3, analysis #2)
^host is matrix glass unless otherwise noted (ol = olivine, pyx = pyroxene, fel = feldspar)

Sample	*n*	TiO_2	Al_2O_3	Fe_2O_3	FeO	MnO	MgO	Total	mol% ülvospinel *Stormer (1983)*	traverse coord. (µm)	location*	crystal-analysis$	host^
97018	20	24.55	2.20	19.29	47.58	1.73	2.84	98.18	72.4	5	r	7-3	
97018	21	24.87	2.22	19.06	48.06	1.78	2.82	98.80	73.0	8	i	7-4	
97018	22	24.95	2.22	19.04	48.20	1.69	2.85	98.96	73.1	22	i	7-5	
97018	23	24.93	2.22	19.00	48.11	1.72	2.86	98.84	73.1	29	i	7-6	
97018	24	24.71	2.17	19.34	47.76	1.77	2.87	98.63	72.4	40	i	7-7	
97018	25	24.91	2.25	19.00	48.12	1.71	2.86	98.85	73.1	59	c	7-8	
97018	26	24.70	2.23	18.99	47.83	1.68	2.81	98.24	73.0	74	i	7-9	
97018	27	24.53	2.23	19.39	47.52	1.73	2.89	98.29	72.3	85	i	7-10	
97018	28	24.30	2.20	19.32	47.12	1.75	2.84	97.53	72.1	90	r	7-11	
97018	29	24.71	2.26	19.10	47.68	1.71	2.93	98.39	72.8	90	r	7-12	
97018	30	24.60	2.25	19.34	47.60	1.75	2.89	98.42	72.4	90	r	7-13	
97018	31	24.77	2.23	19.18	47.79	1.75	2.91	98.62	72.7	39	i	7-14	
97018	32	24.92	2.25	19.02	47.95	1.80	2.90	98.84	73.0	58	c	7-15	
Er97KS	1	24.52	2.31	19.78	47.83	1.73	2.83	99.00	72.0		c	1-1	
Er97KS	2	24.78	2.24	19.37	48.09	1.65	2.86	98.97	72.6		c	1-2	
Er97KS	3	24.45	2.25	20.04	47.57	1.77	2.92	99.00	71.4		c	1-3	
Er97KS	4	24.87	2.22	19.60	48.25	1.70	2.88	99.51	72.3		c	2-1	
Er97KS	5	24.70	2.29	19.54	47.97	1.69	2.89	99.07	72.4		c	2-2	
Er97KS	6	24.81	2.25	19.50	48.16	1.70	2.85	99.26	72.5		c	2-3	
Er97KS	7	24.62	2.22	19.78	47.86	1.75	2.87	99.09	71.9		c	3-1	
Er97KS	8	24.81	2.28	19.45	48.11	1.78	2.83	99.27	72.5		c	3-2	
Er97KS	9	24.12	2.27	19.90	47.15	1.66	2.86	97.96	71.4	5	r	4-1	
Er97KS	10	24.02	2.25	20.22	47.05	1.66	2.89	98.08	70.9	12	c	4-2	
Er97KS	11	24.03	2.28	20.15	46.87	1.77	2.94	98.04	70.9	27	r	4-3	
Er97KS	12	23.88	2.26	20.38	46.85	1.71	2.88	97.97	70.6	10	c	4-4	
Er97KS	13	23.92	2.22	20.33	46.78	1.76	2.90	97.91	70.6	5	r	5-1	
Er97KS	14	24.13	2.23	20.08	47.01	1.75	2.92	98.12	71.1	5	r	5-2	
Er97KS	15	24.38	2.26	19.78	47.41	1.81	2.86	98.50	71.7	17	i	5-3	
Er97KS	16	24.37	2.25	19.68	47.58	1.65	2.82	98.36	71.9	27	i	5-4	
Er97KS	17	24.61	2.25	20.02	47.89	1.74	2.92	99.44	71.6	36	i	5-5	
Er97KS	18	24.57	2.20	19.92	47.80	1.73	2.89	99.12	71.6	47	i	5-6	
Er97KS	19	24.67	2.29	19.82	48.04	1.75	2.86	99.43	72.0	62	i	5-7	
Er97KS	20	24.31	2.21	20.23	47.51	1.68	2.91	98.85	71.1	73	i	5-8	
Er97KS	21	24.55	2.20	19.91	47.88	1.66	2.86	99.06	71.7	85	c	5-9	
Er97KS	22	24.37	2.20	20.38	47.59	1.82	2.87	99.23	70.9	44	i	5-10	
Er97KS	23	24.57	2.28	19.95	47.90	1.71	2.88	99.28	71.7	42	i	5-11	

Table D.4.3 Electron Microprobe Analyses of Titanomagnetite in Tephra

r = rim, I = intermediate, c = core
* = small crystal (< 20μm)
$ = crystal number & analysis number (e.g. 3-2 = crystal #3, analysis #2)
^host is matrix glass unless otherwise noted (ol = olivine, pyx = pyroxene, fel = feldspar)

Sample	*n*	TiO_2	Al_2O_3	Fe_2O_3	FeO	MnO	MgO	Total	mol% ülvospinel *Stormer (1983)*	traverse coord. (μm)	location*	crystal-analysis$	host^
Er97KS	24	24.20	2.25	19.76	47.35	1.69	2.77	98.01	71.7		c	6-1	
Er97KS	25	24.13	2.29	20.10	47.39	1.59	2.84	98.33	71.3		c	6-2	
Er97KS	26	24.35	2.18	19.55	47.25	1.69	2.90	97.93	71.9		c	7-1	
Er97KS	27	24.01	2.15	20.35	47.07	1.65	2.87	98.09	70.6		c	7-2	
Er97KS	28	24.13	2.21	20.01	47.01	1.74	2.91	98.02	71.1		c	8-1	
Er97KS	29	24.38	2.19	19.79	47.43	1.71	2.88	98.38	71.6		c	9-1	
1999	1	23.93	2.30	20.40	46.94	1.75	2.88	98.19	70.6		r	1-1	
1999	2	24.23	2.04	20.13	47.24	1.76	2.83	98.22	70.9		c	1-2	
1999	3	24.18	2.24	20.06	47.34	1.72	2.81	98.35	71.2		c	1-3	
1999	4	24.27	2.33	19.97	47.50	1.74	2.82	98.63	71.5		c	1-4	
1999	5	23.99	2.27	20.21	46.97	1.78	2.85	98.07	70.9		c	1-5	
1999	6	24.16	2.21	20.28	47.28	1.71	2.87	98.50	70.9		r	1-6	
1999	7	23.89	2.29	20.76	47.10	1.73	2.85	98.61	70.2		c	1-7	
1999	8	24.17	2.27	19.95	47.25	1.70	2.84	98.19	71.4		c	1-8	
1999	9	24.08	2.25	20.37	47.14	1.78	2.87	98.49	70.7		c	1-9	
1999	10	24.20	2.36	20.14	47.26	1.82	2.89	98.66	71.2		c	1-10	
1999	11	24.37	2.75	20.31	47.89	1.67	2.99	99.99	71.7		c	2-1	fel
1999	12	24.64	2.74	19.82	48.15	1.65	3.00	100.00	72.5		c	2-2	fel
1999	13	24.46	2.46	20.34	48.04	1.69	2.87	99.86	71.5		c	3-1	fel
1999	14	24.54	2.45	20.36	48.17	1.73	2.87	100.12	71.5		c	4-1	fel
1999	15	24.78	2.49	20.04	48.17	1.86	2.96	100.30	72.0		c	5-1	fel
Er99KS	1	24.35	2.25	19.88	47.45	1.78	2.85	98.55	71.6		c	1-1	
Er99KS	2	24.23	2.30	19.93	47.32	1.75	2.84	98.37	71.5		c	2-1	
Er99KS	3	23.81	2.27	20.73	46.83	1.77	2.87	98.27	70.1		c	2-2	
Er99KS	4	24.26	2.26	20.08	47.48	1.76	2.80	98.65	71.3		c	3-1	
Er99KS	5	23.57	2.78	20.61	46.86	1.70	2.82	98.33	70.8		c	3-2	
Er99KS	6	24.07	2.21	20.37	47.03	1.82	2.89	98.39	70.6		c	3-3	
Er99KS	7	23.91	2.55	20.14	47.09	1.78	2.79	98.26	71.3		c	3-4	
Er99KS	8	23.74	2.30	20.67	46.69	1.72	2.92	98.03	70.1		c	4-1	
Er99KS	9	24.00	2.33	20.50	47.14	1.76	2.87	98.60	70.6		c	5-1	
Er99KS	10	23.75	2.27	20.70	46.85	1.65	2.87	98.09	70.1		c	6-1	
Er99KS	11	24.30	2.28	19.59	47.45	1.70	2.79	98.10	72.0		c	6-2	
Er99KS	12	24.45	2.28	19.28	47.35	1.76	2.87	97.98	72.4		r	6-3	
Er99KS	13	24.41	2.27	19.39	47.37	1.74	2.86	98.03	72.2		c	6-4	
Er99KS	14	24.27	2.31	19.54	47.30	1.64	2.87	97.92	72.0		c	6-5	
DEC2000	1	24.56	2.31	19.67	47.91	1.69	2.82	98.94	72.2		r	1-1	
DEC2000	2	24.53	2.30	19.77	47.68	1.84	2.86	98.98	71.9		i	1-2	

Table D.4.3 Electron Microprobe Analyses of Titanomagnetite in Tephra

r = rim, I = intermediate, c = core
* = small crystal (< 20μm)
$ = crystal number & analysis number (e.g. 3-2 = crystal #3, analysis #2)
^host is matrix glass unless otherwise noted (ol = olivine, pyx = pyroxene, fel = feldspar)

Sample	*n*	TiO_2	Al_2O_3	Fe_2O_3	FeO	MnO	MgO	Total	mol% ülvospinel *Stormer (1983)*	traverse coord. (μm)	location*	crystal-analysis$	host^
DEC2000	3	24.47	2.29	19.98	47.60	1.81	2.91	99.04	71.6		c	1-3	
DEC2000	4	24.60	2.25	19.76	47.91	1.69	2.86	99.07	72.0		c	2-1	
DEC2000	5	23.92	2.26	20.57	47.06	1.75	2.82	98.38	70.4		r	3-1	
DEC2000	6	24.38	2.28	20.05	47.70	1.81	2.77	98.99	71.5		i	3-2	
DEC2000	7	24.35	2.25	20.20	47.75	1.72	2.80	99.07	71.3		c	3-3	
DEC2000	8	24.44	2.36	19.97	47.79	1.77	2.82	99.15	71.7		c	4-1	
DEC2000	9	24.68	2.29	19.55	47.88	1.78	2.87	99.05	72.3		c	5-1	
DEC2000	10	24.54	2.32	19.93	47.89	1.73	2.86	99.26	71.8		c	6-1	
Y2K	1	23.98	2.33	20.41	46.99	1.73	2.92	98.34	70.7		r	1-1	
Y2K	2	24.74	2.34	19.39	47.92	1.76	2.89	99.05	72.6		i	1-2	
Y2K	3	24.71	2.42	19.49	47.93	1.81	2.89	99.25	72.5		c	1-3	
Y2K	4	24.43	2.31	19.44	47.53	1.76	2.80	98.27	72.3		r	2-1	
Y2K	5	23.94	3.10	20.41	47.64	1.74	2.82	99.64	71.8		c	2-2	
Y2K	6	24.14	4.42	19.12	48.32	1.77	2.83	100.59	75.1		r	2-3	
Y2K	7	24.64	2.37	19.37	47.80	1.72	2.90	98.80	72.6		c	2-4	
Y2K	8	23.84	3.02	20.52	47.38	1.75	2.85	99.37	71.4		c	3-1	
Y2K	9	23.96	2.25	20.76	47.14	1.74	2.87	98.72	70.2		r	3-2	
E2001	1	24.97	2.17	20.22	48.63	1.72	2.90	100.59	71.6		c	1-1	
E2001	2	24.59	2.21	20.67	48.06	1.70	2.98	100.22	70.8		c	1-2	
E2001	3	24.81	2.28	19.94	48.09	1.82	2.95	99.89	71.9		c	2-1	
E2001	4	24.69	2.32	20.28	48.06	1.77	2.98	100.10	71.4		c	2-2	
E2001	5	24.89	2.23	20.09	48.14	1.90	2.98	100.23	71.7		c	3-1	
E2001	6	24.74	2.25	20.37	48.35	1.75	2.88	100.34	71.4		c	3-2	
E2001	7	24.69	2.19	20.31	48.11	1.81	2.89	100.00	71.3		c	4-1	
E2001	8	24.98	2.23	19.98	48.53	1.78	2.89	100.39	72.0		c	4-2	
E2001	9	24.74	2.27	20.53	48.34	1.72	2.96	100.56	71.2		c	5-1	
E2001	10	24.83	2.31	20.30	48.33	1.75	2.98	100.49	71.5		c	5-2	
JAN2004	1	24.44	2.26	19.75	47.59	1.76	2.84	98.63	71.8		r	1-1	
JAN2004	2	24.72	2.24	19.39	47.85	1.72	2.90	98.82	72.5		i	1-2	
JAN2004	3	24.16	2.16	20.22	47.30	1.73	2.82	98.37	70.9		c	1-3	
JAN2004	4	24.39	2.34	19.68	47.59	1.70	2.84	98.53	72.0		r	2-1	
JAN2004	5	24.46	2.29	19.67	47.76	1.73	2.78	98.70	72.0		c	2-2	
JAN2004	6	24.22	2.34	19.88	47.29	1.73	2.87	98.32	71.6		c	3-1	
JAN2004	7	24.48	2.30	19.63	47.53	1.77	2.90	98.60	72.0		c	4-1	
JAN2004	8	24.29	2.38	19.81	47.28	1.79	2.91	98.47	71.7		c	5-1	
JAN2004	9	24.54	2.24	19.03	47.52	1.76	2.79	97.88	72.8		c	6-1	
JAN2004	10	24.70	2.68	19.24	48.01	1.79	2.89	99.31	73.2		c	7-1	

Table D.4.3 Electron Microprobe Analyses of Titanomagnetite in Tephra

r = rim, I = intermediate, c = core
* = small crystal (< 20μm)
$ = crystal number & analysis number (e.g. 3-2 = crystal #3, analysis #2)
^host is matrix glass unless otherwise noted (ol = olivine, pyx = pyroxene, fel = feldspar)

Sample	*n*	TiO_2	Al_2O_3	Fe_2O_3	FeO	MnO	MgO	Total	mol% ülvospinel *Stormer (1983)*	traverse coord. (μm)	location*	crystal-analysis$	host^
Erpyx01	1	24.67	2.23	20.22	47.72	1.88	3.03	99.75	71.3		c	1-1	pyx
Erpyx01	2	24.48	2.25	20.48	47.65	1.67	3.07	99.59	70.9		c	2-1	pyx
Erpyx01	3	24.86	2.40	19.68	48.09	1.74	3.03	99.79	72.4		c	3-1	pyx
Erpyx01	4	24.52	2.61	19.55	47.69	1.68	3.00	99.04	72.5		c	4-1	pyx
Erpyx01	5	25.17	2.59	18.99	48.52	1.73	3.02	100.02	73.7		c*	5-1	pyx
Erpyx01	6	24.50	2.63	20.11	47.24	1.65	3.39	99.51	71.6		c*	6-1	pyx
Erpyx01	7	24.59	2.64	19.45	47.73	1.67	3.04	99.12	72.7		c	7-1	pyx
Erpyx01	8	24.91	2.66	19.25	48.26	1.57	3.08	99.72	73.3		c	7-2	pyx
Erpyx01	9	24.70	2.58	19.48	47.81	1.74	3.05	99.36	72.7		c	8-1	pyx
Erpyx01	10	25.14	2.52	19.15	48.26	1.75	3.12	99.93	73.3		c	9-1	pyx
Erpyx01	11	24.33	2.52	20.09	47.56	1.67	2.99	99.15	71.6		c	10-1	pyx
Erpyx01	12	23.88	2.28	21.32	46.34	1.69	3.42	98.93	69.1		c	11-1	pyx
Erpyx01	13	24.75	2.60	19.49	48.09	1.64	3.01	99.58	72.8		c	12-1	pyx
Erpyx01	14	24.57	2.40	20.69	46.71	1.71	3.79	99.87	70.4		c	13-1	pyx
Erpyx01	15	25.01	2.63	19.22	48.45	1.63	3.02	99.96	73.4		c	14-1	pyx
Erpyx01	16	24.74	2.55	19.84	48.05	1.65	3.08	99.90	72.3		c	15-1	pyx
Erpyx01	17	24.82	2.50	19.32	47.98	1.71	3.02	99.34	72.9		c	16-1	pyx
Erpyx01	18	24.59	2.69	19.50	47.79	1.66	3.04	99.28	72.7		c	17-1	pyx
Erpyx01	19	25.01	2.52	19.58	48.30	1.61	3.16	100.18	72.7		c	18-1	pyx
Erpyx01	20	24.74	2.51	19.75	48.31	1.72	2.88	99.90	72.4		c	19-1	pyx
Erpyx01	21	24.23	2.12	20.37	47.18	1.74	2.97	98.61	70.6		c	20-1	pyx
Erpyx01	22	24.01	2.17	20.71	47.00	1.70	2.98	98.56	70.1		c*	21-1	pyx

Table D.5. Electron Microprobe Analyses of Fluorapatites in Tephra

Sample	79302	79302	79302	79302	79302	79302	85010	85010	85010	85010	85010	85010	91101
host^	gl	gl	gl	gl	gl	gl				gl	mag	gl	mag/gl
xtyl-anal.													1-1
SiO_2	0.39	0.40	0.55	0.25	0.34	0.36	0.43	0.45	0.43	0.47	0.60	0.46	0.25
FeO	0.41	0.31	0.67	0.26	0.25	0.41	0.44	0.31	0.31	0.69	1.26	0.55	0.54
MnO	0.11	0.08	0.10	0.10	0.10	0.07	0.13	0.16	0.14	0.11	0.16	0.12	0.12
CaO	53.40	53.49	53.61	53.55	53.23	53.61	54.72	54.00	54.08	53.32	53.49	53.88	54.11
SrO	0.16	0.16	0.18	0.11	0.11	0.17	0.09	0.13	0.10	0.08	0.07	0.08	0.09
P_2O_5	40.70	41.15	41.09	41.59	41.86	41.27	41.19	41.10	41.38	41.00	41.41	40.98	41.10
F	3.17	2.92	3.46	3.26	3.24	2.93	3.03	3.02	3.27	3.10	2.91	3.15	2.97
Cl	0.12	0.14	0.11	0.12	0.11	0.11	0.11	0.14	0.14	0.12	0.15	0.13	0.12
Sum	98.46	98.84	99.76	99.25	99.24	98.94	100.14	99.31	99.85	98.89	100.04	99.35	99.30
O=F,Cl	1.36	1.26	1.48	1.40	1.39	1.26	1.30	1.31	1.41	1.33	1.26	1.36	1.28
Total	97.10	97.38	98.28	97.85	97.85	97.68	98.84	98.00	98.44	97.56	98.78	98.00	98.02

^(ol = olivine, gl = matrix glass, mag = magnetite)

Table D.5. Electron Microprobe Analyses of Fluorapatites in Tephra, Continued

Sample	91101	91101	91101	91101	91101	92101	92101	92101	92101	92101	93102	93102	93102
host^	mag/gl	gl	mag/gl	gl	mag/gl	gl	gl	gl	gl	mag/gl	ol	mag	mag
xtyl-anal.	1-2	2-1	3-1	4-1	5-1	1-1	1-2	2-1	2-2	3-1	1-1	2-1	2-2
SiO_2	0.36	0.35	0.40	0.40	0.44	0.13	0.28	0.41	0.30	0.21	0.35	0.29	0.28
FeO	0.48	0.37	0.61	0.56	0.82	0.34	0.26	0.32	0.30	0.57	0.76	0.59	0.72
MnO	0.13	0.12	0.14	0.16	0.14	0.11	0.12	0.11	0.09	0.14	0.14	0.15	0.10
CaO	53.56	54.48	53.77	53.97	53.54	54.99	54.59	54.14	54.24	54.12	54.21	53.92	53.70
SrO	0.09	0.12	0.12	0.10	0.13	0.13	0.10	0.11	0.14	0.07	0.13	0.11	0.13
P_2O_5	41.13	40.98	40.84	41.13	41.42	41.39	41.65	41.33	41.45	42.06	41.52	41.05	41.21
F	3.12	2.93	3.75	3.09	3.17	3.19	3.30	3.22	3.18	3.07	3.38	2.65	2.83
Cl	0.13	0.13	0.14	0.14	0.14	0.10	0.11	0.13	0.13	0.12	0.11	0.13	0.13
Sum	98.98	98.47	98.77	98.56	98.79	100.37	100.40	98.77	98.89	100.36	100.61	98.89	98.09
O=F,Cl	1.34	1.26	1.61	1.33	1.36	1.37	1.41	1.38	1.37	1.32	1.45	1.14	1.22
Total	97.65	98.21	98.16	98.23	98.43	99.01	98.99	98.39	98.48	99.04	99.16	97.75	97.87

^(ol = olivine, gl = matrix glass, mag = magnetite)

Table D.5. Electron Microprobe Analyses of Fluorapatites in Tephra, Continued

Sample	93102	93102	Er96	Er96	Er96	Er96	Er96	Er96	Er96	Er96	1999	1999	1999
host^	mag/gl	gl	mag/gl	gl	gl	mag/gl	ol	ol	ol	ol	mag/gl	gl	gl
xtyl-anal.	3-1	4-1	1-1	2-1	2-2	3-1	4-1	4-2	5-1	5-2	1-1	2-1	3-1
SiO_2	0.32	0.33	0.08	0.16	0.10	0.41	0.29	0.39	0.30	0.31	0.20	0.21	0.43
FeO	0.43	0.59	0.87	0.84	0.80	0.98	0.58	0.69	0.48	0.45	0.59	0.47	0.41
MnO	0.12	0.15	0.15	0.15	0.12	0.15	0.15	0.15	0.12	0.13	0.11	0.12	0.08
CaO	54.40	53.60	54.17	54.29	53.97	53.74	54.53	54.40	53.15	53.89	53.10	53.13	53.21
SrO	0.11	0.09	0.11	0.11	0.10	0.11	0.10	0.09	0.12	0.10	0.08	0.12	0.10
P_2O_5	41.75	41.70	41.42	41.72	42.03	41.50	41.15	41.30	41.81	41.45	40.95	40.84	40.88
F	3.10	3.06	2.99	2.94	3.27	3.21	3.34	2.90	2.81	2.84	2.66	3.36	2.99
Cl	0.12	0.12	0.12	0.11	0.12	0.14	0.12	0.10	0.14	0.13	0.13	0.14	0.14
Sum	100.36	99.63	99.90	100.12	100.31	100.23	100.25	99.96	98.90	99.30	97.82	98.48	98.23
O=F,Cl	1.33	1.32	1.24	1.26	1.40	1.38	1.43	1.24	1.22	1.23	1.15	1.45	1.29
Total	99.02	98.32	98.66	98.85	98.91	98.85	98.81	98.72	97.68	98.08	96.67	97.03	96.94

^(ol = olivine, gl = matrix glass, mag = magnetite)

Table D.5. Electron Microprobe Analyses of Fluorapatites in Tephra, Continued

Sample	1999	1999	1999	DEC2000	DEC2000	DEC2000	DEC2000	Y2K	Y2K	Y2K	Y2K	Y2K	Y2K
host^	gl	gl		gl	gl	ol	ol	ol	ol	ol	ol	ol	gl
xtyl-anal.	4-1	4-2		1-1	2-1	3-1	4-1	1-1	2-1	2-2	3-1	4-1	5-1
SiO_2	0.37	0.37	0.43	0.40	0.43	0.34	0.46	0.44	0.44	0.42	0.36	0.39	0.40
FeO	0.26	0.22	0.49	0.52	0.56	0.73	1.10	0.81	0.47	0.31	0.24	0.53	0.69
MnO	0.11	0.11	0.09	0.10	0.08	0.12	0.12	0.11	0.09	0.11	0.08	0.09	0.09
CaO	53.16	53.10	53.19	53.14	53.39	53.23	53.12	54.17	53.37	53.23	53.59	53.61	53.78
SrO	0.09	0.09	0.13	0.13	0.15	0.14	0.11	0.13	0.10	0.13	0.12	0.14	0.14
P_2O_5	40.87	41.06	40.65	40.41	40.31	40.80	40.62	40.66	40.23	40.69	40.75	40.39	40.29
F	2.90	3.00	3.18	2.82	2.73	2.92	2.91	2.71	2.94	2.81	2.82	3.21	2.58
Cl	0.12	0.13	0.12	0.13	0.13	0.14	0.12	0.13	0.14	0.13	0.14	0.12	0.14
Sum	97.89	98.06	98.26	97.65	97.79	98.43	98.57	99.17	97.76	97.83	98.11	98.49	98.13
O=F,Cl	1.25	1.29	1.37	1.22	1.18	1.26	1.25	1.17	1.27	1.21	1.22	1.38	1.12
Total	96.64	96.77	96.90	96.43	96.61	97.17	97.31	98.00	96.50	96.61	96.89	97.11	97.00

^(ol = olivine, gl = matrix glass, mag = magnetite)

Table D.5. Electron Microprobe Analyses of Fluorapatites in Tephra, Continued

Sample	Y2K	Y2K	Y2K	E2001	E2001	E2001	E2001	E2001	JAN2004	JAN2004	JAN2004
host^	gl	gl	gl	gl	gl	gl	gl	gl	gl	gl	gl
xtyl-anal.	6-1	6-2	7-1	1-1	1-2	1-3	1-4	1-5	1-1	2-1	2-2
SiO_2	0.38	0.35	0.30	0.40	0.35	0.32	0.35	0.45	0.36	0.34	0.32
FeO	0.55	0.49	0.79	0.18	0.25	0.19	0.23	0.24	0.49	0.60	0.27
MnO	0.10	0.10	0.10	0.09	0.10	0.10	0.07	0.08	0.09	0.11	0.10
CaO	53.03	53.05	52.81	53.36	53.60	53.40	53.44	53.44	53.05	53.47	53.19
SrO	0.12	0.10	0.14	0.11	0.13	0.12	0.09	0.16	0.11	0.16	0.11
P_2O_5	40.91	41.05	40.85	40.48	40.78	40.74	40.93	40.50	40.76	40.53	40.64
F	2.99	3.18	3.11	3.08	2.99	2.92	3.17	3.21	3.10	3.45	3.09
Cl	0.13	0.14	0.12	0.13	0.14	0.13	0.13	0.12	0.13	0.12	0.13
Sum	98.19	98.47	98.31	97.81	98.35	97.80	98.40	98.20	98.02	98.78	97.84
O=F,Cl	1.29	1.37	1.34	1.32	1.29	1.28	1.36	1.38	1.34	1.48	1.33
Total	96.90	97.10	96.97	96.49	97.06	96.64	97.04	96.82	96.68	97.30	96.51

^(cl = olivine, gl = matrix glass, mag = magnetite)

Appendix D.6. Electron Microprobe Traverses of Anorthoclase Feldspar Megacrysts

Electron Microprobe traverses were performed on eight anorthoclase feldspar megacrysts from four bombs. The feldspars were sectioned perpendicular to the c-axis using a rock trim saw and mounted and polished for analysis. The traverses were made perpendicular to textural zoning in the crystals. Analytical errors are calculated from counting statistics (Table D.6.1.)

Table D.6.1. Statistical error (2σ) for analyses of feldspar calculated from counting statistics

SiO_2 (wt%)	Al_2O_3 (wt%)	CaO (wt%)	Na_2O (wt%)	K_2O (wt%)	FeO (ppm)	SrO (ppm)	BaO (ppm)
0.25	0.14	0.07	0.12	0.07	140	200	240

Figures D.6.1. – D.6.4: EMP traverse of anorthoclase feldspar 84505-01

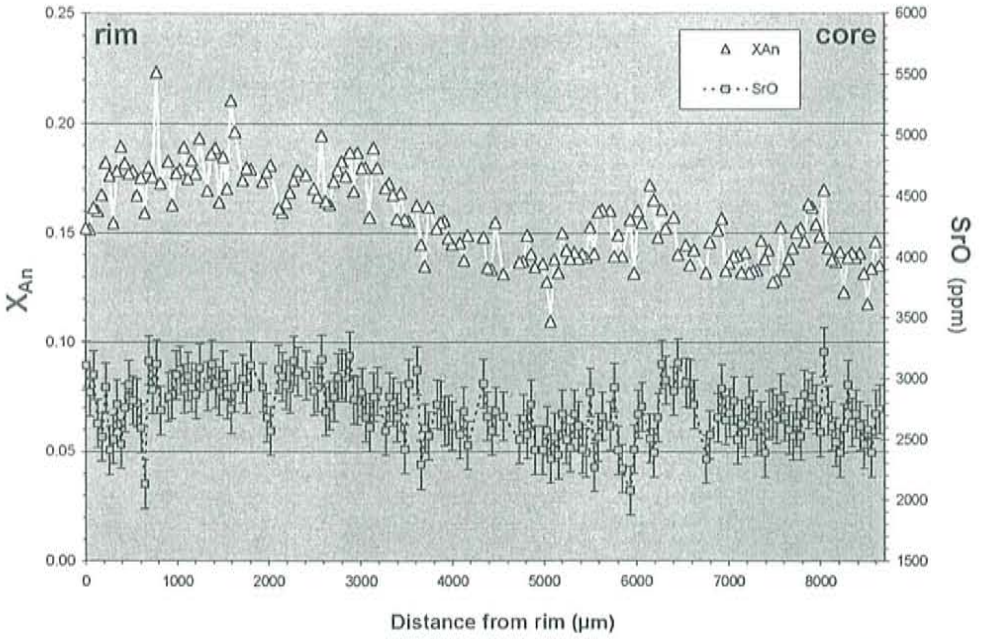

Figure D.6.1. Core - Rim EMP traverse of anorthoclase feldspar 84505-01 showing mol fraction of anorthite (X_{An}) and SrO (ppm). Analytical errors shown at 2σ level (errors for X_{An} are smaller than symbol)

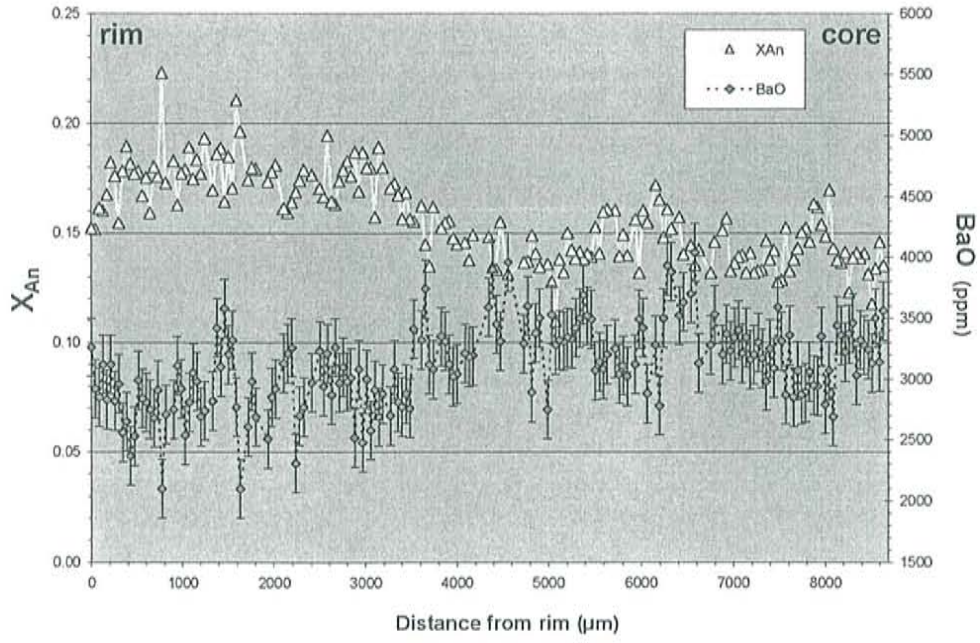

Figure D.6.2. Core - Rim EMP traverse of anorthoclase feldspar 84505-01 showing mol fraction of anorthite (X_{An}) and BaO (ppm). Analytical errors shown at 2σ level (errors for X_{An} are smaller than symbol)

Figures D.6.1. – D.6.4: EMP traverse of anorthoclase feldspar 84505-01

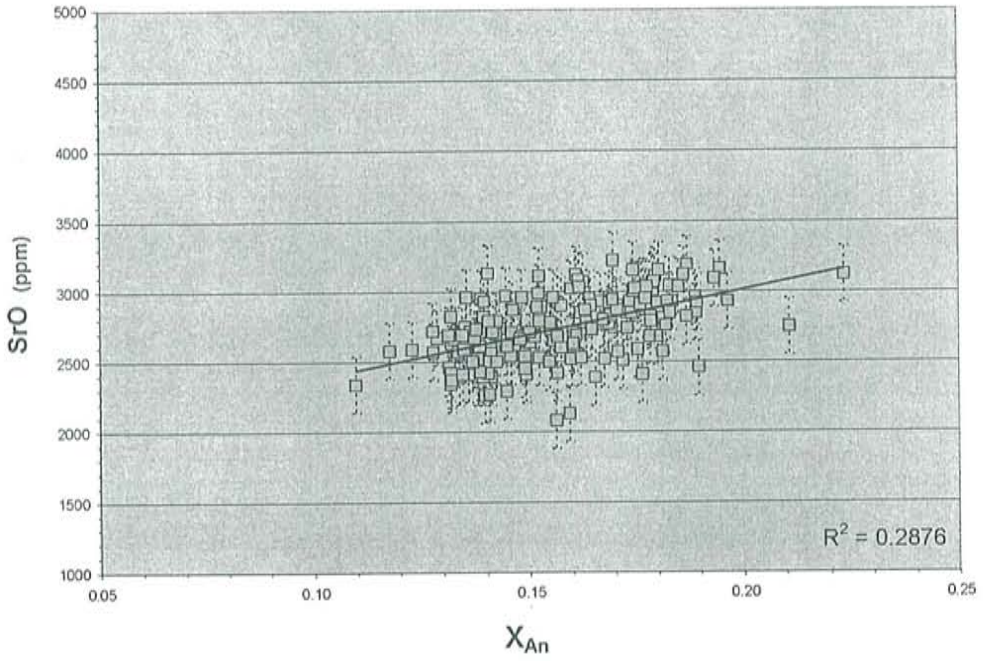

Figure D.6.3. Mol fraction anorthite (X_{An}) versus SrO for core - rim EMP traverse of anorthoclase feldspar 84505-01

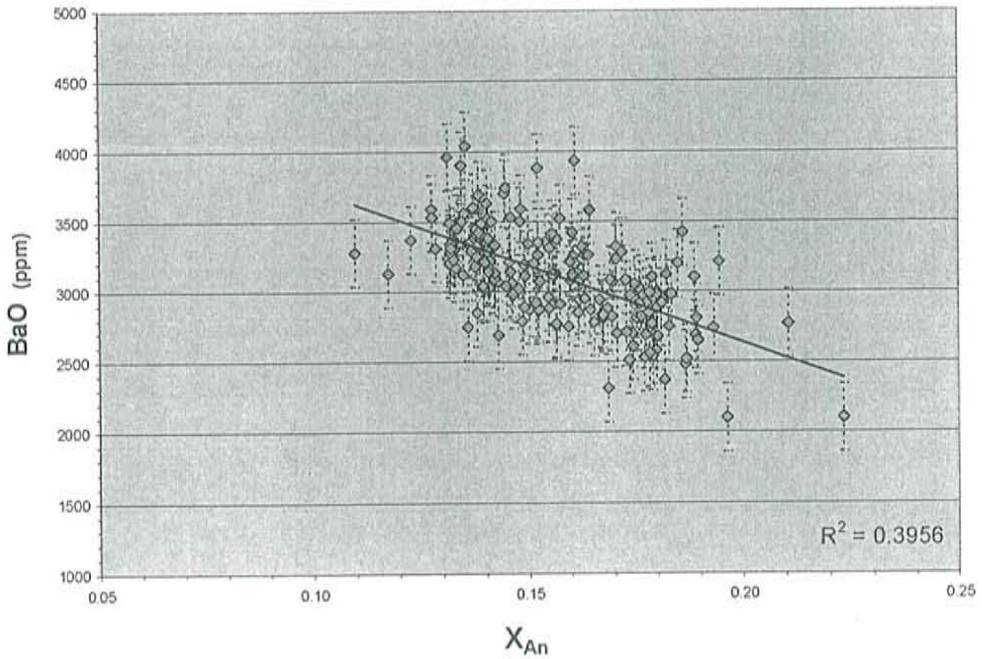

Figure D.6.4. Mol fraction anorthite (X_{An}) versus BaO for core - rim EMP traverse of anorthoclase feldspar 84505-01

Figures D.6.5. – D.6.8: EMP traverse of anorthoclase feldspar 84505-02

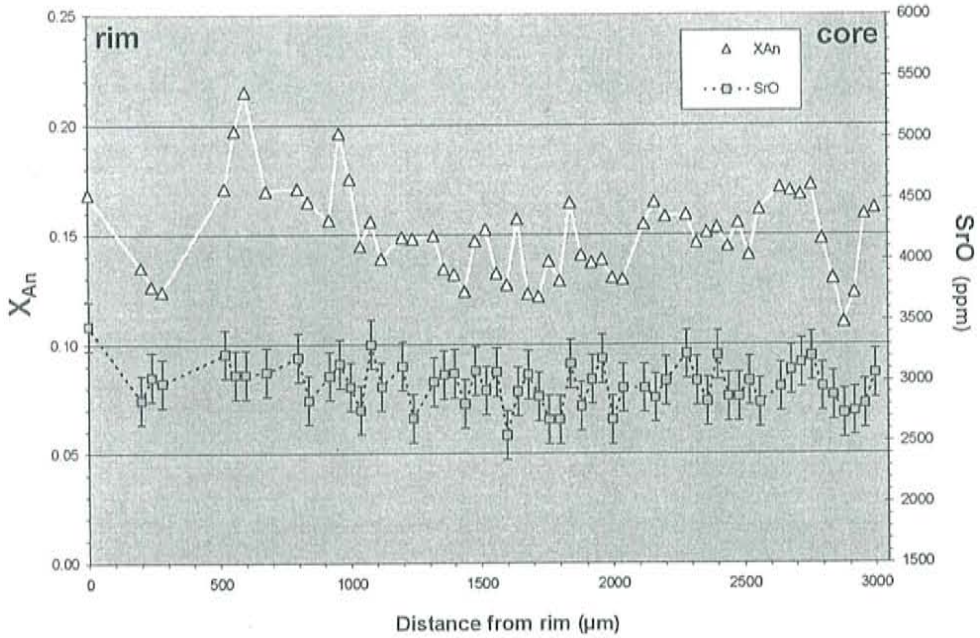

Figure D.6.5. Core - Rim EMP traverse of anorthoclase feldspar 84505-02 showing mol fraction of anorthite (X_{An}) and SrO (ppm). Analytical errors shown at 2σ level (errors for X_{An} are smaller than symbol)

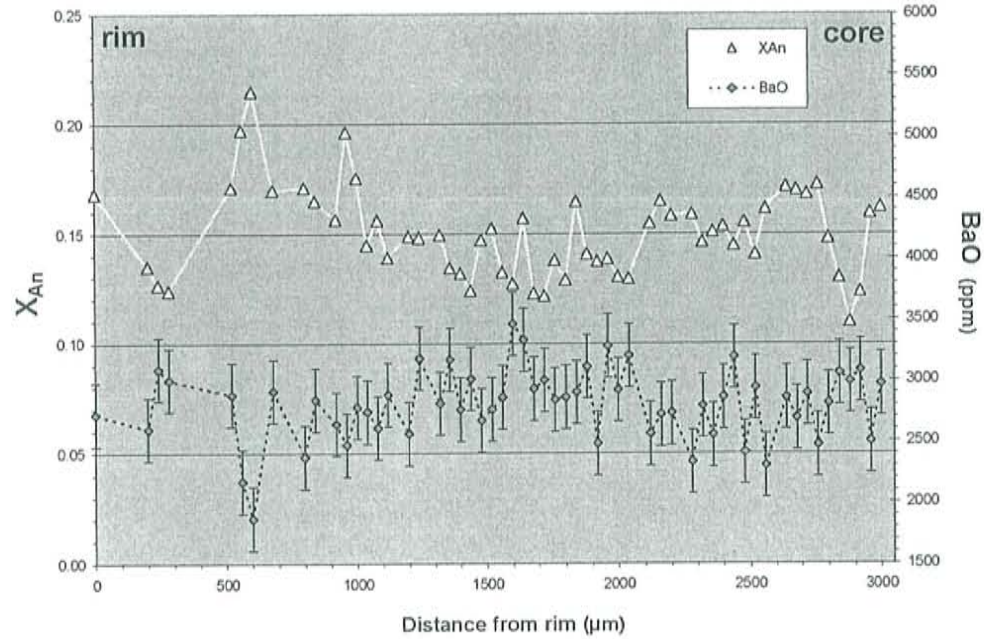

Figure D.6.6. Core - Rim EMP traverse of anorthoclase feldspar 84505-02 showing mol fraction of anorthite (X_{An}) and BaO (ppm). Analytical errors shown at 2σ level (errors for X_{An} are smaller than symbol)

Figures D.6.5. – D.6.8: EMP traverse of anorthoclase feldspar 84505-03

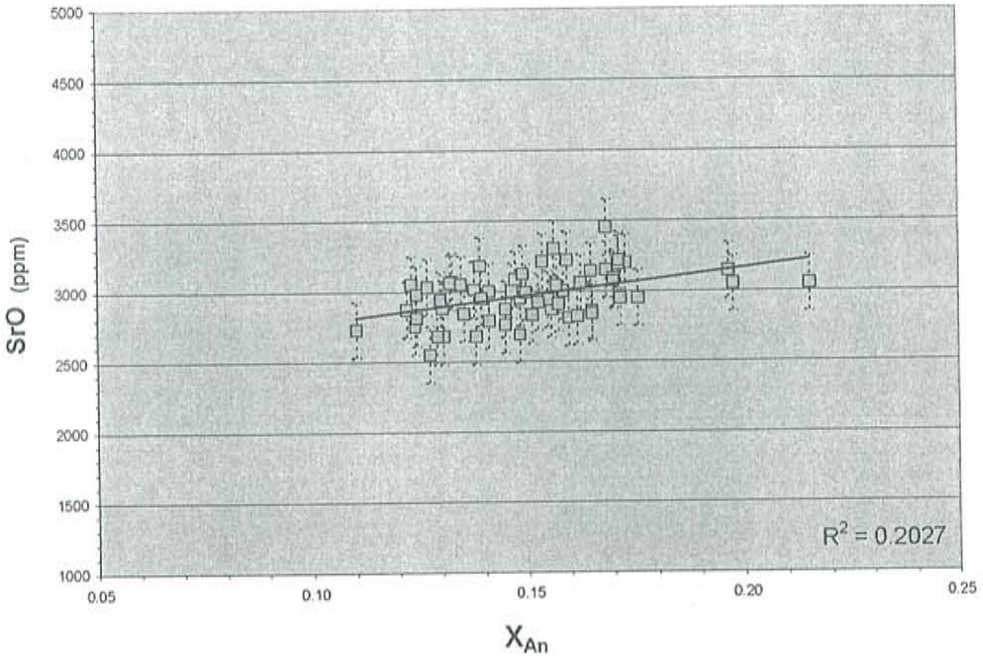

Figure D.6.7. Mol fraction anorthite (X_{An}) versus SrO for core - rim EMP traverse of anorthoclase feldspar 84505-02

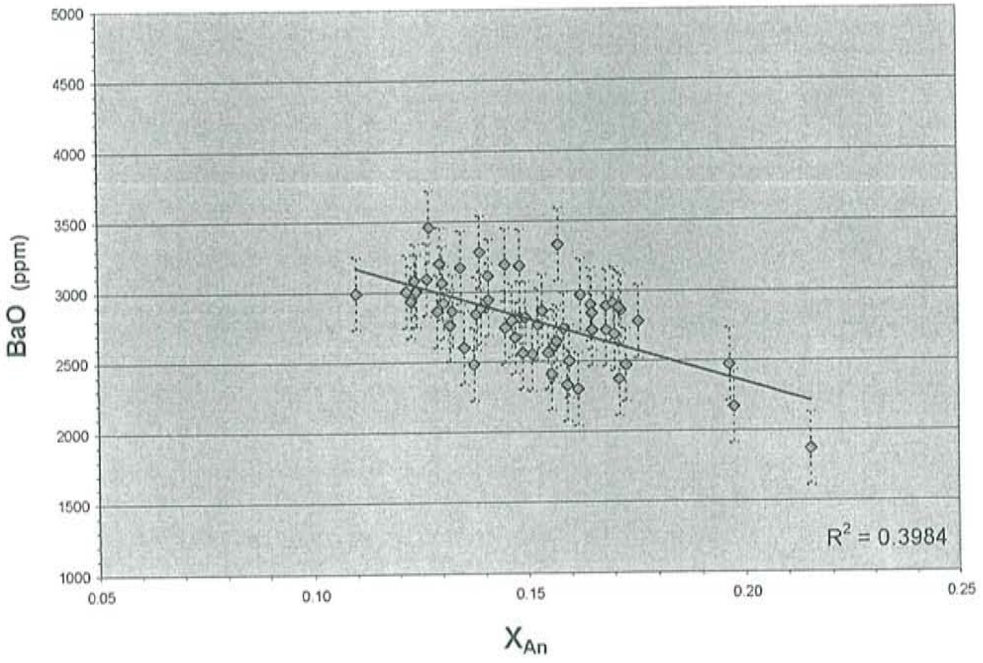

Figure D.6.8. Mol fraction anorthite (X_{An}) versus BaO for core - rim EMP traverse of anorthoclase feldspar 84505-02

Figures D.6.9. – D.6.12: EMP traverse of anorthoclase feldspar 84505-03

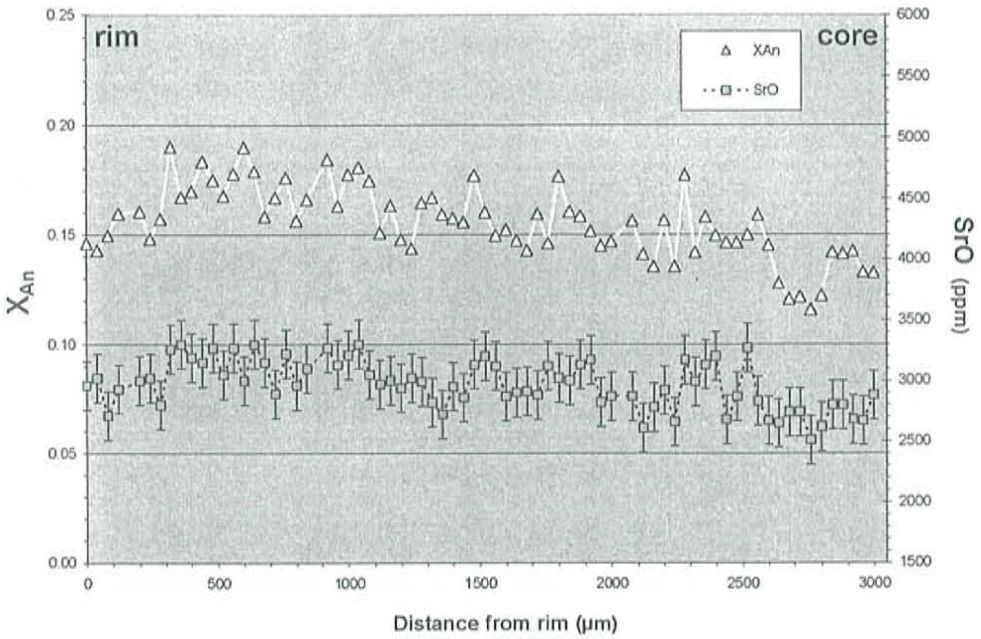

Figure D.6.9. Core - Rim EMP traverse of anorthoclase feldspar 84505-03 showing mol fraction of anorthite (X_{An}) and SrO (ppm). Analytical errors shown at 2σ level (errors for X_{An} are smaller than symbol)

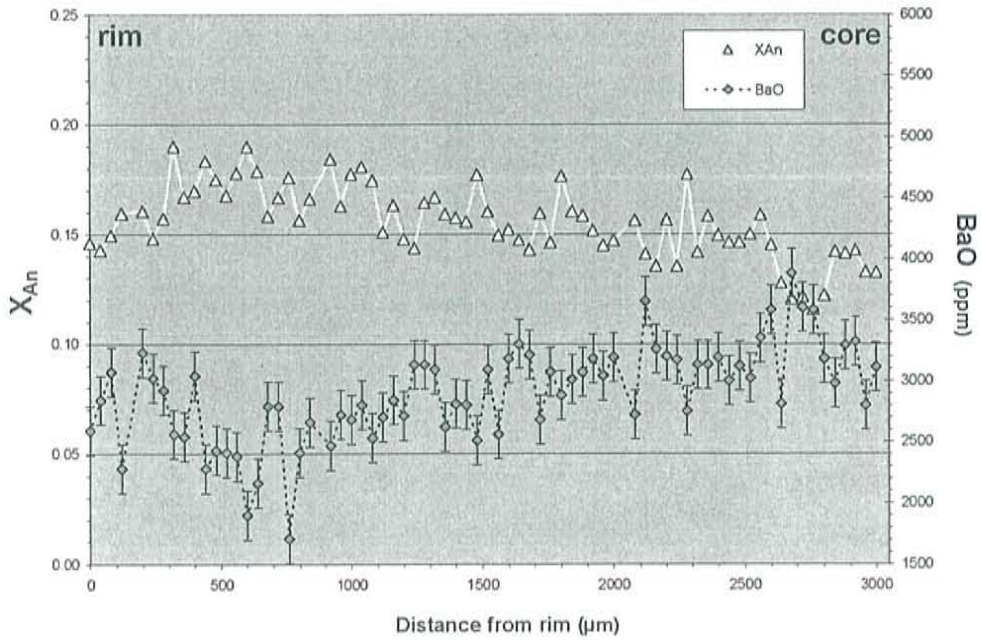

Figure D.6.10. Core - Rim EMP traverse of anorthoclase feldspar 84505-03 showing mol fraction of anorthite (X_{An}) and BaO (ppm). Analytical errors shown at 2σ level (errors for X_{An} are smaller than symbol)

Figures D.6.9. – D.6.12: EMP traverse of anorthoclase feldspar 84505-03

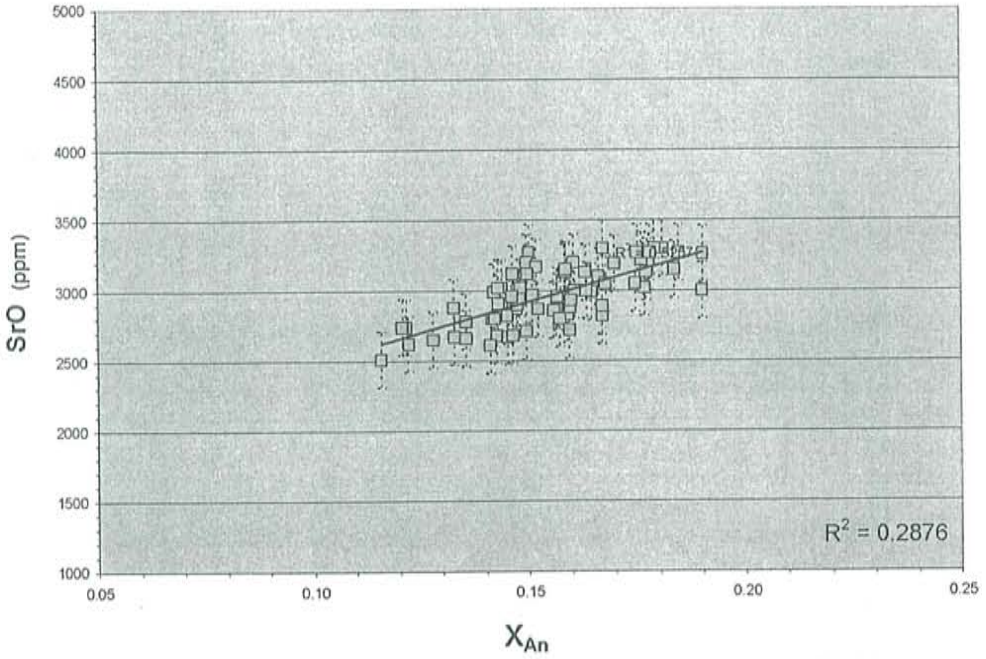

Figure D.6.11. Mol fraction anorthite (X_{An}) versus SrO for core - rim EMP traverse of anorthoclase feldspar 84505-03

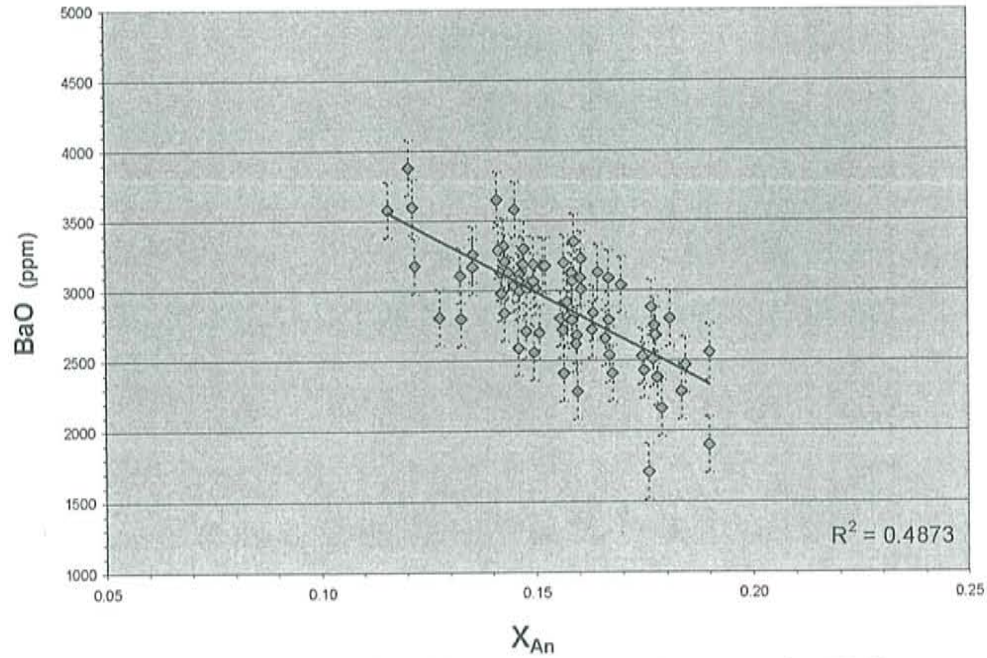

Figure D.6.12. Mol fraction anorthite (X_{An}) versus BaO for core - rim EMP traverse of anorthoclase feldspar 84505-03

Figures D.6.13. – D.6.16: EMP traverse of anorthoclase feldspar 85010-01

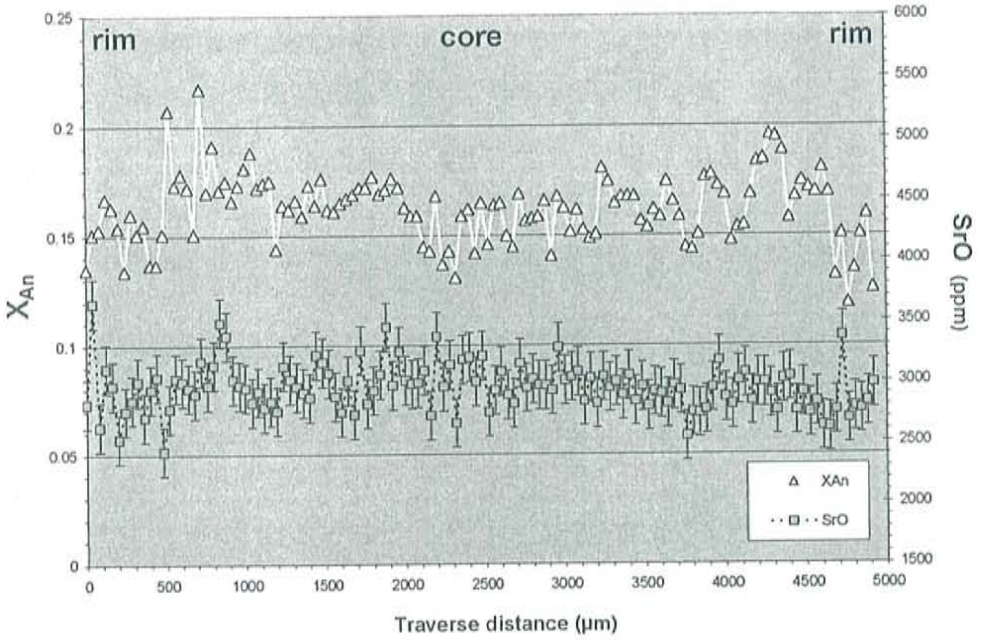

Figure D.6.13. Rim - Rim EMP traverse of anorthoclase feldspar 85010-01 showing mol fraction of anorthite (X_{An}) and SrO (ppm). Analytical errors shown at 2σ level (errors for X_{An} are smaller than symbol)

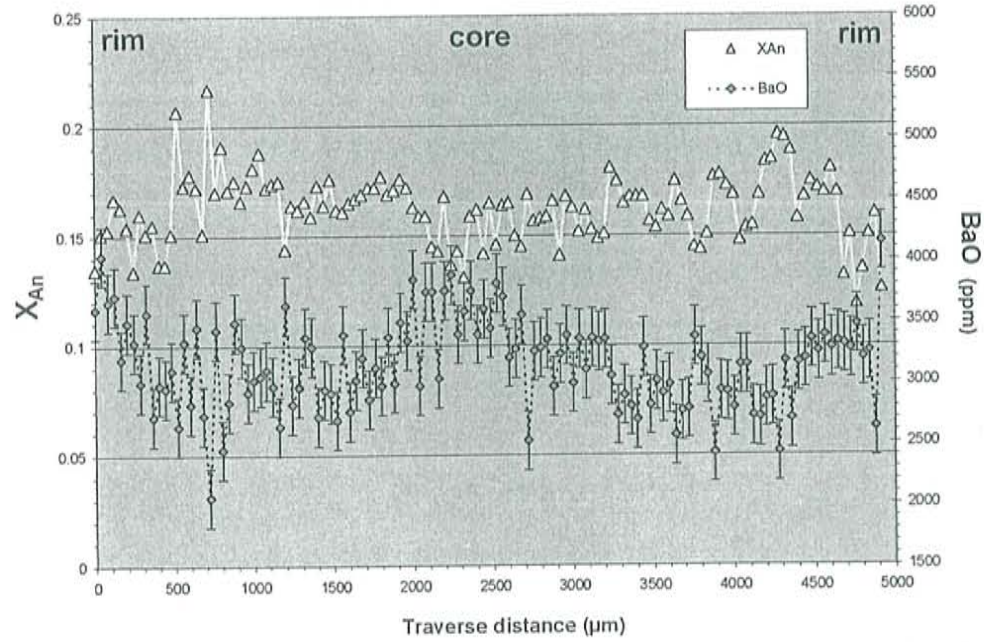

Figure D.6.14. Rim - Rim EMP traverse of anorthoclase feldspar 85010-01 showing mol fraction of anorthite (X_{An}) and BaO (ppm). Analytical errors shown at 2σ level (errors for X_{An} are smaller than symbol)

Figures D.6.13. – D.6.16: EMP traverse of anorthoclase feldspar 85010-01

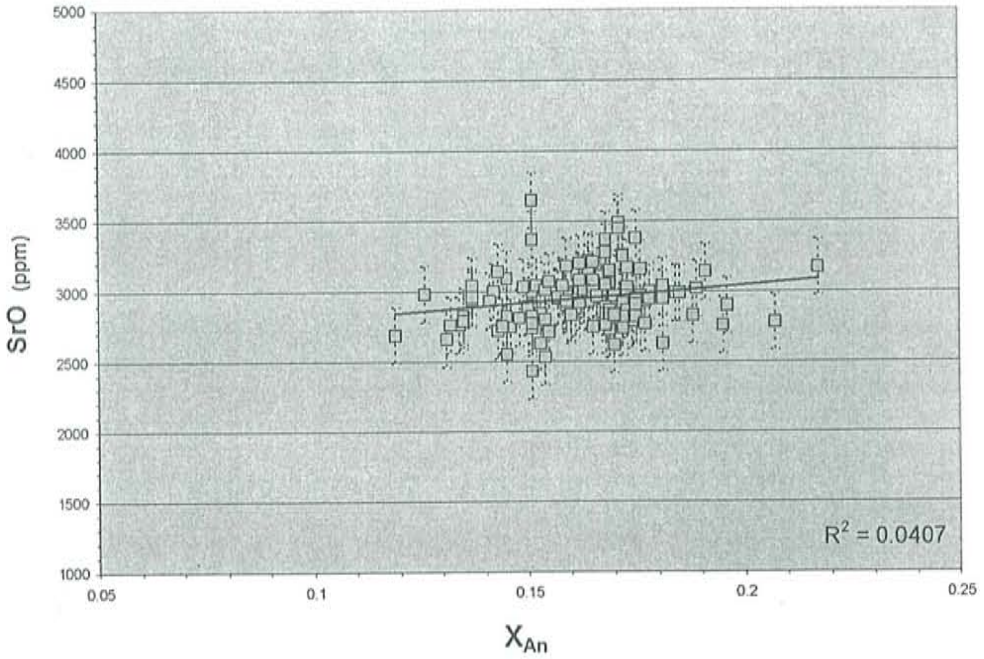

Figure D.6.15. Mol fraction anorthite (X_{An}) versus SrO for core - rim EMP traverse of anorthoclase feldspar 85010-01

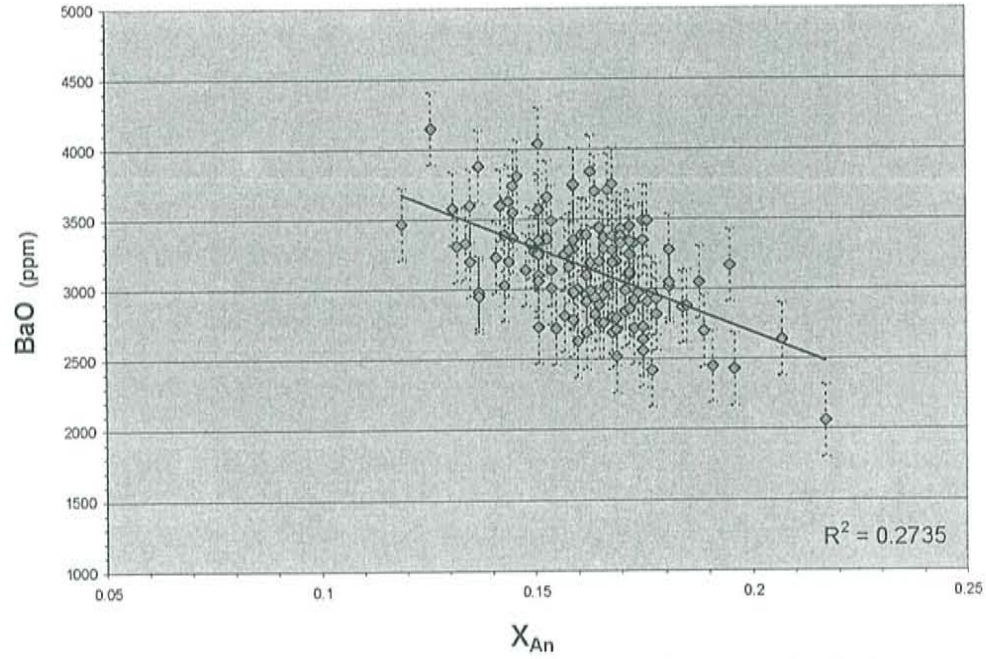

Figure D.6.16. Mol fraction anorthite (X_{An}) versus BaO for core - rim EMP traverse of anorthoclase feldspar 85010-01

Figures D.6.17. – D.6.20: EMP traverse of anorthoclase feldspar 85010-02

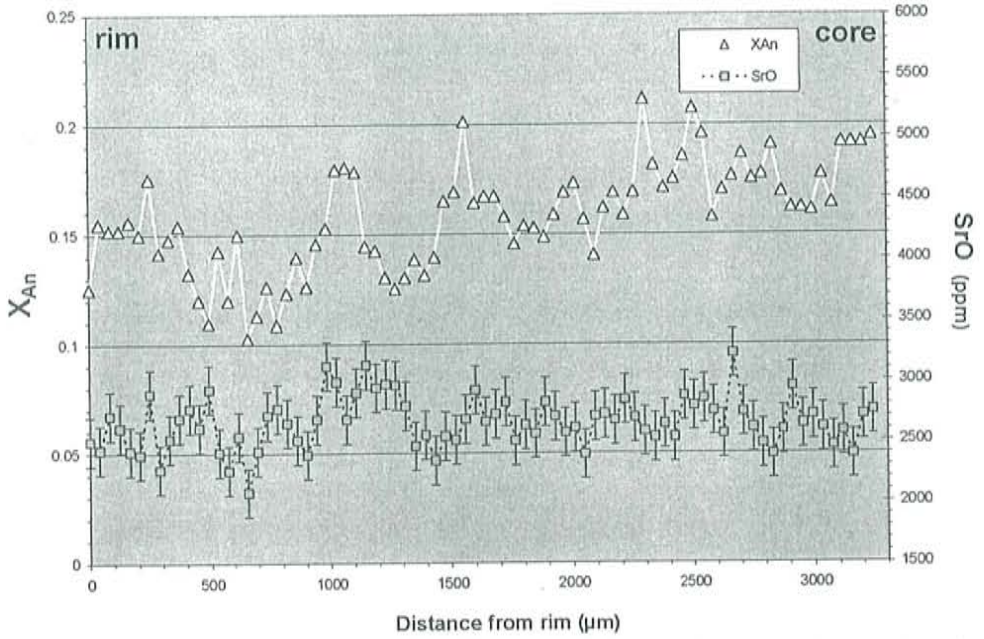

Figure D.6.17. Rim - Rim EMP traverse of anorthoclase feldspar 85010-02 showing mol fraction of anorthite (X_{An}) and SrO (ppm). Analytical errors shown at 2σ level (errors for X_{An} are smaller than symbol)

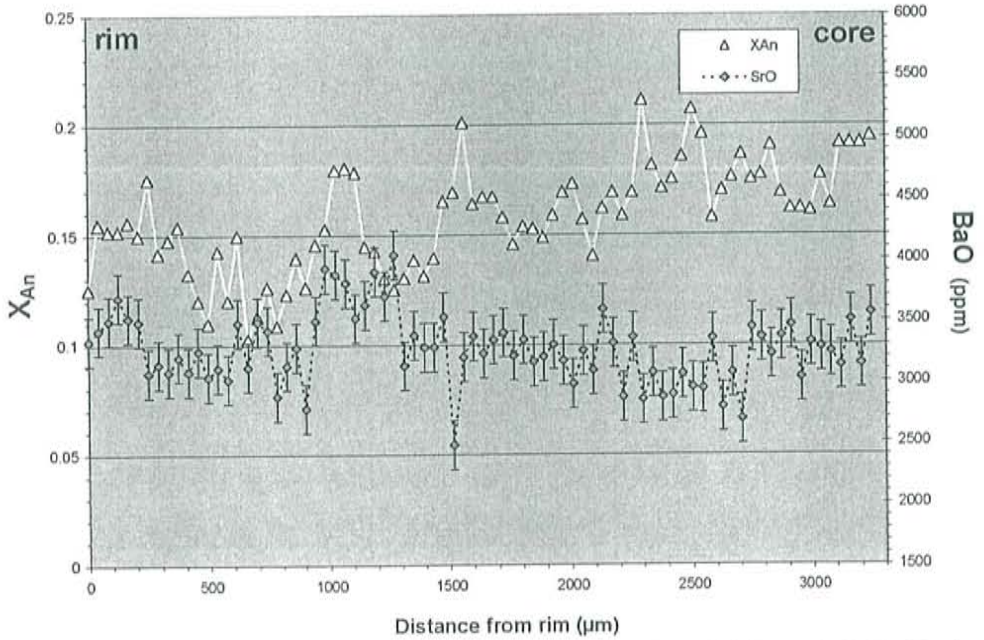

Figure D.6.18. Rim - Rim EMP traverse of anorthoclase feldspar 85010-02 showing mol fraction of anorthite (X_{An}) and BaO (ppm). Analytical errors shown at 2σ level (errors for X_{An} are smaller than symbol)

Figures D.6.17. – D.6.20: EMP traverse of anorthoclase feldspar 85010-02

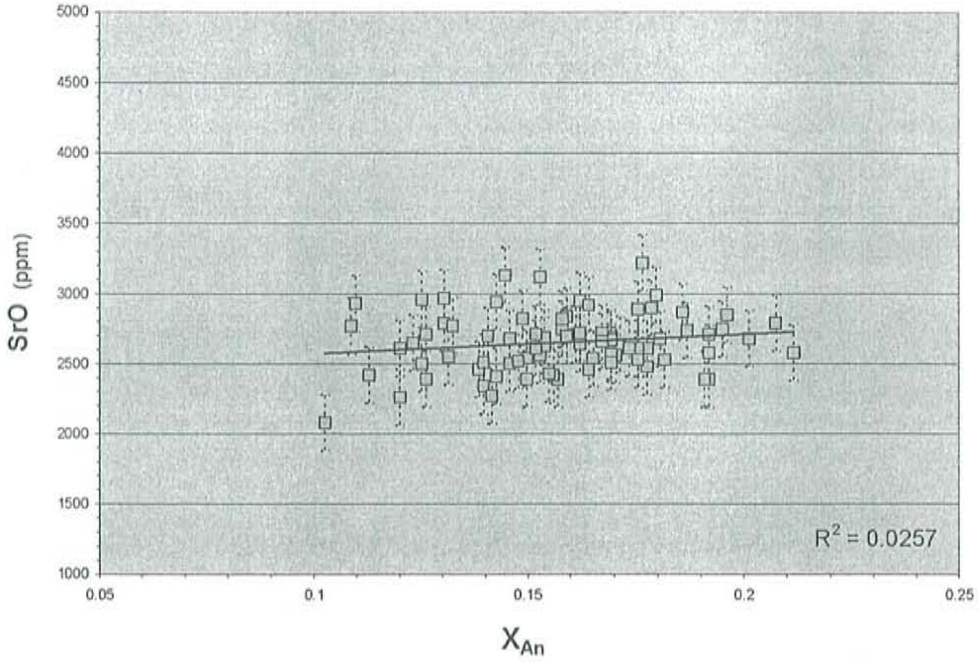

Figure D.6.19. Mol fraction anorthite (X_{An}) versus SrO for core - rim EMP traverse of anorthoclase feldspar 85010-02

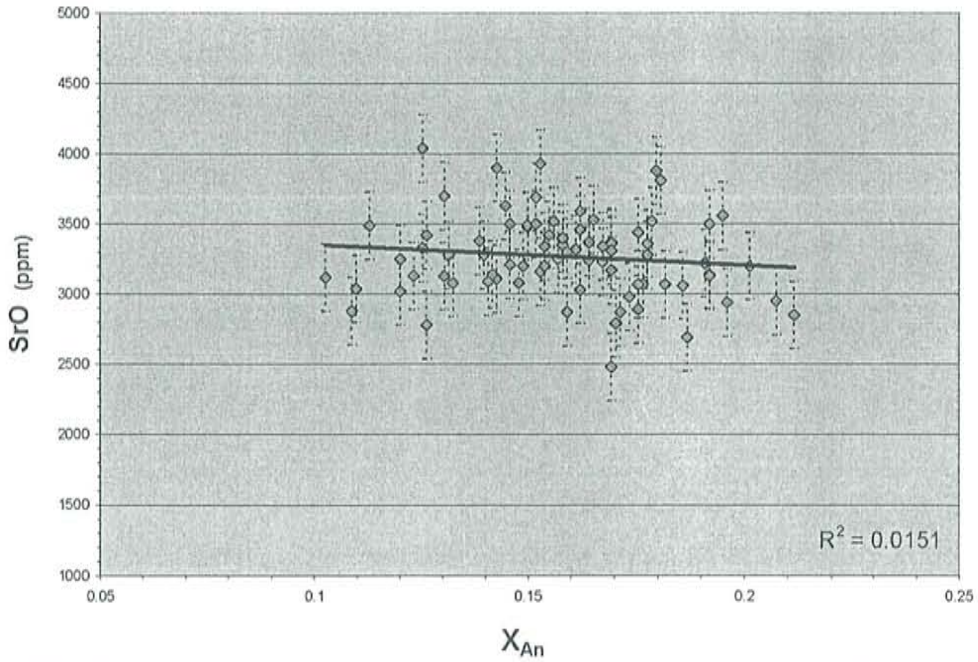

Figure D.6.20. Mol fraction anorthite (X_{An}) versus BaO for core - rim EMP traverse of anorthoclase feldspar 85010-02

Figures D.6.21. – D.6.24: EMP traverse of anorthoclase feldspar 85010-04

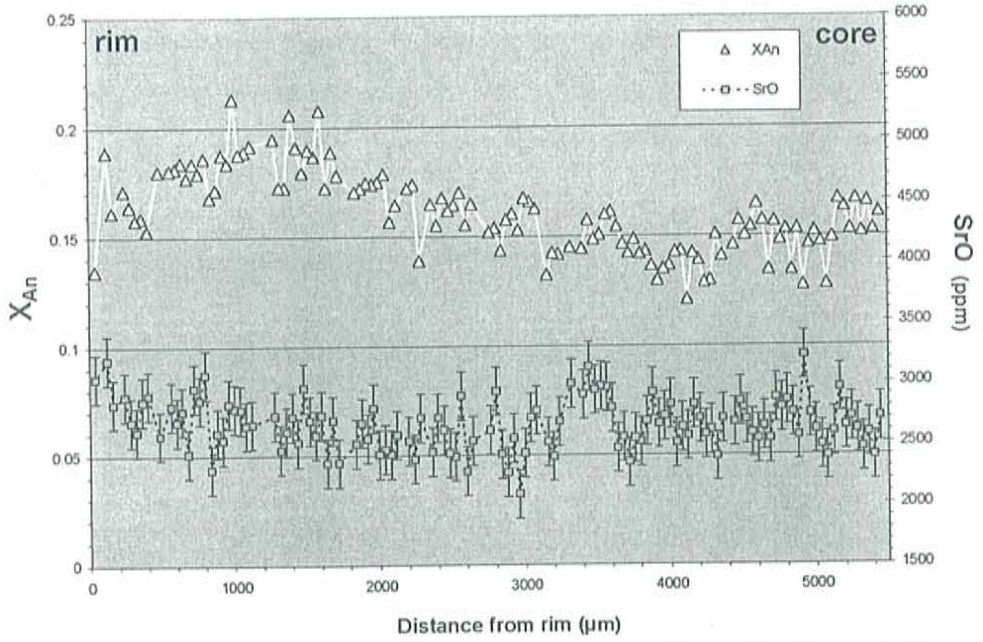

Figure D.6.21. Core - Rim EMP traverse of anorthoclase feldspar 85010-04 showing mol fraction of anorthite (X_{An}) and SrO (ppm). Analytical errors shown at 2σ level (errors for X_{An} are smaller than symbol)

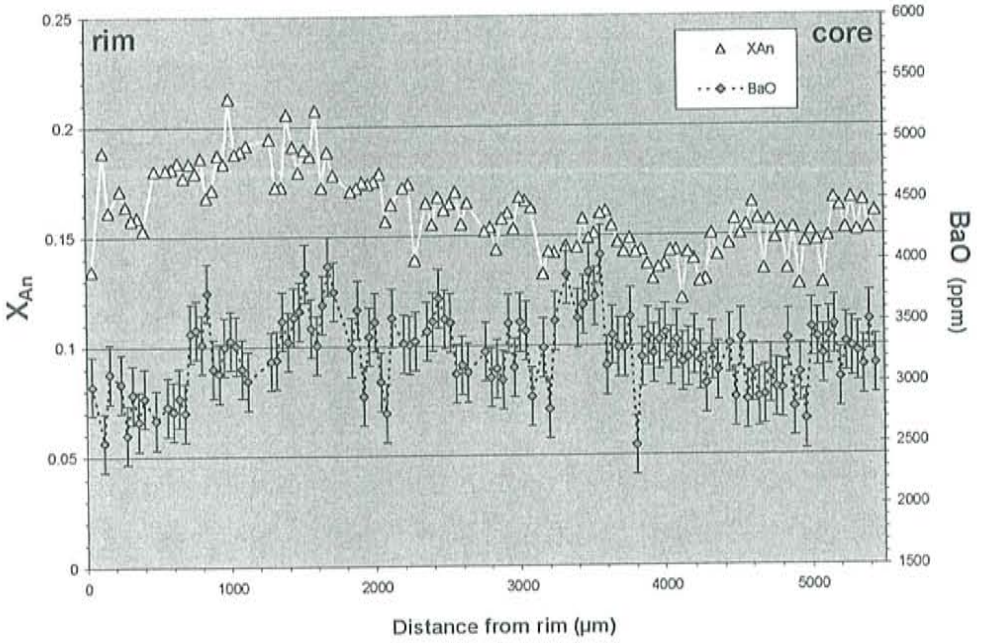

Figure D.6.21. Core - Rim EMP traverse of anorthoclase feldspar 85010-04 showing mol fraction of anorthite (X_{An}) and BaO (ppm). Analytical errors shown at 2σ level (errors for X_{An} are smaller than symbol)

Figures D.6.21. – D.6.24: EMP traverse of anorthoclase feldspar 85010-04

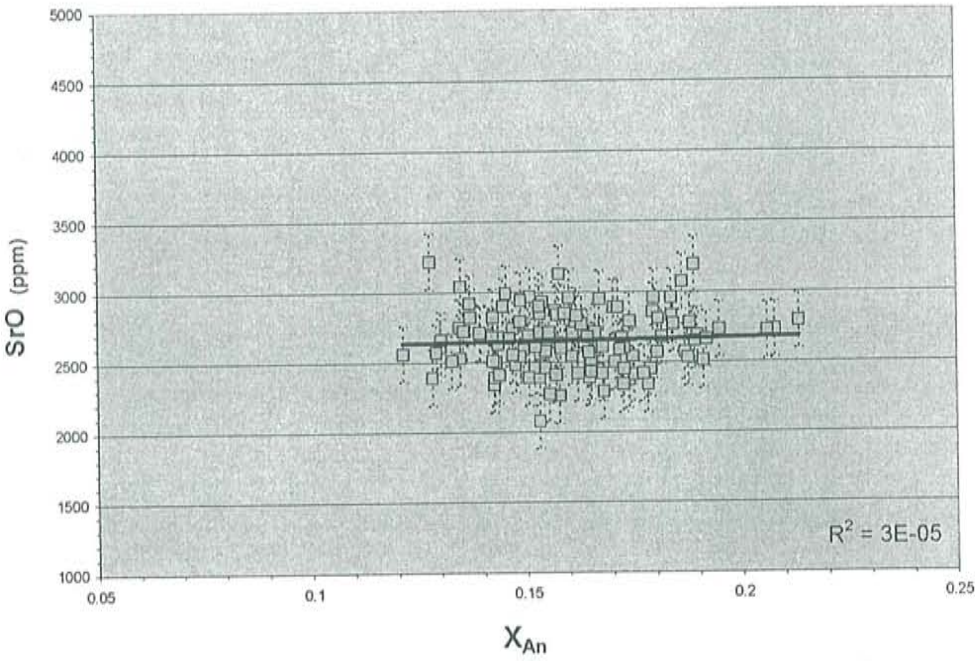

Figure D.6.23. Mol fraction anorthite (X_{An}) versus SrO for core - rim EMP traverse of anorthoclase feldspar 85010-04

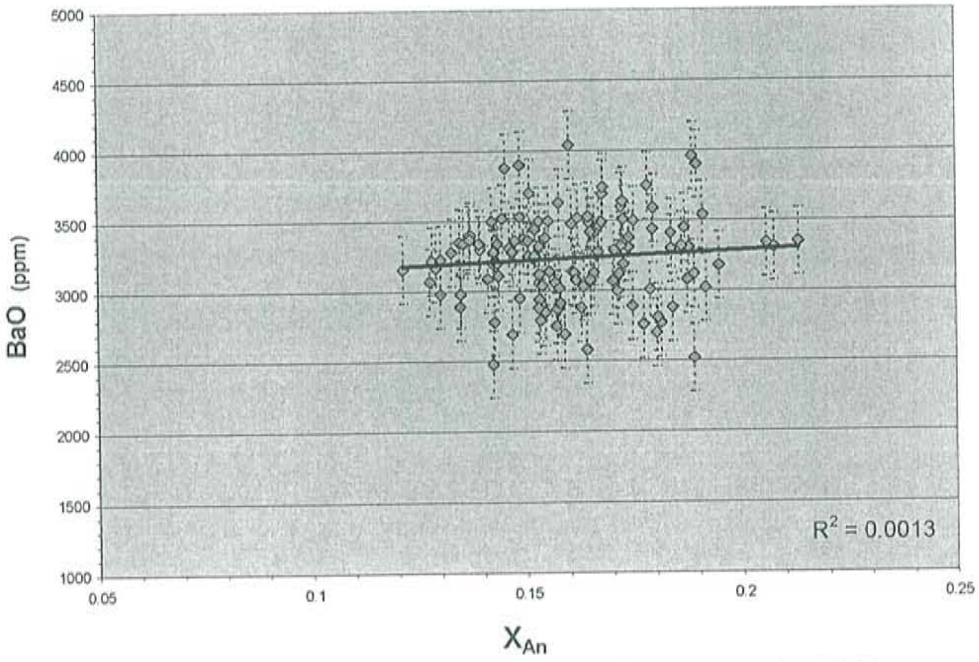

Figure D.6.24. Mol fraction anorthite (X_{An}) versus BaO for core - rim EMP traverse of anorthoclase feldspar 85010-04

Figures D.6.25. – D.6.28: EMP traverse of anorthoclase feldspar 1999-01

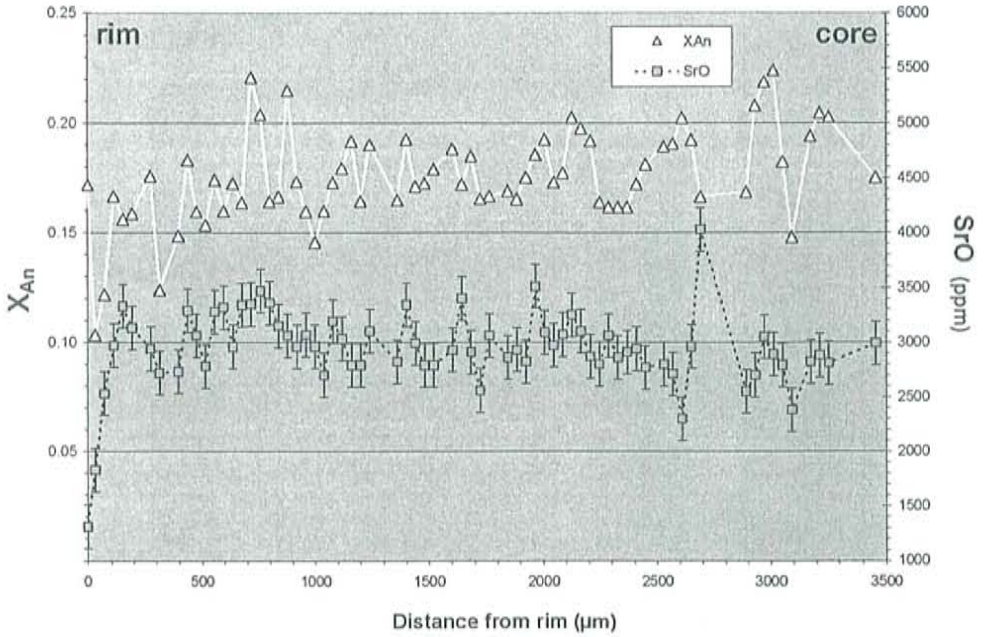

Figure D.6.25. Core - Rim EMP traverse of anorthoclase feldspar 1999-01 showing mol fraction of anorthite (X_{An}) and SrO (ppm). Analytical errors shown at 2σ level (errors for X_{An} are smaller than symbol). Note: different SrO scale (1000 – 6000ppm)

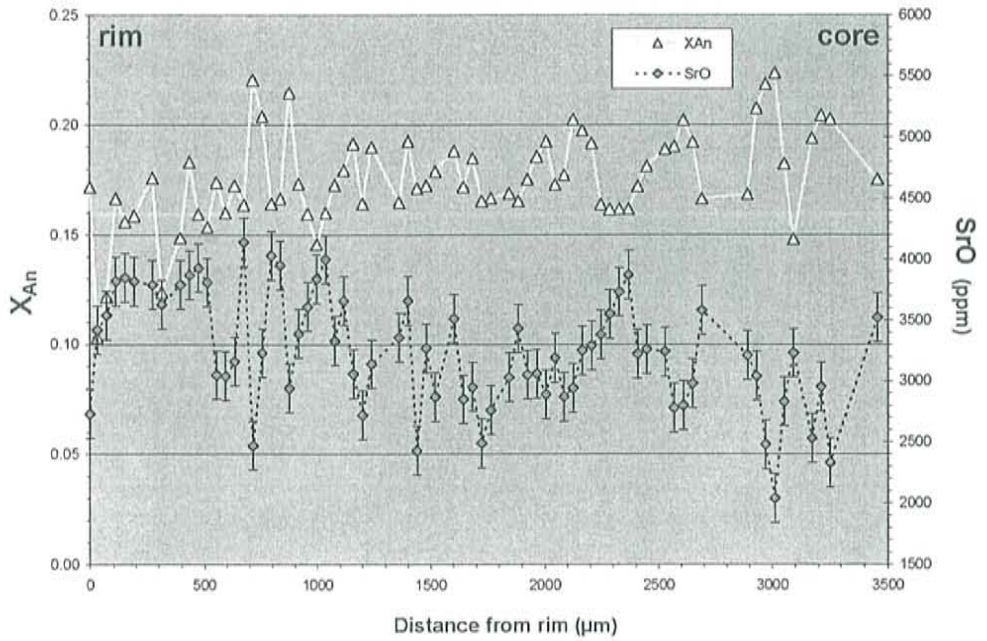

Figure D.6.26. Core - Rim EMP traverse of anorthoclase feldspar 1999-01 showing mol fraction of anorthite (X_{An}) and BaO (ppm). Analytical errors shown at 2σ level (errors for X_{An} are smaller than symbol).

Figures D.6.25. – D.6.28: EMP traverse of anorthoclase feldspar 1999-01

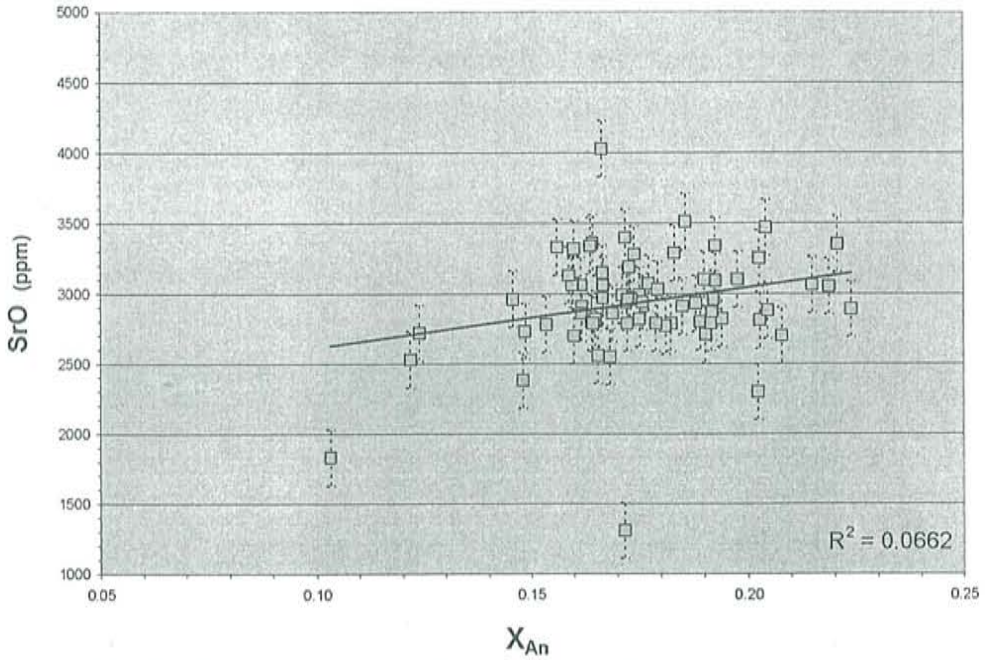

Figure D.6.27. Mol fraction anorthite (X_{An}) versus SrO for core - rim EMP traverse of anorthoclase feldspar 1999-01

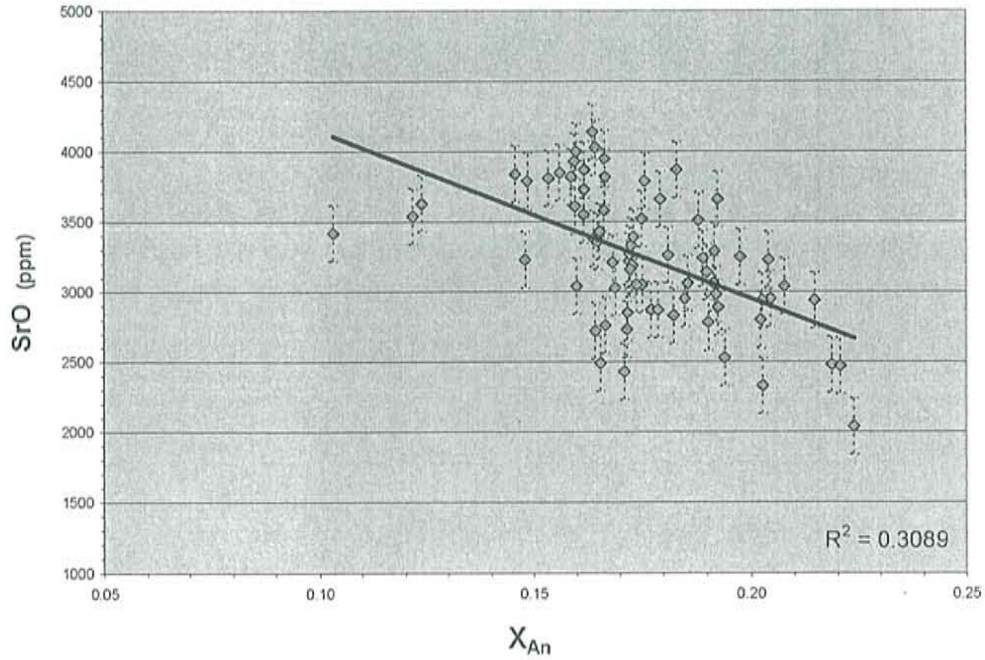

Figure D.6.28. Mol fraction anorthite (X_{An}) versus BaO for core - rim EMP traverse of anorthoclase feldspar 1999-01

Figures D.6.29. – D.6.32: EMP traverse of anorthoclase feldspar DEC2000-03

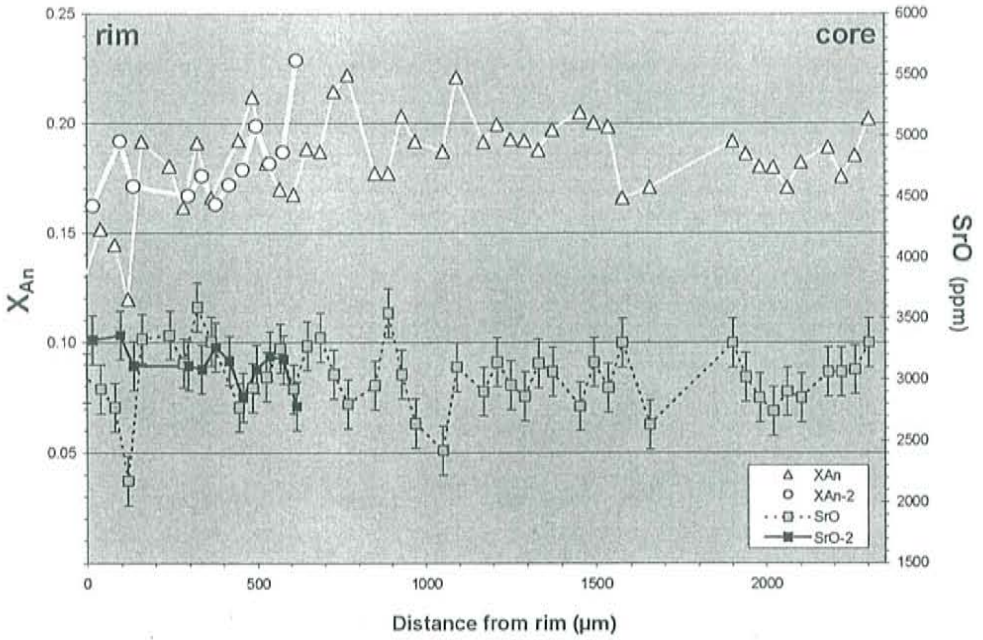

Figure D.6.29. Core - Rim EMP traverse of anorthoclase feldspar DEC2000-03 showing mol fraction of anorthite (X_{An}) and SrO (ppm). XAn-2 and SrO-2 are data from a traverse made ~500µm orthogonal to the longer traverse. Analytical errors shown at 2σ level (errors for X_{An} are smaller than symbol).

Figures D.6.29. – D.6.32: EMP traverse of anorthoclase feldspar DEC2000-03

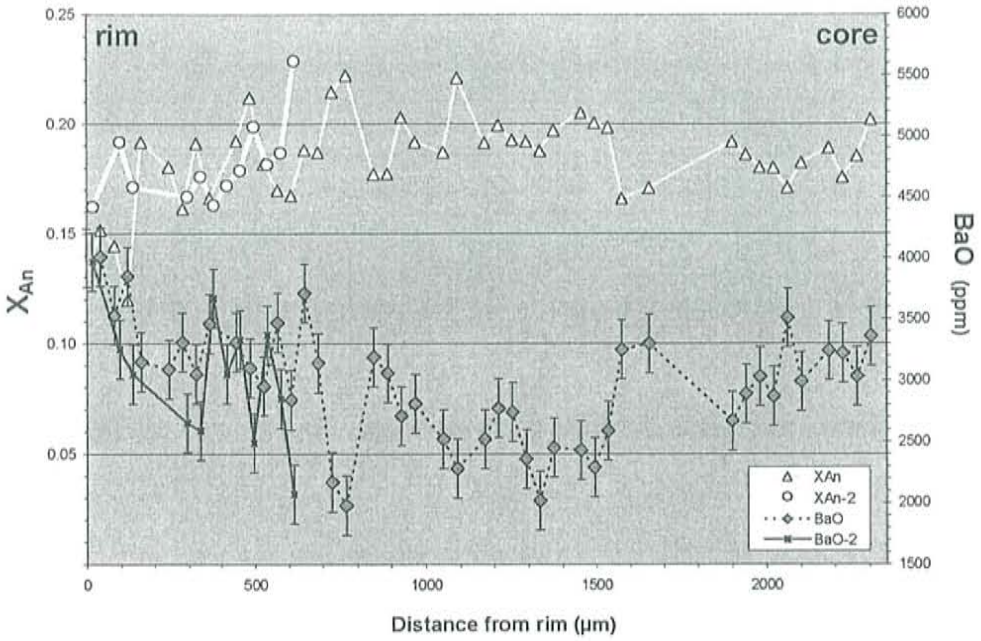

Figure D.6.30. Core - Rim EMP traverse of anorthoclase feldspar DEC2000-03 showing mol fraction of anorthite (X_{An}) and BaO (ppm). XAn-2 and SrO-2 are data from a traverse made ~500µm orthogonal to the longer traverse. Analytical errors shown at 2σ level (errors for X_{An} are smaller than symbol).

Figures D.6.29. – D.6.32: EMP traverse of anorthoclase feldspar DEC2000-03

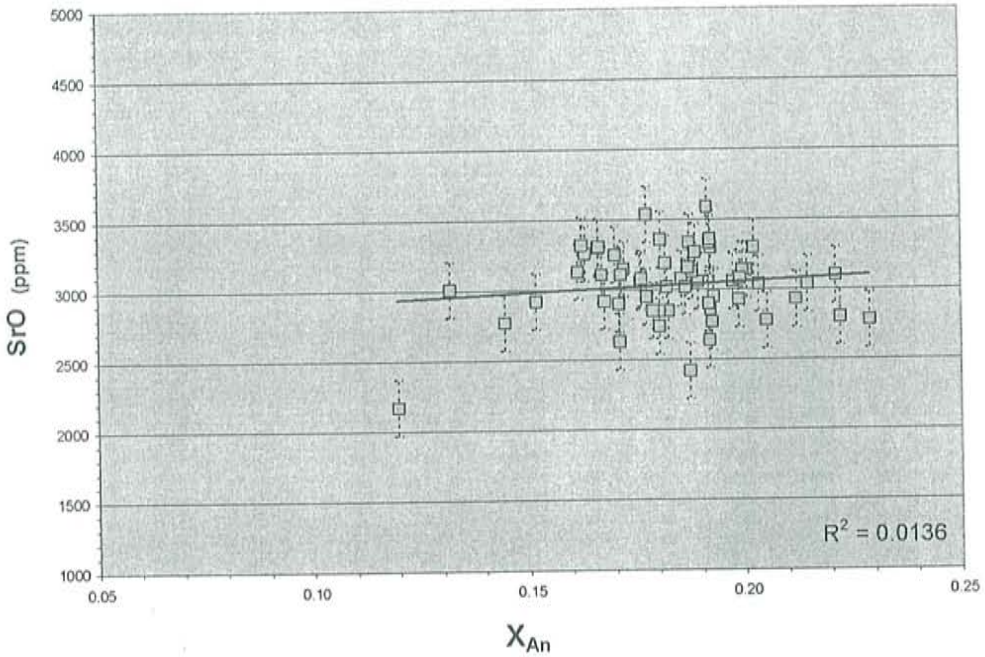

Figure D.6.31. Mol fraction anorthite (X_{An}) versus SrO for core - rim EMP traverses of anorthoclase feldspar DEC2000-03

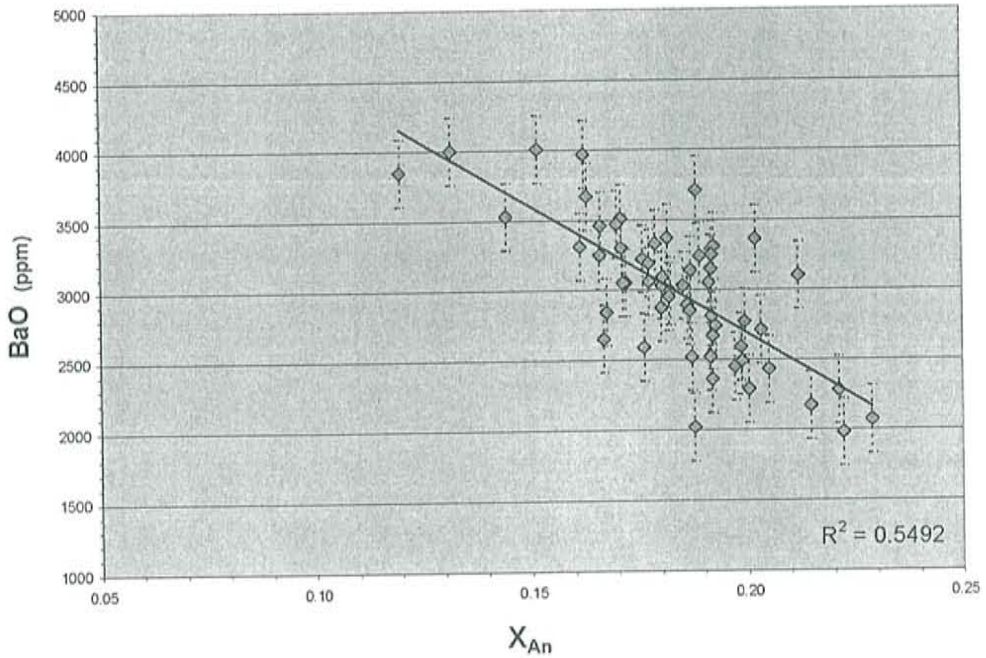

Figure D.6.32. Mol fraction anorthite (X_{An}) versus BaO for core - rim EMP traverses of anorthoclase feldspar DEC2000-03

Table D.6.2. Core - Rim EMP Traverse of Anorthoclase Feldspar Phenocryst

Sample: 84505-01

Total traverse distance (μm): 8643

Step size (μm): 43

n = cumulative # of analyses

EMP # = analysis point ID from run data

n	EMP #	distance from rim	SiO_2 (wt%)	Al_2O_3 (wt%)	CaO (wt%)	Na_2O (wt%)	K_2O (wt%)	FeO (ppm)	SrO (ppm)	BaO (ppm)	Total (wt%)	Endmember Mol. Fractions An	Ab	Or
1	1	8643	63.72	22.20	2.84	7.76	3.43	1560	2750	3560	100.74	0.14	0.67	0.20
2	2	8600	63.35	22.55	3.03	7.69	3.28	1520	2710	3140	100.64	0.15	0.67	0.19
3	3	8557	63.34	22.34	2.77	7.71	3.41	1600	2390	3500	100.31	0.13	0.67	0.20
4	4	8514	63.96	22.01	2.46	7.69	3.78	1860	2580	3130	100.65	0.12	0.67	0.22
5	5	8471	63.58	22.23	2.73	7.72	3.50	1890	2460	3240	100.52	0.13	0.67	0.20
6	6	8428	63.40	22.39	2.94	7.66	3.40	2010	2610	3280	100.58	0.14	0.67	0.19
7	7	8385	63.33	22.28	2.90	7.70	3.48	1740	2710	3320	100.48	0.14	0.66	0.20
8	8	8342	62.76	22.33	2.92	7.71	3.28	1780	2640	3030	99.74	0.14	0.67	0.19
9	9	8299	62.91	22.43	2.92	7.76	3.43	1590	2950	3460	100.24	0.14	0.67	0.19
10	10	8256	63.80	21.89	2.58	7.74	3.67	1680	2590	3370	100.43	0.12	0.67	0.21
11	11	8213	63.33	22.40	3.03	7.89	3.44	1610	2390	3220	100.81	0.14	0.67	0.19
12	12	8170	63.56	22.35	2.85	7.72	3.41	1380	2480	3360	100.61	0.14	0.67	0.19
13	13	8127	63.41	22.45	2.90	7.78	3.39	1350	2610	3440	100.67	0.14	0.67	0.19
14	14	8084	63.43	22.46	2.99	7.78	3.28	1780	2740	2690	100.65	0.14	0.67	0.19
15	15	8041	62.64	22.85	3.55	7.76	2.81	1620	3220	3070	100.42	0.17	0.67	0.16
16	16	7998	63.17	22.60	3.11	7.83	3.13	1630	2560	2790	100.55	0.15	0.67	0.18
17	17	7955	62.82	22.72	3.20	7.70	3.06	1880	2750	3350	100.30	0.15	0.67	0.18
18	18	7912	62.77	22.78	3.37	7.70	2.94	1570	2850	2940	100.29	0.16	0.67	0.17
19	19	7869	63.11	22.96	3.38	7.64	2.97	1590	2790	2950	100.79	0.16	0.67	0.17
20	20	7826	63.34	22.45	3.05	7.64	3.29	1610	2870	3060	100.52	0.15	0.67	0.19
21	21	7783	63.08	22.81	3.14	7.64	3.08	1560	2530	2890	100.44	0.15	0.67	0.18
22	22	7740	63.36	22.61	3.10	7.66	3.10	1620	2640	2870	100.54	0.15	0.67	0.18
23	23	7697	63.38	22.50	2.98	7.78	3.16	1610	2530	3070	100.52	0.14	0.68	0.18
24	24	7654	62.61	22.31	2.89	7.70	3.43	1520	2580	2850	99.63	0.14	0.67	0.20
25	25	7611	62.99	22.28	2.79	7.82	3.43	1630	2690	3360	100.08	0.13	0.67	0.19
26	26	7568	62.46	22.67	3.15	7.66	3.10	1620	2840	2870	99.77	0.15	0.67	0.18
27	27	7525	63.32	22.19	2.68	7.75	3.57	1700	2670	3310	100.28	0.13	0.67	0.20
28	29	7482	63.81	22.02	2.67	7.74	3.51	1650	2720	3590	100.54	0.13	0.67	0.20
29	30	7439	63.29	22.27	2.91	7.59	3.28	1640	2700	3090	100.10	0.14	0.67	0.19
30	31	7396	63.27	22.44	2.87	7.69	3.35	1650	2390	3250	100.35	0.14	0.67	0.19
31	32	7353	63.38	22.44	3.05	7.75	3.21	1460	2610	2980	100.53	0.15	0.67	0.18
32	33	7310	62.97	22.41	2.78	7.73	3.41	1310	2570	3170	100.00	0.13	0.67	0.20
33	34	7267	63.56	22.21	2.76	7.76	3.38	1710	2700	3300	100.44	0.13	0.67	0.19
34	35	7224	63.62	22.24	2.74	7.75	3.42	1540	2820	3200	100.53	0.13	0.67	0.20
35	36	7181	63.39	22.63	2.98	7.97	3.15	1800	2560	3160	100.88	0.14	0.68	0.18
36	37	7138	63.12	22.34	2.73	7.66	3.45	1480	2630	3340	100.04	0.13	0.67	0.20
37	38	7095	63.17	22.41	2.88	7.59	3.35	1510	2500	3210	100.12	0.14	0.67	0.19
38	39	7052	62.65	22.60	2.92	7.80	3.27	1710	2820	3400	100.04	0.14	0.67	0.19
39	40	7009	63.97	22.22	2.85	7.70	3.43	1540	2720	3340	100.93	0.14	0.67	0.20
40	41	6966	63.45	22.56	2.78	7.77	3.41	1850	2660	3230	100.74	0.13	0.67	0.19
41	42	6923	62.32	22.74	3.24	7.70	2.95	1470	2920	3370	99.72	0.16	0.67	0.17
42	43	6880	62.47	22.74	3.17	7.82	3.03	1730	2680	3200	99.99	0.15	0.68	0.17
43	45	6794	62.40	22.54	3.03	7.64	3.30	1610	2540	3530	99.68	0.15	0.67	0.19
44	46	6751	62.82	22.29	2.75	7.64	3.54	1500	2340	3280	99.74	0.13	0.67	0.20
45	50	6622	63.00	22.44	2.96	7.73	3.24	1840	2790	3130	100.15	0.14	0.67	0.19
46	51	6579	63.68	22.13	2.84	7.65	3.57	1660	2960	4040	100.73	0.14	0.66	0.20
47	52	6536	63.65	22.34	3.04	7.60	3.49	1670	2970	3700	100.96	0.14	0.66	0.20
48	54	6450	63.72	22.06	2.93	7.64	3.48	1920	3130	3630	100.70	0.14	0.66	0.20
49	55	6407	63.20	22.63	3.30	7.66	3.17	1740	2900	3520	100.77	0.16	0.66	0.18
50	57	6321	62.88	22.41	3.22	7.71	3.34	1890	2990	3880	100.42	0.15	0.66	0.19
51	58	6278	62.43	22.72	3.34	7.57	3.10	2080	3120	3930	100.07	0.16	0.66	0.18
52	59	6235	63.38	22.60	3.13	7.83	3.24	1740	2680	3500	100.98	0.15	0.67	0.18
53	60	6192	62.67	22.87	3.48	7.72	2.98	1900	2390	2780	100.43	0.17	0.67	0.17
54	61	6149	63.12	22.85	3.60	7.66	2.91	1750	2510	3280	100.90	0.17	0.66	0.17
55	63	6063	63.06	22.60	3.23	7.66	3.14	1490	2770	2880	100.40	0.15	0.67	0.18
56	64	6020	63.07	22.62	3.35	7.66	3.14	1570	2710	3420	100.60	0.16	0.66	0.18
57	65	5977	63.87	22.31	2.76	7.75	3.46	1530	2420	3490	100.88	0.13	0.67	0.20
58	66	5934	63.55	22.65	3.24	7.59	3.16	1520	2080	3120	100.87	0.16	0.66	0.18
59	68	5848	63.62	22.31	2.95	7.78	3.38	1590	2260	3020	100.73	0.14	0.67	0.19
60	69	5805	63.20	22.37	3.14	7.70	3.31	1500	2410	3110	100.42	0.15	0.66	0.19
61	70	5762	63.38	22.43	2.92	7.68	3.42	1840	2930	3040	100.61	0.14	0.66	0.20
62	71	5719	63.33	22.80	3.33	7.64	3.00	1800	2610	3250	100.86	0.16	0.67	0.17
63	74	5633	63.33	22.58	3.38	7.74	3.07	2130	2690	3200	100.90	0.16	0.67	0.17

Table D.6.2. Core - Rim EMP Traverse of Anorthoclase Feldspar Phenocryst

Sample: 84505-01

Total traverse distance (μm): 8643

Step size (μm): 43

n = cumulative # of analyses

EMP # = analysis point ID from run data

n	EMP #	distance from rim	SiO_2 (wt%)	Al_2O_3 (wt%)	CaO (wt%)	Na_2O (wt%)	K_2O (wt%)	FeO (ppm)	SrO (ppm)	BaO (ppm)	Total (wt%)	Endmember Mol. Fractions An	Ab	Or
64	75	5590	63.25	22.77	3.36	7.79	3.04	1670	2520	3080	100.94	0.16	0.67	0.17
65	76	5547	63.79	22.32	2.97	7.75	3.44	1770	2270	3140	100.99	0.14	0.66	0.19
66	77	5504	63.19	22.29	3.20	7.71	3.20	1750	2890	3070	100.36	0.15	0.67	0.18
67	78	5461	63.78	22.27	2.90	7.67	3.42	1760	2390	3490	100.80	0.14	0.67	0.20
68	79	5418	63.76	22.22	2.93	7.65	3.49	1590	2420	3520	100.81	0.14	0.66	0.20
69	80	5375	63.11	22.17	2.94	7.76	3.59	1800	2610	3690	100.37	0.14	0.66	0.20
70	81	5332	63.39	22.16	2.99	7.73	3.51	1950	2710	3500	100.59	0.14	0.66	0.20
71	82	5289	63.73	22.19	2.89	7.65	3.52	1540	2430	3420	100.71	0.14	0.66	0.20
72	83	5246	63.41	22.42	2.98	7.71	3.35	1730	2500	3330	100.63	0.14	0.67	0.19
73	84	5203	63.33	22.46	3.12	7.58	3.32	1710	2710	3340	100.58	0.15	0.66	0.19
74	86	5160	63.62	22.06	2.75	7.62	3.67	1540	2370	3310	100.45	0.13	0.66	0.21
75	87	5117	63.87	22.29	2.88	7.65	3.50	1570	2520	3320	100.93	0.14	0.66	0.20
76	88	5074	63.41	21.78	2.29	7.62	4.00	1550	2340	3280	99.82	0.11	0.66	0.23
77	89	5031	63.96	22.02	2.70	7.72	3.69	1710	2570	3530	100.87	0.13	0.66	0.21
78	90	4988	64.04	22.14	2.87	7.83	3.40	1950	2410	2750	100.99	0.14	0.67	0.19
79	92	4902	63.61	22.25	2.81	7.63	3.58	1870	2410	3500	100.66	0.13	0.66	0.20
80	93	4859	63.57	22.21	2.94	7.66	3.43	1740	2790	3380	100.60	0.14	0.66	0.20
81	94	4816	63.48	22.49	3.13	7.72	3.27	1740	2540	2890	100.80	0.15	0.67	0.19
82	95	4773	63.32	22.04	2.87	7.67	3.55	1470	2670	3600	100.22	0.14	0.66	0.20
83	96	4730	63.87	22.32	2.86	7.68	3.51	1570	2500	3290	100.98	0.14	0.66	0.20
84	100	4558	63.48	22.18	2.74	7.65	3.62	1660	2690	3960	100.50	0.13	0.66	0.21
85	102	4472	63.31	22.56	3.25	7.66	3.25	1590	2730	3310	100.78	0.16	0.66	0.18
86	103	4429	63.78	22.14	2.81	7.74	3.58	1740	2570	3450	100.83	0.13	0.66	0.20
87	104	4386	63.38	22.31	2.80	7.68	3.50	1840	2690	3900	100.51	0.13	0.67	0.20
88	105	4343	63.55	22.43	3.07	7.57	3.28	1640	2960	3590	100.71	0.15	0.66	0.19
89	110	4171	63.38	22.47	3.10	7.59	3.34	1660	2450	3190	100.61	0.15	0.66	0.19
90	111	4128	63.50	22.51	2.90	7.78	3.43	1880	2730	3180	100.90	0.14	0.67	0.19
91	112	4085	63.52	22.37	3.06	7.73	3.34	1590	2540	3210	100.76	0.15	0.67	0.19
92	114	3999	63.12	22.33	3.03	7.61	3.44	1500	2610	3040	100.25	0.14	0.66	0.20
93	115	3956	63.19	22.62	3.08	7.64	3.32	1670	2660	3020	100.58	0.15	0.66	0.19
94	116	3913	63.38	22.74	3.26	7.74	3.12	1700	2650	3120	100.99	0.16	0.67	0.18
95	117	3870	63.41	22.56	3.21	7.56	3.24	1640	2780	3310	100.74	0.15	0.66	0.19
96	118	3827	63.47	22.62	3.20	7.71	3.22	1340	2790	3350	100.96	0.15	0.67	0.18
97	121	3741	63.27	22.60	3.36	7.57	3.09	1840	2530	3080	100.64	0.16	0.66	0.18
98	122	3698	63.80	22.27	2.84	7.63	3.71	1710	2590	3120	100.99	0.13	0.66	0.21
99	123	3655	63.38	22.29	3.07	7.76	3.38	1750	2290	3740	100.66	0.14	0.67	0.19
100	124	3612	63.22	22.69	3.41	7.66	3.08	1790	3070	3320	100.88	0.16	0.66	0.18
101	127	3526	63.30	22.54	3.24	7.64	3.23	1590	2960	3410	100.75	0.16	0.66	0.18
102	128	3483	63.30	22.69	3.26	7.67	3.09	1460	2420	2760	100.68	0.16	0.67	0.18
103	129	3440	62.81	22.97	3.56	7.80	2.92	1620	2770	2880	100.79	0.17	0.67	0.16
104	130	3397	63.35	22.65	3.28	7.74	3.07	1310	2680	2770	100.76	0.16	0.67	0.17
105	131	3354	62.81	22.99	3.50	7.68	2.93	1610	2810	2810	100.63	0.17	0.66	0.17
106	132	3311	62.60	22.89	3.58	7.56	2.90	1650	2850	3080	100.29	0.17	0.66	0.17
107	133	3268	62.91	22.96	3.56	7.64	2.95	1890	2570	2700	100.73	0.17	0.66	0.17
108	135	3182	62.50	23.11	3.74	7.65	2.72	1630	2900	2880	100.45	0.18	0.66	0.16
109	136	3139	62.56	23.22	4.00	7.72	2.65	1620	2850	2690	100.87	0.19	0.66	0.15
110	137	3096	63.19	22.45	3.29	7.70	3.10	1540	2600	2910	100.43	0.16	0.67	0.18
111	139	3053	62.23	23.03	3.75	7.66	2.74	2140	2680	2580	100.15	0.18	0.66	0.16
112	140	3010	62.51	23.07	3.74	7.65	2.72	1850	2890	3000	100.47	0.18	0.66	0.16
113	141	2967	62.61	23.21	3.91	7.69	2.61	1720	2820	2480	100.73	0.19	0.66	0.15
114	142	2924	62.68	22.87	3.56	7.75	2.90	1850	2830	3080	100.54	0.17	0.67	0.16
115	143	2881	62.76	23.06	3.90	7.64	2.66	1930	3190	2520	100.79	0.19	0.66	0.15
116	144	2838	62.35	23.08	3.70	7.77	2.74	2030	3010	3010	100.45	0.18	0.67	0.16
117	145	2795	62.69	23.08	3.83	7.63	2.76	1810	3040	2980	100.77	0.18	0.66	0.16
118	146	2752	62.11	23.09	3.73	7.64	2.78	1900	3010	3100	100.14	0.18	0.66	0.16
119	147	2709	63.04	23.02	3.62	7.66	2.81	1570	2850	2970	100.89	0.17	0.67	0.16
120	148	2666	63.41	22.74	3.38	7.68	2.93	1510	2780	3260	100.90	0.16	0.67	0.17
121	149	2623	62.99	22.68	3.44	7.69	2.97	1950	2730	2870	100.53	0.16	0.67	0.17
122	150	2580	62.51	23.32	4.05	7.61	2.53	2110	3160	3210	100.86	0.19	0.66	0.15
123	155	2537	63.03	22.94	3.49	7.70	2.95	2110	2930	2940	100.91	0.17	0.67	0.17
124	156	2494	62.59	22.91	3.55	7.64	2.91	1950	2900	3230	100.41	0.17	0.66	0.17
125	158	2408	62.76	22.97	3.71	7.66	2.89	1960	3030	2970	100.78	0.18	0.66	0.16
126	160	2322	62.16	23.12	3.77	7.76	2.70	1920	3060	2770	100.27	0.18	0.67	0.15
127	161	2279	62.98	23.00	3.65	7.76	2.69	1650	3150	2700	100.83	0.17	0.67	0.15
128	162	2236	63.16	22.82	3.56	7.79	2.88	1680	2920	2310	100.91	0.17	0.67	0.16

Table D.6.2. Core - Rim EMP Traverse of Anorthoclase Feldspar Phenocryst

Sample: 84505-01

Total traverse distance (μm): 8643

Step size (μm): 43

n = cumulative # of analyses

EMP # = analysis point ID from run data

n	EMP #	distance from rim	SiO_2 (wt%)	Al_2O_3 (wt%)	CaO (wt%)	Na_2O (wt%)	K_2O (wt%)	FeO (ppm)	SrO (ppm)	BaO (ppm)	Total (wt%)	Endmember Mol. Fractions An	Ab	Or
129	163	2193	63.19	22.81	3.44	7.70	3.05	1480	2950	3260	100.96	0.16	0.66	0.17
130	164	2150	62.66	22.79	3.36	7.72	3.16	1820	3020	3210	100.49	0.16	0.66	0.18
131	165	2107	63.20	22.70	3.38	7.71	3.05	1970	3080	3130	100.85	0.16	0.67	0.17
132	167	2021	62.75	23.13	3.78	7.66	2.72	1610	2570	2920	100.74	0.18	0.66	0.15
133	168	1978	62.78	23.09	3.71	7.64	2.79	1860	2680	2850	100.75	0.18	0.66	0.16
134	169	1935	62.84	23.08	3.63	7.74	2.79	1720	2930	2510	100.80	0.17	0.67	0.16
135	172	1806	62.67	23.23	3.75	7.64	2.77	1600	3110	2690	100.79	0.18	0.66	0.16
136	173	1763	62.87	22.94	3.72	7.51	2.83	1780	2920	2980	100.63	0.18	0.66	0.16
137	174	1720	63.17	22.88	3.65	7.68	2.81	1890	3000	2610	100.93	0.17	0.67	0.16
138	176	1634	62.34	23.47	4.09	7.57	2.58	1750	2930	2100	100.72	0.20	0.66	0.15
139	177	1591	62.14	23.61	4.40	7.62	2.31	1820	2750	2770	100.82	0.21	0.66	0.13
140	178	1548	62.76	23.00	3.57	7.66	2.92	1630	2870	3320	100.69	0.17	0.66	0.17
141	179	1505	62.41	23.17	3.90	7.70	2.73	1530	3030	3200	100.69	0.18	0.66	0.15
142	180	1462	62.78	22.87	3.44	7.66	3.03	1710	2900	3580	100.60	0.16	0.66	0.17
143	181	1419	62.01	23.34	3.96	7.66	2.59	1560	2960	3100	100.32	0.19	0.66	0.15
144	182	1376	62.68	23.23	3.88	7.57	2.77	1760	3120	3420	100.95	0.19	0.66	0.16
145	183	1333	63.27	22.73	3.52	7.57	2.94	1780	2940	2820	100.77	0.17	0.66	0.17
146	185	1247	62.14	23.43	4.06	7.71	2.53	1580	3090	2740	100.61	0.19	0.66	0.14
147	186	1204	62.56	23.06	3.73	7.76	2.74	1650	2870	2690	100.57	0.18	0.67	0.16
148	187	1161	62.68	23.14	3.86	7.78	2.63	2090	2930	2980	100.89	0.18	0.67	0.15
149	188	1118	62.63	22.99	3.69	7.78	2.80	1740	3020	3050	100.67	0.17	0.67	0.16
150	189	1075	62.74	23.32	3.94	7.61	2.60	1680	2920	2810	100.95	0.19	0.66	0.15
151	190	1032	62.75	23.06	3.75	7.69	2.78	1650	3070	2540	100.75	0.18	0.66	0.16
152	191	989	62.96	23.03	3.70	7.65	2.77	1670	3030	2920	100.88	0.18	0.66	0.16
153	192	946	63.12	22.87	3.44	7.74	3.03	1630	2870	3110	100.97	0.16	0.67	0.17
154	193	903	62.77	23.14	3.84	7.67	2.79	1830	2850	2750	100.94	0.18	0.66	0.16
155	195	817	62.78	22.96	3.62	7.64	2.97	1980	2740	2710	100.71	0.17	0.66	0.17
156	197	774	61.08	23.92	4.73	7.68	2.17	1740	3120	2100	100.28	0.22	0.65	0.12
157	198	731	62.42	23.11	3.69	7.68	2.83	1730	2910	2910	100.49	0.18	0.66	0.16
158	199	688	61.92	23.16	3.79	7.73	2.74	1750	3150	2680	100.10	0.18	0.67	0.15
159	200	645	63.18	22.72	3.39	7.81	3.12	1860	2130	2750	100.89	0.16	0.67	0.18
160	201	602	62.25	22.89	3.69	7.71	2.86	2290	2590	2810	100.17	0.18	0.66	0.16
161	204	559	62.45	23.07	3.50	7.72	2.88	2110	2800	2840	100.40	0.17	0.67	0.16
162	205	516	62.27	23.01	3.75	7.71	2.75	1760	2820	2990	100.24	0.18	0.67	0.16
163	206	473	62.61	23.02	3.75	7.77	2.83	1710	2950	2530	100.70	0.18	0.66	0.16
164	207	430	62.59	23.01	3.81	7.68	2.74	1960	2760	2370	100.54	0.18	0.66	0.16
165	208	387	62.63	23.17	3.99	7.68	2.66	1900	2460	2650	100.83	0.19	0.66	0.15
166	209	344	63.00	22.94	3.76	7.84	2.67	2070	2790	2560	100.95	0.18	0.67	0.15
167	211	301	63.48	22.61	3.23	7.69	3.18	1770	2500	2960	100.91	0.15	0.66	0.18
168	212	258	61.94	22.97	3.67	7.62	2.84	1760	2410	2820	99.75	0.18	0.66	0.16
169	213	215	62.75	23.16	3.83	7.67	2.77	1970	2930	3120	100.97	0.18	0.66	0.16
170	214	172	63.00	22.76	3.49	7.55	3.05	1980	2520	2830	100.59	0.17	0.66	0.17
171	215	129	62.96	22.72	3.35	7.59	3.21	1840	2630	3120	100.59	0.16	0.66	0.18
172	216	86	63.13	22.56	3.41	7.76	3.10	1830	3030	2850	100.73	0.16	0.66	0.17
173	217	43	63.37	22.51	3.17	7.66	3.23	1790	2890	2920	100.68	0.15	0.66	0.18
174	219	0	63.21	22.41	3.17	7.59	3.26	2130	3110	3260	100.48	0.15	0.66	0.19

Table D.6.3. Core - Rim EMP Traverse of Anorthoclase Feldspar Phenocryst

Sample: 84505-02

Total traverse distance (μm): 3000

Step size (μm): 40

n = cumulative # of analyses

EMP # = analysis point ID from run data

n	EMP #	distance from rim	SiO_2 (wt%)	Al_2O_3 (wt%)	CaO (wt%)	Na_2O (wt%)	K_2O (wt%)	FeO (ppm)	SrO (ppm)	BaO (ppm)	Total (wt%)	Endmember Mol. Fractions An	Ab	Or
1	1	3000	63.14	22.80	3.37	7.66	3.01	1730	3060	2970	100.76	0.16	0.67	0.17
2	3	2960	63.03	22.86	3.34	7.65	3.12	1780	2810	2500	100.72	0.16	0.66	0.18
3	4	2920	63.03	21.81	2.70	8.04	3.86	1900	2750	3080	100.21	0.12	0.67	0.21
4	5	2880	62.62	21.44	2.50	8.36	4.27	2090	2730	2990	99.98	0.11	0.67	0.22
5	6	2840	63.54	22.20	2.76	7.82	3.65	2030	2880	3060	100.78	0.13	0.67	0.20
6	7	2800	63.08	22.64	3.14	7.83	3.28	2350	2950	2810	100.77	0.15	0.67	0.18
7	8	2760	61.63	22.96	3.61	7.68	2.91	1990	3200	2470	99.56	0.17	0.66	0.16
8	9	2720	62.12	22.98	3.54	7.74	2.91	2020	3150	2890	100.09	0.17	0.67	0.17
9	10	2680	62.70	23.00	3.62	7.83	2.89	2150	3090	2690	100.83	0.17	0.67	0.16
10	11	2640	62.72	23.11	3.60	7.75	2.85	2520	2950	2860	100.87	0.17	0.67	0.16
11	14	2560	63.00	22.91	3.37	7.72	2.91	2520	2820	2300	100.66	0.16	0.67	0.17
12	15	2520	63.42	22.32	2.97	7.85	3.31	2270	3000	2940	100.69	0.14	0.67	0.19
13	16	2480	63.19	22.69	3.28	7.79	3.11	2320	2870	2410	100.82	0.16	0.67	0.18
14	17	2440	62.91	22.49	3.04	7.77	3.31	2370	2870	3190	100.36	0.14	0.67	0.19
15	18	2400	62.26	22.64	3.22	7.76	3.13	1880	3210	2860	99.80	0.15	0.67	0.18
16	19	2360	62.94	22.69	3.19	7.80	3.17	1840	2830	2550	100.50	0.15	0.67	0.18
17	20	2320	63.05	22.64	3.11	7.84	3.26	2000	3000	2790	100.68	0.15	0.67	0.18
18	21	2280	63.00	22.92	3.31	7.70	3.03	2080	3220	2330	100.72	0.16	0.67	0.17
19	23	2200	62.82	22.76	3.33	7.78	3.02	2160	3000	2730	100.50	0.16	0.67	0.17
20	24	2160	62.32	22.83	3.48	7.77	2.97	2190	2860	2720	100.13	0.17	0.67	0.17
21	26	2120	62.60	22.70	3.23	7.69	3.11	1860	2940	2560	100.06	0.15	0.67	0.18
22	28	2040	62.77	22.28	2.74	7.80	3.61	1770	2940	3200	99.98	0.13	0.67	0.20
23	29	2000	63.64	22.12	2.79	7.85	3.67	1960	2680	2920	100.83	0.13	0.67	0.20
24	30	1960	62.68	22.27	2.89	7.52	3.60	1770	3180	3280	99.77	0.14	0.66	0.21
25	31	1920	63.37	22.32	2.88	7.78	3.38	1800	3010	2480	100.46	0.14	0.67	0.19
26	32	1880	63.04	22.28	2.95	7.67	3.51	2190	2790	3110	100.25	0.14	0.66	0.20
27	33	1840	62.20	22.79	3.47	7.73	3.05	2070	3140	2900	100.04	0.16	0.66	0.17
28	34	1800	62.57	22.29	2.74	7.77	3.71	1610	2680	2860	99.78	0.13	0.66	0.21
29	35	1760	63.75	22.31	2.90	7.70	3.51	1910	2680	2840	100.92	0.14	0.66	0.20
30	36	1720	63.86	21.96	2.55	7.62	3.91	2270	2870	3000	100.71	0.12	0.66	0.22
31	37	1680	63.94	22.08	2.56	7.64	3.75	2180	3050	2930	100.78	0.12	0.66	0.21
32	38	1640	62.83	22.94	3.31	7.74	3.15	1910	2910	3330	100.79	0.16	0.66	0.18
33	39	1600	63.78	22.11	2.70	7.86	3.67	1830	2550	3460	100.89	0.13	0.67	0.21
34	40	1560	63.33	22.26	2.77	7.74	3.52	1830	3070	2860	100.40	0.13	0.67	0.20
35	41	1520	63.37	22.60	3.20	7.74	3.15	2590	2920	2760	100.89	0.15	0.67	0.18
36	42	1480	62.86	22.53	3.10	7.71	3.33	2560	3080	2670	100.36	0.15	0.66	0.19
37	43	1440	62.61	22.19	2.60	7.69	3.80	2340	2810	3010	99.71	0.12	0.66	0.21
38	44	1400	63.13	22.48	2.77	7.77	3.56	2140	3060	2760	100.50	0.13	0.67	0.20
39	45	1360	63.56	22.33	2.84	7.75	3.55	2230	3050	3170	100.86	0.13	0.67	0.20
40	46	1320	63.42	22.52	3.08	7.54	3.27	2560	2990	2810	100.66	0.15	0.66	0.19
41	49	1240	62.98	22.53	3.13	7.77	3.34	2040	2690	3180	100.53	0.15	0.66	0.19
42	50	1200	63.52	22.64	3.12	7.72	3.21	1710	3120	2560	100.95	0.15	0.67	0.18
43	52	1120	62.76	22.40	2.91	7.63	3.55	1830	2950	2880	100.00	0.14	0.66	0.20
44	53	1080	63.13	22.77	3.31	7.74	3.20	2060	3300	2610	100.94	0.16	0.66	0.18
45	54	1040	63.21	22.48	3.03	7.78	3.24	2130	2760	2740	100.50	0.14	0.67	0.18
46	55	1000	62.07	23.15	3.70	7.67	2.90	1510	2950	2780	100.21	0.18	0.66	0.16
47	56	960	62.30	23.41	4.15	7.66	2.58	1900	3140	2470	100.84	0.20	0.66	0.15
48	57	920	63.03	22.63	3.25	7.65	3.02	1710	3040	2640	100.31	0.16	0.67	0.17
49	60	840	62.36	22.99	3.42	7.65	2.92	2350	2840	2840	100.13	0.16	0.67	0.17
50	61	800	62.50	23.13	3.60	7.79	2.82	1910	3190	2370	100.58	0.17	0.67	0.16
51	64	680	62.10	23.18	3.59	7.80	2.88	1820	3070	2910	100.32	0.17	0.67	0.16
52	66	600	61.92	23.85	4.52	7.67	2.19	1710	3050	1870	100.82	0.22	0.66	0.12
53	67	560	62.09	23.56	4.10	7.62	2.44	1930	3050	2170	100.53	0.20	0.66	0.14
54	68	520	62.27	23.07	3.58	7.63	2.90	2090	3220	2880	100.27	0.17	0.66	0.17
55	75	280	63.05	22.31	2.59	7.77	3.51	2720	2980	3000	100.10	0.12	0.68	0.20
56	76	240	63.18	22.43	2.68	7.83	3.61	2120	3030	3090	100.56	0.13	0.67	0.20
57	77	200	63.62	22.39	2.86	7.81	3.50	2090	2840	2600	100.93	0.14	0.67	0.20
58	82	0	62.49	23.34	3.58	7.90	2.83	2530	3450	2720	101.00	0.17	0.67	0.16

Table D.6.4. Core - Rim EMP Traverse of Anorthoclase Feldspar Phenocryst

Sample: 84505-03

Total traverse distance (μm): 3000

Step size (μm): 40

n = cumulative # of analyses

EMP # = analysis point ID from run data

n	EMP #	distance from rim	SiO_2 (wt%)	Al_2O_3 (wt%)	CaO (wt%)	Na_2O (wt%)	K_2O (wt%)	FeO (ppm)	SrO (ppm)	BaO (ppm)	Total (wt%)	Endmember Mol. Fractions An	Ab	Or
1	1	3000	63.68	22.20	2.77	7.60	3.65	1960	2880	3110	100.69	0.13	0.66	0.21
2	2	2960	63.21	22.25	2.80	7.70	3.66	2060	2670	2800	100.37	0.13	0.66	0.21
3	3	2920	62.72	22.31	2.99	7.64	3.49	2200	2680	3320	99.97	0.14	0.66	0.20
4	4	2880	63.13	22.33	2.96	7.72	3.39	1830	2800	3290	100.32	0.14	0.67	0.19
5	5	2840	63.65	22.57	2.96	7.65	3.44	2330	2800	2980	101.08	0.14	0.66	0.20
6	6	2800	63.62	22.27	2.55	7.69	3.76	2300	2620	3180	100.69	0.12	0.66	0.21
7	7	2760	63.46	22.08	2.43	7.65	3.91	1970	2510	3580	100.33	0.12	0.66	0.22
8	8	2720	62.94	22.14	2.58	7.77	3.84	1950	2740	3600	100.09	0.12	0.66	0.22
9	9	2680	64.06	21.88	2.47	7.42	3.86	2000	2740	3880	100.56	0.12	0.66	0.22
10	10	2640	63.65	22.36	2.70	7.83	3.64	1670	2650	2810	100.89	0.13	0.67	0.20
11	11	2600	62.78	22.41	3.03	7.62	3.44	1630	2670	3580	100.06	0.15	0.66	0.20
12	12	2560	63.11	22.75	3.31	7.70	3.03	2020	2830	3350	100.70	0.16	0.67	0.17
13	13	2520	63.42	22.54	3.10	7.64	3.16	2240	3270	3020	100.71	0.15	0.67	0.18
14	14	2480	62.96	22.37	3.07	7.70	3.31	2110	2870	3120	100.22	0.15	0.67	0.19
15	15	2440	62.35	22.44	3.05	7.68	3.24	1890	2680	3000	99.52	0.15	0.67	0.19
16	16	2400	63.32	22.51	3.12	7.66	3.28	1790	3200	3190	100.71	0.15	0.66	0.19
17	17	2360	63.28	22.69	3.29	7.69	3.06	1880	3130	3130	100.83	0.16	0.67	0.17
18	18	2320	63.32	22.46	2.96	7.70	3.30	2120	2990	3130	100.56	0.14	0.67	0.19
19	19	2280	62.63	23.04	3.73	7.73	2.80	2090	3170	2750	100.73	0.18	0.66	0.16
20	20	2240	63.49	22.34	2.85	7.77	3.48	2060	2660	3170	100.72	0.14	0.67	0.20
21	21	2200	63.28	22.47	3.28	7.67	3.14	1870	2920	3200	100.63	0.16	0.66	0.18
22	22	2160	63.44	22.30	2.81	7.63	3.43	2240	2780	3260	100.43	0.14	0.67	0.20
23	23	2120	62.52	22.37	2.93	7.63	3.35	1870	2610	3650	99.61	0.14	0.67	0.19
24	25	2080	62.71	22.80	3.28	7.70	3.16	1980	2870	2720	100.41	0.16	0.66	0.18
25	27	2000	62.92	22.57	3.07	7.68	3.26	1960	2870	3190	100.30	0.15	0.67	0.19
26	28	1960	63.21	22.55	3.02	7.62	3.34	2060	2820	3040	100.53	0.15	0.66	0.19
27	29	1920	63.19	22.63	3.16	7.63	3.26	1850	3170	3180	100.69	0.15	0.66	0.19
28	30	1880	63.12	22.59	3.31	7.64	3.16	2110	3130	3070	100.64	0.16	0.66	0.18
29	31	1840	62.40	22.87	3.38	7.70	3.15	2340	3000	3010	100.33	0.16	0.66	0.18
30	32	1800	62.57	22.96	3.71	7.65	2.87	1940	3020	2880	100.53	0.18	0.66	0.16
31	33	1760	63.15	22.55	3.08	7.80	3.24	2050	3120	3070	100.64	0.15	0.67	0.18
32	34	1720	61.92	22.68	3.34	7.64	3.11	2000	2880	2680	99.45	0.16	0.66	0.18
33	35	1680	62.30	22.62	3.00	7.73	3.29	2120	2910	3210	99.77	0.14	0.67	0.19
34	36	1640	63.49	22.51	3.09	7.74	3.24	2040	2900	3300	100.90	0.15	0.67	0.18
35	37	1600	63.33	22.64	3.19	7.73	3.20	2030	2870	3180	100.89	0.15	0.67	0.18
36	38	1560	63.57	22.48	3.12	7.73	3.20	1780	3120	2560	100.85	0.15	0.67	0.18
37	39	1520	62.75	22.74	3.36	7.76	3.02	2010	3200	3090	100.46	0.16	0.67	0.17
38	40	1480	62.44	23.28	3.70	7.70	2.70	2470	3130	2510	100.62	0.18	0.67	0.15
39	41	1440	62.57	22.66	3.24	7.63	3.19	2130	2860	2800	100.07	0.16	0.66	0.18
40	42	1400	62.01	22.60	3.30	7.74	3.02	1950	2950	2810	99.44	0.16	0.67	0.17
41	43	1360	63.18	22.64	3.35	7.68	3.21	2100	2720	2620	100.79	0.16	0.66	0.18
42	44	1320	62.20	22.87	3.48	7.63	2.98	2160	2820	3090	99.95	0.17	0.66	0.17
43	45	1280	62.90	22.75	3.45	7.68	3.07	2020	2990	3130	100.67	0.16	0.66	0.17
44	46	1240	63.49	22.41	3.00	7.69	3.31	2120	3020	3130	100.73	0.14	0.67	0.19
45	47	1200	63.64	22.58	3.07	7.62	3.29	2010	2940	2710	100.96	0.15	0.66	0.19
46	48	1160	62.82	22.75	3.44	7.71	3.05	2350	3000	2840	100.59	0.16	0.66	0.17
47	49	1120	62.36	22.61	3.16	7.70	3.21	1940	2970	2700	99.80	0.15	0.67	0.18
48	50	1080	62.80	22.95	3.70	7.79	2.82	2080	3050	2530	100.84	0.17	0.67	0.16
49	51	1040	62.48	22.90	3.79	7.65	2.77	1900	3300	2800	100.38	0.18	0.66	0.16
50	52	1000	61.85	23.25	3.72	7.67	2.83	1630	3210	2680	100.08	0.18	0.66	0.16
51	53	960	62.01	22.69	3.43	7.82	2.94	1810	3130	2720	99.67	0.16	0.67	0.17
52	54	920	62.52	23.17	3.87	7.72	2.67	1690	3270	2470	100.69	0.18	0.66	0.15
53	56	840	62.84	22.90	3.46	7.66	2.95	1540	3100	2660	100.52	0.17	0.67	0.17
54	57	800	62.30	22.70	3.27	7.69	3.08	1740	2960	2410	99.75	0.16	0.67	0.18
55	58	760	62.81	23.09	3.69	7.77	2.74	1730	3220	1710	100.77	0.18	0.67	0.16
56	59	720	62.84	22.94	3.50	7.75	2.90	1900	2890	2790	100.69	0.17	0.67	0.17
57	60	680	63.15	22.85	3.32	7.74	3.04	1730	3150	2790	100.87	0.16	0.67	0.17
58	61	640	61.60	23.01	3.76	7.76	2.73	1570	3300	2160	99.57	0.18	0.67	0.15
59	62	600	62.03	23.58	3.95	7.71	2.44	1710	3000	1900	100.37	0.19	0.67	0.14
60	63	560	62.84	23.26	3.70	7.65	2.74	1940	3270	2380	100.95	0.18	0.67	0.16
61	64	520	62.30	23.02	3.53	7.83	2.78	1960	3050	2410	100.21	0.17	0.67	0.16

Table D.6.4. Core - Rim EMP Traverse of Anorthoclase Feldspar Phenocryst

Sample: 84505-03

Total traverse distance (μm): 3000

Step size (μm): 40

n = cumulative # of analyses

EMP # = analysis point ID from run data

n	EMP #	distance from rim	SiO_2 (wt%)	Al_2O_3 (wt%)	CaO (wt%)	Na_2O (wt%)	K_2O (wt%)	FeO (ppm)	SrO (ppm)	BaO (ppm)	Total (wt%)	Endmember Mol. Fractions An	Ab	Or
62	65	480	62.39	23.03	3.65	7.69	2.80	1950	3270	2430	100.33	0.18	0.67	0.16
63	66	440	62.37	23.34	3.82	7.68	2.57	1830	3150	2280	100.51	0.18	0.67	0.15
64	67	400	63.09	22.99	3.55	7.67	2.93	1970	3190	3040	101.05	0.17	0.66	0.17
65	68	360	63.03	22.80	3.49	7.59	3.03	1950	3300	2540	100.73	0.17	0.66	0.17
66	69	320	61.82	23.46	4.01	7.72	2.61	1730	3260	2560	100.37	0.19	0.66	0.15
67	70	280	62.73	22.81	3.31	7.75	3.11	1960	2800	2920	100.47	0.16	0.67	0.18
68	71	240	62.48	22.69	3.10	7.65	3.36	2000	3020	3020	100.08	0.15	0.66	0.19
69	72	200	62.47	22.90	3.40	7.85	3.01	2170	3000	3230	100.47	0.16	0.67	0.17
70	75	120	62.74	22.79	3.34	7.79	2.96	2230	2930	2280	100.35	0.16	0.67	0.17
71	76	80	63.33	22.60	3.13	7.72	3.21	1950	2710	3070	100.76	0.15	0.67	0.18
72	77	40	62.52	22.52	3.04	7.86	3.36	2120	3020	2840	100.10	0.14	0.67	0.19
73	78	0	62.70	22.59	3.06	7.74	3.26	1750	2960	2590	100.08	0.15	0.67	0.19

Table D.6.5. Rim-to-Rim EMP Traverse of Anorthoclase Feldspar Phenocryst

Sample: 85010-01

Total traverse distance (μm): 4920

Step size (μm): 40

N = cumulative # of analyses

EMP # = analysis point ID from run data

n	EMP #	distance from rim	SiO_2 (wt%)	Al_2O_3 (wt%)	CaO (wt%)	Na_2O (wt%)	K_2O (wt%)	FeO (ppm)	SrO (ppm)	BaO (ppm)	Total (wt%)	Endmember Mol. Fractions An	Ab	Or
1	1	0	63.49	22.17	2.82	7.33	3.59	2440	2820	3600	100.28	0.14	0.64	0.20
2	2	40	62.63	22.72	3.14	7.34	3.29	2030	3650	4040	100.09	0.15	0.64	0.19
3	3	80	62.42	22.68	3.18	7.34	3.23	2010	2630	3660	99.68	0.15	0.64	0.19
4	4	120	62.87	23.00	3.50	7.35	3.13	2430	3110	3710	100.77	0.17	0.63	0.18
5	6	160	62.13	22.72	3.37	7.50	3.18	1800	2970	3190	99.69	0.16	0.65	0.18
6	7	200	62.98	22.76	3.22	7.50	3.30	2070	2530	3490	100.57	0.15	0.65	0.19
7	10	240	63.27	22.56	2.81	7.55	3.67	2340	2760	3330	100.71	0.13	0.65	0.21
8	12	280	62.45	22.89	3.33	7.57	3.11	2080	2850	3000	100.15	0.16	0.66	0.18
9	13	320	63.23	22.69	3.16	7.47	3.36	1730	3000	3570	100.74	0.15	0.65	0.19
10	14	360	63.23	22.79	3.25	7.52	3.26	2290	2710	2720	100.82	0.16	0.65	0.19
11	15	400	63.78	22.45	2.88	7.45	3.54	2140	2940	2980	100.90	0.14	0.64	0.20
12	16	440	63.56	22.46	2.88	7.38	3.49	1950	3040	2950	100.57	0.14	0.64	0.20
13	17	480	63.09	22.65	3.17	7.47	3.38	1990	2430	3100	100.51	0.15	0.65	0.19
14	18	520	61.36	23.77	4.30	7.29	2.49	1820	2780	2640	99.94	0.21	0.63	0.14
15	19	560	62.75	22.94	3.62	7.44	3.01	1890	3030	3330	100.57	0.17	0.64	0.17
16	20	600	62.35	23.22	3.72	7.39	2.88	1960	3000	2820	100.34	0.18	0.64	0.16
17	21	640	61.86	23.25	3.57	7.30	2.87	2050	2950	3450	99.69	0.17	0.64	0.17
18	22	680	63.10	22.70	3.16	7.41	3.39	1960	2900	2730	100.51	0.15	0.64	0.19
19	23	720	61.14	24.07	4.53	7.43	2.32	2010	3170	2060	100.22	0.22	0.64	0.13
20	24	760	62.68	23.26	3.57	7.53	2.95	1830	2970	3430	100.81	0.17	0.65	0.17
21	25	800	61.88	23.35	3.98	7.42	2.70	1860	3140	2450	100.07	0.19	0.64	0.15
22	26	840	62.60	23.03	3.59	7.55	2.95	2010	3490	2840	100.55	0.17	0.65	0.17
23	27	880	62.12	23.22	3.65	7.39	2.96	1940	3380	3490	100.22	0.18	0.64	0.17
24	28	920	62.93	22.99	3.49	7.44	3.11	1830	3020	3290	100.78	0.17	0.64	0.18
25	29	960	62.72	23.19	3.63	7.44	3.01	2060	2970	2920	100.78	0.17	0.64	0.17
26	30	1000	62.68	23.35	3.80	7.31	2.85	1780	2950	3020	100.76	0.18	0.63	0.16
27	31	1040	61.72	23.37	3.91	7.42	2.90	1820	2830	3050	100.08	0.19	0.65	0.17
28	32	1080	62.03	22.90	3.58	7.32	2.98	1840	2920	3100	99.60	0.17	0.64	0.17
29	33	1120	62.13	23.21	3.63	7.37	2.96	1850	2790	2970	100.04	0.17	0.64	0.17
30	34	1160	62.68	23.30	3.68	7.46	2.89	1690	2840	2640	100.74	0.18	0.64	0.16
31	35	1200	62.74	22.59	3.01	7.44	3.44	1750	2760	3630	100.04	0.14	0.65	0.20
32	36	1240	63.09	22.94	3.45	7.48	3.11	1820	3130	2820	100.85	0.16	0.64	0.18
33	37	1280	62.87	23.00	3.40	7.37	3.02	1790	3020	2960	100.45	0.16	0.64	0.17
34	38	1320	62.27	22.84	3.46	7.45	3.03	1590	2960	3370	99.83	0.17	0.65	0.17
35	39	1360	62.58	23.05	3.33	7.49	3.11	2030	2910	3290	100.38	0.16	0.65	0.18
36	40	1400	62.70	23.17	3.63	7.37	2.87	2180	2870	2720	100.51	0.17	0.64	0.16
37	42	1440	62.58	22.89	3.43	7.49	2.98	1820	3220	2940	100.16	0.16	0.65	0.17
38	43	1480	62.34	23.23	3.68	7.40	2.91	2020	3160	2910	100.37	0.18	0.64	0.17
39	44	1520	62.74	22.91	3.39	7.43	3.01	1680	3070	2690	100.23	0.16	0.64	0.17
40	45	1560	62.71	23.02	3.37	7.44	3.05	1740	2880	3390	100.39	0.16	0.64	0.17
41	46	1600	62.86	23.19	3.47	7.43	2.92	1890	2750	2760	100.61	0.17	0.64	0.17
42	47	1640	62.29	22.91	3.48	7.42	2.98	1910	3010	3020	99.88	0.17	0.65	0.17
43	48	1680	62.46	22.81	3.52	7.42	3.07	1930	2730	3200	100.06	0.17	0.64	0.18
44	49	1720	62.74	23.08	3.60	7.40	2.99	1830	3260	2860	100.60	0.17	0.64	0.17
45	50	1760	61.90	22.88	3.56	7.49	3.00	1740	2820	3120	99.60	0.17	0.65	0.17
46	51	1800	62.50	23.11	3.71	7.46	2.86	1960	2930	2970	100.43	0.18	0.65	0.16
47	52	1840	62.67	23.11	3.54	7.37	2.97	1780	3060	3370	100.47	0.17	0.64	0.17
48	53	1880	62.42	23.03	3.57	7.36	2.92	2010	3450	2990	100.16	0.17	0.64	0.17
49	54	1920	62.22	23.13	3.67	7.40	2.94	2010	2970	3490	100.21	0.18	0.64	0.17
50	55	1960	62.73	23.05	3.61	7.34	2.97	1950	3250	3340	100.55	0.17	0.63	0.17
51	56	2000	62.57	23.06	3.41	7.37	3.10	1900	3010	3840	100.39	0.16	0.64	0.18
52	59	2040	62.57	22.84	3.32	7.46	3.16	1960	2980	2970	100.15	0.16	0.65	0.18
53	60	2080	63.26	22.99	3.35	7.38	3.19	1960	2990	3740	101.03	0.16	0.63	0.18
54	61	2120	62.82	22.57	3.02	7.35	3.46	1600	3090	3740	100.06	0.15	0.64	0.20
55	62	2160	63.20	22.61	2.99	7.48	3.42	2130	2720	3030	100.48	0.14	0.65	0.20
56	63	2200	62.25	22.95	3.49	7.48	3.17	1810	3370	3750	100.23	0.17	0.65	0.18
57	64	2240	63.82	22.54	2.89	7.37	3.61	1950	2960	3880	101.11	0.14	0.63	0.20
58	65	2280	63.38	22.56	3.00	7.38	3.46	1870	3140	3390	100.62	0.14	0.64	0.20
59	66	2320	63.43	22.38	2.74	7.39	3.61	1870	2660	3580	100.36	0.13	0.64	0.21
60	67	2360	62.74	22.89	3.32	7.39	3.18	2000	3180	3750	100.40	0.16	0.64	0.18

Table D.6.5. Rim-to-Rim EMP Traverse of Anorthoclase Feldspar Phenocryst

Sample: 85010-01

Total traverse distance (μm): 4920

Step size (μm): 40

N = cumulative # of analyses

EMP # = analysis point ID from run data

n	EMP #	distance from rim	SiO_2 (wt%)	Al_2O_3 (wt%)	CaO (wt%)	Na_2O (wt%)	K_2O (wt%)	FeO (ppm)	SrO (ppm)	BaO (ppm)	Total (wt%)	Endmember Mol. Fractions An	Ab	Or
61	68	2400	62.59	22.89	3.38	7.39	3.09	1750	3200	3390	100.16	0.16	0.64	0.18
62	69	2440	63.34	22.65	2.99	7.55	3.47	1770	3000	3600	100.83	0.14	0.65	0.20
63	70	2480	62.85	22.97	3.46	7.43	3.01	1660	3210	3440	100.55	0.17	0.64	0.17
64	71	2520	63.06	22.67	3.05	7.45	3.39	1870	2750	3810	100.46	0.15	0.64	0.19
65	72	2560	62.95	22.59	3.43	7.36	3.20	1950	2930	3700	100.38	0.16	0.64	0.18
66	73	2600	62.41	22.92	3.44	7.51	3.05	1810	3080	3200	100.13	0.17	0.65	0.17
67	74	2640	63.30	22.58	3.14	7.46	3.28	1790	2890	3270	100.55	0.15	0.64	0.19
68	75	2680	63.49	22.62	3.04	7.62	3.36	1880	2820	3550	100.95	0.15	0.66	0.19
69	77	2720	62.81	22.99	3.54	7.46	2.98	1830	3150	2520	100.52	0.17	0.64	0.17
70	78	2760	62.69	22.75	3.28	7.45	3.19	1880	2950	3250	100.16	0.16	0.65	0.18
71	79	2800	63.04	22.89	3.31	7.44	3.15	1900	3020	3280	100.64	0.16	0.64	0.18
72	80	2840	62.54	22.83	3.32	7.53	3.19	1910	2970	3350	100.23	0.16	0.65	0.18
73	81	2880	62.41	22.98	3.47	7.42	3.07	2060	2970	2960	100.15	0.17	0.64	0.18
74	82	2920	63.42	22.42	2.95	7.43	3.58	2110	2930	3230	100.61	0.14	0.64	0.20
75	83	2960	62.35	22.96	3.49	7.44	3.06	1810	3280	3380	100.14	0.17	0.65	0.18
76	84	3000	62.47	22.88	3.41	7.38	3.11	2070	3010	2990	100.05	0.16	0.64	0.18
77	85	3040	62.54	22.61	3.17	7.44	3.39	1670	3040	3350	99.96	0.15	0.65	0.19
78	86	3080	63.02	22.85	3.39	7.34	3.14	2080	3080	3100	100.56	0.16	0.63	0.18
79	87	3120	62.62	22.95	3.20	7.52	3.30	2000	2840	3360	100.41	0.15	0.65	0.19
80	88	3160	63.37	22.34	3.12	7.42	3.32	1880	3030	3330	100.39	0.15	0.64	0.19
81	89	3200	63.19	22.76	3.16	7.41	3.38	2110	2820	3350	100.73	0.15	0.64	0.19
82	90	3240	62.58	23.35	3.79	7.32	2.83	1950	3040	3050	100.67	0.18	0.63	0.16
83	91	3280	62.66	23.13	3.68	7.47	2.94	1930	2950	2730	100.65	0.18	0.65	0.17
84	92	3320	62.71	22.93	3.46	7.45	3.02	2760	3000	2890	100.43	0.17	0.65	0.17
85	99	3360	62.77	22.91	3.51	7.50	2.89	2150	2890	2800	100.36	0.17	0.65	0.16
86	100	3400	62.78	23.16	3.52	7.49	2.95	1950	3050	2690	100.68	0.17	0.65	0.17
87	101	3440	62.43	23.02	3.50	7.44	3.06	1830	2840	3280	100.23	0.17	0.65	0.17
88	102	3480	63.01	22.91	3.28	7.46	3.19	1460	2960	2810	100.56	0.16	0.64	0.18
89	103	3520	63.03	22.68	3.22	7.40	3.13	1980	2800	3010	100.25	0.15	0.64	0.18
90	104	3560	63.18	22.98	3.40	7.50	3.07	2000	2920	2910	100.90	0.16	0.65	0.17
91	105	3600	62.95	23.00	3.33	7.52	3.12	1900	2900	2980	100.70	0.16	0.65	0.18
92	106	3640	62.72	23.17	3.68	7.43	2.94	1700	2820	2560	100.63	0.18	0.64	0.17
93	107	3680	62.26	23.14	3.46	7.43	3.08	1710	2970	2760	100.11	0.17	0.65	0.18
94	108	3720	62.90	23.05	3.33	7.45	3.10	1880	2930	2780	100.59	0.16	0.64	0.18
95	109	3760	63.19	22.80	3.04	7.45	3.28	1790	2550	3370	100.53	0.15	0.64	0.19
96	110	3800	63.35	22.62	3.02	7.34	3.29	1950	2750	3200	100.41	0.14	0.63	0.19
97	111	3840	63.24	22.77	3.17	7.36	3.27	2100	2740	3060	100.60	0.15	0.64	0.19
98	112	3880	62.30	23.18	3.69	7.34	2.95	1890	2770	2420	100.16	0.18	0.64	0.17
99	114	3920	62.57	23.26	3.73	7.37	2.82	1890	2950	2930	100.52	0.18	0.64	0.16
100	115	3960	62.33	23.35	3.62	7.41	2.84	1760	3170	2920	100.33	0.17	0.64	0.16
101	116	4000	62.76	22.84	3.53	7.45	3.01	2020	2870	2790	100.35	0.17	0.65	0.17
102	117	4040	63.53	22.69	3.10	7.31	3.39	1750	2810	3140	100.79	0.15	0.63	0.19
103	118	4080	62.73	22.72	3.22	7.36	3.20	1950	3010	3140	100.03	0.15	0.64	0.18
104	119	4120	63.15	22.66	3.24	7.46	3.23	1780	3070	2720	100.49	0.16	0.64	0.18
105	121	4160	62.52	23.11	3.54	7.32	3.01	1880	2840	2710	100.24	0.17	0.63	0.17
106	122	4200	62.69	23.54	3.87	7.38	2.81	1880	2990	2870	101.07	0.18	0.63	0.16
107	123	4240	62.23	23.61	3.87	7.29	2.67	2250	2990	2880	100.49	0.19	0.63	0.15
108	124	4280	61.80	23.70	4.10	7.37	2.51	2050	2900	2430	100.23	0.20	0.64	0.14
109	125	4320	61.87	23.59	4.07	7.35	2.62	2040	2760	3170	100.30	0.20	0.64	0.15
110	126	4360	61.85	23.39	3.94	7.39	2.60	1880	3020	2700	99.94	0.19	0.64	0.15
111	127	4400	63.13	22.94	3.32	7.44	3.19	1600	3040	3160	100.79	0.16	0.64	0.18
112	128	4440	62.39	23.02	3.50	7.45	3.05	1660	2760	3190	100.18	0.17	0.65	0.17
113	129	4480	62.64	22.92	3.66	7.36	2.92	1700	2910	3350	100.30	0.18	0.64	0.17
114	130	4520	62.70	23.25	3.61	7.45	2.94	1930	2740	3250	100.73	0.17	0.64	0.17
115	131	4560	62.69	23.09	3.56	7.46	2.92	1640	2830	3380	100.50	0.17	0.65	0.17
116	132	4600	62.50	23.31	3.80	7.40	2.75	1750	2630	3280	100.52	0.18	0.64	0.16
117	133	4640	62.69	23.02	3.57	7.48	3.04	1840	2620	3330	100.57	0.17	0.65	0.17
118	135	4680	64.01	22.40	2.78	7.42	3.59	2720	2760	3310	101.07	0.13	0.64	0.20
119	136	4720	63.24	22.72	3.17	7.39	3.27	2250	3370	3270	100.67	0.15	0.64	0.19
120	137	4760	63.82	22.20	2.50	7.36	3.97	2400	2690	3470	100.69	0.12	0.64	0.23
121	138	4800	63.42	22.18	2.82	7.38	3.62	2040	2790	3200	100.23	0.14	0.64	0.21
122	139	4840	62.87	22.79	3.15	7.46	3.28	1930	2770	3250	100.34	0.15	0.65	0.19

Table D.6.5. Rim-to-Rim EMP Traverse of Anorthoclase Feldspar Phenocryst

Sample: 85010-01

Total traverse distance (μm): 4920

Step size (μm): 40

N = cumulative # of analyses

EMP # = analysis point ID from run data

n	EMP #	distance from rim	SiO_2 (wt%)	Al_2O_3 (wt%)	CaO (wt%)	Na_2O (wt%)	K_2O (wt%)	FeO (ppm)	SrO (ppm)	BaO (ppm)	Total (wt%)	Endmember Mol. Fractions An	Ab	Or
123	140	4880	62.97	22.95	3.36	7.38	2.99	1890	2830	2630	100.38	0.16	0.64	0.17
124	141	4920	63.90	22.20	2.66	7.52	3.79	2990	2980	4150	101.07	0.13	0.65	0.22

Table D.6.6. Core - Rim EMP Traverse of Anorthoclase Feldspar Phenocryst

Sample: 85010-02

Total traverse distance (μm): 3239

Step size (μm): 41

n = cumulative # of analyses

EMP # = analysis point ID from run data

n	EMP #	distance from rim	SiO_2 (wt%)	Al_2O_3 (wt%)	CaO (wt%)	Na_2O (wt%)	K_2O (wt%)	FeO (ppm)	SrO (ppm)	BaO (ppm)	Total (wt%)	Endmember Mol. Fractions An	Ab	Or
1	1	3239	62.2	23.4	4.0	7.4	2.7	1820	2750	3560	100.41	0.20	0.66	0.16
2	2	3198	62.4	23.5	3.9	7.3	2.8	1890	2710	3140	100.63	0.19	0.65	0.16
3	3	3157	62.4	23.5	3.9	7.3	2.8	2140	2390	3500	100.61	0.19	0.65	0.16
4	4	3116	61.9	23.2	3.9	7.4	2.9	2050	2580	3130	100.03	0.19	0.66	0.17
5	5	3075	63.1	22.7	3.4	7.4	3.3	2020	2460	3240	100.65	0.16	0.66	0.19
6	6	3034	62.5	23.0	3.6	7.3	3.1	1970	2610	3280	100.28	0.18	0.65	0.18
7	7	2993	62.8	22.8	3.3	7.3	3.3	1850	2710	3320	100.32	0.16	0.65	0.19
8	8	2952	63.1	22.8	3.3	7.4	3.3	1820	2640	3030	100.63	0.16	0.66	0.19
9	9	2911	62.6	22.7	3.3	7.3	3.3	2040	2950	3460	100.03	0.16	0.65	0.19
10	10	2870	62.8	23.1	3.5	7.3	3.0	2050	2590	3370	100.42	0.17	0.65	0.18
11	11	2829	62.0	23.4	3.9	7.3	2.8	1590	2390	3220	100.13	0.19	0.65	0.16
12	12	2788	62.7	23.3	3.6	7.4	2.9	1670	2480	3360	100.74	0.18	0.66	0.17
13	13	2747	62.6	23.1	3.6	7.3	3.1	1650	2610	3440	100.47	0.18	0.65	0.18
14	14	2706	61.4	23.5	3.8	7.4	2.9	1770	2740	2690	99.64	0.19	0.66	0.17
15	15	2665	62.5	23.3	3.6	7.5	2.9	1980	3220	3070	100.61	0.18	0.66	0.17
16	16	2624	62.7	23.2	3.5	7.3	3.1	1830	2560	2790	100.51	0.17	0.65	0.18
17	17	2583	63.1	22.8	3.2	7.4	3.3	2090	2750	3350	100.60	0.16	0.65	0.19
18	18	2542	61.5	23.6	4.0	7.3	2.7	2070	2850	2940	99.84	0.20	0.65	0.16
19	19	2501	62.0	23.7	4.2	7.3	2.5	1710	2790	2950	100.53	0.21	0.65	0.14
20	20	2460	62.0	23.4	3.8	7.3	2.9	2000	2870	3060	100.10	0.19	0.65	0.17
21	21	2419	62.9	23.1	3.6	7.4	3.1	1830	2530	2890	100.86	0.18	0.66	0.18
22	22	2378	62.6	23.0	3.5	7.4	3.0	1920	2640	2870	100.20	0.17	0.66	0.18
23	23	2337	62.6	23.2	3.7	7.4	2.9	2060	2530	3070	100.63	0.18	0.65	0.17
24	24	2296	62.0	23.8	4.3	7.3	2.4	2300	2580	2850	100.54	0.21	0.65	0.14
25	25	2255	62.8	23.0	3.5	7.3	3.1	2210	2690	3360	100.34	0.17	0.64	0.18
26	26	2214	63.1	22.8	3.2	7.4	3.2	1710	2840	2870	100.53	0.16	0.65	0.19
27	27	2173	62.4	23.1	3.4	7.4	3.0	1970	2670	3310	100.13	0.17	0.66	0.18
28	29	2132	63.2	22.8	3.3	7.5	3.3	2090	2720	3590	100.89	0.16	0.66	0.19
29	30	2091	63.4	22.5	2.9	7.5	3.6	2130	2700	3090	100.63	0.14	0.67	0.21
30	31	2050	63.0	22.8	3.2	7.4	3.3	1790	2390	3250	100.54	0.16	0.66	0.19
31	32	2009	62.6	22.9	3.5	7.4	3.0	1670	2610	2980	100.16	0.17	0.66	0.18
32	33	1968	62.2	23.2	3.4	7.4	3.0	1880	2570	3170	100.06	0.17	0.66	0.18
33	34	1927	63.1	22.8	3.3	7.4	3.3	2100	2700	3300	100.66	0.16	0.66	0.19
34	35	1886	63.2	22.5	3.0	7.5	3.5	1970	2820	3200	100.48	0.15	0.67	0.20
35	36	1845	63.0	22.7	3.1	7.6	3.5	1860	2560	3160	100.57	0.15	0.67	0.20
36	37	1804	63.3	22.8	3.2	7.4	3.4	1730	2630	3340	100.82	0.15	0.65	0.20
37	38	1763	63.5	22.4	3.0	7.4	3.5	2100	2500	3210	100.55	0.15	0.65	0.21
38	39	1722	63.2	22.7	3.2	7.3	3.3	1870	2820	3400	100.43	0.16	0.65	0.19
39	40	1681	62.3	23.0	3.4	7.5	3.1	1890	2720	3340	100.16	0.17	0.67	0.18
40	41	1640	63.0	23.0	3.4	7.3	3.2	1850	2660	3230	100.72	0.17	0.65	0.19
41	42	1599	62.5	22.9	3.3	7.4	3.2	2010	2920	3370	100.09	0.16	0.66	0.19
42	43	1558	61.7	23.6	4.1	7.2	2.6	1700	2680	3200	100.04	0.20	0.65	0.15
43	44	1517	62.7	22.9	3.5	7.2	3.2	1880	2510	2480	100.26	0.17	0.64	0.18
44	45	1476	62.8	23.0	3.4	7.4	3.2	1590	2540	3530	100.50	0.17	0.65	0.19
45	46	1435	63.8	22.4	2.9	7.4	3.7	1580	2340	3280	100.89	0.14	0.66	0.21
46	47	1394	63.7	22.2	2.7	7.4	3.9	1680	2550	3280	100.68	0.13	0.65	0.23
47	49	1353	63.2	22.4	2.8	7.4	3.8	1990	2460	3380	100.28	0.14	0.66	0.22
48	50	1312	63.5	22.2	2.7	7.4	4.0	1850	2790	3130	100.48	0.13	0.66	0.23
49	51	1271	64.0	22.2	2.6	7.4	3.9	2000	2960	4040	100.81	0.13	0.66	0.23
50	52	1230	63.9	22.2	2.7	7.2	3.9	1890	2970	3700	100.69	0.13	0.64	0.22
51	53	1189	63.4	22.5	2.9	7.4	3.6	1810	2940	3900	100.58	0.14	0.65	0.21
52	54	1148	63.2	22.6	2.9	7.4	3.5	2070	3130	3630	100.47	0.14	0.66	0.20
53	55	1107	62.5	23.2	3.6	7.3	3.0	2420	2900	3520	100.52	0.18	0.65	0.18
54	56	1066	62.7	23.3	3.7	7.3	2.9	2000	2680	3810	100.70	0.18	0.65	0.17
55	57	1025	62.2	23.1	3.7	7.3	3.1	1630	2990	3880	100.20	0.18	0.65	0.18
56	58	984	63.4	22.7	3.1	7.4	3.4	1670	3120	3930	100.74	0.15	0.66	0.20
57	59	943	63.5	22.4	3.0	7.4	3.6	1830	2680	3500	100.58	0.15	0.65	0.21
58	60	902	64.0	22.1	2.6	7.4	3.9	1990	2390	2780	100.76	0.13	0.66	0.23
59	61	861	63.7	22.4	2.9	7.5	3.7	2190	2510	3280	100.93	0.14	0.66	0.22

Table D.6.6. Core - Rim EMP Traverse of Anorthoclase Feldspar Phenocryst

Sample: 85010-02

Total traverse distance (μm): 3239

Step size (μm): 41

n = cumulative # of analyses

EMP # = analysis point ID from run data

n	EMP #	distance from rim	SiO_2 (wt%)	Al_2O_3 (wt%)	CaO (wt%)	Na_2O (wt%)	K_2O (wt%)	FeO (ppm)	SrO (ppm)	BaO (ppm)	Total (wt%)	Endmember Mol. Fractions An	Ab	Or
60	62	820	64.1	22.1	2.5	7.4	4.0	1940	2650	3130	100.71	0.12	0.66	0.23
61	63	779	63.7	21.8	2.2	7.4	4.4	2000	2770	2880	100.26	0.11	0.66	0.26
62	64	738	64.0	22.0	2.6	7.6	4.0	1990	2710	3420	100.81	0.13	0.67	0.23
63	65	697	64.3	21.8	2.3	7.4	4.3	1920	2420	3490	100.75	0.11	0.66	0.25
64	66	656	64.3	21.5	2.1	7.3	4.7	1820	2080	3120	100.64	0.10	0.65	0.27
65	67	615	63.7	22.5	3.1	7.5	3.5	2040	2540	3480	100.98	0.15	0.67	0.20
66	68	574	64.0	22.1	2.5	7.5	4.1	2130	2260	3020	100.89	0.12	0.66	0.24
67	69	533	63.1	22.3	2.9	7.5	3.6	1950	2410	3110	100.10	0.14	0.67	0.21
68	70	492	63.7	21.9	2.2	7.3	4.4	1640	2930	3040	100.17	0.11	0.65	0.26
69	71	451	63.5	22.1	2.4	7.4	4.1	1850	2610	3250	100.21	0.12	0.66	0.24
70	72	410	63.7	22.3	2.7	7.3	4.0	1490	2770	3080	100.66	0.13	0.65	0.23
71	74	369	62.6	22.4	3.1	7.5	3.4	1830	2690	3200	99.71	0.15	0.67	0.20
72	75	328	62.5	22.6	3.0	7.4	3.6	1680	2520	3080	99.91	0.15	0.66	0.21
73	76	287	63.5	22.5	2.9	7.5	3.5	1750	2270	3140	100.66	0.14	0.66	0.21
74	77	246	62.5	23.2	3.6	7.4	3.0	2170	2890	3070	100.52	0.18	0.66	0.18
75	78	205	62.8	22.5	3.0	7.5	3.5	1850	2390	3490	100.07	0.15	0.66	0.21
76	79	164	63.3	22.8	3.2	7.5	3.3	1640	2420	3520	100.93	0.16	0.66	0.19
77	80	123	63.2	22.8	3.1	7.4	3.4	1900	2610	3690	100.84	0.15	0.66	0.20
78	81	82	63.4	22.8	3.1	7.5	3.3	2000	2710	3500	100.83	0.15	0.66	0.19
79	82	41	63.2	22.8	3.2	7.4	3.4	2270	2430	3420	100.85	0.16	0.65	0.20
80	83	0	63.8	22.3	2.6	7.5	3.8	2190	2500	3330	100.84	0.13	0.66	0.22

Table D.6.6. Core - Rim EMP Traverse of Anorthoclase Feldspar Phenocryst

Sample: 85010-02

Total traverse distance (μm): 3239

Step size (μm): 41

n = cumulative # of analyses

EMP # = analysis point ID from run data

n	EMP #	distance from rim	SiO_2 (wt%)	Al_2O_3 (wt%)	CaO (wt%)	Na_2O (wt%)	K_2O (wt%)	FeO (ppm)	SrO (ppm)	BaO (ppm)	Total (wt%)	Endmember Mol. Fractions An	Ab	Or
60	62	820	64.1	22.1	2.5	7.4	4.0	1940	2650	3130	100.71	0.12	0.66	0.23
61	63	779	63.7	21.8	2.2	7.4	4.4	2000	2770	2880	100.26	0.11	0.66	0.26
62	64	738	64.0	22.0	2.6	7.6	4.0	1990	2710	3420	100.81	0.13	0.67	0.23
63	65	697	64.3	21.8	2.3	7.4	4.3	1920	2420	3490	100.75	0.11	0.66	0.25
64	66	656	64.3	21.5	2.1	7.3	4.7	1820	2080	3120	100.64	0.10	0.65	0.27
65	67	615	63.7	22.5	3.1	7.5	3.5	2040	2540	3480	100.98	0.15	0.67	0.20
66	68	574	64.0	22.1	2.5	7.5	4.1	2130	2260	3020	100.89	0.12	0.66	0.24
67	69	533	63.1	22.3	2.9	7.5	3.6	1950	2410	3110	100.10	0.14	0.67	0.21
68	70	492	63.7	21.9	2.2	7.3	4.4	1640	2930	3040	100.17	0.11	0.65	0.26
69	71	451	63.5	22.1	2.4	7.4	4.1	1850	2610	3250	100.21	0.12	0.66	0.24
70	72	410	63.7	22.3	2.7	7.3	4.0	1490	2770	3080	100.66	0.13	0.65	0.23
71	74	369	62.6	22.4	3.1	7.5	3.4	1830	2690	3200	99.71	0.15	0.67	0.20
72	75	328	62.5	22.6	3.0	7.4	3.6	1680	2520	3080	99.91	0.15	0.66	0.21
73	76	287	63.5	22.5	2.9	7.5	3.5	1750	2270	3140	100.66	0.14	0.66	0.21
74	77	246	62.5	23.2	3.6	7.4	3.0	2170	2890	3070	100.52	0.18	0.66	0.18
75	78	205	62.8	22.5	3.0	7.5	3.5	1850	2390	3490	100.07	0.15	0.66	0.21
76	79	164	63.3	22.8	3.2	7.5	3.3	1640	2420	3520	100.93	0.16	0.66	0.19
77	80	123	63.2	22.8	3.1	7.4	3.4	1900	2610	3690	100.84	0.15	0.66	0.20
78	81	82	63.4	22.8	3.1	7.5	3.3	2000	2710	3500	100.83	0.15	0.66	0.19
79	82	41	63.2	22.8	3.2	7.4	3.4	2270	2430	3420	100.85	0.16	0.65	0.20
80	83	0	63.8	22.3	2.6	7.5	3.8	2190	2500	3330	100.84	0.13	0.66	0.22

Table D.6.7. Core - Rim EMP Traverse of Anorthoclase Feldspar Phenocryst

Sample: 85010-04

Total traverse distance (μm): 5440

Step size (μm): 40

n = cumulative # of analyses

EMP # = analysis point ID from run data

n	EMP #	distance from rim	SiO_2 (wt%)	Al_2O_3 (wt%)	CaO (wt%)	Na_2O (wt%)	K_2O (wt%)	FeO (ppm)	SrO (ppm)	BaO (ppm)	Total (wt%)	Endmember Mol. Fractions An	Ab	Or
1	2	5440	63.08	22.75	3.34	7.57	3.12	1620	2710	3140	100.58	0.16	0.66	0.18
2	3	5400	62.62	22.51	3.20	7.66	3.23	1960	2390	3500	99.97	0.15	0.66	0.18
3	4	5360	63.07	22.98	3.47	7.62	3.08	1960	2580	3130	100.91	0.17	0.66	0.18
4	5	5320	63.25	22.55	3.18	7.56	3.33	1950	2460	3240	100.66	0.15	0.66	0.19
5	6	5280	63.03	22.98	3.47	7.61	2.98	2470	2610	3280	100.86	0.17	0.66	0.17
6	7	5240	63.52	22.50	3.20	7.58	3.29	1950	2710	3320	100.87	0.15	0.66	0.19
7	8	5200	62.69	22.88	3.45	7.73	3.11	1720	2640	3030	100.56	0.16	0.66	0.18
8	9	5160	62.47	22.84	3.48	7.50	3.18	1900	2950	3460	100.18	0.17	0.65	0.18
9	10	5120	63.28	22.58	3.12	7.64	3.32	1760	2590	3370	100.70	0.15	0.66	0.19
10	11	5080	63.94	22.17	2.67	7.59	3.71	1800	2390	3220	100.85	0.13	0.66	0.21
11	12	5040	62.75	22.53	3.08	7.62	3.38	1850	2480	3360	100.16	0.15	0.66	0.19
12	13	5000	63.57	22.47	3.17	7.55	3.38	1710	2610	3440	100.89	0.15	0.66	0.19
13	14	4960	62.83	22.76	3.08	7.63	3.38	2000	2740	2690	100.45	0.15	0.66	0.19
14	15	4920	63.48	22.12	2.66	7.46	3.88	1810	3220	3070	100.38	0.13	0.65	0.22
15	16	4880	63.35	22.63	3.21	7.58	3.37	1750	2560	2790	100.85	0.15	0.65	0.19
16	17	4840	63.69	22.16	2.81	7.58	3.66	1840	2750	3350	100.64	0.13	0.66	0.21
17	18	4800	63.28	22.64	3.16	7.48	3.33	1750	2850	2940	100.62	0.15	0.65	0.19
18	19	4760	63.06	22.59	3.07	7.50	3.39	1790	2790	2950	100.37	0.15	0.66	0.20
19	20	4720	62.85	22.64	3.28	7.60	3.27	1700	2870	3060	100.36	0.16	0.66	0.19
20	21	4680	63.21	22.17	2.80	7.62	3.50	2020	2530	2890	99.96	0.13	0.66	0.20
21	22	4640	63.28	22.71	3.28	7.64	3.12	2680	2640	2870	100.79	0.16	0.66	0.18
22	23	4600	62.66	23.09	3.42	7.62	2.94	3030	2530	3070	100.59	0.16	0.67	0.17
23	24	4560	63.26	22.54	3.22	7.61	3.28	2110	2580	2850	100.69	0.15	0.66	0.19
24	25	4520	63.10	22.58	3.14	7.62	3.29	1790	2690	3360	100.46	0.15	0.66	0.19
25	26	4480	62.99	22.54	3.28	7.56	3.29	1810	2840	2870	100.37	0.16	0.66	0.19
26	27	4440	63.22	22.38	3.02	7.53	3.43	1920	2670	3310	100.36	0.15	0.66	0.20
27	30	4360	62.98	22.38	2.94	7.56	3.53	2010	2700	3090	100.21	0.14	0.66	0.20
28	31	4320	63.12	22.64	3.17	7.63	3.38	1870	2390	3250	100.67	0.15	0.66	0.19
29	32	4280	63.89	22.04	2.68	7.46	3.73	1780	2610	2980	100.56	0.13	0.65	0.22
30	33	4240	63.65	22.12	2.68	7.56	3.71	2400	2570	3170	100.49	0.13	0.66	0.21
31	34	4200	62.95	22.43	2.91	7.67	3.50	2070	2700	3300	100.25	0.14	0.66	0.20
32	35	4160	63.48	22.32	2.92	7.49	3.46	1810	2820	3200	100.44	0.14	0.66	0.20
33	36	4120	63.97	21.99	2.55	7.63	3.86	1680	2560	3160	100.70	0.12	0.66	0.22
34	37	4080	62.77	22.51	2.95	7.44	3.51	1650	2630	3340	99.84	0.14	0.65	0.20
35	38	4040	63.54	22.36	2.99	7.57	3.48	1710	2500	3210	100.68	0.14	0.66	0.20
36	39	4000	63.83	22.32	2.85	7.51	3.60	1820	2820	3400	100.86	0.14	0.66	0.21
37	40	3960	63.59	22.28	2.83	7.53	3.74	1980	2720	3340	100.70	0.14	0.65	0.21
38	41	3920	63.58	22.25	2.71	7.53	3.72	2150	2660	3230	100.59	0.13	0.66	0.21
39	42	3880	63.41	22.18	2.88	7.59	3.74	1900	2920	3370	100.54	0.14	0.65	0.21
40	43	3840	62.41	22.42	3.04	7.72	3.48	2010	2680	3200	99.82	0.14	0.66	0.20
41	44	3800	62.39	22.37	3.02	7.76	3.53	1890	2510	2480	99.81	0.14	0.66	0.20
42	45	3760	63.32	22.41	3.11	7.59	3.37	1870	2540	3530	100.54	0.15	0.66	0.19
43	46	3720	63.50	22.32	2.98	7.57	3.53	1990	2340	3280	100.64	0.14	0.66	0.20
44	47	3680	63.33	22.55	3.04	7.56	3.32	1860	2550	3280	100.54	0.15	0.66	0.19
45	49	3640	63.27	22.67	3.20	7.53	3.31	1850	2460	3380	100.70	0.15	0.66	0.19
46	50	3600	62.80	22.84	3.35	7.49	3.23	1760	2790	3130	100.45	0.16	0.65	0.19
47	51	3560	63.26	22.90	3.32	7.54	3.17	1760	2960	4040	100.92	0.16	0.66	0.18
48	52	3520	63.46	22.68	3.13	7.56	3.32	1820	2970	3700	100.88	0.15	0.66	0.19
49	53	3480	62.92	22.57	3.09	7.53	3.43	1860	2940	3900	100.35	0.15	0.66	0.20
50	54	3440	63.36	22.58	3.31	7.67	3.24	2040	3130	3630	100.85	0.16	0.66	0.18
51	55	3400	63.46	22.46	3.03	7.60	3.47	1790	2900	3520	100.75	0.14	0.66	0.20
52	57	3320	63.30	22.64	3.03	7.49	3.54	2130	2990	3880	100.79	0.15	0.65	0.20
53	59	3240	63.56	22.49	2.95	7.57	3.51	1930	2680	3500	100.85	0.14	0.66	0.20
54	60	3200	63.69	22.35	2.98	7.61	3.49	1820	2390	2780	100.88	0.14	0.66	0.20
55	61	3160	63.92	22.15	2.77	7.56	3.75	1730	2510	3280	100.83	0.13	0.65	0.21
56	63	3080	63.16	22.65	3.39	7.55	3.19	1970	2770	2880	100.69	0.16	0.66	0.18
57	64	3040	62.19	22.80	3.46	7.57	3.06	1930	2710	3420	99.79	0.17	0.66	0.18
58	65	3000	62.17	22.81	3.46	7.48	3.08	2080	2420	3490	99.79	0.17	0.65	0.18
59	66	2960	63.18	22.44	3.17	7.58	3.25	2160	2080	3120	100.38	0.15	0.66	0.19
60	67	2920	62.72	22.83	3.39	7.74	3.13	2150	2540	3480	100.59	0.16	0.66	0.18
61	68	2880	63.27	22.64	3.29	7.65	3.14	2310	2260	3020	100.72	0.16	0.66	0.18
62	69	2840	63.56	22.39	2.99	7.66	3.36	2060	2410	3110	100.71	0.14	0.66	0.19
63	70	2800	63.30	22.59	3.20	7.53	3.37	1890	2930	3040	100.65	0.15	0.65	0.19

Table D.6.7. Core - Rim EMP Traverse of Anorthoclase Feldspar Phenocryst

Sample: 85010-04

Total traverse distance (μm): 5440

Step size (μm): 40

n = cumulative # of analyses

EMP # = analysis point ID from run data

n	EMP #	distance from rim	SiO_2 (wt%)	Al_2O_3 (wt%)	CaO (wt%)	Na_2O (wt%)	K_2O (wt%)	FeO (ppm)	SrO (ppm)	BaO (ppm)	Total (wt%)	Endmember Mol. Fractions An	Ab	Or
64	71	2760	62.86	22.57	3.17	7.53	3.41	1770	2610	3250	100.25	0.15	0.65	0.19
65	75	2640	63.01	22.86	3.46	7.65	3.10	1620	2520	3080	100.81	0.17	0.66	0.18
66	76	2600	63.15	22.86	3.27	7.65	3.22	1840	2270	3140	100.85	0.16	0.66	0.18
67	77	2560	63.05	22.99	3.54	7.56	2.96	1810	2890	3070	100.82	0.17	0.66	0.17
68	78	2520	62.36	22.91	3.44	7.62	3.09	2400	2390	3490	100.27	0.16	0.66	0.18
69	79	2480	62.58	22.87	3.39	7.63	3.11	1800	2420	3520	100.36	0.16	0.66	0.18
70	80	2440	62.51	22.92	3.52	7.61	3.15	2000	2610	3690	100.45	0.17	0.65	0.18
71	81	2400	63.28	22.60	3.25	7.59	3.33	1810	2710	3500	100.81	0.16	0.66	0.19
72	82	2360	62.55	22.91	3.44	7.55	3.18	1710	2430	3420	100.36	0.17	0.65	0.18
73	84	2280	63.47	22.38	2.90	7.49	3.65	1700	2710	3340	100.66	0.14	0.65	0.21
74	86	2240	62.69	23.03	3.62	7.58	2.94	1830	2370	3310	100.60	0.17	0.66	0.17
75	87	2200	61.73	23.01	3.54	7.43	3.01	1650	2520	3320	99.42	0.17	0.65	0.17
76	89	2120	63.17	22.92	3.44	7.55	3.15	1790	2570	3530	100.96	0.16	0.66	0.18
77	90	2080	62.57	22.73	3.29	7.62	3.27	1820	2410	2750	100.23	0.16	0.66	0.19
78	91	2040	62.88	23.07	3.71	7.52	2.93	1820	2450	3010	100.81	0.18	0.65	0.17
79	92	2000	61.99	23.06	3.61	7.48	2.94	1730	2410	3500	99.78	0.18	0.65	0.17
80	93	1960	62.83	22.90	3.65	7.59	3.01	2030	2790	3380	100.76	0.17	0.66	0.17
81	94	1920	62.91	23.04	3.64	7.56	2.94	1800	2540	2890	100.78	0.17	0.66	0.17
82	95	1880	62.45	23.14	3.57	7.54	2.98	1870	2670	3600	100.35	0.17	0.66	0.17
83	96	1840	61.95	22.81	3.59	7.64	3.05	1760	2500	3290	99.73	0.17	0.66	0.17
84	99	1720	62.89	23.25	3.70	7.57	2.84	2130	2340	3750	101.00	0.18	0.66	0.16
85	100	1680	62.02	23.49	3.92	7.59	2.59	2360	2690	3960	100.41	0.19	0.66	0.15
86	101	1640	63.01	22.99	3.60	7.62	2.89	2120	2340	3640	100.85	0.17	0.66	0.17
87	102	1600	61.85	23.62	4.33	7.53	2.44	1960	2730	3310	100.51	0.21	0.65	0.14
88	103	1560	62.89	23.21	3.88	7.54	2.70	2320	2570	3450	100.98	0.19	0.66	0.16
89	104	1520	62.33	23.38	3.95	7.53	2.69	1730	2690	3900	100.61	0.19	0.66	0.15
90	105	1480	61.48	23.13	3.76	7.62	2.81	2210	2960	3590	99.56	0.18	0.66	0.16
91	106	1440	62.61	23.34	3.98	7.51	2.70	1920	2510	3540	100.83	0.19	0.65	0.15
92	108	1400	62.22	23.56	4.29	7.57	2.39	2170	2720	3340	100.77	0.21	0.66	0.14
93	109	1360	62.00	22.96	3.57	7.56	2.90	2900	2600	3510	99.80	0.17	0.66	0.17
94	110	1320	62.59	22.97	3.57	7.60	2.85	2890	2450	3190	100.40	0.17	0.66	0.16
95	111	1280	61.97	23.54	4.07	7.52	2.68	2740	2730	3180	100.66	0.19	0.65	0.15
96	115	1120	61.70	23.34	3.95	7.46	2.65	1820	2660	3020	99.85	0.19	0.65	0.15
97	116	1080	62.48	23.47	3.92	7.52	2.72	2170	2650	3120	100.87	0.19	0.66	0.16
98	117	1040	62.35	23.27	3.90	7.53	2.71	2230	2780	3310	100.50	0.19	0.66	0.16
99	118	1000	61.51	23.95	4.45	7.62	2.23	1800	2790	3350	100.42	0.21	0.66	0.13
100	119	960	62.79	23.19	3.78	7.51	2.72	1900	2830	3300	100.77	0.18	0.66	0.16
101	121	920	62.70	23.32	3.90	7.52	2.73	1840	2530	3080	100.90	0.19	0.66	0.16
102	122	880	63.12	22.96	3.59	7.61	2.93	1970	2590	3120	100.96	0.17	0.66	0.17
103	123	840	62.52	22.96	3.54	7.72	2.97	2040	2290	3740	100.45	0.17	0.66	0.17
104	124	800	62.55	23.33	3.89	7.56	2.77	2230	3070	3320	100.86	0.19	0.66	0.16
105	125	760	61.98	23.07	3.72	7.59	2.79	2490	2860	3440	99.93	0.18	0.66	0.16
106	127	720	62.44	23.20	3.80	7.54	2.77	2180	2960	3410	100.46	0.18	0.66	0.16
107	128	680	62.85	23.11	3.71	7.58	2.90	1970	2420	2760	100.93	0.18	0.66	0.17
108	129	640	62.49	23.08	3.86	7.60	2.80	1570	2770	2880	100.55	0.18	0.66	0.16
109	130	600	62.15	23.20	3.78	7.53	2.88	1910	2680	2770	100.35	0.18	0.65	0.16
110	131	560	61.93	23.16	3.75	7.52	2.84	1710	2810	2810	99.96	0.18	0.66	0.16
111	133	480	62.66	23.33	3.76	7.61	2.80	1700	2570	2700	100.89	0.18	0.66	0.16
112	135	400	62.21	22.54	3.18	7.59	3.28	1720	2900	2880	99.57	0.15	0.66	0.19
113	136	360	62.46	22.65	3.28	7.47	3.25	1890	2850	2690	99.88	0.16	0.65	0.19
114	137	320	62.51	22.67	3.29	7.55	3.23	1920	2600	2910	100.00	0.16	0.66	0.19
115	139	280	63.09	22.91	3.43	7.68	2.98	2160	2680	2580	100.84	0.16	0.67	0.17
116	140	240	62.73	22.97	3.59	7.59	3.02	1790	2890	3000	100.72	0.17	0.66	0.17
117	142	160	63.14	22.91	3.35	7.64	2.95	2350	2830	3080	100.78	0.16	0.67	0.17
118	143	120	62.57	23.24	3.95	7.58	2.71	1960	3190	2520	100.86	0.19	0.66	0.15
119	145	40	62.85	22.37	2.82	7.65	3.65	2160	3040	2980	100.11	0.13	0.66	0.21

Table D.6.7. Core - Rim EMP Traverse of Anorthoclase Feldspar Phenocryst

Sample: 85010-04

Total traverse distance (μm): 5440

Step size (μm): 40

n = cumulative # of analyses

EMP # = analysis point ID from run data

n	EMP #	distance from rim		SiO_2 (wt%)	Al_2O_3 (wt%)	CaO (wt%)	Na_2O (wt%)	K_2O (wt%)	FeO (ppm)	SrO (ppm)	BaO (ppm)	Total (wt%)	Endmember Mol. Fractions An	Ab	Or
1	1	3455	62.63	22.96	3.57	7.35	2.97	1710	2990	3520	100.29	0.18	0.65	0.17	
2	6	3254	62.02	23.49	4.17	7.50	2.39	2420	2810	2330	100.32	0.20	0.66	0.14	
3	7	3213	62.26	23.39	4.16	7.20	2.64	1660	2880	2950	100.40	0.20	0.64	0.15	
4	8	3173	62.04	23.31	4.01	7.48	2.62	2080	2820	2530	100.20	0.19	0.66	0.15	
5	10	3093	63.15	22.37	3.07	7.51	3.42	1620	2380	3230	100.24	0.15	0.66	##	
6	11	3052	62.45	23.21	3.82	7.61	2.81	1900	2790	2830	100.66	0.18	0.66	0.16	
7	12	3012	61.61	23.80	4.67	7.49	2.22	2060	2890	2040	100.48	0.22	0.65	0.13	
8	13	2972	61.66	23.73	4.50	7.30	2.40	1770	3050	2480	100.32	0.22	0.64	0.14	
9	14	2932	61.90	23.72	4.31	7.49	2.42	2190	2700	3040	100.64	0.21	0.65	0.14	
10	15	2891	63.04	22.68	3.46	7.41	3.10	1840	2550	3210	100.45	0.17	0.65	0.18	
11	20	2690	62.74	22.89	3.40	7.49	2.92	2750	4030	3580	100.47	0.17	0.66	0.17	
12	21	2650	62.17	23.35	3.99	7.49	2.71	2070	2960	2980	100.52	0.19	0.65	0.16	
13	22	2609	61.94	23.48	4.17	7.36	2.63	1660	2300	2800	100.25	0.20	0.65	0.15	
14	23	2569	62.19	23.43	3.96	7.45	2.81	1860	2710	2780	100.57	0.19	0.65	0.16	
15	24	2529	62.05	23.25	3.93	7.50	2.76	1520	2800	3240	100.24	0.19	0.65	0.16	
16	26	2448	62.86	23.12	3.73	7.36	2.98	1730	2770	3260	100.84	0.18	0.65	0.17	
17	27	2408	62.80	22.86	3.46	7.17	3.08	1820	2940	3220	100.16	0.17	0.65	0.18	
18	28	2368	63.21	22.62	3.35	7.50	3.18	1710	2910	3870	100.71	0.16	0.66	0.18	
19	29	2328	63.16	22.83	3.29	7.28	3.26	1820	2860	3730	100.66	0.16	0.65	0.19	
20	30	2287	63.01	22.72	3.36	7.49	3.26	1580	3060	3550	100.65	0.16	0.65	0.19	
21	31	2247	62.73	22.55	3.36	7.36	3.19	1710	2800	3380	99.98	0.16	0.65	0.19	
22	32	2207	62.14	23.42	3.99	7.49	2.74	1870	2870	3290	100.59	0.19	0.65	0.16	
23	33	2167	62.06	23.55	4.15	7.56	2.66	1610	3100	3250	100.78	0.20	0.65	0.15	
24	34	2126	62.19	23.60	4.19	7.40	2.62	1960	3250	2940	100.82	0.20	0.65	0.15	
25	35	2086	62.75	23.03	3.56	7.10	3.08	1920	3070	2870	100.30	0.18	0.64	0.18	
26	36	2046	62.76	22.86	3.59	7.45	3.10	2040	2970	3190	100.58	0.17	0.65	0.18	
27	37	2005	62.00	23.18	3.97	7.37	2.78	1710	3090	2890	100.06	0.19	0.65	0.16	
28	38	1965	62.50	23.18	3.86	7.49	2.84	1390	3510	3060	100.68	0.19	0.65	0.16	
29	39	1925	62.54	23.01	3.61	7.42	2.98	1910	2820	3050	100.34	0.18	0.65	0.17	
30	40	1885	62.61	23.16	3.50	7.77	3.01	1960	2930	3430	100.88	0.17	0.67	0.17	
31	41	1844	62.86	23.00	3.47	7.38	3.11	1540	2860	3030	100.58	0.17	0.65	0.18	
32	43	1764	63.02	23.02	3.47	7.61	3.01	2010	3060	2760	100.92	0.17	0.66	0.17	
33	44	1724	63.09	22.87	3.46	7.63	3.04	1520	2560	2490	100.76	0.17	0.66	0.17	
34	45	1683	62.75	23.14	3.76	7.24	2.92	1770	2910	2950	100.57	0.18	0.64	0.17	
35	46	1643	62.84	22.89	3.52	7.34	3.08	1680	3400	2850	100.47	0.17	0.65	0.18	
36	47	1603	62.75	22.94	3.67	6.83	2.92	1580	2930	3510	99.91	0.19	0.63	0.18	
37	49	1522	62.64	23.04	3.70	7.50	2.84	2020	2790	2870	100.49	0.18	0.66	0.16	
38	50	1482	63.01	23.01	3.57	7.59	2.86	1920	2790	3270	100.83	0.17	0.66	0.16	
39	51	1442	62.21	22.49	3.38	7.02	3.10	1320	2990	2430	98.87	0.17	0.64	0.19	
40	52	1401	62.43	23.18	3.83	7.00	2.86	1630	3340	3660	100.17	0.19	0.64	0.17	
41	53	1361	62.91	22.78	3.39	7.47	3.07	1790	2820	3360	100.42	0.16	0.66	0.18	
42	56	1240	62.42	23.40	3.94	7.49	2.72	1550	3100	3140	100.74	0.19	0.65	0.16	
43	57	1200	62.64	22.85	3.39	7.49	3.11	1930	2790	2720	100.22	0.16	0.66	0.18	
44	58	1160	62.43	23.39	3.98	7.42	2.81	2110	2790	3060	100.82	0.19	0.65	0.16	
45	59	1120	62.80	23.01	3.56	7.01	3.03	1920	3030	3660	100.26	0.18	0.64	0.18	
46	60	1079	62.64	22.95	3.53	7.33	3.05	2350	3190	3330	100.39	0.17	0.65	0.18	
47	61	1039	63.09	22.81	3.29	7.38	3.29	1510	2700	4000	100.68	0.16	0.65	0.19	
48	62	999	63.23	22.50	2.96	7.29	3.51	1680	2960	3840	100.34	0.15	0.65	0.21	
49	63	959	62.55	22.74	3.27	7.37	3.23	1620	3070	3610	99.99	0.16	0.65	0.19	
50	64	918	62.77	22.92	3.59	7.43	3.07	1730	2960	3390	100.58	0.17	0.65	0.18	
51	65	878	61.81	23.61	4.37	7.31	2.33	1920	3060	2940	100.23	0.21	0.65	0.14	
52	66	838	62.72	22.85	3.43	7.41	3.15	1590	3150	3950	100.43	0.17	0.65	0.18	
53	67	797	63.13	22.72	3.29	7.16	3.18	1680	3360	4030	100.39	0.16	0.65	0.19	
54	68	757	62.05	23.34	4.03	6.87	2.78	1830	3470	3230	99.92	0.20	0.63	0.17	
55	69	717	61.39	23.86	4.57	7.41	2.29	2280	3350	2470	100.33	0.22	0.65	0.13	
56	70	677	62.92	22.81	3.33	7.33	3.16	1720	3340	4140	100.47	0.16	0.65	0.18	
57	71	636	62.68	22.93	3.54	7.39	3.03	1820	2960	3160	100.35	0.17	0.65	0.18	
58	72	596	62.93	22.63	3.33	7.52	3.25	1710	3320	3040	100.47	0.16	0.65	0.19	
59	73	556	62.59	23.00	3.57	7.29	3.16	1750	3280	3050	100.42	0.17	0.64	0.18	
60	74	516	63.10	22.65	3.17	7.47	3.31	2550	2780	3810	100.60	0.15	0.66	0.19	
61	75	475	62.93	22.74	3.29	7.44	3.23	2380	3060	3930	100.57	0.16	0.65	0.19	
62	76	435	62.59	23.11	3.77	7.38	2.90	1490	3290	3870	100.62	0.18	0.65	0.17	

Table D.6.7. Core - Rim EMP Traverse of Anorthoclase Feldspar Phenocryst

Sample: 85010-04

Total traverse distance (μm): 5440

Step size (μm): 40

n = cumulative # of analyses

EMP # = analysis point ID from run data

n	EMP #	distance from rim		SiO_2 (wt%)	Al_2O_3 (wt%)	CaO (wt%)	Na_2O (wt%)	K_2O (wt%)	FeO (ppm)	SrO (ppm)	BaO (ppm)	Total (wt%)	Endmember Mol. Fractions An	Ab	Or
63	77	395	63.27	22.51	3.09	7.53	3.45	1760	2730	3790	100.68	0.15	0.65	##	
64	79	314	63.72	21.97	2.56	7.45	3.91	2000	2720	3630	100.44	0.12	0.65	##	
65	80	274	62.44	22.92	3.63	7.35	3.11	2240	2940	3790	100.35	0.18	0.64	0.18	
66	82	194	62.99	22.62	3.24	7.23	3.41	1810	3130	3820	100.37	0.16	0.64	##	
67	83	153	63.04	22.77	3.22	7.37	3.40	1790	3330	3850	100.69	0.16	0.65	##	
68	84	113	62.86	22.85	3.39	7.30	3.15	2060	2970	3820	100.44	0.17	0.65	0.18	
69	85	73	63.94	22.11	2.51	7.46	3.89	1950	2530	3540	100.71	0.12	0.65	##	
70	86	32	64.02	21.66	2.16	7.47	4.42	2170	1830	3420	100.46	0.10	0.65	##	
71	87	0	63.02	22.70	3.54	7.54	2.86	4620	1310	2730	100.53	0.17	0.66	0.17	

Table D.6.8. Core - Rim EMP Traverse of Anorthoclase Feldspar Phenocryst

Sample: 1999-01

Total traverse distance (μm): 3455

Step size (μm): 40

n = cumulative # of analyses

EMP # = analysis point ID from run data

												Endmember Mol. Fractions		
n	EMP #	distance from rim	SiO_2 (wt%)	Al_2O_3 (wt%)	CaO (wt%)	Na_2O (wt%)	K_2O (wt%)	FeO (ppm)	SrO (ppm)	BaO (ppm)	Total (wt%)	An	Ab	Or
1	1	3455	62.63	22.96	3.57	7.35	2.97	1710	2990	3520	100.29	0.18	0.65	0.17
2	6	3254	62.02	23.49	4.17	7.50	2.39	2420	2810	2330	100.32	0.20	0.66	0.14
3	7	3213	62.26	23.39	4.16	7.20	2.64	1660	2880	2950	100.40	0.20	0.64	0.15
4	8	3173	62.04	23.31	4.01	7.48	2.62	2080	2820	2530	100.20	0.19	0.66	0.15
5	10	3093	63.15	22.37	3.07	7.51	3.42	1620	2380	3230	100.24	0.15	0.66	##
6	11	3052	62.45	23.21	3.82	7.61	2.81	1900	2790	2830	100.66	0.18	0.66	0.16
7	12	3012	61.61	23.80	4.67	7.49	2.22	2060	2890	2040	100.48	0.22	0.65	0.13
8	13	2972	61.66	23.73	4.50	7.30	2.40	1770	3050	2480	100.32	0.22	0.64	0.14
9	14	2932	61.90	23.72	4.31	7.49	2.42	2190	2700	3040	100.64	0.21	0.65	0.14
10	15	2891	63.04	22.68	3.46	7.41	3.10	1840	2550	3210	100.45	0.17	0.65	0.18
11	20	2690	62.74	22.89	3.40	7.49	2.92	2750	4030	3580	100.47	0.17	0.66	0.17
12	21	2650	62.17	23.35	3.99	7.49	2.71	2070	2960	2980	100.52	0.19	0.65	0.16
13	22	2609	61.94	23.48	4.17	7.36	2.63	1660	2300	2800	100.25	0.20	0.65	0.15
14	23	2569	62.19	23.43	3.96	7.45	2.81	1860	2710	2780	100.57	0.19	0.65	0.16
15	24	2529	62.05	23.25	3.93	7.50	2.76	1520	2800	3240	100.24	0.19	0.65	0.16
16	26	2448	62.86	23.12	3.73	7.36	2.98	1730	2770	3260	100.84	0.18	0.65	0.17
17	27	2408	62.80	22.86	3.46	7.17	3.08	1820	2940	3220	100.16	0.17	0.65	0.18
18	28	2368	63.21	22.62	3.35	7.50	3.18	1710	2910	3870	100.71	0.16	0.66	0.18
19	29	2328	63.16	22.83	3.29	7.28	3.26	1820	2860	3730	100.66	0.16	0.65	0.19
20	30	2287	63.01	22.72	3.36	7.49	3.26	1580	3060	3550	100.65	0.16	0.65	0.19
21	31	2247	62.73	22.55	3.36	7.36	3.19	1710	2800	3380	99.98	0.16	0.65	0.19
22	32	2207	62.14	23.42	3.99	7.49	2.74	1870	2870	3290	100.59	0.19	0.65	0.16
23	33	2167	62.06	23.55	4.15	7.56	2.66	1610	3100	3250	100.78	0.20	0.65	0.15
24	34	2126	62.19	23.60	4.19	7.40	2.62	1960	3250	2940	100.82	0.20	0.65	0.15
25	35	2086	62.75	23.03	3.56	7.10	3.08	1920	3070	2870	100.30	0.18	0.64	0.18
26	36	2046	62.76	22.86	3.59	7.45	3.10	2040	2970	3190	100.58	0.17	0.65	0.18
27	37	2005	62.00	23.18	3.97	7.37	2.78	1710	3090	2890	100.06	0.19	0.65	0.16
28	38	1965	62.50	23.18	3.86	7.49	2.84	1390	3510	3060	100.68	0.19	0.65	0.16
29	39	1925	62.54	23.01	3.61	7.42	2.98	1910	2820	3050	100.34	0.18	0.65	0.17
30	40	1885	62.61	23.16	3.50	7.77	3.01	1960	2930	3430	100.88	0.17	0.67	0.17
31	41	1844	62.86	23.00	3.47	7.38	3.11	1540	2860	3030	100.58	0.17	0.65	0.18
32	43	1764	63.02	23.02	3.47	7.61	3.01	2010	3060	2760	100.92	0.17	0.66	0.17
33	44	1724	63.09	22.87	3.46	7.63	3.04	1520	2560	2490	100.76	0.17	0.66	0.17
34	45	1683	62.75	23.14	3.76	7.24	2.92	1770	2910	2950	100.57	0.18	0.64	0.17
35	46	1643	62.84	22.89	3.52	7.34	3.08	1680	3400	2850	100.47	0.17	0.65	0.18
36	47	1603	62.75	22.94	3.67	6.83	2.92	1580	2930	3510	99.91	0.19	0.63	0.18
37	49	1522	62.64	23.04	3.70	7.50	2.84	2020	2790	2870	100.49	0.18	0.66	0.16
38	50	1482	63.01	23.01	3.57	7.59	2.86	1920	2790	3270	100.83	0.17	0.66	0.16
39	51	1442	62.21	22.49	3.38	7.02	3.10	1320	2990	2430	98.87	0.17	0.64	0.19
40	52	1401	62.43	23.18	3.83	7.00	2.86	1630	3340	3660	100.17	0.19	0.64	0.17
41	53	1361	62.91	22.78	3.39	7.47	3.07	1790	2820	3360	100.42	0.16	0.66	0.18
42	56	1240	62.42	23.40	3.94	7.49	2.72	1550	3100	3140	100.74	0.19	0.65	0.16
43	57	1200	62.64	22.85	3.39	7.49	3.11	1930	2790	2720	100.22	0.16	0.66	0.18
44	58	1160	62.43	23.39	3.98	7.42	2.81	2110	2790	3060	100.82	0.19	0.65	0.16
45	59	1120	62.80	23.01	3.56	7.01	3.03	1920	3030	3660	100.26	0.18	0.64	0.18
46	60	1079	62.64	22.95	3.53	7.33	3.05	2350	3190	3330	100.39	0.17	0.65	0.18
47	61	1039	63.09	22.81	3.29	7.38	3.29	1510	2700	4000	100.68	0.16	0.65	0.19
48	62	999	63.23	22.50	2.96	7.29	3.51	1680	2960	3840	100.34	0.15	0.65	0.21
49	63	959	62.55	22.74	3.27	7.37	3.23	1620	3070	3610	99.99	0.16	0.65	0.19
50	64	918	62.77	22.92	3.59	7.43	3.07	1730	2960	3390	100.58	0.17	0.65	0.18
51	65	878	61.81	23.61	4.37	7.31	2.33	1920	3060	2940	100.23	0.21	0.65	0.14
52	66	838	62.72	22.85	3.43	7.41	3.15	1590	3150	3950	100.43	0.17	0.65	0.18
53	67	797	63.13	22.72	3.29	7.16	3.18	1680	3360	4030	100.39	0.16	0.65	0.19
54	68	757	62.05	23.34	4.03	6.87	2.78	1830	3470	3230	99.92	0.20	0.63	0.17
55	69	717	61.39	23.86	4.57	7.41	2.29	2280	3350	2470	100.33	0.22	0.65	0.13
56	70	677	62.92	22.81	3.33	7.33	3.16	1720	3340	4140	100.47	0.16	0.65	0.18
57	71	636	62.68	22.93	3.54	7.39	3.03	1820	2960	3160	100.35	0.17	0.65	0.18
58	72	596	62.93	22.63	3.33	7.52	3.25	1710	3320	3040	100.47	0.16	0.65	0.19

Table D.6.8. Core - Rim EMP Traverse of Anorthoclase Feldspar Phenocryst

Sample: 1999-01

Total traverse distance (μm): 3455

Step size (μm): 40

n = cumulative # of analyses

EMP # = analysis point ID from run data

n	EMP #	distance from rim	SiO_2 (wt%)	Al_2O_3 (wt%)	CaO (wt%)	Na_2O (wt%)	K_2O (wt%)	FeO (ppm)	SrO (ppm)	BaO (ppm)	Total (wt%)	Endmember Mol. Fractions An	Ab	Or
59	73	556	62.59	23.00	3.57	7.29	3.16	1750	3280	3050	100.42	0.17	0.64	0.18
60	74	516	63.10	22.65	3.17	7.47	3.31	2550	2780	3810	100.60	0.15	0.66	0.19
61	75	475	62.93	22.74	3.29	7.44	3.23	2380	3060	3930	100.57	0.16	0.65	0.19
62	76	435	62.59	23.11	3.77	7.38	2.90	1490	3290	3870	100.62	0.18	0.65	0.17
63	77	395	63.27	22.51	3.09	7.53	3.45	1760	2730	3790	100.68	0.15	0.65	##
64	79	314	63.72	21.97	2.56	7.45	3.91	2000	2720	3630	100.44	0.12	0.65	##
65	80	274	62.44	22.92	3.63	7.35	3.11	2240	2940	3790	100.35	0.18	0.64	0.18
66	82	194	62.99	22.62	3.24	7.23	3.41	1810	3130	3820	100.37	0.16	0.64	##
67	83	153	63.04	22.77	3.22	7.37	3.40	1790	3330	3850	100.69	0.16	0.65	##
68	84	113	62.86	22.85	3.39	7.30	3.15	2060	2970	3820	100.44	0.17	0.65	0.18
69	85	73	63.94	22.11	2.51	7.46	3.89	1950	2530	3540	100.71	0.12	0.65	##
70	86	32	64.02	21.66	2.16	7.47	4.42	2170	1830	3420	100.46	0.10	0.65	##
71	87	0	63.02	22.70	3.54	7.54	2.86	4620	1310	2730	100.53	0.17	0.66	0.17

Table D.6.9. Core - Rim EMP Traverse of Anorthoclase Feldspar Phenocryst
Sample: DEC2000-03
Total traverse distance (μm): 2304
Step size (μm): 40
n = cumulative # of analyses
EMP # = analysis point ID from run data

n	EMP #	distance from rim	SiO_2 (wt%)	Al_2O_3 (wt%)	CaO (wt%)	Na_2O (wt%)	K_2O (wt%)	FeO (ppm)	SrO (ppm)	BaO (ppm)	Total (wt%)	Endmember Mol. Fractions An	Ab	Or
1	1	2304	61.90	23.53	4.13	7.39	2.49	1600	3300	3360	100.26	0.20	0.65	0.65
2	2	2264	62.58	23.30	3.83	7.55	2.72	1900	3080	3030	100.77	0.19	0.66	0.66
3	3	2223	62.60	23.09	3.66	7.62	2.79	1920	3060	3220	100.56	0.18	0.66	0.66
4	4	2183	62.54	23.21	3.93	7.55	2.66	1780	3060	3240	100.68	0.19	0.66	0.66
5	6	2102	62.85	23.23	3.77	7.57	2.67	1840	2850	2990	100.86	0.18	0.66	0.66
6	7	2061	62.62	23.22	3.56	7.67	2.87	1680	2900	3510	100.75	0.17	0.67	0.67
7	8	2021	62.23	23.09	3.71	7.54	2.71	1700	2740	2870	100.02	0.18	0.66	0.66
8	9	1981	62.37	23.27	3.75	7.54	2.86	2050	2850	3030	100.59	0.18	0.66	0.66
9	10	1940	62.53	23.42	3.85	7.57	2.61	2090	3020	2890	100.77	0.19	0.66	0.66
10	11	1900	62.77	23.43	3.95	7.54	2.48	2240	3300	2670	100.98	0.19	0.66	0.66
11	17	1657	63.20	23.02	3.53	7.58	2.80	2710	2630	3300	101.00	0.17	0.67	0.67
12	19	1576	63.02	22.97	3.45	7.75	2.76	2920	3300	3250	100.91	0.17	0.68	0.68
13	20	1536	62.50	23.64	4.10	7.59	2.38	2070	2930	2590	100.97	0.20	0.66	0.66
14	21	1495	62.50	23.47	4.21	7.71	2.38	1580	3140	2290	100.97	0.20	0.66	0.66
15	22	1455	61.89	23.52	4.24	7.58	2.30	1660	2780	2430	100.21	0.21	0.66	0.66
16	24	1374	62.48	23.37	4.08	7.58	2.41	1960	3060	2450	100.66	0.20	0.66	0.66
17	25	1334	62.32	23.15	3.90	7.71	2.50	1520	3130	2020	100.24	0.19	0.67	0.67
18	26	1293	62.06	23.27	3.97	7.59	2.48	2560	2860	2360	100.14	0.19	0.66	0.66
19	27	1253	62.65	23.37	4.00	7.63	2.48	2220	2950	2740	100.92	0.19	0.67	0.67
20	28	1212	62.04	23.50	4.16	7.67	2.39	2060	3140	2770	100.55	0.20	0.66	0.66
21	29	1172	62.59	23.42	3.98	7.60	2.54	1880	2900	2520	100.86	0.19	0.66	0.66
22	31	1091	61.71	23.86	4.66	7.74	2.04	2220	3100	2280	100.77	0.22	0.66	0.66
23	32	1051	62.11	23.35	3.91	7.67	2.60	1960	2420	2520	100.33	0.19	0.66	0.66
24	34	970	62.55	23.32	3.89	7.44	2.50	2190	2640	2810	100.47	0.19	0.66	0.66
25	35	929	62.07	23.73	4.23	7.59	2.37	2030	3040	2710	100.76	0.20	0.66	0.66
26	36	889	62.78	23.13	3.69	7.71	2.70	2200	3540	3060	100.89	0.18	0.67	0.67
27	37	849	63.29	22.82	3.66	7.54	2.83	2070	2950	3190	100.96	0.18	0.66	0.66
28	39	768	61.71	24.00	4.65	7.64	2.03	2130	2800	1980	100.72	0.22	0.66	0.66
29	40	727	62.03	23.87	4.46	7.62	2.12	2140	3040	2170	100.83	0.21	0.66	0.66
30	41	687	62.78	23.30	3.87	7.64	2.54	2250	3340	3140	101.00	0.19	0.67	0.67
31	42	646	62.32	23.35	3.84	7.41	2.68	1820	3270	3710	100.49	0.19	0.66	0.66
32	43	606	63.11	23.00	3.50	7.70	2.89	1850	2920	2840	100.96	0.17	0.67	0.67
33	44	566	62.91	22.98	3.50	7.58	2.85	1630	3250	3470	100.65	0.17	0.67	0.67
34	45	525	62.62	23.11	3.76	7.61	2.61	2390	3020	2950	100.54	0.18	0.67	0.67
35	46	485	62.20	23.82	4.34	7.55	2.07	2200	2930	3100	100.81	0.21	0.67	0.67
36	47	444	62.41	23.51	3.99	7.58	2.56	1840	2770	3310	100.83	0.19	0.66	0.66
37	49	363	63.10	22.95	3.42	7.58	2.92	1640	3310	3460	100.82	0.17	0.67	0.67
38	50	323	62.68	23.32	3.90	7.41	2.63	1540	3590	3050	100.75	0.19	0.66	0.66
39	51	283	63.06	22.97	3.35	7.71	2.85	1750	3130	3310	100.76	0.16	0.67	0.67
40	52	242	62.57	23.27	3.75	7.62	2.75	2140	3360	3090	100.82	0.18	0.66	0.66
41	54	161	62.60	23.44	3.95	7.52	2.57	1900	3330	3150	100.92	0.19	0.66	0.66
42	55	121	64.14	21.97	2.50	7.58	3.92	2000	2170	3850	100.89	0.12	0.66	0.66
43	56	80	63.40	22.38	2.96	7.48	3.42	2150	2770	3530	100.49	0.14	0.66	0.66
44	57	40	62.97	22.66	3.13	7.70	3.04	2550	2920	4010	100.46	0.15	0.67	0.67
45	58	0	63.79	22.15	2.70	7.46	3.64	3020	3010	4000	100.74	0.13	0.66	0.66
46	2-01	615	61.66	24.06	4.70	7.46	1.98	2170	2780	2070	100.55	0.23	0.66	0.66
47	2-02	575	62.56	23.44	3.86	7.65	2.51	1960	3160	2850	100.83	0.19	0.67	0.67
48	2-03	535	62.62	23.20	3.80	7.67	2.73	1820	3190	3370	100.86	0.18	0.66	0.66
49	2-04	495	61.90	23.70	4.12	7.61	2.39	1900	3080	2490	100.48	0.20	0.66	0.66
50	2-05	456	62.84	23.05	3.67	7.56	2.69	2030	2850	3330	100.62	0.18	0.67	0.67
51	2-06	416	62.91	22.89	3.55	7.58	2.80	2020	3150	3050	100.55	0.17	0.67	0.67
52	2-07	376	62.87	22.89	3.42	7.77	2.94	1920	3260	3670	100.77	0.16	0.67	0.67
53	2-08	336	62.91	23.20	3.64	7.60	2.76	1750	3080	2590	100.85	0.18	0.67	0.67
54	2-09	296	63.17	22.94	3.48	7.66	2.92	1830	3110	2650	100.92	0.17	0.67	0.67
55	2-13	137	62.63	22.97	3.51	7.51	2.85	2060	3110	3050	100.30	0.17	0.66	0.66
56	2-14	97	62.32	23.51	4.04	7.73	2.54	1940	3360	3250	100.99	0.19	0.66	0.66
57	2-16	17	63.01	23.03	3.37	7.64	2.99	2180	3320	3970	100.99	0.16	0.67	0.67

Appendix D.7. Electron Microprobe Analyses of pyrrhotite (wt. %)

S	Ca	Mn	Fe	Co	Ni	Cu	Total	Sample
37.538	0.043	0.132	60.774	0	0.023	0.394	98.904	E2001-01
37.363	0.005	0.190	60.731	0.012	0.003	0.334	98.638	E2001-02
37.404	0.004	0.218	60.736	0	0	0.417	98.779	E2001-05
37.207	0.033	0.225	60.324	0	0	0.390	98.179	E2001-06
37.171	0.013	0.192	60.788	0	0	0.328	98.492	E2001-07
37.177	0.002	0.180	60.487	0	0.005	0.304	98.155	E2001-08
37.171	0.005	0.181	60.243	0	0	0.458	98.058	E2001-09

Appendix D.8. Electron Microprobe Analyses of Matrix Glass

Table D.8.1. Average EMP Analyses of Matrix Glass from Tephra Erupted between 1972-2004

Table D.8.1. Average Electron Microprobe Analyses of Matrix Glass from Tephra Erupted Between 1972 and 2004 from Erebus Volcano

Sample	86022		80300		85009		81401		84505		84500		83207		82418	
n	12		6		13		17		12		14		14		12	
	mean	1σ	mean	1σ	mean	1σ	mean	1σ	mean	1σ	mean	1σ	mean	1σ	mean	1σ
SiO_2	55.41	0.37	55.01	0.28	55.63	0.26	55.08	0.12	55.90	0.17	55.61	0.24	55.75	0.16	55.82	0.18
TiO_2	1.01	0.06	0.99	0.08	0.97	0.05	1.01	0.04	0.98	0.06	0.98	0.04	0.99	0.05	1.00	0.04
Al_2O_3	19.74	0.13	19.98	0.19	19.70	0.13	20.05	0.10	19.69	0.08	19.71	0.14	19.74	0.08	19.75	0.11
$FeO^‡$	5.48	0.16	5.34	0.07	5.45	0.11	5.31	0.09	5.40	0.11	5.57	0.15	5.52	0.11	5.50	0.18
MnO	0.28	0.02	0.26	0.03	0.28	0.02	0.27	0.03	0.28	0.02	0.29	0.02	0.29	0.02	0.28	0.02
MgO	0.83	0.09	0.82	0.03	0.92	0.17	0.80	0.02	0.83	0.04	0.93	0.16	0.84	0.04	0.85	0.03
CaO	1.79	0.06	1.89	0.03	1.81	0.04	1.86	0.05	1.75	0.05	1.80	0.06	1.75	0.06	1.74	0.04
Na_2O	9.04	0.10	9.09	0.10	8.93	0.11	9.09	0.10	8.99	0.08	8.96	0.11	8.99	0.11	8.96	0.10
K_2O	5.62	0.10	5.71	0.08	5.50	0.10	5.65	0.06	5.43	0.09	5.42	0.09	5.41	0.07	5.35	0.13
P_2O_5	0.26	0.03	0.23	0.01	0.28	0.05	0.26	0.04	0.28	0.03	0.27	0.04	0.27	0.04	0.27	0.03
SO_2	0.09	0.02	0.08	0.01	0.08	0.01	0.08	0.01	0.07	0.01	0.07	0.02	0.07	0.02	0.06	0.01
F	0.29	0.06	0.23	0.12	0.31	0.08	0.18	0.09	0.26	0.13	0.26	0.10	0.26	0.10	0.27	0.07
Cl	0.16	0.02	0.16	0.02	0.15	0.02	0.16	0.02	0.14	0.01	0.15	0.01	0.14	0.02	0.15	0.01

Sample	81410		81003		79302		78325		77015		25724		25723		2E2	
n	10		15		16		16		13		20		18		17	
	mean	1σ	mean	1σ	mean	1σ	mean	1σ	mean	1σ	mean	1σ	mean	1σ	mean	1σ
SiO_2	55.69	0.20	55.74	0.18	55.73	0.20	55.78	0.13	55.78	0.14	55.62	0.16	55.70	0.16	55.75	0.14
TiO_2	1.01	0.04	1.02	0.03	1.02	0.06	1.02	0.06	1.01	0.03	1.05	0.05	1.03	0.04	1.02	0.05
Al_2O_3	19.71	0.10	19.64	0.13	19.63	0.12	19.61	0.08	19.65	0.15	19.58	0.12	19.60	0.10	19.67	0.10
$FeO^‡$	5.43	0.08	5.49	0.20	5.41	0.10	5.41	0.09	5.42	0.10	5.59	0.10	5.52	0.14	5.38	0.14
MnO	0.28	0.02	0.27	0.02	0.26	0.03	0.28	0.03	0.27	0.03	0.28	0.02	0.29	0.02	0.28	0.02
MgO	0.82	0.03	0.84	0.03	0.83	0.06	0.80	0.04	0.83	0.02	0.86	0.03	0.85	0.02	0.83	0.02
CaO	1.84	0.06	1.86	0.05	1.83	0.05	1.89	0.04	1.84	0.04	1.85	0.04	1.92	0.08	1.88	0.07
Na_2O	8.80	0.09	8.82	0.10	8.85	0.23	8.80	0.09	8.86	0.09	8.82	0.08	8.73	0.20	8.85	0.16
K_2O	5.64	0.08	5.61	0.08	5.67	0.07	5.70	0.06	5.63	0.08	5.61	0.06	5.58	0.14	5.64	0.07
P_2O_5	0.28	0.04	0.28	0.03	0.27	0.04	0.26	0.05	0.26	0.04	0.28	0.04	0.29	0.04	0.28	0.05
SO_2	0.08	0.02	0.08	0.02	0.08	0.02	0.08	0.02	0.07	0.02	0.08	0.02	0.08	0.02	0.07	0.02
F	0.28	0.08	0.21	0.08	0.26	0.08	0.20	0.11	0.22	0.07	0.23	0.08	0.25	0.06	0.19	0.07
Cl	0.15	0.02	0.15	0.01	0.15	0.02	0.16	0.01	0.16	0.01	0.16	0.01	0.16	0.02	0.15	0.02

Sample	82416		83220		88104		89001		91101		92101		93102		E96-01	
n	9		6		17		20		19		20		17		20	
	mean	1σ	mean	1σ	mean	1σ	mean	1σ	mean	1σ	mean	1σ	mean	1σ	mean	1σ
SiO_2	55.02	0.19	54.93	0.14	54.97	0.19	55.12	0.27	55.09	0.26	54.85	0.25	55.17	0.30	55.12	0.21
TiO_2	1.01	0.04	1.03	0.06	1.03	0.05	0.99	0.05	1.01	0.04	1.02	0.05	1.01	0.06	1.02	0.04
Al_2O_3	20.07	0.08	20.01	0.05	19.90	0.16	19.91	0.13	19.83	0.16	19.90	0.14	19.79	0.19	19.91	0.09
$FeO^‡$	5.37	0.08	5.41	0.08	5.45	0.09	5.46	0.07	5.43	0.10	5.50	0.08	5.42	0.11	5.32	0.08
MnO	0.28	0.03	0.27	0.03	0.28	0.03	0.28	0.03	0.27	0.03	0.28	0.03	0.27	0.03	0.27	0.03
MgO	0.84	0.03	0.82	0.02	0.84	0.04	0.83	0.03	0.84	0.03	0.84	0.03	0.82	0.02	0.83	0.03
CaO	1.89	0.05	1.89	0.05	1.86	0.04	1.88	0.05	1.88	0.05	1.88	0.05	1.88	0.05	1.87	0.04
Na_2O	9.04	0.15	9.14	0.07	9.13	0.08	9.02	0.09	9.06	0.10	9.15	0.10	9.06	0.11	9.09	0.11
K_2O	5.57	0.10	5.67	0.07	5.65	0.07	5.59	0.05	5.65	0.04	5.65	0.11	5.64	0.07	5.64	0.09
P_2O_5	0.28	0.05	0.26	0.04	0.29	0.04	0.30	0.05	0.28	0.05	0.29	0.05	0.28	0.04	0.27	0.05
SO_2	0.07	0.03	0.07	0.02	0.07	0.01	0.08	0.02	0.08	0.02	0.07	0.01	0.08	0.02	0.08	0.02
F	0.20	0.07	0.15	0.09	0.17	0.10	0.19	0.07	0.21	0.07	0.20	0.07	0.23	0.07	0.21	0.08
Cl	0.15	0.02	0.15	0.02	0.15	0.01	0.16	0.02	0.16	0.02	0.15	0.02	0.15	0.02	0.15	0.02

Table D.8.1. Continued

Sample	ERB12-21-97		1999		DEC2000		E2001		JAN2004	
n	18		16		11		20		15	
	mean	1σ	mean	1σ	mean	1σ	mean	1σ	mean	1σ
SiO_2	55.11	0.18	55.00	0.25	54.73	0.22	54.94	0.24	54.95	0.29
TiO_2	1.03	0.05	1.02	0.04	1.02	0.06	1.02	0.03	1.04	0.04
Al_2O_3	19.85	0.09	19.83	0.15	19.93	0.19	19.92	0.17	19.87	0.17
FeO‡	5.34	0.09	5.38	0.16	5.43	0.12	5.39	0.09	5.45	0.11
MnO	0.27	0.03	0.28	0.03	0.28	0.02	0.28	0.03	0.27	0.04
MgO	0.83	0.03	0.83	0.04	0.84	0.03	0.83	0.03	0.82	0.03
CaO	1.88	0.06	1.86	0.06	1.89	0.05	1.87	0.07	1.90	0.06
Na_2O	9.07	0.09	9.13	0.12	9.21	0.08	9.13	0.11	9.10	0.14
K_2O	5.65	0.08	5.68	0.07	5.73	0.05	5.67	0.09	5.65	0.05
P_2O_5	0.30	0.05	0.31	0.03	0.28	0.05	0.29	0.03	0.27	0.04
SO_2	0.08	0.02	0.08	0.02	0.08	0.01	0.08	0.02	0.09	0.02
F	0.25	0.06	0.24	0.09	0.20	0.04	0.22	0.05	0.23	0.06
Cl	0.16	0.01	0.16	0.01	0.16	0.02	0.16	0.01	0.16	0.02

*Analyses normalized to 100 wt%
n = Number of analyses averaged
‡Total Fe as FeO

Table D.8.2. Electron Microprobe Analyses of Matrix Glass from Tephra

Sample	n	SiO_2	TiO_2	Al_2O_3	FeO*	MnO	MgO	CaO	Na_2O	K_2O	P_2O_5	SO_2	F	Cl
25724	1	55.52	1.10	19.54	5.73	0.29	0.83	1.94	8.82	5.47	0.27	0.07	0.23	0.19
25724	2	55.59	1.13	19.43	5.65	0.30	0.89	1.88	8.75	5.58	0.27	0.05	0.30	0.17
25724	3	55.40	1.11	19.50	5.70	0.33	0.85	1.85	8.85	5.70	0.27	0.09	0.20	0.15
25724	4	55.79	1.06	19.43	5.57	0.26	0.84	1.84	8.96	5.54	0.25	0.09	0.21	0.16
25724	5	55.76	1.10	19.42	5.49	0.26	0.84	1.82	8.86	5.62	0.29	0.06	0.32	0.16
25724	6	55.45	1.08	19.69	5.71	0.29	0.81	1.82	8.72	5.62	0.27	0.06	0.35	0.13
25724	7	55.46	1.04	19.70	5.58	0.27	0.85	1.86	8.85	5.59	0.34	0.11	0.20	0.16
25724	8	55.37	1.01	19.75	5.65	0.26	0.90	1.83	8.86	5.62	0.36	0.09	0.14	0.17
25724	9	55.61	1.05	19.60	5.62	0.25	0.87	1.86	8.75	5.64	0.20	0.10	0.28	0.16
25724	10	55.63	0.99	19.73	5.43	0.29	0.86	1.92	8.88	5.60	0.33	0.08	0.11	0.15
25724	11	55.43	1.05	19.50	5.61	0.28	0.91	1.87	8.87	5.57	0.33	0.10	0.32	0.17
25724	12	55.72	0.97	19.60	5.70	0.29	0.78	1.88	8.63	5.59	0.26	0.08	0.35	0.16
25724	13	55.62	1.08	19.65	5.55	0.28	0.85	1.86	8.73	5.72	0.22	0.07	0.21	0.14
25724	14	55.69	1.09	19.47	5.74	0.26	0.87	1.78	8.77	5.58	0.35	0.07	0.19	0.15
25724	15	55.70	1.03	19.44	5.54	0.28	0.87	1.79	8.87	5.69	0.32	0.07	0.24	0.15
25724	16	55.87	1.03	19.44	5.57	0.30	0.84	1.80	8.69	5.67	0.30	0.11	0.23	0.16
25724	17	55.46	1.11	19.76	5.52	0.27	0.86	1.85	8.78	5.64	0.24	0.08	0.28	0.15
25724	18	55.91	1.02	19.63	5.47	0.24	0.88	1.88	8.90	5.49	0.25	0.07	0.09	0.17
25724	19	55.72	0.99	19.64	5.46	0.28	0.85	1.82	8.89	5.62	0.29	0.12	0.14	0.17
25724	20	55.60	1.01	19.61	5.55	0.26	0.86	1.80	8.89	5.62	0.27	0.10	0.29	0.15
2E2	1	55.74	1.03	19.92	4.97	0.24	0.86	1.77	9.14	5.77	0.28	0.09	0.06	0.15
2E2	2	55.98	1.00	19.51	5.44	0.27	0.80	1.77	8.94	5.71	0.32	0.05	0.08	0.13
2E2	3	55.79	1.09	19.61	5.29	0.30	0.83	1.75	8.89	5.67	0.32	0.08	0.26	0.13
2E2	4	55.67	1.03	19.54	5.36	0.32	0.84	1.89	9.05	5.59	0.27	0.07	0.21	0.17
2E2	5	55.78	1.04	19.53	5.24	0.30	0.83	1.93	8.88	5.74	0.31	0.09	0.21	0.14
2E2	6	55.70	1.01	19.64	5.50	0.28	0.84	1.87	8.85	5.55	0.30	0.06	0.27	0.13
2E2	7	55.85	0.98	19.67	5.36	0.30	0.81	1.89	8.90	5.56	0.25	0.07	0.19	0.16
2E2	8	55.70	1.05	19.73	5.51	0.32	0.82	2.00	8.68	5.60	0.21	0.06	0.15	0.17
2E2	9	55.93	1.11	19.66	5.49	0.26	0.84	2.00	8.46	5.66	0.23	0.10	0.13	0.14
2E2	10	55.46	1.05	19.66	5.54	0.25	0.81	1.86	8.99	5.61	0.30	0.09	0.24	0.14
2E2	11	55.70	1.11	19.62	5.35	0.28	0.82	1.88	8.85	5.60	0.31	0.05	0.25	0.17
2E2	12	55.79	1.02	19.75	5.35	0.30	0.86	1.89	8.67	5.63	0.20	0.07	0.30	0.17
2E2	13	55.75	0.98	19.70	5.43	0.23	0.82	1.89	8.90	5.64	0.20	0.04	0.27	0.15
2E2	14	55.49	0.99	19.77	5.42	0.27	0.87	1.91	8.95	5.56	0.36	0.09	0.18	0.14
2E2	15	55.79	0.93	19.74	5.52	0.26	0.80	1.84	8.85	5.64	0.28	0.08	0.12	0.14
2E2	16	55.95	1.03	19.62	5.24	0.28	0.85	1.83	8.72	5.80	0.28	0.08	0.16	0.18
2E2	17	55.72	0.99	19.68	5.45	0.28	0.84	1.96	8.67	5.60	0.33	0.07	0.25	0.16
25723	1	55.84	1.02	19.62	5.51	0.32	0.82	1.91	8.57	5.60	0.29	0.09	0.24	0.16
25723	2	55.82	0.97	19.52	5.47	0.31	0.87	2.01	8.79	5.47	0.32	0.07	0.20	0.18
25723	3	55.61	1.08	19.42	5.59	0.30	0.85	1.89	9.03	5.41	0.25	0.07	0.32	0.18
25723	4	55.84	1.03	19.76	5.41	0.25	0.81	1.86	8.44	5.77	0.30	0.08	0.29	0.17
25723	5	55.94	1.00	19.59	5.28	0.29	0.87	1.95	8.60	5.72	0.30	0.07	0.25	0.14
25723	6	55.79	1.01	19.58	5.44	0.29	0.87	1.87	8.57	5.72	0.31	0.12	0.27	0.16
25723	7	55.53	1.06	19.61	5.49	0.33	0.87	1.90	8.77	5.74	0.25	0.11	0.16	0.18
25723	8	55.54	1.07	19.54	5.98	0.28	0.85	2.16	8.39	5.40	0.29	0.11	0.22	0.17
25723	9	55.93	1.01	19.73	5.50	0.29	0.85	1.92	8.49	5.50	0.31	0.05	0.26	0.16
25723	10	55.83	0.99	19.56	5.46	0.28	0.87	1.89	8.97	5.30	0.29	0.07	0.35	0.14
25723	11	55.69	0.99	19.72	5.43	0.29	0.85	1.87	8.68	5.67	0.26	0.08	0.28	0.19
25723	12	55.71	1.00	19.46	5.58	0.31	0.83	2.05	8.67	5.72	0.18	0.08	0.25	0.17
25723	13	55.66	1.07	19.58	5.48	0.28	0.90	1.90	8.79	5.64	0.22	0.11	0.24	0.12
25723	14	55.66	1.02	19.56	5.61	0.28	0.83	1.87	8.81	5.61	0.35	0.07	0.17	0.17
25723	15	55.52	1.06	19.64	5.55	0.25	0.85	1.96	8.79	5.58	0.31	0.05	0.26	0.17
25723	16	55.36	1.00	19.60	5.59	0.28	0.85	1.84	9.12	5.52	0.33	0.05	0.33	0.15
25723	17	55.58	1.05	19.77	5.60	0.24	0.86	1.85	8.83	5.59	0.27	0.08	0.13	0.15
25723	18	55.83	1.14	19.47	5.47	0.30	0.86	1.88	8.86	5.44	0.32	0.09	0.21	0.14
77015	1	55.76	0.98	19.52	5.42	0.29	0.85	1.83	8.88	5.69	0.24	0.09	0.28	0.17
77015	2	55.62	1.01	19.74	5.37	0.28	0.86	1.77	8.99	5.62	0.26	0.04	0.27	0.16
77015	3	55.72	1.02	19.36	5.57	0.33	0.81	1.86	8.85	5.81	0.23	0.04	0.25	0.14
77015	4	55.74	1.00	19.56	5.53	0.26	0.80	1.87	8.84	5.63	0.27	0.08	0.24	0.17
77015	5	55.88	1.07	19.46	5.41	0.28	0.85	1.80	8.81	5.66	0.24	0.08	0.29	0.15
77015	6	55.93	1.01	19.63	5.25	0.27	0.84	1.84	8.91	5.59	0.24	0.09	0.26	0.14
77015	7	55.89	1.05	19.86	5.43	0.26	0.80	1.81	8.72	5.68	0.20	0.08	0.06	0.17
77015	8	55.50	0.99	19.76	5.51	0.25	0.82	1.88	8.92	5.68	0.27	0.05	0.22	0.13
77015	9	55.96	1.02	19.73	5.40	0.28	0.81	1.84	8.70	5.64	0.24	0.09	0.14	0.17
77015	10	55.80	1.02	19.62	5.49	0.31	0.81	1.92	8.85	5.51	0.25	0.11	0.15	0.15
77015	11	55.93	0.96	19.77	5.31	0.25	0.84	1.88	8.80	5.55	0.30	0.08	0.18	0.16

Sample	n	SiO_2	TiO_2	Al_2O_3	FeO*	MnO	MgO	CaO	Na_2O	K_2O	P_2O_5	SO_2	F	Cl
77015	12	55.68	0.99	19.59	5.52	0.23	0.80	1.84	8.90	5.59	0.34	0.05	0.33	0.16
77015	13	55.69	1.01	19.81	5.29	0.28	0.86	1.85	9.01	5.50	0.26	0.06	0.23	0.17
78325	1	55.78	1.05	19.57	5.40	0.29	0.83	1.88	8.81	5.64	0.24	0.07	0.31	0.14
78325	2	55.90	0.96	19.57	5.28	0.29	0.72	1.89	8.80	5.70	0.30	0.10	0.32	0.17
78325	3	55.87	1.00	19.79	5.27	0.32	0.85	1.95	8.70	5.65	0.26	0.11	0.07	0.15
78325	4	55.62	1.11	19.60	5.46	0.28	0.77	1.92	8.84	5.71	0.28	0.08	0.17	0.16
78325	5	55.90	1.06	19.55	5.38	0.30	0.82	1.87	8.87	5.69	0.28	0.09	0.01	0.17
78325	6	55.87	1.13	19.55	5.40	0.26	0.81	1.84	8.72	5.66	0.27	0.09	0.22	0.16
78325	7	55.91	1.08	19.54	5.39	0.32	0.74	1.90	8.77	5.78	0.19	0.12	0.10	0.16
78325	8	55.67	1.06	19.59	5.45	0.31	0.77	1.90	8.81	5.65	0.24	0.11	0.27	0.15
78325	9	55.72	0.94	19.68	5.34	0.26	0.84	1.92	8.77	5.72	0.26	0.06	0.33	0.15
78325	10	55.87	0.95	19.51	5.43	0.26	0.80	1.89	8.80	5.68	0.24	0.06	0.36	0.15
78325	11	55.68	0.99	19.68	5.41	0.23	0.75	1.96	8.96	5.68	0.34	0.07	0.10	0.16
78325	12	55.88	1.07	19.60	5.34	0.25	0.85	1.83	8.70	5.82	0.14	0.07	0.27	0.17
78325	13	55.87	0.98	19.65	5.47	0.29	0.82	1.85	8.68	5.67	0.31	0.08	0.17	0.16
78325	14	55.48	1.03	19.58	5.60	0.26	0.83	1.85	8.86	5.75	0.27	0.06	0.28	0.15
78325	15	55.85	0.96	19.61	5.55	0.29	0.81	1.95	8.71	5.61	0.28	0.08	0.16	0.14
78325	16	55.64	1.00	19.73	5.39	0.26	0.83	1.87	8.96	5.73	0.24	0.08	0.11	0.16
79302	1	55.51	1.02	19.59	5.45	0.28	0.81	1.89	8.93	5.75	0.27	0.09	0.29	0.12
79302	2	55.92	0.91	19.74	5.34	0.25	0.79	1.84	8.57	5.73	0.27	0.10	0.36	0.18
79302	3	55.53	1.06	19.72	5.39	0.33	0.86	1.82	8.86	5.63	0.28	0.10	0.26	0.15
79302	4	55.24	0.95	19.73	5.31	0.27	0.83	1.90	9.10	5.71	0.33	0.08	0.39	0.15
79302	5	55.74	1.02	19.62	5.58	0.23	0.81	1.82	8.96	5.54	0.24	0.08	0.20	0.16
79302	6	55.88	1.01	19.53	5.38	0.27	0.83	1.92	8.74	5.62	0.30	0.09	0.27	0.17
79302	7	55.53	0.95	19.81	5.44	0.26	0.82	1.79	8.79	5.72	0.28	0.10	0.36	0.16
79302	8	55.93	1.05	19.67	5.43	0.30	0.82	1.84	8.68	5.69	0.23	0.04	0.14	0.19
79302	9	55.76	1.05	19.88	5.34	0.25	0.81	1.78	8.70	5.74	0.28	0.08	0.20	0.14
79302	10	55.89	1.08	19.62	5.36	0.27	0.80	1.81	8.77	5.70	0.21	0.08	0.28	0.14
79302	11	55.78	1.13	19.54	5.37	0.26	0.83	1.87	8.82	5.71	0.34	0.09	0.11	0.15
79302	12	55.56	1.06	19.43	5.21	0.23	0.80	1.77	9.55	5.50	0.27	0.08	0.38	0.14
79302	13	55.90	1.02	19.62	5.51	0.25	0.77	1.79	8.86	5.60	0.28	0.07	0.19	0.15
79302	14	55.92	1.00	19.53	5.52	0.22	0.86	1.78	8.72	5.74	0.25	0.09	0.22	0.15
79302	15	55.90	1.09	19.44	5.50	0.22	0.81	1.83	8.80	5.64	0.27	0.05	0.27	0.17
79302	16	55.66	1.00	19.65	5.50	0.30	1.02	1.79	8.71	5.68	0.19	0.06	0.29	0.15
80300	1	55.11	0.92	19.91	5.43	0.29	0.85	1.89	9.08	5.57	0.23	0.09	0.25	0.19
80300	2	54.97	1.02	19.80	5.37	0.28	0.81	1.94	9.05	5.75	0.20	0.06	0.40	0.15
80300	3	55.13	0.93	20.06	5.37	0.23	0.84	1.88	9.04	5.70	0.24	0.08	0.11	0.17
80300	4	55.20	1.10	19.93	5.22	0.23	0.80	1.87	9.17	5.74	0.22	0.07	0.10	0.15
80300	5	54.47	1.05	20.33	5.34	0.29	0.79	1.85	9.23	5.81	0.23	0.08	0.17	0.14
80300	6	55.21	0.91	19.87	5.30	0.26	0.84	1.90	8.96	5.73	0.24	0.08	0.33	0.19
81003	1	55.92	1.05	19.69	5.27	0.26	0.84	1.88	8.73	5.52	0.24	0.08	0.36	0.14
81003	2	55.86	1.00	19.73	5.55	0.24	0.81	1.89	8.82	5.55	0.19	0.09	0.13	0.16
81003	3	55.91	1.01	19.60	5.36	0.27	0.83	1.86	8.83	5.63	0.30	0.08	0.17	0.14
81003	4	55.57	1.02	19.85	5.37	0.27	0.78	1.86	8.93	5.59	0.30	0.08	0.23	0.15
81003	5	55.92	1.08	19.51	5.43	0.27	0.80	1.87	8.68	5.63	0.31	0.09	0.26	0.15
81003	6	55.75	1.01	19.70	5.58	0.31	0.86	1.84	8.74	5.56	0.29	0.09	0.13	0.16
81003	7	55.49	1.03	19.64	5.56	0.30	0.85	2.02	8.75	5.48	0.28	0.07	0.39	0.14
81003	8	55.90	0.98	19.67	5.38	0.31	0.83	1.88	8.85	5.54	0.28	0.05	0.17	0.15
81003	9	55.80	1.00	19.49	5.61	0.26	0.90	1.88	8.71	5.69	0.27	0.04	0.18	0.17
81003	10	55.87	1.06	19.58	5.53	0.25	0.81	1.79	8.98	5.60	0.23	0.06	0.13	0.14
81003	11	55.79	0.94	19.84	5.26	0.24	0.83	1.81	8.86	5.76	0.29	0.10	0.15	0.12
81003	12	55.73	1.02	19.77	5.40	0.23	0.84	1.85	8.82	5.62	0.27	0.09	0.21	0.14
81003	13	55.34	1.05	19.44	6.09	0.29	0.86	1.82	8.72	5.66	0.32	0.08	0.20	0.15
81003	14	55.54	1.03	19.56	5.49	0.27	0.88	1.83	8.98	5.71	0.30	0.10	0.17	0.15
81003	15	55.78	1.02	19.53	5.48	0.27	0.85	1.85	8.89	5.63	0.28	0.07	0.23	0.13
81401	1	55.23	1.01	19.95	5.29	0.25	0.79	1.88	8.99	5.60	0.22	0.09	0.33	0.16
81401	2	55.23	1.04	20.00	5.32	0.25	0.80	1.90	9.04	5.58	0.29	0.09	0.11	0.15
81401	3	55.01	0.97	19.98	5.32	0.25	0.81	1.83	9.26	5.68	0.25	0.10	0.18	0.16
81401	4	55.05	1.10	20.11	5.14	0.31	0.81	1.86	8.95	5.71	0.24	0.07	0.31	0.16
81401	5	55.14	0.97	20.06	5.35	0.22	0.76	1.88	9.17	5.61	0.26	0.08	0.15	0.14
81401	6	54.94	1.00	20.22	5.39	0.28	0.83	1.94	9.11	5.56	0.29	0.07	0.00	0.16
81401	7	55.19	1.03	20.04	5.33	0.23	0.76	1.89	8.93	5.70	0.30	0.07	0.16	0.18
81401	8	54.86	0.98	20.11	5.31	0.28	0.82	1.87	9.14	5.66	0.26	0.08	0.25	0.19
81401	9	55.27	1.06	19.91	5.22	0.29	0.81	1.80	9.07	5.71	0.25	0.04	0.20	0.19
81401	10	55.19	1.04	20.08	5.31	0.27	0.82	1.79	9.08	5.72	0.29	0.08	0.00	0.15
81401	11	55.03	0.94	20.24	5.19	0.33	0.82	1.79	9.10	5.76	0.23	0.06	0.16	0.14
81401	12	55.00	1.02	20.11	5.50	0.33	0.79	1.83	9.09	5.64	0.17	0.07	0.12	0.16

Sample	n	SiO_2	TiO_2	Al_2O_3	FeO*	MnO	MgO	CaO	Na_2O	K_2O	P_2O_5	SO_2	F	Cl
81401	13	54.99	0.97	20.02	5.37	0.30	0.80	1.87	9.06	5.71	0.24	0.05	0.26	0.14
81401	14	55.00	1.06	19.95	5.23	0.30	0.80	1.93	9.15	5.62	0.32	0.08	0.20	0.15
81401	15	54.91	1.00	19.91	5.38	0.26	0.80	1.87	9.27	5.61	0.32	0.08	0.21	0.17
81401	16	55.16	1.02	20.05	5.28	0.26	0.78	1.83	9.13	5.62	0.21	0.09	0.23	0.16
81401	17	55.11	1.04	20.08	5.42	0.27	0.77	1.86	8.98	5.58	0.26	0.06	0.21	0.15
81410	1	55.86	1.03	19.51	5.53	0.27	0.79	1.90	8.95	5.57	0.25	0.09	0.12	0.15
81410	2	55.54	1.02	19.75	5.58	0.28	0.83	1.81	8.93	5.53	0.29	0.08	0.23	0.12
81410	3	55.61	1.03	19.86	5.42	0.27	0.78	1.80	8.83	5.56	0.26	0.08	0.34	0.15
81410	4	55.36	1.05	19.66	5.44	0.33	0.80	1.77	8.84	5.76	0.38	0.07	0.39	0.16
81410	5	55.73	0.97	19.59	5.39	0.27	0.80	1.89	8.78	5.69	0.27	0.09	0.37	0.16
81410	6	55.47	0.99	19.74	5.45	0.29	0.84	1.93	8.77	5.69	0.28	0.09	0.30	0.16
81410	7	55.81	1.06	19.73	5.39	0.26	0.84	1.86	8.66	5.73	0.25	0.05	0.24	0.12
81410	8	55.88	0.92	19.72	5.39	0.25	0.87	1.87	8.79	5.56	0.28	0.08	0.24	0.16
81410	9	55.99	1.03	19.72	5.30	0.28	0.80	1.77	8.70	5.66	0.24	0.10	0.24	0.17
81410	10	55.70	0.96	19.78	5.42	0.27	0.82	1.80	8.75	5.61	0.29	0.06	0.35	0.17
82416	1	55.06	1.03	20.09	5.40	0.31	0.86	1.87	8.95	5.61	0.29	0.03	0.12	0.17
82416	2	54.83	1.02	19.96	5.43	0.26	0.87	1.96	9.20	5.56	0.27	0.08	0.21	0.14
82416	3	55.07	1.01	20.18	5.45	0.28	0.85	1.97	8.81	5.45	0.30	0.08	0.23	0.14
82416	4	54.82	0.98	20.15	5.44	0.27	0.80	1.90	9.25	5.49	0.23	0.04	0.25	0.16
82416	5	55.03	0.98	20.05	5.21	0.23	0.86	1.86	9.04	5.76	0.24	0.13	0.27	0.15
82416	6	55.06	0.99	20.05	5.37	0.29	0.82	1.91	9.09	5.55	0.39	0.08	0.09	0.13
82416	7	54.87	1.09	20.09	5.34	0.28	0.81	1.85	9.17	5.71	0.24	0.04	0.17	0.17
82416	8	55.03	0.96	20.09	5.40	0.32	0.83	1.80	9.02	5.51	0.32	0.07	0.32	0.15
82416	9	55.43	1.02	19.95	5.31	0.29	0.85	1.92	8.88	5.50	0.24	0.07	0.16	0.18
82418	1	55.90	1.00	19.81	5.49	0.27	0.85	1.79	8.83	5.26	0.25	0.06	0.35	0.14
82418	2	55.55	1.04	19.86	5.54	0.28	0.86	1.76	8.90	5.34	0.26	0.06	0.41	0.15
82418	3	56.09	0.98	19.79	5.10	0.28	0.82	1.73	9.06	5.42	0.28	0.06	0.25	0.13
82418	4	55.69	0.99	19.73	5.76	0.26	0.88	1.71	8.96	5.29	0.29	0.05	0.25	0.14
82418	5	55.99	0.95	19.64	5.65	0.24	0.82	1.80	8.93	5.34	0.24	0.09	0.14	0.17
82418	6	55.71	1.06	19.73	5.61	0.26	0.82	1.75	9.02	5.31	0.30	0.04	0.23	0.17
82418	7	55.85	1.01	19.69	5.46	0.25	0.86	1.77	8.95	5.44	0.25	0.07	0.24	0.16
82418	8	55.72	1.03	19.85	5.64	0.30	0.84	1.74	8.80	5.32	0.31	0.07	0.23	0.16
82418	9	56.00	0.97	19.83	5.52	0.32	0.85	1.68	8.89	5.15	0.28	0.04	0.32	0.16
82418	10	55.63	0.98	19.89	5.54	0.30	0.90	1.71	9.07	5.17	0.27	0.07	0.30	0.15
82418	11	55.71	1.04	19.53	5.42	0.29	0.84	1.75	9.04	5.58	0.28	0.07	0.29	0.16
82418	12	56.02	0.94	19.69	5.26	0.29	0.81	1.68	9.08	5.56	0.22	0.07	0.26	0.13
83220	1	54.99	0.99	20.04	5.41	0.25	0.79	1.90	9.14	5.59	0.30	0.06	0.23	0.12
83220	2	54.88	1.06	20.08	5.35	0.22	0.85	1.95	9.11	5.70	0.25	0.08	0.08	0.15
83220	3	54.66	1.07	19.97	5.49	0.29	0.82	1.95	9.21	5.64	0.29	0.04	0.19	0.18
83220	4	55.02	1.12	19.94	5.52	0.27	0.81	1.88	9.02	5.76	0.24	0.06	0.00	0.16
83220	5	55.00	0.99	20.03	5.34	0.31	0.82	1.85	9.15	5.59	0.27	0.10	0.21	0.15
83220	6	55.03	0.96	19.97	5.36	0.28	0.80	1.84	9.20	5.72	0.20	0.09	0.19	0.16
83207	1	55.83	1.01	19.81	5.62	0.27	0.75	1.86	8.71	5.45	0.24	0.08	0.24	0.12
83207	2	55.66	1.08	19.76	5.54	0.30	0.79	1.79	9.08	5.26	0.28	0.04	0.28	0.13
83207	3	55.57	1.03	19.63	5.58	0.32	0.83	1.72	9.05	5.43	0.26	0.05	0.38	0.15
83207	4	55.60	1.00	19.75	5.59	0.27	0.88	1.75	9.00	5.44	0.24	0.04	0.31	0.15
83207	5	55.65	0.97	19.75	5.70	0.28	0.84	1.78	9.04	5.35	0.20	0.11	0.21	0.11
83207	6	55.63	1.00	19.77	5.58	0.29	0.86	1.75	8.96	5.34	0.33	0.08	0.29	0.13
83207	7	55.83	1.08	19.76	5.40	0.31	0.87	1.81	8.98	5.29	0.22	0.08	0.23	0.13
83207	8	55.92	1.00	19.88	5.29	0.29	0.86	1.62	8.92	5.49	0.26	0.06	0.28	0.13
83207	9	55.87	0.96	19.63	5.59	0.29	0.88	1.70	8.85	5.45	0.27	0.10	0.23	0.18
83207	10	55.80	1.00	19.58	5.43	0.25	0.84	1.78	9.08	5.43	0.27	0.03	0.40	0.12
83207	11	55.78	0.96	19.83	5.49	0.32	0.83	1.68	9.15	5.46	0.24	0.09	0.00	0.16
83207	12	55.56	0.94	19.72	5.53	0.28	0.85	1.80	9.00	5.47	0.31	0.09	0.32	0.14
83207	13	55.66	0.88	19.69	5.52	0.26	0.85	1.74	9.12	5.40	0.34	0.09	0.31	0.14
83207	14	56.13	0.94	19.74	5.33	0.31	0.83	1.71	8.94	5.41	0.29	0.05	0.20	0.12
84500	1	55.54	0.97	19.74	5.41	0.30	0.89	1.84	9.01	5.47	0.30	0.05	0.32	0.16
84500	2	55.51	0.97	19.73	5.58	0.28	1.33	1.90	8.70	5.26	0.24	0.05	0.29	0.15
84500	3	55.67	0.96	19.66	5.77	0.30	0.83	1.81	8.98	5.34	0.30	0.06	0.17	0.15
84500	4	55.69	0.94	19.69	5.53	0.29	1.28	1.78	8.83	5.36	0.23	0.09	0.13	0.15
84500	5	56.11	0.94	19.88	5.28	0.27	0.87	1.68	9.04	5.43	0.29	0.07	0.00	0.13
84500	6	55.35	0.98	19.84	5.68	0.26	0.87	1.84	9.00	5.37	0.27	0.10	0.27	0.16
84500	7	55.54	1.07	19.84	5.63	0.24	0.91	1.79	8.84	5.30	0.31	0.09	0.29	0.14
84500	8	55.78	1.05	19.62	5.37	0.27	0.87	1.77	9.04	5.42	0.31	0.09	0.25	0.15
84500	9	55.43	0.94	19.95	5.51	0.26	0.87	1.85	8.83	5.57	0.23	0.05	0.36	0.15
84500	10	55.63	0.97	19.49	5.63	0.31	0.87	1.83	9.05	5.41	0.24	0.07	0.33	0.15
84500	11	55.23	1.00	19.80	5.72	0.32	0.84	1.84	9.01	5.49	0.25	0.09	0.26	0.16

Sample	n	SiO_2	TiO_2	Al_2O_3	FeO*	MnO	MgO	CaO	Na_2O	K_2O	P_2O_5	SO_2	F	Cl
84500	12	55.83	0.97	19.69	5.62	0.31	0.82	1.70	8.96	5.52	0.19	0.03	0.21	0.13
84500	13	55.82	0.99	19.47	5.49	0.29	0.87	1.74	9.10	5.37	0.33	0.05	0.36	0.12
84500	14	55.34	0.98	19.59	5.80	0.31	0.82	1.79	9.02	5.56	0.24	0.05	0.35	0.13
84505	1	56.00	0.98	19.55	5.41	0.26	0.84	1.71	8.88	5.58	0.31	0.05	0.29	0.14
84505	2	55.79	1.05	19.74	5.47	0.31	0.83	1.79	9.12	5.43	0.24	0.07	0.00	0.16
84505	3	55.93	0.99	19.78	5.23	0.26	0.74	1.64	9.12	5.54	0.27	0.07	0.28	0.14
84505	4	55.55	1.02	19.71	5.56	0.30	0.83	1.75	9.02	5.46	0.26	0.08	0.31	0.14
84505	5	55.88	0.98	19.62	5.32	0.25	0.82	1.81	9.00	5.41	0.30	0.06	0.42	0.15
84505	6	55.82	0.84	19.79	5.47	0.30	0.82	1.77	8.89	5.48	0.33	0.08	0.29	0.12
84505	7	55.79	0.94	19.78	5.45	0.28	0.80	1.75	9.04	5.35	0.28	0.08	0.34	0.15
84505	8	55.83	0.95	19.77	5.35	0.29	0.86	1.82	8.90	5.39	0.29	0.08	0.33	0.14
84505	9	55.89	1.04	19.66	5.31	0.29	0.86	1.78	8.92	5.48	0.30	0.04	0.30	0.13
84505	10	56.16	1.00	19.58	5.54	0.29	0.84	1.78	8.98	5.29	0.31	0.07	0.00	0.15
84505	11	56.20	1.01	19.61	5.27	0.23	0.81	1.71	9.02	5.42	0.26	0.06	0.27	0.12
84505	12	55.92	1.01	19.65	5.41	0.27	0.92	1.72	8.99	5.29	0.28	0.07	0.31	0.15
85009	1	55.69	0.98	19.55	5.56	0.25	0.86	1.80	8.94	5.64	0.22	0.06	0.34	0.12
85009	2	55.80	0.94	19.85	5.47	0.25	0.79	1.76	8.95	5.44	0.22	0.08	0.28	0.16
85009	3	55.80	0.93	19.77	5.42	0.25	0.81	1.82	9.05	5.52	0.16	0.06	0.25	0.16
85009	4	55.77	1.01	19.56	5.51	0.29	0.86	1.81	8.77	5.48	0.27	0.09	0.42	0.16
85009	5	55.83	0.98	19.71	5.23	0.32	0.87	1.81	8.86	5.56	0.36	0.09	0.26	0.12
85009	6	55.46	0.92	19.86	5.43	0.28	0.84	1.82	8.97	5.53	0.30	0.08	0.35	0.16
85009	7	55.46	1.01	19.77	5.44	0.29	0.86	1.77	9.05	5.48	0.27	0.10	0.34	0.17
85009	8	55.54	1.03	19.54	5.36	0.28	1.27	1.83	8.89	5.51	0.28	0.08	0.25	0.16
85009	9	55.10	0.96	19.73	5.54	0.28	1.33	1.85	8.86	5.52	0.31	0.07	0.28	0.15
85009	10	55.63	0.98	19.62	5.32	0.26	0.90	1.85	9.01	5.50	0.29	0.08	0.44	0.12
85009	11	56.09	1.06	19.63	5.47	0.25	0.87	1.86	8.68	5.33	0.27	0.07	0.27	0.15
85009	12	55.78	0.90	19.61	5.43	0.31	0.84	1.83	9.05	5.34	0.30	0.05	0.40	0.17
85009	13	55.26	0.93	19.91	5.68	0.30	0.82	1.71	9.01	5.65	0.34	0.08	0.16	0.15
86022	1	55.79	0.95	19.64	5.38	0.28	0.82	1.74	8.96	5.67	0.26	0.12	0.23	0.16
86022	2	54.66	1.04	19.87	5.83	0.27	0.84	1.78	9.18	5.71	0.22	0.09	0.35	0.17
86022	3	55.31	1.05	19.67	5.32	0.28	0.83	1.82	9.06	5.74	0.30	0.09	0.36	0.17
86022	4	55.37	0.98	19.88	5.61	0.32	0.82	1.89	8.91	5.59	0.26	0.07	0.15	0.15
86022	5	55.21	1.03	19.84	5.49	0.30	0.85	1.85	9.10	5.50	0.31	0.11	0.27	0.15
86022	6	55.74	1.12	19.62	5.57	0.26	0.56	1.71	9.02	5.69	0.24	0.08	0.28	0.11
86022	7	54.90	1.04	19.95	5.53	0.27	0.82	1.82	9.10	5.73	0.31	0.05	0.30	0.17
86022	8	55.61	1.05	19.64	5.31	0.30	0.88	1.83	8.88	5.74	0.25	0.07	0.25	0.17
86022	9	55.64	0.92	19.60	5.42	0.29	0.87	1.79	9.07	5.53	0.27	0.10	0.32	0.17
86022	10	55.92	0.98	19.59	5.41	0.27	0.81	1.70	8.98	5.52	0.22	0.10	0.35	0.15
86022	11	55.37	1.03	19.79	5.29	0.27	0.95	1.79	9.22	5.54	0.25	0.07	0.26	0.17
86022	12	55.37	0.93	19.81	5.64	0.30	0.89	1.79	9.00	5.48	0.22	0.10	0.33	0.15
88104	1	54.92	1.05	19.92	5.43	0.30	0.82	1.87	9.11	5.71	0.32	0.08	0.12	0.16
88104	2	54.77	1.08	19.93	5.43	0.26	0.81	1.89	9.13	5.71	0.30	0.06	0.24	0.16
88104	3	54.97	1.01	19.96	5.52	0.26	0.86	1.87	9.06	5.66	0.25	0.06	0.17	0.15
88104	4	54.91	1.07	20.12	5.36	0.27	0.87	1.84	9.11	5.61	0.31	0.07	0.11	0.13
88104	5	55.09	1.06	19.90	5.45	0.32	0.82	1.92	8.93	5.63	0.32	0.07	0.09	0.19
88104	6	54.92	0.98	19.92	5.48	0.24	0.89	1.89	9.05	5.59	0.28	0.09	0.31	0.16
88104	7	54.83	1.01	19.84	5.53	0.27	0.84	1.82	9.20	5.72	0.34	0.07	0.20	0.13
88104	8	55.17	1.02	19.59	5.55	0.25	0.86	1.87	9.06	5.65	0.34	0.08	0.21	0.14
88104	9	54.99	1.01	19.93	5.37	0.29	0.89	1.82	9.11	5.56	0.28	0.07	0.32	0.13
88104	10	54.95	1.03	19.83	5.56	0.31	0.88	1.82	9.18	5.67	0.29	0.07	0.08	0.14
88104	11	55.26	0.99	19.64	5.49	0.25	0.76	1.86	9.03	5.67	0.34	0.08	0.28	0.14
88104	12	55.01	1.07	19.74	5.37	0.34	0.85	1.97	9.17	5.52	0.32	0.09	0.22	0.16
88104	13	54.60	1.10	20.10	5.48	0.28	0.90	1.83	9.25	5.67	0.23	0.08	0.14	0.15
88104	14	54.69	0.98	20.02	5.37	0.28	0.84	1.90	9.15	5.82	0.27	0.08	0.26	0.14
88104	15	55.24	0.97	20.13	5.27	0.29	0.79	1.79	9.17	5.67	0.30	0.03	0.01	0.14
88104	16	54.91	0.96	20.00	5.39	0.31	0.86	1.88	9.27	5.61	0.30	0.07	0.08	0.16
88104	17	55.24	1.10	19.74	5.56	0.29	0.79	1.83	9.17	5.59	0.21	0.08	0.02	0.16
89001	1	54.98	1.02	19.88	5.45	0.32	0.84	1.86	8.93	5.65	0.36	0.09	0.25	0.16
89001	2	55.24	1.01	19.86	5.37	0.25	0.84	1.92	8.99	5.63	0.22	0.08	0.21	0.19
89001	3	55.54	0.96	19.79	5.34	0.28	0.79	1.86	9.15	5.61	0.23	0.06	0.00	0.15
89001	4	55.06	1.04	19.92	5.41	0.28	0.84	1.92	9.07	5.60	0.28	0.07	0.17	0.12
89001	5	55.29	0.98	19.95	5.44	0.30	0.80	1.80	9.02	5.53	0.22	0.05	0.25	0.16
89001	6	54.68	0.97	20.13	5.53	0.28	0.89	1.95	9.01	5.60	0.32	0.08	0.24	0.14
89001	7	54.89	0.96	20.04	5.42	0.29	0.81	1.92	8.96	5.67	0.33	0.06	0.25	0.16
89001	8	54.89	1.09	20.00	5.53	0.31	0.81	1.87	9.02	5.56	0.34	0.06	0.17	0.18
89001	9	54.77	1.01	20.13	5.49	0.31	0.85	1.89	9.01	5.52	0.29	0.07	0.28	0.17
89001	10	55.31	0.92	19.86	5.57	0.27	0.88	1.88	8.79	5.61	0.32	0.06	0.16	0.17

Sample	n	SiO_2	TiO_2	Al_2O_3	FeO*	MnO	MgO	CaO	Na_2O	K_2O	P_2O_5	SO_2	F	Cl
89001	11	55.07	1.08	19.91	5.34	0.28	0.83	1.92	9.04	5.68	0.32	0.08	0.09	0.17
89001	12	54.83	0.98	20.10	5.57	0.30	0.80	1.90	9.04	5.58	0.27	0.09	0.15	0.19
89001	13	55.54	1.01	19.72	5.41	0.23	0.84	1.86	8.90	5.63	0.29	0.06	0.17	0.17
89001	14	54.97	0.99	20.04	5.33	0.26	0.86	1.90	9.13	5.57	0.29	0.09	0.20	0.15
89001	15	55.55	0.96	19.70	5.50	0.31	0.77	1.72	9.19	5.57	0.20	0.05	0.10	0.17
89001	16	55.40	1.06	19.81	5.40	0.23	0.77	1.90	8.96	5.52	0.35	0.10	0.16	0.15
89001	17	55.03	1.01	19.82	5.50	0.23	0.82	1.83	9.04	5.64	0.35	0.11	0.30	0.14
89001	18	54.83	1.03	19.95	5.51	0.31	0.83	1.92	9.10	5.55	0.32	0.10	0.20	0.16
89001	19	55.30	0.85	19.85	5.47	0.25	0.87	1.91	9.05	5.49	0.29	0.10	0.20	0.16
89001	#	55.14	0.96	19.78	5.53	0.23	0.86	1.93	8.98	5.58	0.35	0.05	0.27	0.13
91101	1	55.34	1.01	19.85	5.34	0.26	0.83	1.94	8.89	5.68	0.20	0.08	0.24	0.16
91101	2	55.11	1.06	19.80	5.48	0.31	0.82	1.79	9.23	5.68	0.17	0.10	0.10	0.15
91101	3	54.93	1.00	20.12	5.57	0.22	0.84	1.84	9.04	5.59	0.26	0.06	0.17	0.15
91101	4	55.53	0.93	19.65	5.35	0.28	0.82	1.82	9.06	5.65	0.32	0.06	0.16	0.15
91101	5	55.31	1.06	19.55	5.45	0.26	0.85	1.91	9.07	5.62	0.29	0.05	0.22	0.19
91101	6	54.82	1.01	20.00	5.30	0.31	0.81	1.92	9.11	5.75	0.34	0.10	0.22	0.15
91101	7	55.14	1.01	19.88	5.52	0.25	0.85	1.95	8.86	5.64	0.30	0.06	0.17	0.16
91101	8	55.43	0.99	19.84	5.33	0.23	0.85	1.90	9.00	5.61	0.22	0.05	0.21	0.16
91101	9	55.50	1.02	19.61	5.41	0.30	0.85	1.86	9.01	5.65	0.33	0.08	0.06	0.14
91101	10	55.21	1.01	19.71	5.31	0.29	0.88	1.85	9.07	5.61	0.31	0.07	0.34	0.17
91101	11	55.04	0.99	19.93	5.39	0.27	0.84	1.87	9.01	5.65	0.24	0.07	0.35	0.15
91101	12	54.60	1.09	20.05	5.34	0.24	0.89	1.91	9.18	5.65	0.31	0.09	0.23	0.19
91101	13	55.21	1.01	19.63	5.51	0.27	0.87	1.91	9.00	5.69	0.27	0.07	0.24	0.14
91101	14	55.00	1.05	19.93	5.35	0.20	0.79	1.92	9.03	5.72	0.28	0.11	0.22	0.15
91101	15	55.13	1.01	19.73	5.45	0.31	0.88	1.82	9.04	5.58	0.29	0.07	0.29	0.16
91101	16	54.82	0.95	19.91	5.62	0.30	0.80	1.90	9.17	5.61	0.26	0.09	0.15	0.18
91101	17	54.90	1.05	19.77	5.59	0.26	0.84	1.92	9.09	5.67	0.28	0.09	0.19	0.15
91101	18	54.93	0.97	19.81	5.51	0.25	0.85	1.84	9.09	5.70	0.35	0.09	0.24	0.17
91101	19	54.79	1.03	20.04	5.37	0.33	0.82	1.86	9.25	5.61	0.28	0.08	0.21	0.13
92101	1	55.01	1.00	19.74	5.60	0.26	0.85	1.95	9.04	5.65	0.35	0.05	0.17	0.15
92101	2	54.79	1.00	20.19	5.49	0.24	0.85	1.93	8.92	5.55	0.31	0.08	0.26	0.18
92101	3	55.03	0.96	19.93	5.32	0.25	0.85	1.81	9.18	5.67	0.30	0.06	0.27	0.15
92101	4	54.94	1.11	19.80	5.50	0.31	0.88	1.86	9.10	5.63	0.31	0.06	0.11	0.17
92101	5	54.74	1.06	19.91	5.49	0.33	0.86	1.91	9.09	5.69	0.32	0.07	0.19	0.15
92101	6	55.06	1.02	19.86	5.49	0.31	0.85	1.90	9.14	5.49	0.23	0.08	0.22	0.16
92101	7	54.32	1.11	20.19	5.57	0.28	0.82	1.83	9.23	5.57	0.30	0.08	0.34	0.17
92101	8	54.94	0.96	19.82	5.46	0.29	0.84	1.89	9.13	5.70	0.30	0.10	0.21	0.15
92101	9	55.21	0.97	20.01	5.38	0.31	0.81	1.88	9.10	5.65	0.25	0.07	0.05	0.13
92101	10	54.66	1.03	19.88	5.51	0.35	0.85	1.94	9.25	5.53	0.29	0.07	0.26	0.16
92101	11	55.26	1.05	19.82	5.49	0.27	0.83	1.92	9.06	5.53	0.23	0.06	0.18	0.12
92101	12	54.73	0.98	19.89	5.49	0.29	0.81	1.88	9.16	5.62	0.40	0.09	0.28	0.14
92101	13	54.69	0.99	19.94	5.58	0.29	0.79	1.86	9.37	5.65	0.17	0.10	0.24	0.13
92101	14	55.00	1.11	19.67	5.64	0.25	0.83	1.89	9.07	5.71	0.23	0.07	0.17	0.15
92101	15	54.56	1.03	19.91	5.49	0.28	0.85	1.88	9.20	5.78	0.32	0.07	0.28	0.16
92101	16	54.62	0.99	19.94	5.49	0.27	0.92	1.88	9.20	5.72	0.35	0.07	0.20	0.16
92101	17	54.84	1.00	19.94	5.44	0.29	0.83	1.92	9.16	5.67	0.31	0.08	0.19	0.14
92101	18	54.65	0.97	19.97	5.62	0.25	0.86	1.89	9.12	5.71	0.35	0.08	0.19	0.15
92101	19	55.26	1.01	19.65	5.49	0.27	0.78	1.76	9.34	5.53	0.28	0.10	0.19	0.13
92101	20	54.71	1.05	19.86	5.51	0.30	0.87	1.77	9.24	5.98	0.25	0.05	0.06	0.17
93102	1	54.89	0.87	19.79	5.38	0.25	0.81	1.96	9.21	5.70	0.29	0.06	0.43	0.16
93102	2	54.57	1.05	20.17	5.57	0.25	0.85	1.85	9.10	5.71	0.27	0.10	0.13	0.18
93102	3	55.05	1.04	19.72	5.45	0.30	0.83	1.92	9.18	5.60	0.27	0.07	0.23	0.13
93102	4	54.98	1.05	19.72	5.57	0.29	0.79	1.89	9.25	5.60	0.26	0.05	0.21	0.16
93102	5	54.98	0.99	19.74	5.46	0.34	0.85	1.97	9.10	5.73	0.22	0.10	0.17	0.16
93102	6	55.45	1.01	19.64	5.47	0.28	0.85	1.84	8.93	5.58	0.34	0.07	0.21	0.12
93102	7	55.31	1.00	19.61	5.51	0.30	0.83	1.81	9.06	5.66	0.29	0.09	0.18	0.16
93102	8	54.99	1.03	19.85	5.49	0.30	0.79	1.92	9.02	5.70	0.19	0.06	0.29	0.14
93102	9	55.40	1.03	19.79	5.29	0.26	0.83	1.91	8.88	5.65	0.32	0.11	0.19	0.16
93102	10	54.91	0.96	19.98	5.55	0.25	0.80	1.89	8.91	5.73	0.35	0.08	0.23	0.14
93102	11	55.64	1.01	19.71	5.29	0.23	0.80	1.81	9.03	5.62	0.22	0.09	0.22	0.13
93102	12	55.40	0.95	19.70	5.38	0.28	0.79	1.83	9.16	5.54	0.28	0.07	0.28	0.14
93102	13	55.53	1.10	19.52	5.28	0.30	0.81	1.89	8.99	5.73	0.25	0.09	0.18	0.14
93102	14	55.60	1.10	19.50	5.38	0.24	0.83	1.84	9.08	5.51	0.27	0.09	0.24	0.15
93102	15	55.12	1.04	20.13	5.29	0.23	0.84	1.86	8.89	5.60	0.29	0.10	0.25	0.17
93102	16	54.94	0.99	19.96	5.54	0.24	0.84	1.91	9.08	5.64	0.32	0.05	0.17	0.13
93102	17	55.13	0.98	19.96	5.24	0.30	0.83	1.84	9.15	5.62	0.28	0.08	0.23	0.16
E96-01	1	54.87	1.05	19.92	5.42	0.31	0.81	1.91	9.06	5.67	0.32	0.06	0.27	0.14
E96-01	2	54.88	1.10	19.90	5.38	0.24	0.83	1.98	9.07	5.72	0.30	0.08	0.14	0.16

Sample	n	SiO_2	TiO_2	Al_2O_3	FeO*	MnO	MgO	CaO	Na_2O	K_2O	P_2O_5	SO_2	F	Cl
E96-01	3	55.31	1.03	19.72	5.45	0.26	0.83	1.83	8.90	5.59	0.29	0.09	0.36	0.13
E96-01	4	55.54	1.02	19.88	5.32	0.29	0.86	1.81	8.94	5.64	0.20	0.06	0.08	0.15
E96-01	5	54.97	1.04	20.08	5.28	0.30	0.83	1.83	9.10	5.74	0.23	0.06	0.19	0.16
E96-01	6	55.39	1.05	19.84	5.40	0.25	0.80	1.90	8.95	5.48	0.30	0.08	0.21	0.15
E96-01	7	54.87	1.00	19.85	5.25	0.29	0.80	1.89	9.19	5.82	0.28	0.10	0.30	0.18
E96-01	8	55.21	1.04	19.90	5.31	0.26	0.80	1.86	9.13	5.61	0.23	0.10	0.22	0.14
E96-01	9	54.89	1.00	19.96	5.36	0.26	0.86	1.88	9.15	5.65	0.31	0.05	0.24	0.19
E96-01	10	54.99	0.99	19.96	5.35	0.23	0.84	1.93	9.17	5.63	0.20	0.10	0.29	0.14
E96-01	11	54.93	1.07	19.97	5.35	0.25	0.81	1.86	9.30	5.54	0.32	0.08	0.18	0.12
E96-01	12	55.04	0.99	19.89	5.48	0.24	0.83	1.90	9.19	5.48	0.27	0.07	0.26	0.17
E96-01	13	55.12	1.01	19.98	5.33	0.26	0.84	1.94	8.98	5.74	0.26	0.06	0.12	0.17
E96-01	14	55.50	1.04	19.87	5.11	0.30	0.86	1.89	8.99	5.58	0.20	0.11	0.18	0.17
E96-01	15	55.00	0.94	20.03	5.27	0.28	0.85	1.83	9.10	5.68	0.31	0.06	0.31	0.15
E96-01	16	55.34	1.05	19.89	5.29	0.28	0.79	1.89	9.03	5.55	0.28	0.12	0.11	0.18
E96-01	17	55.21	1.01	19.82	5.24	0.30	0.83	1.82	9.28	5.66	0.28	0.07	0.14	0.15
E96-01	18	55.06	1.04	19.98	5.28	0.32	0.83	1.87	9.09	5.62	0.28	0.05	0.21	0.18
E96-01	19	55.07	0.96	20.00	5.36	0.29	0.86	1.86	9.07	5.64	0.26	0.06	0.26	0.13
E96-01	20	55.29	1.02	19.76	5.26	0.29	0.88	1.84	9.07	5.69	0.38	0.08	0.13	0.13
97018	1	55.08	1.10	19.75	5.33	0.29	0.85	1.88	9.10	5.69	0.30	0.05	0.17	0.14
97018	2	55.28	1.04	19.85	5.21	0.33	0.88	1.82	8.96	5.64	0.28	0.09	0.23	0.17
97018	3	55.02	1.07	19.83	5.27	0.22	0.86	1.99	9.10	5.63	0.39	0.07	0.19	0.16
97018	4	55.32	1.02	19.88	5.30	0.21	0.78	1.99	9.05	5.61	0.22	0.08	0.23	0.15
97018	5	55.31	0.99	19.96	5.33	0.25	0.84	1.83	9.02	5.60	0.20	0.06	0.25	0.15
97018	6	54.93	1.02	19.87	5.45	0.27	0.83	1.89	9.11	5.63	0.26	0.08	0.29	0.18
97018	7	55.32	1.09	19.77	5.13	0.29	0.80	1.86	9.13	5.67	0.30	0.06	0.24	0.16
97018	8	54.92	1.02	19.76	5.34	0.27	0.85	1.97	9.27	5.73	0.34	0.08	0.14	0.14
97018	9	55.27	0.98	19.90	5.33	0.24	0.81	1.79	8.99	5.70	0.28	0.06	0.32	0.14
97018	10	54.76	1.08	19.99	5.39	0.27	0.83	1.83	9.17	5.66	0.30	0.05	0.30	0.17
97018	11	54.99	1.04	19.90	5.35	0.25	0.83	1.86	9.08	5.65	0.38	0.06	0.24	0.17
97018	12	55.30	0.91	19.71	5.25	0.27	0.85	1.81	9.02	5.83	0.33	0.08	0.30	0.15
97018	13	55.10	1.02	19.84	5.43	0.29	0.86	1.92	9.11	5.58	0.25	0.10	0.14	0.17
97018	14	55.18	1.05	19.99	5.45	0.29	0.78	1.86	8.99	5.46	0.30	0.07	0.24	0.16
97018	15	54.89	1.03	19.96	5.41	0.31	0.83	1.96	8.88	5.66	0.31	0.10	0.34	0.15
97018	16	55.06	0.99	19.74	5.36	0.28	0.82	1.82	9.13	5.73	0.34	0.06	0.28	0.20
97018	17	55.24	1.07	19.76	5.31	0.27	0.79	1.93	9.01	5.61	0.27	0.10	0.30	0.16
97018	18	54.97	1.03	19.76	5.45	0.23	0.82	1.85	9.11	5.71	0.30	0.10	0.30	0.15
1999bomb	1	55.30	0.99	19.66	5.51	0.34	0.81	1.83	8.95	5.73	0.36	0.07	0.11	0.15
1999bomb	2	55.12	1.02	19.85	5.29	0.30	0.81	1.88	9.10	5.63	0.28	0.07	0.29	0.16
1999bomb	3	55.12	1.03	19.90	5.43	0.32	0.86	1.82	8.90	5.69	0.29	0.05	0.24	0.18
1999bomb	4	55.09	0.98	19.87	5.16	0.31	0.86	1.83	9.26	5.68	0.28	0.08	0.24	0.16
1999bomb	5	54.54	1.09	19.91	5.80	0.22	0.90	2.01	9.11	5.48	0.31	0.08	0.21	0.14
1999bomb	6	55.10	1.01	19.69	5.42	0.24	0.83	1.88	9.11	5.71	0.30	0.10	0.25	0.15
1999bomb	7	54.55	0.99	20.13	5.54	0.31	0.79	1.92	9.15	5.74	0.32	0.10	0.13	0.15
1999bomb	8	55.15	1.04	19.87	5.24	0.28	0.84	1.87	9.06	5.75	0.27	0.07	0.20	0.18
1999bomb	9	55.00	1.02	19.61	5.36	0.28	0.86	1.80	9.10	5.69	0.36	0.08	0.52	0.15
1999bomb	10	55.43	1.07	19.59	5.29	0.28	0.77	1.85	9.11	5.69	0.28	0.06	0.28	0.14
1999bomb	11	55.03	1.02	19.87	5.30	0.30	0.82	1.82	9.21	5.65	0.32	0.10	0.18	0.18
1999bomb	12	55.25	1.05	19.91	5.12	0.31	0.82	1.80	8.97	5.79	0.36	0.07	0.19	0.16
1999bomb	13	54.80	0.95	20.11	5.44	0.24	0.80	1.81	9.31	5.63	0.24	0.06	0.28	0.15
1999bomb	14	54.82	1.05	19.80	5.48	0.27	0.85	1.86	9.25	5.64	0.32	0.10	0.23	0.14
1999bomb	15	54.92	1.08	19.76	5.35	0.23	0.81	1.82	9.30	5.66	0.32	0.09	0.35	0.13
1999bomb	16	54.83	0.98	19.81	5.41	0.29	0.90	2.00	9.12	5.76	0.28	0.07	0.22	0.17
Dec2000	1	54.99	0.94	19.93	5.41	0.27	0.90	1.85	9.18	5.67	0.27	0.07	0.17	0.18
Dec2000	2	54.80	1.05	19.90	5.27	0.26	0.85	1.95	9.23	5.73	0.31	0.10	0.20	0.17
Dec2000	3	54.83	1.11	19.93	5.54	0.28	0.87	1.87	9.03	5.74	0.19	0.05	0.22	0.15
Dec2000	4	54.96	1.10	19.93	5.28	0.29	0.86	1.81	9.18	5.73	0.29	0.07	0.16	0.15
Dec2000	5	55.05	0.99	19.53	5.44	0.27	0.83	1.86	9.27	5.79	0.32	0.08	0.24	0.13
Dec2000	6	54.73	1.01	20.06	5.35	0.26	0.79	1.89	9.25	5.83	0.28	0.07	0.13	0.17
Dec2000	7	54.42	0.98	20.22	5.45	0.32	0.84	1.88	9.30	5.67	0.27	0.09	0.21	0.18
Dec2000	8	54.49	1.08	20.14	5.52	0.29	0.81	1.89	9.16	5.72	0.25	0.08	0.23	0.16
Dec2000	9	54.79	1.02	19.74	5.36	0.26	0.89	1.96	9.29	5.69	0.31	0.10	0.25	0.13
Dec2000	10	54.46	0.95	19.82	5.70	0.29	0.83	1.97	9.24	5.78	0.26	0.08	0.24	0.15
Dec2000	11	54.55	0.99	20.04	5.41	0.30	0.84	1.90	9.25	5.75	0.37	0.08	0.20	0.14
E2001	1	55.18	1.10	20.05	5.26	0.27	0.81	1.72	8.98	5.72	0.32	0.04	0.20	0.16
E2001	2	55.26	0.99	19.74	5.38	0.30	0.80	1.95	8.95	5.66	0.32	0.09	0.23	0.15
E2001	3	54.86	1.04	20.10	5.37	0.26	0.82	1.74	9.22	5.66	0.33	0.07	0.17	0.16
E2001	4	55.05	1.02	19.70	5.49	0.26	0.83	1.93	9.20	5.63	0.27	0.07	0.19	0.14
E2001	5	55.04	1.00	20.03	5.38	0.30	0.83	1.80	9.05	5.59	0.26	0.10	0.30	0.15

Sample	n	SiO_2	TiO_2	Al_2O_3	FeO*	MnO	MgO	CaO	Na_2O	K_2O	P_2O_5	SO_2	F	Cl
E2001	6	54.96	1.05	19.65	5.60	0.27	0.83	1.82	9.08	5.71	0.24	0.11	0.27	0.18
E2001	7	55.01	0.97	19.84	5.39	0.19	0.82	1.87	9.12	5.78	0.31	0.10	0.24	0.15
E2001	8	54.94	0.99	19.99	5.31	0.26	0.78	1.89	9.14	5.76	0.26	0.08	0.22	0.18
E2001	9	54.59	1.00	20.16	5.37	0.29	0.83	1.90	9.39	5.56	0.27	0.05	0.22	0.17
E2001	10	54.78	1.04	20.08	5.32	0.26	0.84	1.90	9.10	5.82	0.23	0.07	0.20	0.16
E2001	11	54.44	1.03	20.14	5.50	0.35	0.85	1.87	9.20	5.73	0.27	0.09	0.18	0.15
E2001	12	54.92	0.99	19.70	5.57	0.31	0.81	1.87	9.23	5.56	0.29	0.07	0.30	0.18
E2001	13	54.45	1.02	20.13	5.39	0.32	0.85	1.91	9.24	5.78	0.31	0.08	0.20	0.13
E2001	14	55.08	1.00	19.91	5.40	0.24	0.83	1.91	9.20	5.58	0.28	0.08	0.14	0.16
E2001	15	55.03	1.06	19.87	5.31	0.29	0.87	1.87	9.10	5.65	0.27	0.10	0.26	0.14
E2001	16	55.21	1.07	19.91	5.32	0.29	0.83	1.84	9.01	5.59	0.24	0.11	0.21	0.18
E2001	17	54.71	1.04	20.05	5.42	0.28	0.88	1.85	9.19	5.67	0.28	0.10	0.17	0.16
E2001	18	55.07	1.02	19.94	5.33	0.28	0.75	1.89	8.93	5.71	0.33	0.09	0.33	0.13
E2001	19	54.95	1.05	19.63	5.37	0.31	0.88	1.97	9.11	5.71	0.36	0.09	0.19	0.16
E2001	20	55.22	0.97	19.84	5.35	0.29	0.86	1.97	9.14	5.49	0.31	0.08	0.15	0.15
Jan2004	1	54.95	1.01	19.94	5.38	0.28	0.80	1.93	9.04	5.68	0.26	0.07	0.32	0.14
Jan2004	2	54.88	1.02	20.00	5.44	0.32	0.85	1.95	8.96	5.60	0.33	0.08	0.20	0.18
Jan2004	3	55.33	1.04	19.64	5.34	0.30	0.81	1.88	9.13	5.61	0.25	0.09	0.23	0.16
Jan2004	4	54.42	1.00	19.94	5.59	0.25	0.87	1.95	9.23	5.69	0.32	0.08	0.30	0.16
Jan2004	5	55.08	1.03	19.71	5.48	0.20	0.79	1.97	8.99	5.72	0.30	0.13	0.23	0.17
Jan2004	6	54.53	1.02	19.89	5.63	0.29	0.84	1.89	9.40	5.60	0.28	0.09	0.15	0.17
Jan2004	7	55.19	1.05	19.72	5.40	0.26	0.85	1.89	9.12	5.62	0.29	0.08	0.17	0.13
Jan2004	8	55.14	1.01	19.90	5.37	0.30	0.89	2.00	8.83	5.60	0.25	0.09	0.27	0.16
Jan2004	9	54.90	1.02	19.87	5.41	0.23	0.77	1.93	9.18	5.70	0.20	0.09	0.34	0.17
Jan2004	10	55.05	0.98	19.87	5.50	0.30	0.82	1.84	9.07	5.66	0.32	0.09	0.17	0.12
Jan2004	11	55.19	1.06	19.96	5.24	0.26	0.78	1.93	9.13	5.70	0.19	0.08	0.14	0.14
Jan2004	12	54.40	1.11	20.30	5.53	0.28	0.84	1.78	9.17	5.71	0.28	0.07	0.20	0.16
Jan2004	13	55.16	1.13	19.65	5.45	0.29	0.80	1.87	9.05	5.59	0.27	0.09	0.26	0.17
Jan2004	14	54.82	1.06	19.78	5.59	0.22	0.80	1.80	9.24	5.64	0.32	0.10	0.26	0.17
Jan2004	15	55.17	1.02	19.96	5.42	0.31	0.81	1.87	8.94	5.58	0.25	0.07	0.25	0.17

*Total Fe as FeO

n = number of analyses

Table D.8.3. Replicate analyses of matrix glass by ICP-MS and estimated analytical precision

Sample Name	80300G	80300g DUP	difference (absolute)	difference (%)	81401g	81401 DUP	difference (absolute)	difference (%)	84505g	84505g DUP	difference (absolute)	difference (%)	mean difference (n = 3) (%)
TiO2 (%)	1.02	1.06	0.03	3.3	1.04	1.03	0.01	0.79	1.02	1.11	0.08	7.8	4.0
Li (ppm)	32.9	29.0	3.9	12	28.1	28.5	0.4	1.3	28.6	29.4	0.8	2.9	5.3
Be	13.4	10.1	3.3	25	10.1	10.0	0.1	1.1	10.2	10.4	0.2	1.5	9.0
Sc	4.97	4.93	0.05	0.93	4.66	4.82	0.16	3.5	5.16	5.03	0.13	2.5	2.3
V	2.23	1.88	0.34	15	1.84	1.88	0.04	2.2	2.51	2.35	0.16	6.4	8.0
Co	2.43	2.10	0.32	13	2.06	2.10	0.04	1.7	2.22	2.66	0.44	20	12
Cu	6.3	7.4	1.1	18	11.8	11.8	0.1	0.58	13.5	9.3	4.2	31	17
Zn	159	162	3	1.6	165	161	3	1.9	180	174	6	3.2	2.2
Ga	31	32	1	2.6	31	31	0	0.25	39	33	7	18	6.8
Rb	147	138	9	6.4	140	138	1	1.1	142	138	4	3.0	3.5
Sr	262	264	2	0.6	246	244	2	1.0	264	282	18	7.0	2.9
Y	85.1	80.8	4.3	5.1	80.2	79.5	0.7	0.83	80.3	89.6	9.3	12	5.8
Zr	1638	1573	65	4.0	1552	1546	6	0.36	1587	1564	24	1.5	1.9
Nb	420	410	10	2.3	408	405	4	0.9	409	408	0	0.08	1.1
Cs	2.02	1.79	0.23	11	1.79	1.77	0.02	1.2	2.00	1.78	0.22	11	7.8
Ba	472	457	15	3.2	440	432	8	1.8	469	462	7	1.5	2.2
La	164	163	1	0.9	162	159	3	1.9	165	184	19	11	4.7
Ce	316	314	2	0.7	315	307	9	2.8	314	356	43	14	5.7
Pr	33.3	34.4	1.1	3.3	33.7	33.1	0.6	1.9	33.2	39.5	6.3	19	8.1
Nd	111	112	2	1.6	111	108	3	2.3	109	131	22	21	8.2
Sm	19.0	19.4	0.3	1.8	19.0	18.8	0.2	1.1	18.5	22.8	4.2	23	8.6
Eu	3.72	3.73	0.02	0.47	3.66	3.60	0.06	1.8	3.66	4.20	0.54	15	5.7
Gd	16.8	14.6	2.2	13	14.5	14.2	0.2	1.5	14.2	17.0	2.8	19	11
Tb	2.63	2.34	0.29	11	2.35	2.33	0.02	0.91	2.28	2.69	0.41	18	9.9
Dy	14.50	13.50	1.00	6.9	13.41	13.20	0.22	1.6	13.22	14.84	1.63	12	6.9
Ho	2.85	2.70	0.15	5.4	2.68	2.64	0.03	1.3	2.68	2.92	0.24	8.9	5.2
Er	7.94	7.67	0.27	3.4	7.67	7.54	0.13	1.7	7.68	8.29	0.61	7.9	4.3
Tm		1.17			1.17	1.16	0.00	0.17	1.21	1.24	0.03	2.4	1.3
Yb	7.70	7.30	0.40	5.2	7.31	7.25	0.06	0.82	7.34	7.68	0.34	4.6	3.5
Lu	1.19	1.15	0.05	4.0	1.15	1.14	0.01	0.65	1.13	1.18	0.05	4.3	3.0
Hf	32.9	30.9	1.9	5.8	30.7	30.4	0.3	0.86	30.2	30.6	0.4	1.2	2.6
Ta	24.8	22.5	2.4	9.5	22.5	22.4	0.2	0.68	22.8	22.1	0.7	3.0	4.4
Pb	8.07	7.49	0.58	7.2	6.73	6.60	0.13	1.9	7.80	7.10	0.71	9.0	6.0
Th	34.6	29.1	5.5	16	29.8	29.3	0.5	1.6	29.6	28.8	0.9	3.0	6.8
U	10.0	8.71	1.3	13	9.01	8.76	0.2	2.7	9.04	8.65	0.4	4.3	6.8

Appendix E. Oxygen isotope analyses

Table E.1. Oxygen Isotope Standard Analyses

	n	Mean measured $\delta^{18}O$ (SMOW)	1σ	Accepted Value $\delta^{18}O$ (SMOW)
Capitan quartz	9	8.47	0.14	*NMT in house*
NBS-28	9	9.39	0.21	9.64

Table E.2. Oxygen Isotope Analyses

Sample	Type	Material	δ18O (‰)‡	replicate difference (‰)
84505G	bomb	glass	5.19	0.191
84505G DUP	bomb	glass	5.38	
85010G	bomb	glass	5.58	0.014
85010G DUP	bomb	glass	5.56	
86024AN	an. phonolite lava	anorthoclase	5.98	0.112
86024AN DUP	an. phonolite lava	anorthoclase	5.87	
82416AN	bomb	anorthoclase	5.79	0.115
82416 DUP	bomb	anorthoclase	5.67	
84505AN	bomb	anorthoclase	5.67	0.193
84505AN DUP	bomb	anorthoclase	5.86	
85010AN	bomb	anorthoclase	5.78	0.173
85010AN DUP	bomb	anorthoclase	5.95	
JAN2004AN	bomb	anorthoclase	5.68	0.049
JAN2004AN DUP	bomb	anorthoclase	5.73	

*G = glass, AN = anorthoclase, DUP = duplicate

‡Corrected to NBS-28

Table E.3. Oxygen isotope analytical data

Date: 6/6/2005

Vessel	Sample ID	Type	Sample wt. (mg)	µmoles O_2	PO_2	PCO_2	µmoles CO_2	yield (%)
1	Capitan Qtz	Quartz	13.62	226.092	0.227	1.317	209.469	92.65
2	Capitan Qtz	Quartz	14.27	236.882	0.262	1.525	243.262	102.69
4	Capitan Qtz	Quartz	13.75	228.250	0.242	1.441	229.591	100.59
5	Capitan Qtz	Quartz	14.60	242.360	0.228	1.503	239.678	98.89
6	Capitan Qtz	Quartz	14.73	244.518	0.285	1.543	246.195	100.69
8	Capitan Qtz	Quartz	14.21	235.886	0.257	1.529	243.914	103.40
9	Capitan Qtz	Quartz	13.80	229.080	0.245	1.473	234.795	102.49
11	Capitan Qtz	Quartz	14.51	240.866	0.256	1.532	244.403	101.47
12	Capitan Qtz	Quartz	14.22	236.052	0.275	1.536	245.054	103.81

Date: 6/7/2005

Vessel	Sample ID	Type	Sample wt. (mg)	µmoles O_2	PO_2	PCO_2	µmoles CO_2	yield (%)
1	NBS-28	Quartz	10.56	175.296	0.191	1.122	177.964	101.52
2	NBS-28	Quartz	11.21	191.232	0.206	1.182	187.640	100.83
4	NBS-28	Quartz	11.52	181.106	0.212	1.259	200.080	104.63
5	NBS-28	Quartz	10.91	190.900	0.200	1.153	182.961	101.02
6	NBS-28	Quartz	11.50	196.046	0.212	1.265	201.051	105.32
8	NBS-28	Quartz	11.81	196.378	0.278	1.310	208.335	106.27
9	NBS-28	Quartz	11.83	210.322	0.227	1.300	206.716	105.26
11	NBS-28	Quartz	12.67	210.322	0.219	1.387	220.820	104.99
12	NBS-28	Quartz	11.90	197.540	0.284	1.291	205.258	103.91

Date: 6/8/2005

Vessel	Sample ID	Type	Sample wt. (mg)	µmoles O_2	PO_2	PCO_2	µmoles CO_2	yield (%)
1	85010g	matrix glass	14.58	242.028	0.227	1.335	212.386	87.75
2	85010g	matrix glass	16.63	276.058	0.263	1.500	239.190	86.64
4	85010An	feldspar	17.59	262.950	0.296	1.693	270.698	102.95
5	85010An	feldspar	18.48	276.257	0.306	1.670	266.934	96.63
6	82416An	feldspar	17.52	260.411	0.310	1.636	261.375	100.37
11	86024An	feldspar	18.74	280.144	0.257	1.664	265.953	94.93
12	86024An	feldspar	17.97	268.633	0.296	1.750	280.035	104.24

Date: 6/8/2005

Vessel	Sample ID	Type	Sample wt. (mg)	µmoles O_2	PO_2	PCO_2	µmoles CO_2	yield (%)
1	84505g	matrix glass	15.83	262.778	0.224	1.475	235.121	89.48
2	84505g	matrix glass	15.50	276.058	0.239	1.444	230.079	83.34
4	84505An	feldspar	16.30	243.668	0.244	1.579	252.067	103.45
5	84505An	feldspar	16.58	247.854	0.226	1.520	242.447	97.82
6	82416An	feldspar	18.06	269.978	0.264	1.711	273.645	101.36
11	Jan2004An	feldspar	14.48	216.461	0.217	1.416	225.529	104.19
12	Jan2004An	feldspar	17.03	254.581	0.260	1.595	254.678	100.04

Figure E.1. Oxygen isotope analyses vs. eruption year

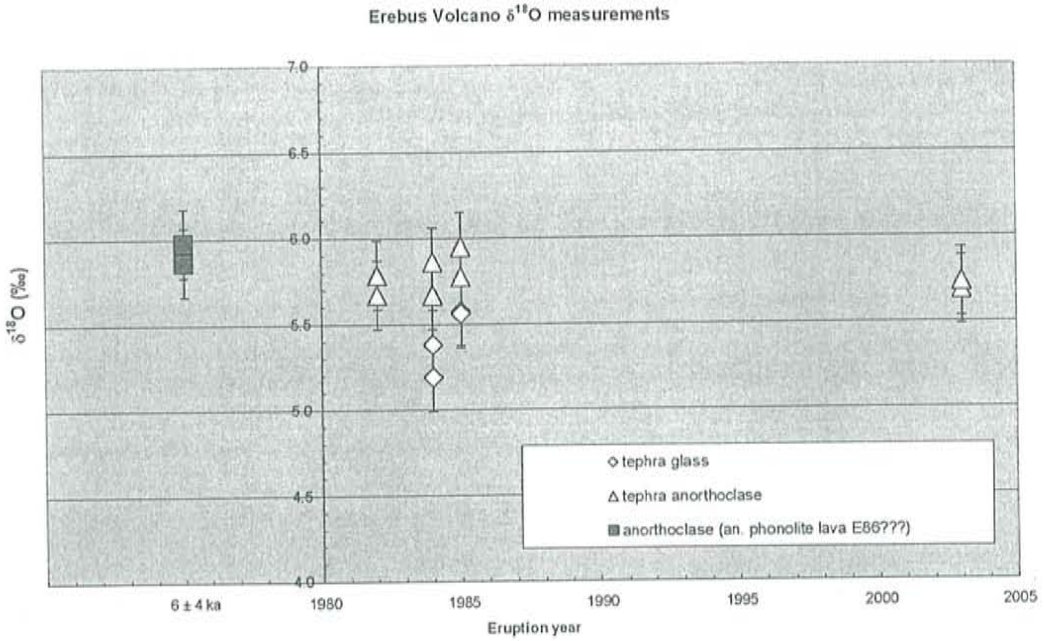

Appendix F. $^{40}Ar/^{39}Ar$ analyses

Table F.1 lists the analytical data from $^{40}Ar/^{39}Ar$ analysis of 9 samples. Two samples (Bomb Peak - Laser & Unknown Sample "E87024") are not discussed in thesis Part B. Oxygen isotopes were measured on anorthoclase from Unknown Sample "E87024" and its age is cited in thesis Part A. The samples is referred to as "E87???".

Anorthoclase samples from Bomb Peak were analyzed by furnace (L#55352) and CO_2 laser (Figure F1; L#55348) to determine the best method of Ar extraction. Both methods yielded comparable, analytically indistinguishable ages (Table F1). The furnace sample released Ar in many steps, whereas the laser sample released more than 80% of its ^{39}Ar in a single step (step B, 4 watts; Table F1). In order to take advantage of the step-heating method the furnace was chosen for all other analyses.

Sample E86024 yielded a concordant, precise age spectrum that is geologically unreasonable. E86024 should be a sample from the "Old Caldera Rim". Other age data and field relationships strongly suggest this sample should be at least < 20 ka. The most plausible explanation is that the sample was mislabeled or switched at some point. The step heating data are shown in Table A1 and the age spectrum is shown in Figure F2.

Inverse isochron diagrams for the samples are shown in figure F3.

Table F.1. $^{40}Ar/^{39}Ar$ analytical data

ID	Power (Watts)	$^{40}Ar/^{39}Ar$	$^{37}Ar/^{39}Ar$	$^{36}Ar/^{39}Ar$ (x 10^{-3})	$^{39}Ar_K$ (x 10^{-15} mol)	K/Ca	$^{40}Ar^*$ (%)	^{39}Ar (%)	Age (Ma)	±1□ (Ma)
Bomb (Laser), Anorthoclase, J=0.0001187±0.25%, D=1.0055±0.001, NM-180x, Lab#=55348-01										
xi A	2	5.926	0.2475	20.46	6.45	2.1	-1.8	7.3	-0.023	0.019
B	4	1.418	0.2101	4.388	71.7	2.4	9.0	88.6	0.027	0.002
C	6	1.903	0.1956	5.672	6.47	2.6	12.2	95.9	0.049	0.009
D	8	3.636	0.1931	11.77	1.61	2.6	4.5	97.7	0.035	0.030
E	10	6.213	0.1970	21.78	0.856	2.6	-3.5	98.7	-0.047	0.047
Xi F	12	9.820	0.1972	31.19	0.623	2.6	6.2	99.4	0.130	0.069
Xi G	16	18.48	0.1965	61.75	0.546	2.6	1.3	100.0	0.05	0.10
Integrated age ± 2□			n=7		88.2	2.4 ±0.0			0.025	0.006
Plateau ± 2□	steps B-E		n=4	MSWD=2.70	80.6	2.4 ±0.2		91.4	0.028	0.007
Isochron±2□	steps B-E		n=4	MSWD=4.03		$^{40}Ar/^{36}Ar$=	293.7±20.3		0.030	0.014
Bomb (Furnace), Anorthoclase, 309.8 mg, J=0.0001183±0.25%, D=1.0055±0.001, NM-180x, Lab#=55352-01										
Xi A	500	146.4	0.2616	489.9	0.830	2.0	1.1	0.2	0.35	0.20
Xi B	600	6.864	0.2258	22.67	11.3	2.3	2.5	3.4	0.036	0.009
Xi C	650	2.454	0.2254	7.661	21.8	2.3	8.0	9.7	0.042	0.004
Xi D	700	1.727	0.2223	5.256	23.2	2.3	10.5	16.3	0.038	0.003
E	750	1.372	0.2199	4.329	47.6	2.3	7.3	29.8	0.021	0.002
F	800	1.171	0.2187	3.652	53.6	2.3	8.5	45.1	0.021	0.002
G	900	1.326	0.2146	4.103	96.2	2.4	9.1	72.6	0.025	0.002
Xi H	1000	2.087	0.2097	6.550	61.9	2.4	7.5	90.2	0.033	0.003
Xi I	1100	5.188	0.2107	16.53	21.9	2.4	5.9	96.4	0.066	0.006
Xi J	1200	10.21	0.2184	33.04	6.59	2.3	4.9	98.3	0.107	0.017
Xi K	1300	7.612	0.2565	23.46	5.09	2.0	9.1	99.8	0.148	0.014
Xi O	1700	12.98	0.4919	39.46	0.789	1.0	10.5	100.0	0.290	0.055
Integrated age ± 2□			n=12		350.8	2.3 ±0.0	K2O=3.68%		0.035	0.005
Plateau ± 2□	steps E-G		n=3	MSWD=2.43	197.4	2.4 ±0.1		56.3	0.023	0.003
Isochron±2□	steps E-G		n=3	MSWD=4.05		$^{40}Ar/^{36}Ar$=	310.7±35.8		0.010	0.009
E87040, Anorthoclase, 265.36 mg, J=0.000126±0.25%, D=1.0055±0.001, NM-180z, Lab#=55363-01										
Xi A	600	7.714	0.3801	27.10	13.0	1.3	-3.6	6.6	-0.063	0.025
xi B	650	1.424	0.3543	4.802	21.5	1.4	1.6	17.5	0.005	0.007
xi C	700	1.110	0.3512	3.697	20.1	1.5	3.1	27.7	0.008	0.009
xi D	750	1.099	0.3441	4.348	12.1	1.5	-15.7	33.8	-0.039	0.010
E	800	1.152	0.3513	3.937	30.0	1.5	0.4	49.0	0.001	0.008
F	900	1.238	0.3589	4.335	40.1	1.4	-2.1	69.4	-0.006	0.005
G	1000	1.328	0.3479	4.595	33.2	1.5	-1.0	86.2	-0.003	0.007
H	1100	2.452	0.3283	8.340	13.3	1.6	0.1	93.0	0.001	0.016
Xi I	1200	6.334	0.3267	19.83	7.08	1.6	8.2	96.6	0.117	0.029
Xi J	1700	4.678	0.3659	13.35	6.69	1.4	16.2	100.0	0.172	0.025
Integrated age ± 2□			n=10		197.1	1.4 ±0.0	K2O=2.26%		0.003	0.008
Plateau ± 2□	steps E-H		n=4	MSWD=0.19	116.7	1.5 ±0.1		59.2	-0.003	0.007
Isochron±2□	steps E-H		n=4	MSWD=0.28		$^{40}Ar/^{36}Ar$=	298.3±34.2		-0.006	0.015
E86003, Anorthoclase, 357 mg, J=0.0001364±0.25%, D=1.0055±0.001, NM-180y, Lab#=55374-01										
xi A	600	2.733	0.2254	9.281	36.2	2.3	-0.1	11.6	-0.001	0.010
B	650	1.359	0.2163	4.485	31.4	2.4	2.9	21.7	0.010	0.007
C	700	1.325	0.2138	4.359	32.8	2.4	3.2	32.2	0.010	0.008
D	750	1.463	0.2075	4.599	19.4	2.5	7.5	38.4	0.027	0.011
E	800	1.558	0.2162	5.024	40.8	2.4	5.1	51.6	0.020	0.006
F	900	1.638	0.2190	4.977	52.1	2.3	10.7	68.3	0.043	0.006
G	1000	1.890	0.2172	6.191	25.7	2.3	3.5	76.5	0.016	0.009
Xi H	1100	2.004	0.2306	6.453	35.0	2.2	5.2	87.8	0.026	0.009
Xi I	1200	4.526	0.2230	13.17	13.5	2.3	14.7	92.1	0.163	0.017
Xi J	1700	1.678	0.2315	4.991	24.6	2.2	12.6	100.0	0.052	0.008
Integrated age ± 2□			n=10		311.5	2.3 ±0.0	K2O=2.46%		0.028	0.006
Plateau ± 2□	steps B-G		n=6	MSWD=3.70	202.2	2.4 ±0.1		64.9	0.023	0.012
Isochron±2□	steps B-G		n=6	MSWD=3.69		$^{40}Ar/^{36}Ar$=	341.9±55.4		-0.033	0.018

Table F1. (continued)

E86031, Anorthoclase, 272.8 mg, J=0.0001184±0.25%, D=1.0055±0.001, NM-180y, Lab#=55370-01

xi	A	600	21.66	1.013	71.54	9.38	0.50	2.7	7.9	0.127	0.023
	B	650	3.670	0.9086	10.01	22.2	0.56	21.2	26.7	0.166	0.004
	C	700	3.403	0.8533	8.744	11.0	0.60	25.9	36.0	0.188	0.006
	D	750	2.569	0.8204	6.699	4.33	0.62	25.2	39.6	0.138	0.010
	E	800	2.862	0.8288	7.290	12.8	0.62	26.8	50.5	0.163	0.005
	F	900	2.900	0.8300	7.138	16.6	0.61	29.3	64.5	0.181	0.004
	G	1000	2.960	0.9302	7.529	9.24	0.55	27.2	72.3	0.171	0.007
xi	H	1100	2.462	1.017	5.615	17.0	0.50	35.7	86.6	0.187	0.004
xi	I	1200	7.253	0.9834	19.98	4.00	0.52	20.2	90.0	0.313	0.014
xi	J	1700	4.398	0.9791	7.827	11.8	0.52	49.1	100.0	0.461	0.005
	Integrated age ± 2□			n=10		118.3	0.56 ±0.0		K2O=1.41%	0.203	0.008
	Plateau ± 2□	steps B-G		n=6	MSWD=5.63	76.125	0.589±0.062		64.4	0.17	0.010
	Isochron±2□	steps B-G		n=6	MSWD=6.76		$^{40}Ar/^{36}Ar$=		302.2±17.8	0.160	0.026

E87025, Anorthoclase, 249.73 mg, J=0.0001182±0.25%, D=1.0055±0.001, NM-180x, Lab#=55347-01

xi	A	600	8.759	0.9244	29.88	10.5	0.55	-0.1	10.6	-0.001	0.012
	B	650	2.347	0.8885	7.628	18.0	0.57	6.6	28.7	0.033	0.004
	C	700	3.207	0.8514	9.950	6.62	0.60	10.2	35.3	0.069	0.007
	D	750	3.317	0.8436	11.35	4.17	0.60	0.6	39.5	0.004	0.010
	E	800	3.305	0.8576	10.97	8.14	0.59	3.8	47.7	0.026	0.008
	F	900	3.668	0.8213	11.94	14.2	0.62	5.3	62.0	0.042	0.006
xi	G	1000	5.347	0.8519	17.37	5.47	0.60	5.1	67.5	0.058	0.011
xi	H	1100	2.442	0.8964	7.337	13.4	0.57	13.9	81.1	0.072	0.005
xi	I	1200	4.794	0.9017	14.77	5.05	0.57	11.2	86.2	0.114	0.011
xi	J	1700	2.324	0.9258	6.396	13.7	0.55	21.6	100.0	0.107	0.005
	Integrated age ± 2□			n=10		99.3	0.58 ±0.0		K2O=1.29%	0.052	0.007
	Plateau ± 2□	steps B-F		n=5	MSWD=8.66	51.099	0.596±0.034		51.5	0.04	0.016
	Isochron±2□	steps B-F		n=5	MSWD=11.11		$^{40}Ar/^{36}Ar$=		303.7±14.6	0.022	0.007

Unknown Sample "E87024", Anorthoclase, 260.84 mg, J=0.0001199±0.25%, D=1.0055±0.001, NM-180w, Lab#=55355-01

	A	600	3.029	0.2976	10.28	33.2	1.7	0.1	16.4	0.001	0.004
	B	650	0.9794	0.2868	3.169	39.1	1.8	5.6	35.7	0.012	0.002
	C	700	1.053	0.2839	3.564	28.0	1.8	1.1	49.5	0.002	0.002
	D	750	1.061	0.2833	3.561	14.8	1.8	1.9	56.8	0.004	0.004
	E	800	1.273	0.2862	4.299	27.4	1.8	1.1	70.3	0.003	0.003
	F	900	1.823	0.2828	6.148	28.8	1.8	1.0	84.5	0.004	0.003
Xi	G	1000	2.353	0.2943	7.460	14.1	1.7	6.9	91.5	0.035	0.005
Xi	H	1100	2.991	0.2901	9.474	11.1	1.8	6.9	96.9	0.044	0.005
Xi	I	1200	9.416	0.2880	27.45	2.86	1.8	14.8	98.3	0.302	0.018
Xi	J	1700	6.195	0.4686	16.45	3.38	1.1	22.1	100.0	0.295	0.014
	Integrated age ± 2□			n=10		202.8	1.8	±0.0	K2O=2.49%	0.018	0.004
	Plateau ± 2□	steps A-F		n=6	MSWD=2.71	171.4	1.8	±0.1	84.5	0.006	0.004
	Isochron±2□	steps A-F		n=6	MSWD=2.54		$^{40}Ar/^{36}Ar$=		290.5±5.3	0.010	0.004

E87037, Anorthoclase, 344.84 mg, J=0.0001205±0.25%, D=1.0055±0.001, NM-180z, Lab#=55367-01

xi	A	600	14.25	0.3400	47.34	14.3	1.5	1.9	5.7	0.060	0.016
xi	B	650	2.272	0.3334	6.599	33.0	1.5	14.9	18.9	0.073	0.003
xi	C	700	2.020	0.3258	5.481	22.0	1.6	20.7	27.6	0.090	0.003
	D	750	1.754	0.3260	4.693	13.3	1.6	21.9	33.0	0.083	0.004
	E	800	1.654	0.3292	4.409	32.9	1.5	22.3	46.1	0.080	0.002
	F	900	1.572	0.3288	4.113	49.8	1.6	23.8	66.0	0.081	0.002
	G	1000	2.063	0.3299	5.782	20.6	1.5	18.0	74.2	0.080	0.004
Xi	H	1100	2.176	0.3414	5.908	30.4	1.5	20.6	86.3	0.097	0.003
Xi	I	1200	4.929	0.3333	12.50	18.1	1.5	25.9	93.5	0.276	0.005
Xi	J	1700	2.680	0.3542	6.785	16.2	1.4	26.0	100.0	0.151	0.004
	Integrated age ± 2□			n=10		250.5	1.5	±0.0	K2O=2.32%	0.100	0.005
	Plateau ± 2□	steps D-G		n=4	MSWD=0.16	116.6	1.6	±0.0	46.5	0.081	0.003
	Isochron±2□	steps D-G		n=4	MSWD=0.24		$^{40}Ar/^{36}Ar$=		296.1±23.2	0.080	0.022

Table F1. (continued)

Ice-Z, Anorthoclase, 326.9 mg, J=0.0001189±0.25%, D=1.0055±0.001, NM-180w, Lab#=55359-01

Xi	A	600	127.1	0.2093	439.6	0.739	2.4	-2.2	0.1	-0.60	0.16
Xi	B	650	10.73	0.1191	33.98	4.05	4.3	6.4	0.9	0.147	0.018
Xi	C	700	4.939	0.0863	14.00	4.17	5.9	16.2	1.7	0.171	0.011
Xi	D	750	3.553	0.0606	9.365	4.23	8.4	22.0	2.5	0.167	0.009
	E	800	2.598	0.0358	6.386	18.4	14.3	27.1	5.9	0.151	0.004
	F	900	1.942	0.0286	4.044	51.5	17.8	38.2	15.5	0.158	0.002
	G	1000	1.665	0.0285	3.166	73.0	17.9	43.6	29.1	0.154	0.002
	H	1100	1.503	0.0298	2.517	141.7	17.1	50.3	55.6	0.161	0.001
	I	1200	1.583	0.0289	2.800	104.2	17.6	47.6	75.0	0.160	0.001
	J	1700	1.493	0.0489	2.496	134.1	10.4	50.5	100.0	0.160	0.001
Integrated age ± 2□				n=10		536.2	14.2	±0.0	K2O=5.30%	0.158	0.003
Plateau ± 2□		steps E-J		n=6	MSWD=3.72	523.0	15.6	±6.0	97.5	0.159	0.002
Isochron±2□		steps E-J		n=6	MSWD=2.33		$^{40}Ar/^{36}Ar$=		283.3±7.9	0.167	0.005

Notes:

Isotopic ratios corrected for blank, radioactive decay, and mass discrimination, not corrected for interfering reactions.

Errors quoted for individual analyses include analytical error only, without interfering reaction or J uncertainties.

Integrated age calculated by summing isotopic measurements of all steps.

Integrated age error calculated by quadratically combining errors of isotopic measurements of all steps.

Plateau age is inverse-variance-weighted mean of selected steps.

Plateau age error is inverse-variance-weighted mean error (Taylor, 1982) times root MSWD where MSWD>1.

Plateau error is weighted error of Taylor (1982).

Decay constants and isotopic abundances after Steiger and Jäger (1977).

"X" or "x" symbol preceding sample ID denotes analyses excluded from plateau age calculations.

"i" symbol preceding sample ID denotes analyses excluded from inverse isochron calculations.

Weight percent K_2O calculated from ^{39}Ar signal, sample weight, and instrument sensitivity.

Ages calculated relative to FC-1 Fish Canyon Tuff sanidine interlaboratory standard at 28.02 Ma (Renne et al., 1998)

Decay Constant (LambdaK (total)) = 5.543e-10/a

Correction factors:

$(^{39}Ar/^{37}Ar)_{Ca}$ = 0.0007 ± 5e-05

$(^{36}Ar/^{37}Ar)_{Ca}$ = 0.00028 ± 1e-05

$(^{38}Ar/^{39}Ar)_{K}$ = 0.0125

$(^{40}Ar/^{39}Ar)_{K}$ = 0.0125 ± 0.0015

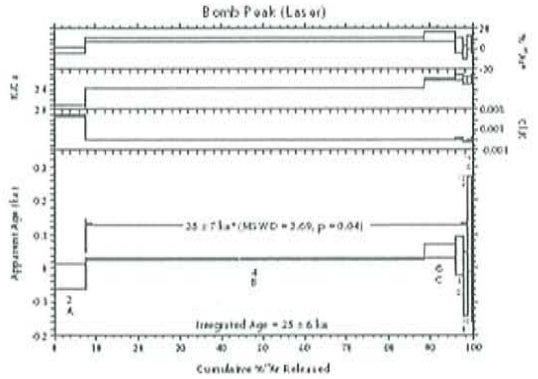

Figure F.1. $^{40}Ar/^{39}Ar$ result of step heating Bomb Peak sample using a CO_2 laser

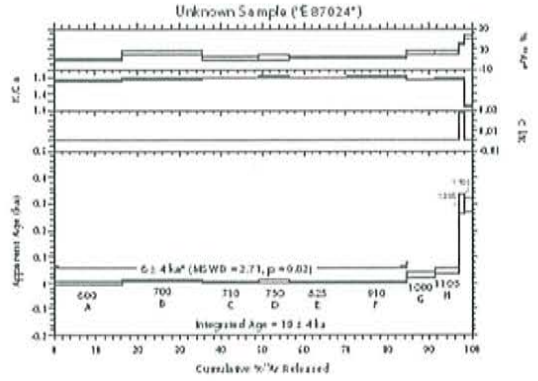

Figure F.2. $^{40}Ar/^{39}Ar$ result of furnace step heating unknown sample. The result gave a geologically unreasonable age for sample E87024.

Figure F.3. Isochron diagrams

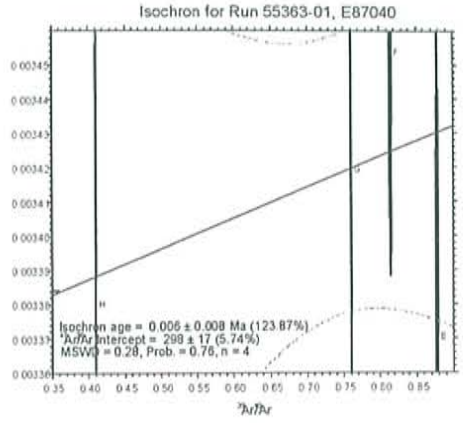

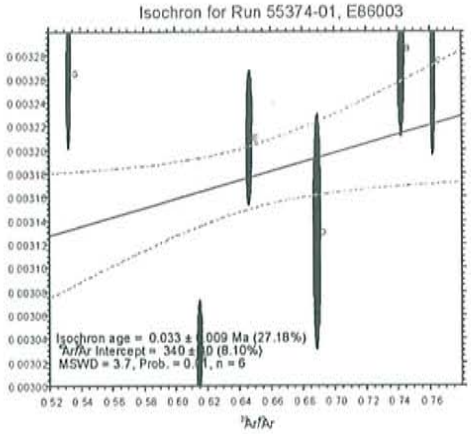

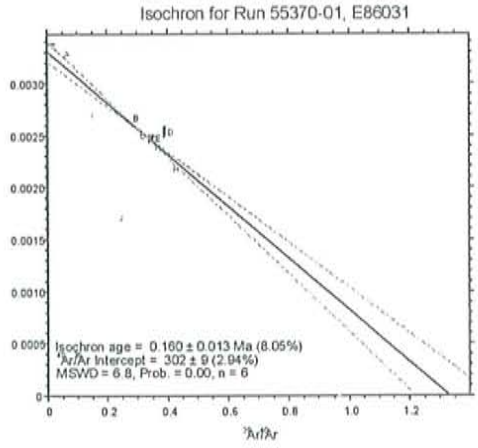

Figure F.3. (continued)

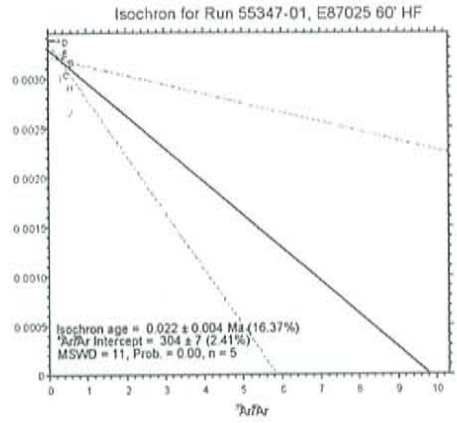

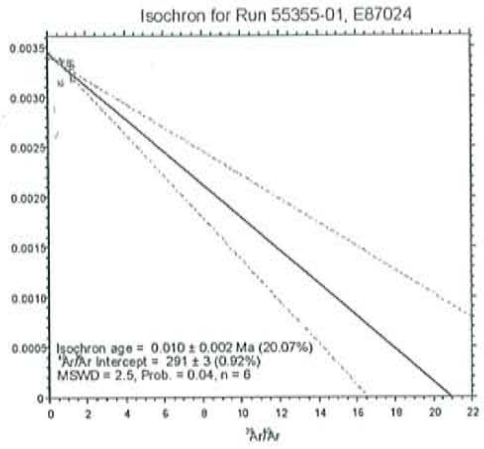

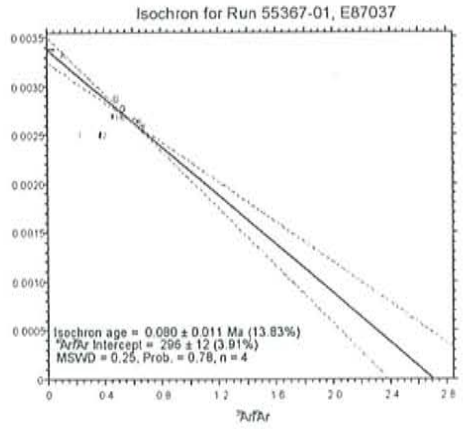

Figure F.3. (continued)

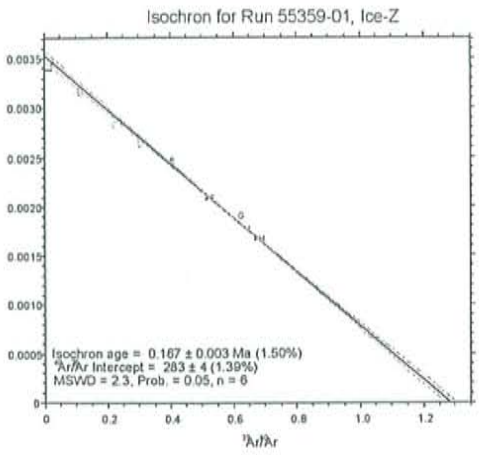

Appendix G. Comprehensive reference list

Albarède, F., 1993. Residence time analysis of geochemical fluctuations in volcanic series. Geochim. Cosmochim. Acta. 57, 615-621.

Allard, P., 1997. Endogenous magma degassing and storage at Mount Etna. Geophysical Research Letters 24, 2219-2222.

Allard, P., Carbonnelle, J., Metrich, N., Loyer, H., Zetttwoog, P., 1994. Sulfur output and magma degassing budget of Stromboli volcano. Nature 368, 326-330.

Anderson, D. J., Lindsley, D.H., 1988. Internally consistent solution models for Fe-Mg-Mn-ti oxides: Fe-Ti oxides. American Mineralogist 73, 714-726.

Andersen D. J., Lindsley D. H., Davidson P. M., 1993. QUILF: A Pascal program to assess equilibria among Fe-Mg-Mn-Ti oxides, pyroxenes, olivine, and quartz. Comp. Geosc. 19, 1333–1350.

Andres, R.J., Rose, W.I., Kyle, P.R., deSilva, S., Francis, P., Gardeweg, M., Moreno Roa, H., 1991. Excessive sulfur dioxide emissions from Chilean volcanoes. J. Volcanol. Geotherm. Res. 46, 323–329.

Armstrong, R.L., 1978. K-Ar dating: Late Cenozoic McMurdo Volcanic Group and dry valley glacial history, Victoria Land, Antarctica. NZ J Geol Geophys 21, 685–698.

Aster, R., Mah, S.Y., Kyle, P., McIntosh, W., Dunbar, N., Johnson, J., Ruiz, M., McNamara, S., 2003. Very long period oscillations of Mount Erebus volcano, J. Geophys. Res., 108 (B11), 2522, doi:10.1029/2002JB002101.

Aster, R., McIntosh, W., Kyle, P., Esser, R., Bartel, B., Dunbar, N., Johns, B., Johnson, J., Karstens, R., Kurnik, C., McGowan, M., McNamara, S., Meertens, C., Pauly, B., Richmond, M., Ruiz, M., 2004. New instrumentation delivers multidisciplinary real-time data from Mount Erebus, Antarctica. EOS trans. AGU., 85, no. 10, 9 March.

Bannister, S., Snieder, R.K., Passier, M.L., 2000. Shear-wave velocities under the Transantarctic Mountains and Terror Rift from surface wave inversion, Geophys. Res. Lett. 27, 281– 284.

Behrendt, J.C., LeMasurier, W.E., Cooper, A.K., Tessensohn, F., Trehu, A., Damaske, D., 1991. Geophysical studies of the West Antarctic rift system. Tectonics 10, 1257–1273.

Belkin, H. E., Kilburn, C.R.J., DeVivo, B., 1993. Sampling and major element chemistry of the Recent (A.D. 1631-1944) Vesuvius activity. J. Volcanol. Geotherm. Res. 58, 273–290.

Caldwell, D., Kyle, P.R., 1994. Mineralogy and geochemistry of ejecta erupted from Mount Erebus, Antarctica between 1972 and 1986, In: Kyle, P.R. (ed) Volcanological and Environmental Studies of Mount Erebus, Antarctica, Antarct. Res. Ser., vol. 66, Am Geophys Union, Washington, D.C. 147–162.

Cashman, K.V., 1990. Textural constraints on the kinetics of crystallization of igneous rocks. In: Nicholls, J., Russell, J.K. (eds) Reviews in mineralogy, vol. 24. Modern methods of igneous petrology, understanding magmatic processes. Mineral. Soc. Am., Washington, D.C. 259-314.

Cashman, K.V., Blundy, J., 2000. Degassing and crystallization of ascending andesite and dacite. Philos. Trans. R. Soc. London. Ser. A, 358, 1487-1513.

Chen, C.H., DePaolo, D.J., Nakada, S., Shieh, Y.N., 1993. Relationship between eruption volume and neodymium isotopic composition at Unzen volcano. Nature. 362, 831-834.

Cooper A.K., Davey F.J., Behrendt J.C., 1987. Seismic stratigraphy and structure of the Victoria Land basin, western Ross Sea, Antarctica. in: Cooper A.K., Davey F.J. (eds) The Antarctic Continental Margin: geology and geophysics of the western Ross Sea. Circum-Pacific Council for Energy and Resources, Houston, 27–65.

Cortés, J.A., Wilson, M., Condliffe, E., Francalanci, L., Chertkoff, D. G., 2005. The evolution of the magmatic system of Stromboli Volcano during the Vancori period (26 – 13.8 ky). J. Volcanol. Geotherm. Res. 147, 1-38.

Couch, S., 2003. Experimental investigation of crystallization kinetics in a haplogranite system. American Mineralogist. 88, 1471-1485.

Couch, S., Harford, C.L., Sparks, R.S.J., and Carroll, M.R., 2003a. Experimental constraints on andesite petrogenesis at the Soufrière Hills Volcano, Montserrat. Journal of Petrology. 44, 1455–1475.

Couch, S., Sparks, R.S.J., and Carroll, M.R., 2003b. The kinetics of degassing induced crystallization at Soufrière Hills Volcano, Montserrat. Journal of Petrology. 44, 1477–1502.

Craig, H., 1961. Standard for reporting concentrations of deuterium and oxygen-18 in natural waters. Science. 133, 1833-1834.

D'Alessandro, Giammanco, S., Parello, F., Valenza, 1997. CO_2 output and $\delta^{13}C(CO_2)$ from Mount Etna as indicators of degassing of shallow asthenosphere. Bull. Volcanol. 58, 455-458.

Devine, J.D., Rutherford, M.J., Norton, G.E., Young, S.R., 2003. Magma storage region processes inferred from geochemistry of Fe-Ti oxides in andesitic magma, Soufrière Hills Volcano, Montserrat, W.I. Journal of Petrology. 44, 1375-1400.

Dunbar, N., Cashman, K., Dupre, R., 1994. Crystallization processes of anorthoclase phenocrysts in the Mount Erebus magmatic system: Evidence from crystal composition, crystal size distributions and volatile contents of melt inclusions. In: Kyle, P.R. (ed.) Volcanological and Environmental Studies of Mount Erebus, Antarctica, Antarct. Res. Ser., 66, AGU, Washington, D. C. 129–146.

Eiler, J.M., 2001. Oxygen isotope variations of basaltic lavas and upper mantle rocks. In: Valley, J.W., Cole, D.R. (eds.), Stable Isotope Geochemistry, Reviews in mineralogy, 43. Min. Soc. Am., Washington, D.C. 319-364.

Elkins, L.T., Grove, T.L., 1990. Ternary feldspar experiments and thermodynamic models. American Mineralogist. 75, 544-559.

Eschenbacher, A. 1998. Open-system degassing of a fractionating, alkaline magma, Mount Erebus, Ross Island, Antarctica. Unpublished Master's Thesis, New Mexico Institute of Mining and Technology, Socorro.

Esser R.P., Kyle P.R., McIntosh W.C., 2004. $^{40}Ar/^{39}Ar$ dating of the eruptive history of Mount Erebus, Antarctica: Volcano evolution. Bull. Volcanol. 66, 671–686.

Esser R.P., McIntosh, W.C., Heizler, M.T., Kyle, P.R., 1997. Excess argon in melt inclusions in zero-age anorthoclase feldspar from Mt. Erebus, Antarctica, as revealed by the $^{40}Ar/^{39}Ar$ method. Geochim. Cosmochim. Acta. 61, 3789–3801.

Finn, C.A., Müller, R.D., Panter, K.S., 2005. A Cenozoic diffuse alkaline magmatic province (DAMP) in the southwest Pacific without rift or plume origin. Geochemistry Geophysics Geosystems. 6, Q02005, doi:10.1029/2004GC000723.

Francalanci, L., Tommasini, S., Conticelli, S., Davies, G. R., 1999. Sr isotope evidence for short magma residence time for the 20th century activity at Stromboli volcano, Italy. Earth. Planet. Sci. Lett. 167, 61-69.

Francalanci, L., Tommasini, S., Conticelli, S., 2004. The volcanic activity of Stromboli in the 1906-1998 AD period: mineralogical, geochemical and isotope data relevant to the understanding of the plumbing system. J. Volcanol. Geotherm. Res. 131, 179-211.
Francis, P., Oppenheimer, C., Stevenson, D., 1993. Endogenous growth of persistently active volcanoes. Nature. 366, 554-557.
Frost, R.B., Lindsley, D.H., Anderson, D.J., 1988. Fe-Ti oxide-silicate equilibria: Assemblages with fayalitic olivine. American Mineralogist, 73, 727-740.
Fujimaki, H., 1986. Partition coefficients of Hf, Zr, and REE between zircon, apatite, and liquid. Contrib. Min. Petrol. 94, 42-45.
Garcia, M.O., Pietruszka, A.J., Rhodes, J. M., 2003. A petrologic perspective of Kilauea Volcano's summit magma reservoir. Journal of Petrology. 44, 2313-2339.
Gerlach, T.M., McGee, K.A., 1994. Total sulfur dioxide emissions and pre-eruption vapor-saturated magma at Mt. St. Helens, 1980-99. Geophysical Research Letters 21, 2833-2836.
Geschwind, C., Rutherford, M.J., 1995. Crystallization of microlites during magma ascent; the fluid mechanics of 1980-1986 eruptions at Mount St. Helens. Bull. Volcanol. 57, 356-370.
Giggenbach, W., Kyle, P., Lyon, G., 1973. Present volcanic activity on Mt. Erebus, Ross Island, Antarctica. Geology. 1, 135– 156.
Goff, F., Love, S., Warren, R., Counce, d., Obenholzner, J., Seibe, C., and Schmidt, S., 2001. Passive infrared remote sensing evidence for large, intermittent CO_2 emissions at Popocatepetl volcano, Mexico. Chemical Geology. 177, 133-156.
Grêt, A., Snieder, R., Aster, R.C., Kyle, P.R., 2005. Monitoring rapid temporal change in a volcano with coda wave interferometry. Geophys Res Lett. 32, L06304, doi:10.1029/2004GL021143.
Hallett, R.B., 1994. Volcanic geology, paleomagnetism, geochronology and geochemistry of the Rio Puerco Necks, west-central New Mexico. Unpublished Ph.D thesis, New Mexico Institute of Mining and Technology, Socorro, New Mexico, U.S.A.
Hallett, R.B., Kyle, P.R., 1993. XRF and INAA determinations of major and trace elements in Geological Survey of Japan igneous and sedimentary rock standards. Geostandards Newsletter. 17, 127-133.
Halliday, A.N., Lee, D.-c., Tommasini, S., Davies, G.R., Paslick, C.R., Fitton, J.G., James, D.E. 1995. Incompatable trace elements in OIB and MORB and source enrichment in the sub-oceanic mantle. Earth. Plan. Sci, Lett. 133, 379-395.
Hammer, J.E., Cashman, K.V., Hoblitt, R.P., Newman, S., 1999. Degassing and microlite crystallization during pre-climatic events of the 1991 eruption of Mt. Pinitubo, Philippines. Bull. Volcanol. 60, 355-380.
Hammer, J.E., Cashman, K.V., Voight, B., 2000. Magmatic processes revealed by textural and compositional trends in Merapi dome lavas. J. Volcanol. Geotherm. Res. 100, 165-192.
Hammer, J.E., Rutherford, M.J., 2002. An experimental study of the kinetics of decompression-induced crystallization in silicic melt. J. Geophys. Res., DOI: 10.1029/2001JB000281.
Harpel, C.J., 2000. Late Quaternary eruptive history of Mount Erebus, Antarctica using $^{40}Ar/^{39}Ar$ geochronology and tephrostratigraphy. Master's Thesis, New Mexico Institute of Mining and Technology, Socorro
Harpel, C.J., Kyle P.R., Caldwell, D.A., McIntosh W.C., Esser R.P., 2004. $^{40}Ar/^{39}Ar$ dating of the eruptive history of Mount Erebus, Antarctica: summit flows and caldera collapse. Bull. Volcanol. 66, 687–702.
Harris, A.J.L., Flynn, L.P., Rothery, D.A., Oppenheimer, C., Sherman, S.B., 1999. Mass flux measurements at active lava lakes: Implications for magma recycling. J. Geophys. Res. 104, 7117-7136.
Hawkesworth, C., Blake, S., Evans, P., Hughes, R., MacDonald, R., Thomas, L.E., Turner, S.P., Zellmer, G., 2000. Time scales of crystal fractionation in magma chambers – integrating physical, isotopic and geochemical perspectives. Journal of Petrology. 41, 991-1006.
Hawkesworth, C., Rhiannon, G., Turner, S., Zellmer, G., 2004. Time scales of magmatic processes. Earth. Planet. Sci. Lett. 218, 1-16.
Higgins, M., 1998. Origin of anorthosite by textural coarsening: Quantitative measurements of a natural sequence of textural development. Journal of Petrology. 39, 1307-1323.
Hofmann, A.W., 1997. Mantle geochemistry: the message from oceanic volcanism. Nature. 385, 219-229.
Housh, T.B., Luhr, J.F., 1991. Plagioclase – melt equilibria in hydrous systems. American Mineralogist. 76, 477-492
Johannes, W., 1978. Melting of plagioclase in the system Ab-An-H_2O at $P_{H2O} \leq 5$ kbars, an equilibrium problem. Contrib. Miner. Petrol. 66, 295-303.
Kazahaya, K., Shinohara, H., Saito, G., 1994. Excessive degassing of Izu-Oshima volcano: magma degassing in a conduit. Bulletin of Volcanology 56, 207-216.
Kelly, P., et al., in prep. Open file report, NMGRL.
Kelley, K.A., Plank, T., Ludden, J., Staudigel, H., 2003. Composition of altered oceanic crust at ODP sites 801 and 1149. Geochemistry, Geophysics, Geosystems 4 (6). Doi:10.1029/2002GC000435.
Kirkpatrick, R.J., 1981. Kinetics of crystallization of igneous rocks. In: Lasaga, A.C., Kirkpatrick, R.J. (eds), Kinetics of geological processes. Reviews in mineralogy, 8. Mineral. Soc. Am., Washington, D.C. 321-398.
Klug, C., Cashman, K.V., 1994. Vesiculation of May 18, 1980, Mount St. Helens magma. Geology. 22, 468-472.
Kyle, P.R., 1976. Geology, mineralogy, and geochemistry of the Late Cenozoic McMurdo Volcanic Group, Victoria Land, Antarctica. Unpublished Ph.D Thesis, Dept. of Geology, Victoria University of Wellington, New Zealand.
Kyle P.R., 1977. Mineralogy and glass chemistry of recent volcanic ejecta from Mt. Erebus, Ross Island, Antarctica. NZ J Geol Geophys. 20, 1123–1146.
Kyle, P., 1986. Volcanic activity of Mount Erebus, 1984 – 1986, Antarct. J. U.S., XXI, 7– 8.
Kyle, P.R., 1990a. McMurdo Volcanic Group-Western Ross Embayment: introduction. in: LeMasurier, W., Thomson, J. (eds) Volcanoes of the Antarctic Plate and Southern Oceans. Antarctic Research Series. Am Geophys Union, Washington, DC. 18–25.
Kyle, P.R., 1990b. Erebus Volcanic Province. in: LeMasurier, W., Thomson, J. (eds) Volcanoes of the Antarctic Plate and Southern Oceans. Antarctic Research Series. Am Geophys Union, Washington, DC
Kyle P.R., Cole, J.W., 1974. Structural control of volcanism in the McMurdo Volcanic Group, Antarctica. Bull Volcanol. 38, 16–25.
Kyle, P., Dibble, R., Giggenbach, W., Keys, J., 1982. Volcanic activity associated with the anorthoclase phonolite lava lake, Mt. Erebus, Antarctica, in: C. Craddock (ed), Antarctic Geosciences, Univ. Wisc. Press, Madison, 735–745.
Kyle P.R., Moore J.A., Thirlwall M.F., 1992. Petrologic evolution of anorthoclase phonolite lavas at Mount Erebus, Ross Island, Antarctica. J. Petrol. 33, 849–875.

Landi, P., Metrich, N., Bertagnini, A., Rosi, M., 2004. Dynamics of magma mixing and degassing recorded in plagioclase at Stromboli (Aeolian Archipelago, Italy). Contrib. Min. Petrol. 147, 213-227.
Larsen, J.F., 2005. Experimental study of plagioclase rim growth around anorthite seed crystals in rhyodacitic melt. American Mineralogist. 90, 417-427.
LeBas, M.J., LeMaitre, R.W., Streckeisen, A., and Zanettin, B., 1986. A chemical classification of volcanic rocks based on the total alkali silica diagram. Journal of Petrology. 27, 745-750.
Le Guern, F., Carbonelle, J., Tazieff, H., 1979. Erte 'Ale lava lake: Heat and gas transfer to the atmosphere, J. Volcanol. Geotherm. Res. 6, 27– 48.
Loomis, T.P., Welber, P.W., 1982. Crystallization processes in the Rocky Hill granodiorite pluton, California: an interpretation based on compositional zoning of plagioclase. Contrib. Mineral. Petrol. 81, 230-239.
Marsh, B.D., 1989. Magma chambers. Annu. Rev. Earth. Planet. Sci. 17, 439-474.
Matsushita, Y., 1973. Oxygen isotope variations in magmatic differentiation processes of the volcanic rocks in Japan. Contrib. Mineral. Petrol. 39, 277-288.
Metrich, N., Rutherford, M.J., 1998. Low pressure crystallization paths of H_2O-saturated basaltic-hawaiitic melts from Mt. Etna; implications for open-system degassing of basaltic volcanoes. Geochim. Cosmochim. Acta. 62, 1195-1205.
Moore J.A., 1986. Mineralogy, geochemistry and petrogenesis of the lavas of Mount Erebus, Antarctica. Unpublished Master's Thesis, New Mexico Institute of Mining and Technology, Socorro, U.S.A.
Moore, J.A., Kyle, P.R., 1987. Volcanic geology of Mount Erebus, Ross Island, Antarctica. Proceedings of the NIPR symposium on Antarctic Geosciences, Tokyo, Japan, Vol.1, 48–65.
Morgan, D.J., Blake, S, 2006. Magmatic residence times of zoned phenocrysts: introduction and application of the binary element diffusion modelling (BEDM) technique. Contrib. Miner. Petrol. 151, 58-70.
Muehlenbachs, K., Byerly, G., 1982. ^{18}O-enrichment of silicic magmas caused by crystal fractionation at the Galapagos spreading center. Contrib. Miner. Petrol. 79, 76-79.
Nakamura, M., 1995. Continuous mixing of crystal mush and replenished magma in the ongoing Unzen eruption. Geology 23, 807–810.
Nekvasil, H., 1992. Tertiary feldspar crystallization in high-temperature felsic magmas. American Mineralogist. 77, 592-604.
Oppenheimer, C., McGonigle, A.J.S., Allard, P., Wooster, M.J., Tsanev, V., 2004. Sulfur, heat, and magma budget of Erta 'Ale lava lake, Ethiopia. Geology 32, 509-512.
Panter, K.S., Hart, S.R., Kyle, P., Blusztanjn, J., Wilch, T., 2000. Geochemistry of Late Cenozoic basalts from the Crary Mountains: characterization of mantle sources in Marie Byrd Land, Antarctica. Chemical Geology 165, 2000.
Panter, K.S., Blusztajn, J., Hart, S.R., Kyle, P.R., Esser, R., McIntosh, W.C., 2006. The Origin of HIMU in the SW Pacific: Evidence from Intraplate Volcanism in Southern New Zealand and Subantarctic Islands. Journal of Petrology (in press).
Pearce, T. H., 1994. Recent work on oscillatory zoning in plagioclase. In: Parsons, I (ed.) Feldspars and their reactions. NATO ASI Series. 421, 313-349.
Powers, H., 1955. Composition and origin of basaltic magma of the Hawaiian Islands. Geochim. Cosmochim. Acta. 7, 77-107.
Reagan, M., Gill, J., Malavassi, E., Garcia, M. O., 1987. Changes in magma composition at Arenal volcano, Costa Rica, 1968-1985: Real-time monitoring of open-system differentiation. Bull. Volcanol. 49, 415-434.
Renne, P.R., Swisher, C.C., Deino, A.L., Karner, D.B., Owens, T.L., DePaolo, D.J., 1998. Intercalibration of standards, absolute ages and uncertainties in $^{40}Ar/^{39}Ar$ dating. Chemical Geology 145, 117-152.
Rose Jr., W.I., Stoiber, R.E., Malinconico, L.L., 1982. Eruptive gas compositions and fluxes of explosive volcanoes: budget of S and Cl emitted from Fuego volcano, Guatemala. In: Thorpe, R.S. (Ed.), Andesites: Orogenic Andesites and Related Rocks. Wiley, New York, NY. 669– 676.
Seaman, S.J., Dyar, M.D., Marinkovic, N., Dunbar, N.W., 2006. An FTIR study of hydrogen in anorthoclase and associated melt inclusions. American Mineralogist. 91, 12-20.
Sheppard, S.M.F., Harris, C., 1985. Hydrogen and oxygen isotope geochemistry of Ascention Island lavas and granites: variation with crystal fractionation and interaction with sea water. Contrib. Mineral. Petrol. 91, 74 -81.
Sims, K.W.W. et al., in prep. Radiogenic isotopic compositions of tephra from the Mount Erebus, Antarctica, lava lake from 1972 – 2004 and comparison with older lavas.
Sims, K.W.W., DePaolo, D.J., 1997. Inferences about mantle magma sources from incompatible element concentration ratios in oceanic basalts. Geochim. Cosmochim. Acta. 61, 765-784.
Sparks, R.S.J., 2003a. Forecasting volcanic eruptions. Earth Planet. Sci. Lett. 210, 1-15.
Sparks, R.S.J., 2003b. Dynamics of magma degassing. In: C. Oppenheimer, C., Barclay, J., Pyle, D. (Eds.), Origins, emissions and impacts of volcanic gases. Geol. Soc. London, Spec. Publ. 213, 5-22.
Steiger, R.H., Jaeger, E., 1977. Subcommission on geochronology: convention on the use of decay constants in geo- and cosmochronology. Earth Planet Sci Lett 36, 359–362.
Stevenson, D.S., Blake, S., 1998. Modeling the dynamics and thermodynamics of volcanic degassing. Bull. Volcanol. 60, 307-317.
Stoiber, R., Williams, S., Huebert, B., 1986. Sulfur and halogen gases at Masaya caldera complex, Nicaragua: Total flux and variations with time. J. Geophys. Res. 91, 2215–2231.
Stormer, J.C., 1983. The effects of recalculation on estimates of temperature and oxygen fugacity from analyses of multicomponent iron-titanium oxides. American Mineralogist. 68, 586-594.
Streck, M.J., Dungan, M.A., Bussy, F., Malavassi, E., 2005. Mineral inventory of continuously erupting basaltic andesites at Arenal volcano, Costa Rica: implications for interpreting monotonous, crystal-rich, mafic arc stratigraphies. J. Volcanol. Geotherm. Res. 140, 133-155.
Sun, S.-S., Hanson, G.N., 1975. Origin of Ross Island basanitoids and limitations upon the heterogeneity of mantle sources for alkali basalts and nephelinites. Contrib. Miner. Petrol. 54, 139-55.
Sun, S.-S., Hanson, G.N., 1976. Rare earth element evidence for differentiation of McMurdo Volcanics, Ross Island, Antarctica. Contrib. Miner. Petrol. 54, 139-155.
Sun, S.-S., McDonough, W.F., 1989. Chemical and isotopic systematics of oceanic basalts: implications for mantle compositions and processes. In: Saunders, A.D., Norry, M.J. (Eds.), Magmatism in Ocean Basins. Geol. Soc. London, Spec. Publ. 42, 313–345.

Tait, S.R., Wörner, G., Bogaard Pvd., Schmincke H-U., 1989. Cumulate nodules as evidence for convective fractionation in a phonolite magma chamber. J. Volcanol. Geotherm. Res. 37, 21-37.
Taylor, H.P., Sheppard, S.M.F., 1986. Igneous Rocks: I. Processes of Isotopic Fractionation and Isotope Systematics. In: Valley, J.W., Taylor, H.P., O'Neil, J.R. (eds.) Reviews in Mineralogy, 16. Stable Isotopes in High Temperature Geological Processes. Min. Soc. Am., Washington, D.C. 227-269.
Taylor, J.R., 1982. An introduction to error analysis: the study of uncertainties in physical measurements. University Science Books, Mill Valley, 1–269.
Tazieff, H., 1984. Nyiragongo: Renewed activity of the lava lake. J. Volcanol. Geotherm. Res., 20, 267– 280.
Tilling, R.I., 1987. Fluctuations in surface height of active lava lakes during 1972-1974 Mauna Ulu eruption, Kilauea Volcano, Hawaii. J. Geophys. Res. 92, 13721-13730.
Tuttle, O.F., Bowen, N.L., 1958. Origin of granite in the light of experimental studies. Geological Society of America, Boulder, Colorado. 153 pp.
Venezky, D.Y., Rutherford, M.J., 1999. Petrology and Fe-Ti oxide reequilibration of the 1991 Mount Unzen mixed magma. J. Volcanol. Geotherm. Res. 89, 213-230.
Wade, J.A., Plank, T., Stern, R.J., Tollstrup, D.L, Gill, J.B., O'Leary, J.C., Eiler, J.M., Moore, R.B., Woodhead, J.D., Trusdell, F., Fischer, T.P., Hilton, D.R., 2005. The May 2003 eruption of Anatahan volcano, Mariana Islands: Geochemical evolution of a silicic island-arc volcano. J. Volcanol. Geotherm. Res. 146, 139-170.
Wallace, P.J., 2005. Volatiles in subduction zone magmas: concentrations and fluxes based on melt inclusion and volcanic gas data. J. Volcanol. Geotherm. Res. 140, 217–240.
Wallace, G.S., Bergantz, G.W., 2005. Reconciling heterogeneity in crystal zoning data: An application of shared characteristic diagrams at Chaos Crags, Lassen Volcanic Center, California. Contrib. Mineral. Petrol. 149, 98-112.
Wardell, L.J., Kyle, P.R., Campbell, A.R., 2003. Carbon dioxide emissions from fumarolic ice towers, Mount Erebus volcano, Antarctica. In: C. Oppenheimer, C., Barclay, J., Pyle, D. (Eds.), Origins, emissions and impacts of volcanic gases. Geol. Soc. London, Spec. Publ. 213, 231-246.
Wardell, L.J., Kyle, P.R., Chaffin, C., 2004. Carbon dioxide and carbon monoxide emission rates from an alkaline intra-plate volcano: Mt. Erebus, Antarctica. J. Volcanol. Geotherm. Res. 131, 109-121.
Wen, S., Nekvasil, H., 1994. SOLVCALC; an interactive graphics program package for calculating the ternary feldspar solvus and for two-feldspar geothermometry. Computers and Geosciences. 20, 1025-1040.
Westrich, H.R., Gerlach, T.M., 1992. Magmatic gas source for the stratospheric SO_2 cloud from the June 15, 1991, eruption of Mount Pinatubo. Geology. 20, 867-870.
Wilson, M., 1989. Igneous Petrogenesis. Unwin Hyman Ltd., London, England. 466 pp.
Witter, J.B., Kress, V.C., Delmelle, P., Stix, J., 2004. Volatile degassing, petrology, and magma dynamics of the Villarrica Lava Lake, Southern Chile. J. Volcanol. Geotherm. Res. 134, 303-337.
Wright, T. L., Fiske, R. S., 1971. Origin of differentiated and hybrid lavas of Kilauea Volcano, Hawaii. J. Petrol. 12, 1-65.
Zhao, Z., Zheng, Y., 2003. Calculation of oxygen isotope fractionation in magmatic rocks. Chemical Geology. 193, 59– 80.